Ollscoil na Gaillimhe
University of Galway

Provided by the author(s) and University of Galway in accordance with publisher policies. Please cite the published version when available.

Title	Unsaturated hydrocarbon combustion chemistry and gasoline and diesel fuel ignition: Experimental and theoretical studies
Author(s)	Li, Yang
Publication Date	2017-12-04
Item record	http://hdl.handle.net/10379/7008

Downloaded 2024-04-26T04:17:11Z

Some rights reserved. For more information, please see the item record link above.

Unsaturated Hydrocarbon Combustion Chemistry and Gasoline and Diesel Fuel Ignition: Experimental and Theoretical Studies

Yang Li
(M. Eng.)

School of Chemistry

Presented for the degree of Ph.D.

of the National University of Ireland, Galway

Supervisor: Prof. Henry J. Curran

Head of School: Prof. Paul V. Murphy

Table of Contents

Abbreviation list……..…….....vi

Abstract……..……..vii

Acknowledgements……...…….....ix

List of Publications……..……...xiii

Flow chart of the thesis……xv

Chapter 1: General introduction……..……...…….....1

1.1 Ignition delay time experiment…….……..2

1.2 Quantum chemistry calculation……...……..12

1.3 Kinetic model development……..32

Chapter 2: Publications……..…….……21

2.1 The oxidation of 2-butene: A high pressure ignition delay, kinetic modeling study and reactivity comparison with isobutene and 1-butene.....21

2.2 An extensive experimental and modeling study of 1-butene oxidation…….43

2.3 Theoretical kinetics analysis for Ḣ atom addition to 1,3-butadiene and related reactions on the $\dot{C}_4H_7$ potential energy surface…….....107

2.4 A comprehensive experimental and modeling study of isobutene oxidation…….....157

2.5 An experimental and modelling study of nitromethane + O_2 + N_2 ignition in a shock tube……..…….243

Chapter 3: Overall conclusions……287

Abbreviation list

AKI	Anti-Knock Index
ATcT	Active Thermochemical Tables
CBS	Complete basis set
DFT	Density functional theory
GA	Group additivity
Geo. & Freq.	Geometry and frequency calculation
HPL	High-pressure limit
HPST	High pressure shock tube
IDT	Ignition delay time
JSR	Jet Stirred Reactor
KAUST	King Abdullah University of Science and Technology
L-J	Lennard-Jones
LLNL	Lawrence Livermore National Laboratory
LPST	Low pressure shock tube
MESS	Master Equation System Solver
MON	Motor octane number
NTC	Negative temperature coefficient
NUIG	National University of Ireland, Galway
OS	Octane sensitivity
PES	Potential energy surface

PRF	Primary reference fuel
QC	Quantum chemistry
RCM	Rapid compression machine
RON	Research octane number
Scan	Dihedral angle scan
SF	Scale factor
SPE	Single point energy
ST	Shock tube
TPRF	Toluene primary reference fuel
ZKE	Zero kelvin energy
ZPE	Zero point energy

Abstract

The primary objective of the work presented in this *Thesis* is to investigate the oxidation chemistry of unsaturated hydrocarbons. Butenes (1-, 2-, iso-butene) and 1,3-butadiene are the shortest olefins with structural isomers and are the simplest conjugated hydrocarbons and were thus selected as candidates to systematically elucidate their combustion chemistry using combined experimental, theoretical and kinetic modelling approaches.

Experimental ignition delay time (IDT) measurements of the butenes were carried out in both a rapid compression machine (RCM) and in a high-pressure shock tube (HPST) at equivalence ratios of 0.5, 1.0, and 2.0 at engine relevant ranges of temperature (650 – 1400 K) and pressure (10 to 50 atm).

A comprehensive chemical kinetic mechanism (AramcoMech 2.0) to describe the combustion of 1- and 2-butene has been developed. It has been validated using the IDT data as measured above in addition to a large variety of literature data: IDTs, species profile data as a function of time and temperature measured in jet-stirred reactors (JSRs), premixed flames, and flow reactors, and laminar flame speed data. Important reactions have been identified via flux and sensitivity analyses including: (a) H-atom abstraction from 1-butene by hydroxyl radicals and molecular oxygen from different carbon sites; (b) addition reactions, including hydrogen atom and hydroxyl radical addition to 1-butene; (c) allylic radical chemistry, including the addition reactions with methyl radical, hydroperoxyl radical and self-recombination; (d) vinylic radical chemistry, including the addition reaction with molecular oxygen; (e) alcohol

radical chemistry, including the Waddington type propagating reaction pathways and alkyl radical low-temperature branching chemical pathways.

Rate constants and thermodynamic properties for Ḣ-atom addition to 1,3-butadiene and related reactions on the $\dot{C}_4H_7$ potential energy surface were calculated using two different series of quantum chemical methods and two different kinetic codes. The calculated results including zero-point energies, single-point energies, rate constants, barrier heights, and thermochemistry were systematically compared among the two quantum chemical methods. Moreover, a systematic investigation of H-atom abstraction by molecular oxygen of primary, secondary and tertiary hydrogen atoms from a series of allylic radicals was carried out using four different quantum chemical methods and two different kinetic codes.

Finally, the autoignition characteristics of two gasoline and diesel fuel blends (volume ratio: 75:25 and 50:50) were studied experimentally over a wide range of temperatures, equivalence ratios, and pressures using both a high-pressure shock tube (HPST) and a rapid compression machine (RCM). The reactivity of these two gasoline and diesel fuel blends were systematically compared with the other pure gasoline fuel samples. Additionally, three surrogates (Primary Reference Fuel (PRF), Toluene PRF (TPRF) and a multi-component surrogate) were carefully formulated for each fuel blend by matching various fuel characteristics (RON, MON, Octane Sensitivity and AKI) with two gasoline surrogate models from LLNL and KAUST being employed to simulate the experimental data.

Acknowledgements

My PhD has been a long journey filled with many challenges and successes. It would not have been possible without the support and mentorship from many people in my academic and personal life.

Firstly, I would like to be deeply grateful to my supervisor, Prof. Henry Curran, for giving me the opportunity to obtain my PhD degree at the Combustion Chemistry Centre (C^3). You opened a door for me to the world of science, to a team with profound knowledge, to a country with beautiful scenery. All these have become a hugely positive experience in my life that I will always be proud of.

A big thank you to Prof. Stephen Klippenstein, who trained me on the Master Equation System Solver (MESS) with great patience.

Many thanks to all of my "second supervisors": Prof. John Simmie, Dr. Chongwen Zhou, Dr. Kieran Somers and Dr. Kuiwen Zhang, I was fully trained on experimental, theoretical and kinetic modelling skills by you throughout my PhD.

A big thank you to Patrick Meier who plays the role of "Guardians of the Facilities", it is because of your great effort on upgrading the heating system, we "Made RCM Great Again!"

Thanks to Prof. Yingjia Zhang, I miss those conversations with you every night in office about the research status in China, in terms of your earnest attitude and extreme hardworking, I always treat you as a role model that young/early-stage researcher should be.

John Bugler, you are the strangest man and biggest "alcoholic" I have ever

met! However, I would like to express my gratitude to you for answering all my “daily questions” with great patience. Together with the other three “alcoholics”: Ultan, Colin and Matteo, I will always miss those “wild nights” in Ireland and after every conference.

Thanks to all of the past and present group members (Jorge, Sinéad, Fiona, Nitin, Jennifer, Yanjin, Gavin), collaborators over in Mechanical Engineering (Rory, Eoin, Sajjad, Karla), and visiting students and researchers I have worked with. I’m very grateful to have had the opportunity to work with people of such extensive knowledge and expertise.

As my favorite sports, I will miss all my “chem-soccer players”: Prof. Donal Leech, Mr. Dermot McGrath, Mr. Séamus Kellehan, Dr. Changyoul Lee and Dr. Mohammadreza Baigmohammadi, different ages and skills have never stopped us enjoying the games!

Thanks to all the PhD students and postdocs in the School of Chemistry, it was my great pleasure to meet with all of you with very different research and cultural background. I hope you all enjoyed the Chinese food I cooked for you!

To my loving girlfriend Alison, it was July 14th, 2014, the date of 2014 FIFA World Cup Final, and our first date. Germany won the game, and you won my heart. From then on, the time I spent with you are truly the best time that I have ever had in my life. Simply, you are my biggest gain in Ireland, and you are the best girl I have ever met!

Last, but not least, to all my family members, and especially to my mum. I’ve spent 22 years in school, traveled all around the world to achieve this final goal. This is for you.

The truth is rarely pure and never simple.

– *Oscar Wilde, The Importance of Being Earnest, 1895.*

Lead Author Publications

Y. Li, C.-W. Zhou, K.P. Somers, K. Zhang, H.J. Curran, "The oxidation of 2-butene: A high pressure ignition delay, kinetic modeling study and reactivity comparison with isobutene and 1-butene", Proc. Combust. Inst. 36 (2017) 403-411.

Y. Li, C.-W. Zhou, H.J. Curran, "An extensive experimental and modeling study of 1-butene oxidation", Combust. Flame, 181 (2017) 198–213.

Y. Li, S.J. Klippenstein, C.-W. Zhou, H.J. Curran, "Theoretical kinetics analysis for Ḣ atom addition to 1,3-butadiene and related reactions on the $\dot{C}_4H_7$ potential energy surface", J. Phys. Chem. A 121 (2017) 7433-7445.

Other Publications (Major Experimentalist)

C.-W. Zhou, **Y. Li,** E. O'Connor, K.P. Somers, S. Thion, C. Keesee, O. Mathieu, E.L. Petersen, T.A. DeVerter, M.A. Oehlschlaeger, G. Kukkadapu, C.-J. Sung, M. Alrefae, F. Khaled, A. Farooq, P. Dirrenberger, P.-A. Glaude, F. Battin-Leclerc, J. Santner, Y. Ju, T. Held, F.M. Haas, F.L. Dryer, H.J. Curran, "A comprehensive experimental and modeling study of isobutene oxidation", Combust. Flame 167 (2016) 353-379.

J.D. Nauclér, **Y. Li,** E.J.K. Nilsson, H.J. Curran, A.A. Konnov, "An experimental and modelling study of nitromethane + O_2 + N_2 ignition in a shock tube", Fuel (2016) 186 629–638.

C.-W. Zhou, **Y. Li,** U. Burke, K.P. Somers, S. Khan, J.W. Hargis, E.L. Petersen, M. AlAbbad, A. Farooq, Y. Pan, Y. Zhang, Z. Huang, J. Lopez, Z. Loparo, S. Vasu, H.J. Curran, "An experimental and chemical kinetic modeling study of 1,3-butadiene combustion: ignition delay time and flame speed measurements", Combust. Flame, in review.

Flow chart of the thesis

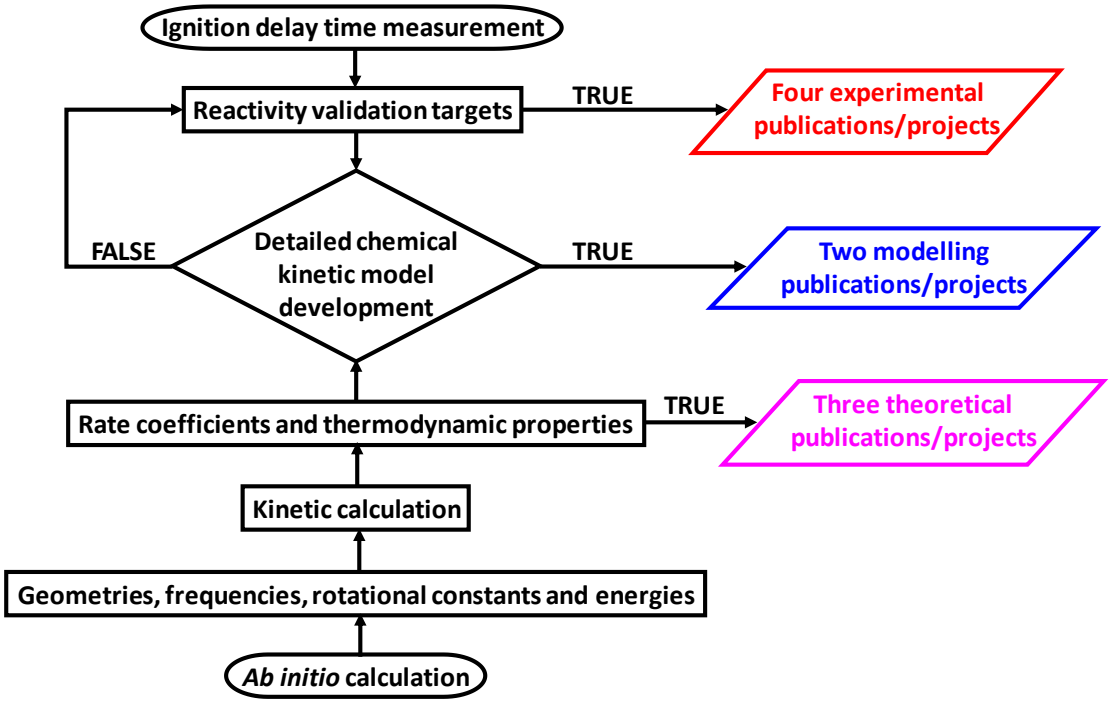

Experimental pblications/projects:

Y. Li et al., Gasoline and Diesel Fuel Ignition, Prepare for submission.
C-W. Zhou, **Y. Li** et al., Combust. Flame 167 (2016) 353-379.
J.D. Nauclér, **Y. Li** et al., Fuel (2016) 186 629–638.
C-W. Zhou, **Y. Li** et al., 1,3-Butadiene Ignition, Prepare for submission.

Modelling publications/projects:

Y. Li et al., Proc. Combust. Inst. 36 (2017) 403-411.
Y. Li et al., Combust. Flame 181 (2017) 198–213.

Theoretical publications/projects:

Y. Li et al., J. Phys. Chem. A 121 (2017) 7433–7445.
Y. Li et al., Thermochemistry Calculation and Group Optimization, Prepare for submission.
Y. Li et al., Allylic Radicals + O_2 Rate Constants Calculation, Prepare for submission.

General introduction

More than 80% of the world's energy supply is generated from combustion. Development of efficient, next generation, advanced engines by using alternative fuels and operating at extreme conditions is one of the most important solutions to increase energy efficiency and sustainability. To realize advanced engine design, the challenges in combustion research are therefore to advance our fundamental understanding of combustion chemistry and dynamics from molecule scales to engine scales and to develop quantitatively predictive tools and innovative combustion technologies, Figure 1, in which the first three steps highlighted in red are the primary focus of this thesis:

- Ignition delay time experiments
- Quantum chemistry calculation
- Kinetic model development

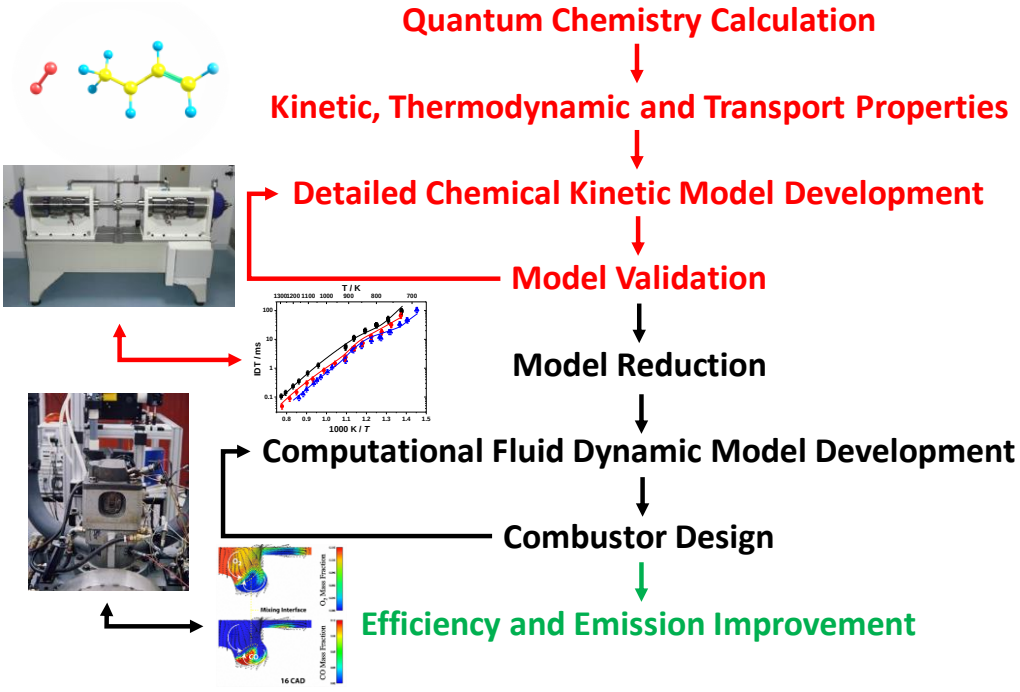

Figure 1. Next generation advanced engine design from molecule to motor.

1. Ignition delay time experiment

Figure 2 is taken from a review paper published by Goldsborough *et al.* [1], which summarizes the operating conditions (temperature and pressure) of the typical experimental facilities used in combustion chemistry research. Shock tubes (STs) and rapid compression machines (RCMs) are suitable reactors to study the ranges of temperature and pressure applicable to engine operating conditions.

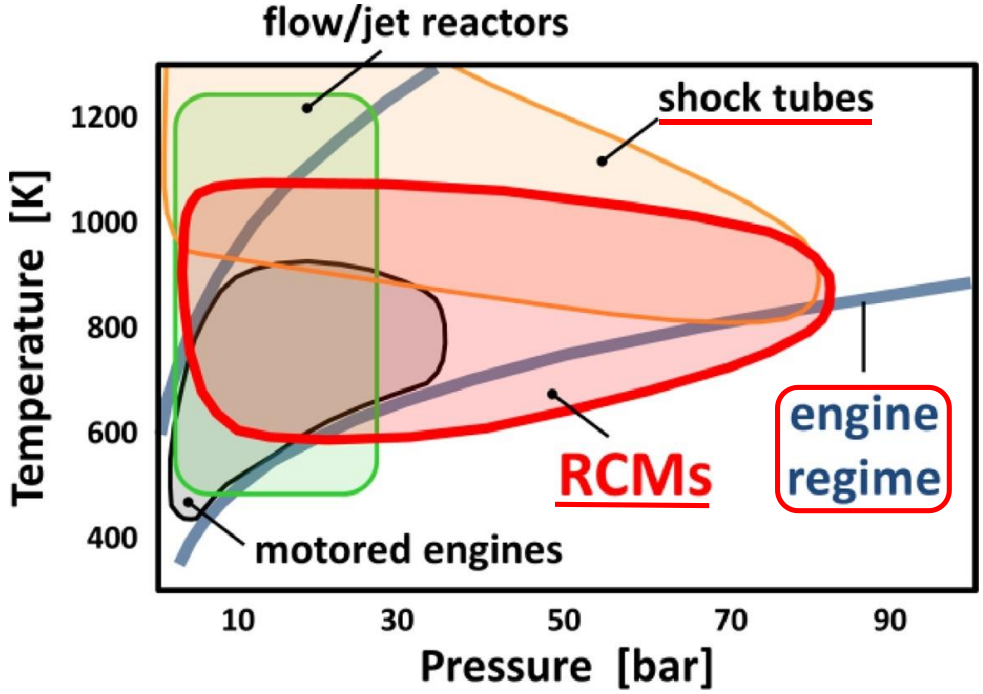

Figure 2. Experimental facilities used in the combustion chemistry research area.

In this study, the ST and Blue RCM at NUIG were utilized to measure ignition delay times (IDT) of five unsaturated hydrocarbons, one nitro compound and two practical gasoline/diesel fuel blends including:

- Iso-butene
- 1-Butene
- Trans-2-butene

- Cis-2-butene
- 1,3-Butadiene
- Nitromethane
- Gasoline/Diesel 75/25 Fuel Blends
- Gasoline/Diesel 50/50 Fuel Blends

Most of the IDT measurements were taken at equivalence ratios of 0.5, 1.0, and 2.0 over a wide temperature range, and across engine relevant pressures, ranging from 10 to 50 atm. The experiments reported in this thesis resulted in the generation of more than 100 data sets with over 1000 IDT points.

Particularly, as a state-of-the-art research facility, there are about 30 RCMs all over the world which were used for autoignition study, Figure 3 [1].

Figure 3. RCM worldwide

Here, as the experimental study of gasoline/diesel fuel blends hasn't been published, instead, a brief introduction and a small part of the results about this

project will be shown in the following section.

Basically, this project is to measure the IDTs of four different gasoline and gasoline diesel fuel blends (supplied by Coryton Advanced Fuels and Haltermann Solutions):

- Coryton Gasoline
- Haltermann Gasoline
- Coryton Gasoline/Diesel (75/25)
- Coryton Gasoline/Diesel (50/50)

Table 1 shows the comparison of properties of four different fuels, which include the research octane number (RON), motor octane number (MON), octane sensitivity and anti-knock index (AKI). In general, these properties all decrease from Coryton Gasoline to Coryton Gasoline/Diesel (50/50).

Table 2 summarizes the experimental conditions of this project, where the IDTs of these fuels were measured at three different equivalence rations (0.5, 1.0 and 2.0) and three different pressures (10, 20 and 40 atm).

Table 1 Comparison of properties of four different fuels.

Fuel	Coryton Gasoline	Haltermann Gasoline	Coryton Gasoline /Diesel (75/25)	Coryton Gasoline /Diesel (50/50)
RON	97.5	91	80	61
MON	86.6	83.4	73.8	55
Sensitivity	10.9	7.6	6.2	6
AKI	92.05	87.2	76.9	58

Table 2 Experimental conditions of this project.

Fuel		Coryton Gasoline	Haltermann Gasoline	Coryton Gasoline /Diesel (75/25)	Coryton Gasoline /Diesel (50/50)
Φ = 0.5	10 atm	–	–	√	√
	20 atm	√	–	√	√
	40 atm	–	–	–	–
Φ = 1.0	10 atm	√	√	√	√
	20 atm	√	√	√	–
	40 atm	√	√	–	–
Φ = 2.0	10 atm	–	–	√	–
	20 atm	√	–	√	–
	40 atm	–	–	–	–
Formula		$C_{6.46}H_{11.39}O_{0.10}$	$C_{6.11}H_{12.07}O_{0.21}$	$C_{7.49}H_{13.28}O_{0.08}$	$C_{8.81}H_{15.69}O_{0.06}$

In order to perform experiments on these extreme low vapor pressure gasoline/diesel fuel blends, the heating system of RCM was systematically upgraded, shown in Table 3.

Here, φ = 1.0, p = 10 atm is selected as representative condition, and the IDT comparison of four different fuels under this condition is shown in Figure 4. At intermediate to high temperature (900 – 1400 K), four fuels present the same reactivity (solid symbols), while at NTC regime (700 – 900 K), the IDT decreases from the fuel high octane number to the one with low octane number fuel (open symbols).

Table 3 Comparison of the key parameters of RCM heating system.

	Old RCM	Upgraded RCM
Target temperature	120 °C	200 °C
Number of heating devices (PID controllers, heating tapes and thermocouples)	11 sets	20 sets
Length of pipeline (From tank to chamber)	6 m	2 m
Size of pipeline and manifold (Inner diameter)	1/4 inch	1/2 inch
Heating of reaction chamber	heating cable	heating cable & heating cartridge
Insulation materials	Glass Fibre Yarn	Glass Fibre Yarn & Calcium-Magnesium Silicate
Pressure gages	Vacuum gauge 5000 mbar gauge	Vacuum gauge 100 Torr gauge 5000 mbar gauge

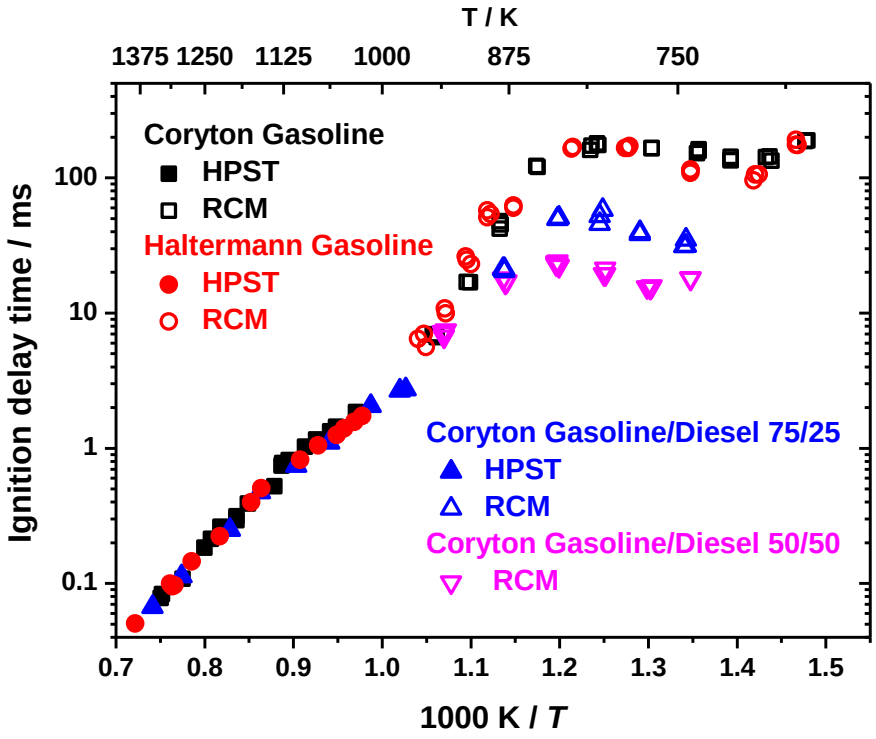

Figure 4. IDT comparison of four different fuels at φ = 1.0, p = 10 atm.

In addition, two different gasoline surrogates: primary reference fuel (PRF; mixture of n-heptane and iso-octane) and toluene primary reference fuels (TPRF; mixture of toluene, n-heptane and iso-octane), were formulated by emulating the AKI, RON and octane sensitivity [2], as shown in Table 4.

Table 4 Gasoline surrogate formulation for four different fuels.

Fuel	Coryton Gasoline		Haltermann Gasoline		Coryton Gasoline /Diesel (75/25)		Coryton Gasoline /Diesel (50/50)	
Surrogate	PRF	TPRF	PRF	TPRF	PRF	TPRF	PRF	TPRF
iso-Octane	92.05	8.1	87.2	54	76.9	35.46	58	14.52
n-Heptane	17.95	14.3	12.8	17	23.1	29.64	42	51.03
Toluene	-	77.6	-	29	-	34.9	-	34.45

Two different kinetic models were employed to carry out the simulation results based on the above surrogates:

- LLNL (1389 species and 5935 reactions) [3]
- KAUST (2768 species and 9236 reactions) [4]

Here, the validation results generated by two different kinetic models and two different gasoline surrogates, at three different equivalence ratios, two different pressures and over different temperature regimes were selected as representatives, shown in Figure 5. In general, both kinetic models and both gasoline surrogates can capture the IDTs over a wide range of temperatures, equivalence ratios and pressures. The KAUST model performs better than the LLNL model, and the PRF surrogate shows a higher reactivity than the TPRF surrogate.

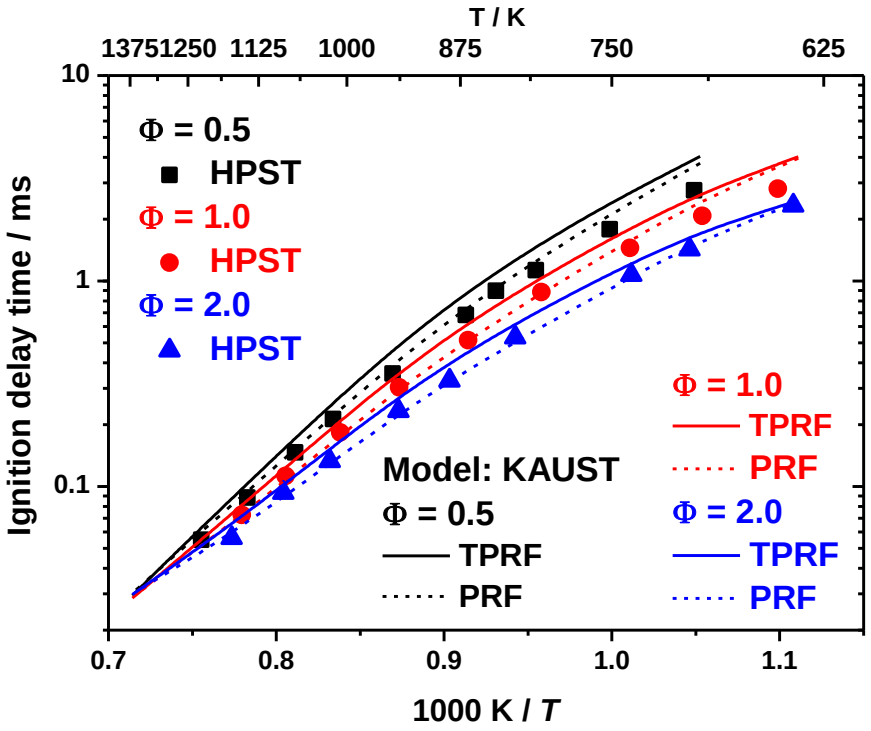

(a) IDT of Coryton Gasoline/Diesel 75/25 at high temperature, p = 20 atm.

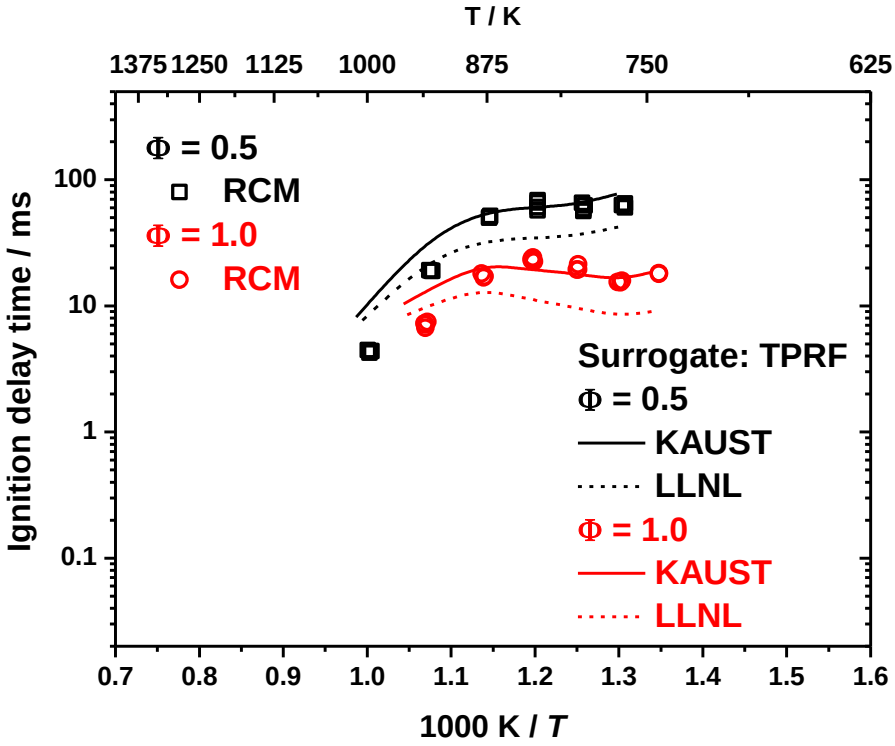

(b) IDT of Coryton Gasoline/Diesel 50/50 at low temperature, p = 10 atm.

Figure 5. Gasoline surrogate model simulation using two kinetic models and two gasoline surrogates, at three equivalence ratios, two pressures and different temperature regimes.

Moreover, in order to systematically compare the reactivity of these four fuels and eliminate the effect of the limited quantity of experimental data presented in Table 2 and the facility effect, constant volume simulations have been consistently performed for these four different fuels, using two different gasoline surrogates and two different kinetic models, at three different equivalence ratios and two different pressures.

Here, simulation results at φ = 1.0 and p = 10 atm were selected as representatives, shown in Figure 6. The reactivity of four fuels were compared as a function different gasoline surrogates and kinetic models.

At intermediate and high temperatures (900 – 1400 K), all four fuels present the same reactivity, which indicates the dominance of oxygen chemistry over this temperature regime. In the NTC regime (700 – 900 K), IDTs decrease from the fuel with the highest octane number (Coryton gasoline) to that with the lowest (50/50 Coryton gasoline/diesel). At 750 K, the discrepancy is about a factor of 1.5 – 2.0. This discrepancy corresponds to the experimental data shown in Figure 4. In general, the LLNL model shows a more pronounced NTC behavior than the KAUST model, and the PRF surrogate shows a more pronounced NTC behavior than the TPRF surrogate. It is worth noting that the simulation results of the Coryton Gasoline using the TPRF surrogate are unreasonably slow, due to the large quantity of toluene (77.6% by volume) in the surrogate shown in Table 4, in order to match the high RON and octane sensitivity.

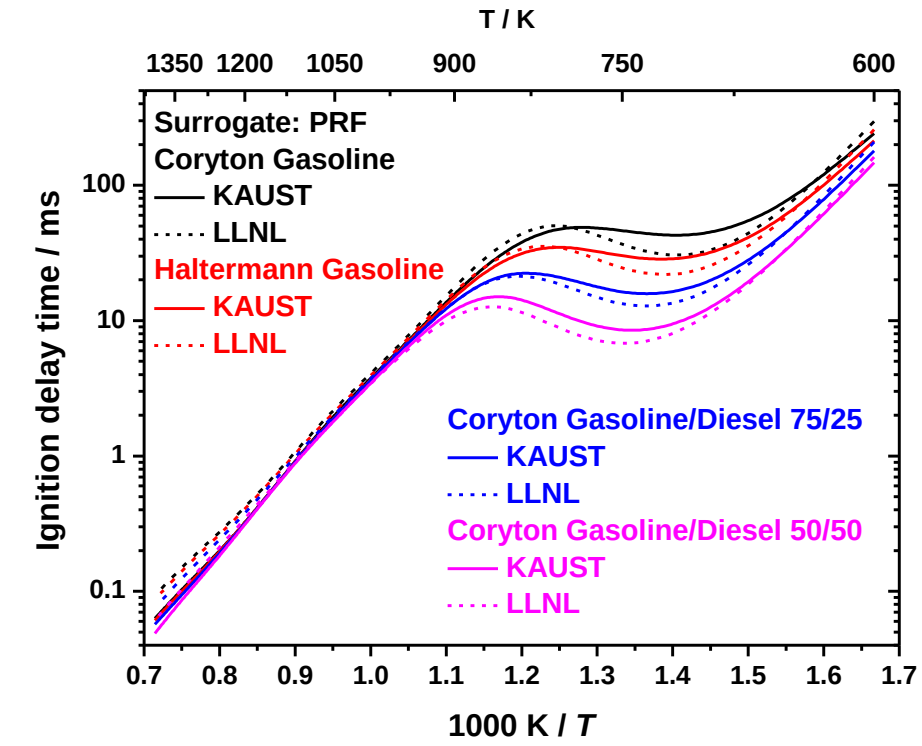

(a) Simulation results by using PRF surrogate

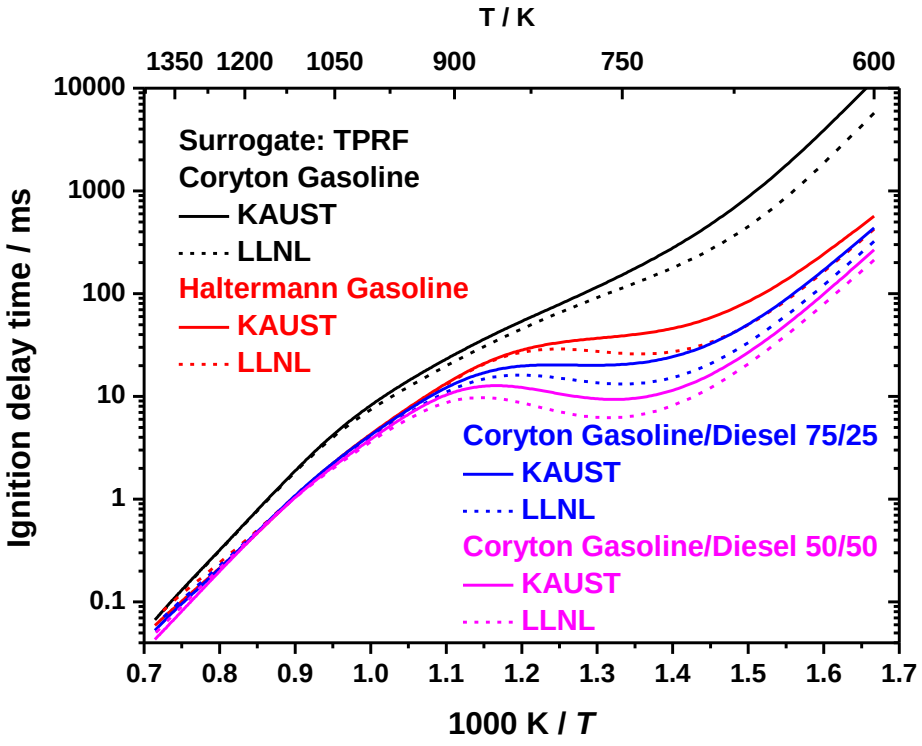

(b) Simulation results by using TPRF surrogate

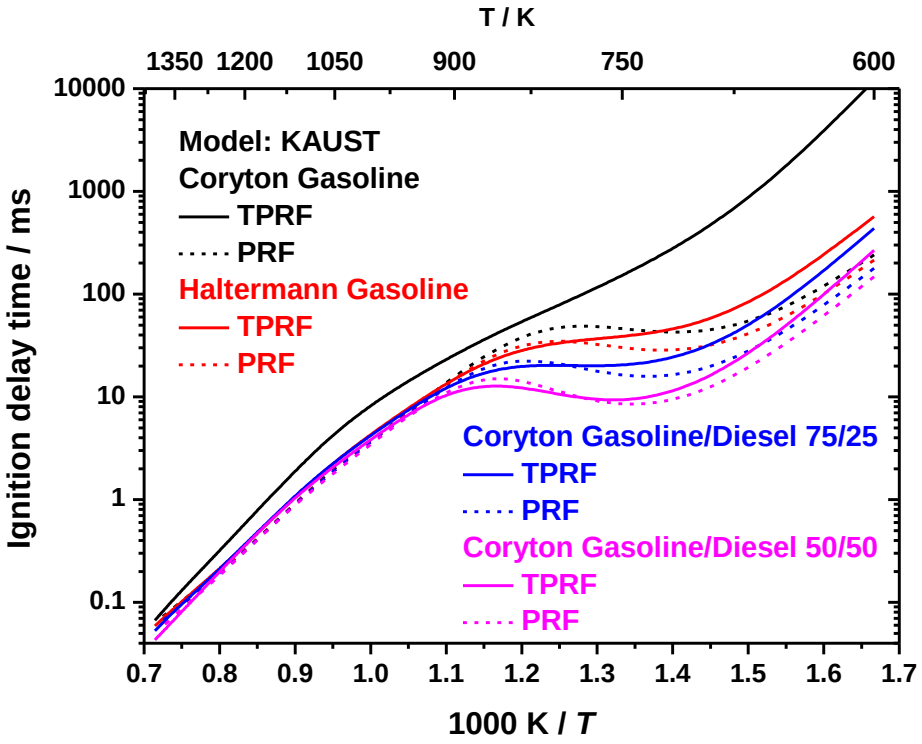

(c) Simulation results by using KAUST model

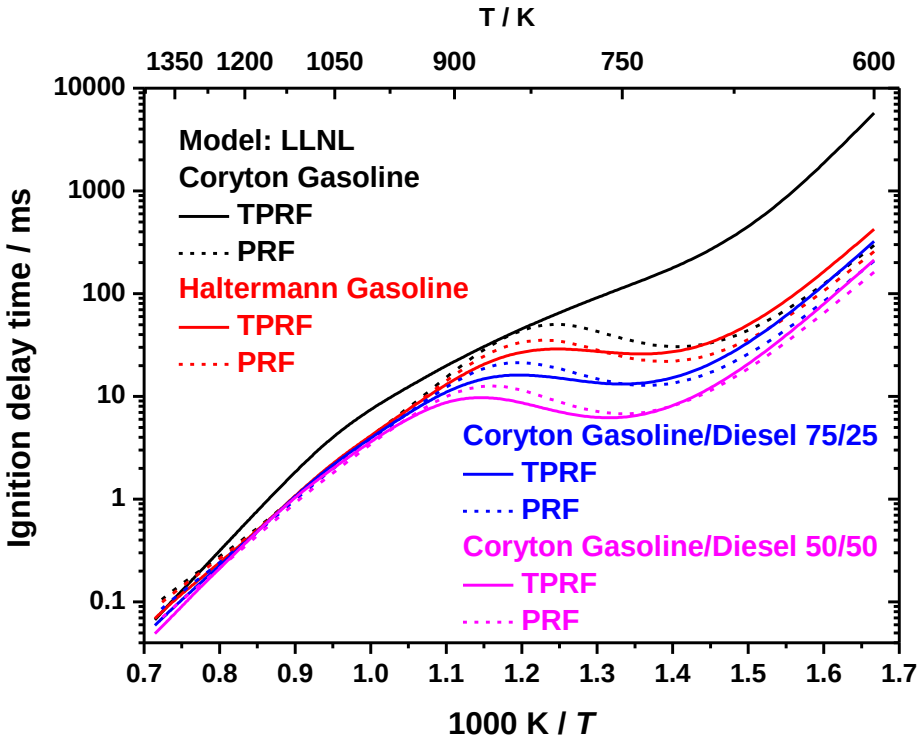

(d) Simulation results by using LLNL model

Figure 6. Constant volume simulation for four fuels at φ = 1.0, p = 10 atm

2. Quantum chemistry calculation

Based on the detailed 1-butene, 2-butene and 1,3-butadiene kinetic models the 1-methylallyl ($\dot{C}_4H_7$1-3) allylic radical was found to be the most important intermediate species involved in the oxidation of linear C_4 unsaturated hydrocarbons. Figure 7 shows the major consumption pathways of this 1-methylallyl ($\dot{C}_4H_7$1-3) allylic radical, one of which includes reactions on the $\dot{C}_4H_7$ potential energy surface (PES) which includes the isomerization, β-scission and chemically activated reactions; the other is direct H-atom abstraction by molecular oxygen. Figure 8 shows the related experimental, theoretical and modelling studies on the $\dot{C}_4H_7$ PES available in the literature.

In this thesis, the rate constants and thermodynamic properties for the above two reaction classes were calculated using four different series of quantum chemical methods and two different kinetic codes.

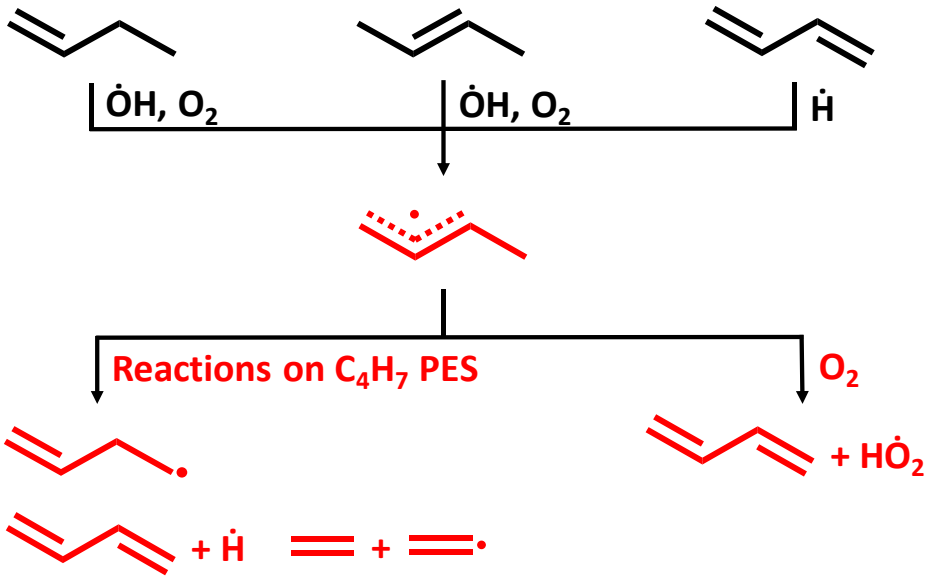

Figure 7. Major consumption pathways of 1-methylallyl ($\dot{C}_4H_7$1-3) allylic radical

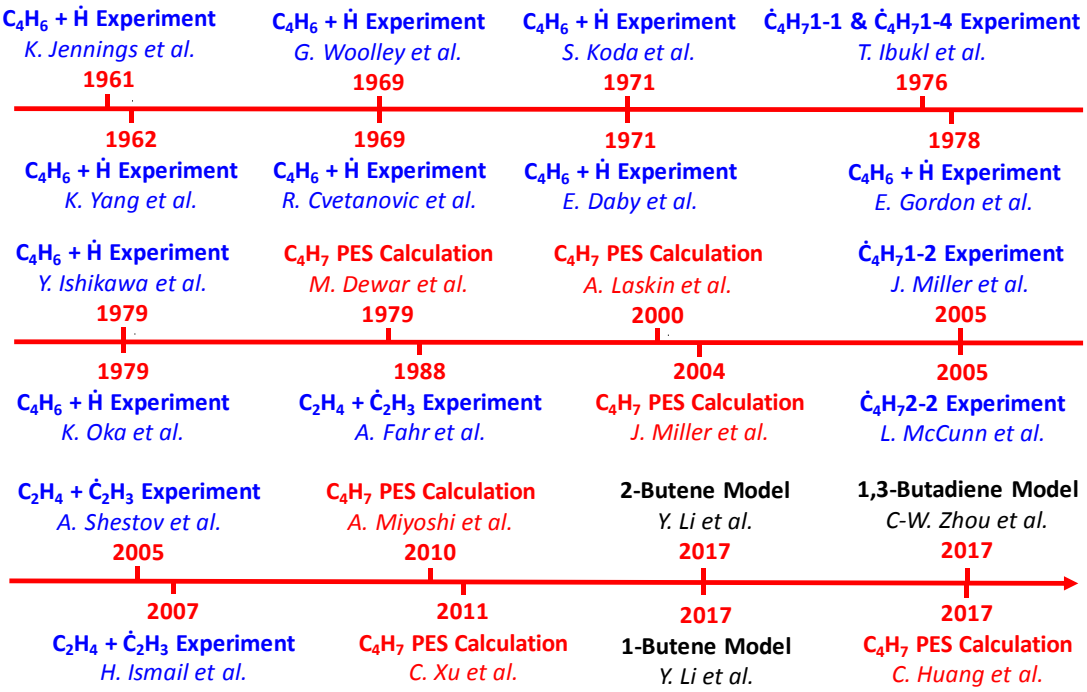

Figure 8. Literature review for the related studies on $\dot{C}_4H_7$ PES. Black: modelling studies, blue: experimental studies, red: theoretical studies.

A series of commercial software and non-commercial codes have been utilized in this theoretical work including the *ab initio* solvers, kinetic solvers, visualization tools and fitting tools, as listed below:

- Spartan 14
- Gaussian 09
- Chemcraft 2.0
- Chemdraw Pro 16.0
- COREL VideoStudio Pro
- MultiWell (THERMO)
- PAPR (MESS)
- ChemDis
- THERM

- CHEMKIN-PRO (FitDat)
- PAC 99
- A series of automation Perl codes from Dr. Kieran Somers
- THERMAKE.xlsm Excel Sheet with VB code from Dr. Kuiwen Zhang
- MESS_TPfit and NASA_CKIN Python codes from Prof. Franklin Goldsmith

In the *ab initio* electronic structure calculations, four different series of methods have been systematically applied and compared, Table 5.

Table 5 Calculation methods employed here.

	Method 1	Method 2	Method 3	Method 4
Targets	Allylic radicals + O_2 1,3-Butadiene + H	Allylic radicals + O_2 1,3-Butadiene + H	Allylic radicals + O_2	Allylic radicals + O_2
Geom. & Freq.	M062X/ 6-311++G(d,p)	wB97XD/ aug-cc-pVTZ	M062X/ 6-311++G(d,p)	M062X/ 6-311++G(d,p)
Scan	M062X/6-311++G(d,p)			
SPE	CCSD(T)/cc-pVTZ	CCSD(T)/aug-cc-pVTZ	CCSD(T)/cc-pVDZ	G4
	CCSD(T)/cc-pVQZ	MP2/aug-cc-pVTZ	CCSD(T)/cc-pVTZ	–
	–	MP2/aug-cc-pVQZ	MP2/cc-pVDZ	–
	–	–	MP2/cc-pVTZ	–
	–	–	MP2/cc-pVQZ	–
ZKE	CBS-APNO/G3/G4			

Different density functional theory (DFT) methods with different basis sets were used for geometry optimizations, vibrational frequency calculations, and in the hindered rotation scans for the lower-frequency modes. In terms of the

electronic single point energy (SPE) calculations, the level of theory decreases from Method 1 to Method 4, which affects the selection of the method for the calculations of different molecular sizes. The zero kelvin energy (ZKE) calculations were carried out using a combined compound method CBS-APNO/G3/G4, which was found to yield results approaching "chemical accuracy" (arbitrarily ≈ 4 kJ mol^{-1} or 1 kcal mol^{-1}) when benchmarked against enthalpy of formation values in the Active Thermochemical Tables (ATcT) [5-7].

Table 6 Detailed parameter treatment.

	Method 1	Method 2	Method 3	Method 4
Targets	Allylic radicals + O_2 1,3-Butadiene + H	Allylic radicals + O_2 1,3-Butadiene + H	Allylic radicals + O_2	Allylic radicals + O_2
SF for ZPE	0.9698	1.0	0.9698	0.9698
SF for Freq.	0.983	1.0	0.983	0.983
CBS Extrapolation	E_{CBS} = $E_{CCSD(T)/cc\text{-}pVQZ}$ + ($E_{CCSD(T)/cc\text{-}pVQZ}$ - $E_{CCSD(T)/cc\text{-}pVTZ}$) * 4^4 / (5^4 - 4^4)	E_{CBS} = $E_{MP2/aug\text{-}cc\text{-}pVQZ}$ - $E_{MP2/aug\text{-}cc\text{-}pVTZ}$ - $E_{CCSD(T)/aug\text{-}cc\text{-}pVTZ}$	E_{CBS} = $E_{CCSD(T)/cc\text{-}pVTZ}$ + ($E_{CCSD(T)/cc\text{-}pVTZ}$ - $E_{CCSD(T)/cc\text{-}pVDZ}$) * 3^4 / 4^4 – 3^4 + $E_{MP2/cc\text{-}pVQZ}$ + ($E_{MP2/cc\text{-}pVQZ}$ - $E_{MP2/cc\text{-}pVTZ}$) * 4^4 / 5^4 – 4^4 - $E_{MP2/cc\text{-}pVTZ}$ - ($E_{MP2/cc\text{-}pVTZ}$ - $E_{MP2/cc\text{-}pVDZ}$) * 3^4 / 4^4 – 3^4	E_{G4}
Corrections	Asymmetric Eckart tunneling effect and hinder rotation treatments			
$H_{f,0K}$	Atomization and isodesmic method			

Table 6 summarized the detailed parameter treatment used in these four different methods including the scale factor (SF) for zero-point energy (ZPE),

vibrational frequencies, the equation for complete basis set (CBS) extrapolation, the correction for the asymmetric Eckart tunneling effect, and the chemically-balanced reaction schemes for 0 K formation enthalpy calculations.

For the MultiWell program suite calculations, the Lamm module [8] was used to calculate both external rotational constants and reduced moments of inertia for the hindered internal rotations. The calculated results were then fitted to truncated Fourier series, which were further used as 1-D hindered internal rotation input in the Thermo module. The high-pressure limit (HPL) rate coefficients were finally calculated by the Thermo module as a function of temperature (298.15 − 2000 K) based on canonical transition-state theory (TST).

The Master Equation System Solver (MESS) was used, in the PAPR program suite calculations, to calculate temperature and pressure-dependent rate coefficients for complex-forming reactions via solution of the one-dimensional ME, with the chemical transformations described using RRKM theory. Rate coefficients for the thermally and chemically activated reactions are obtained at temperatures ranging from 298.15 − 2000 K, and at pressures ranging from 0.01 to 100 atm. The internal rotors corresponding to methyl and ethyl like torsions were treated as one-dimensional hindered rotors with hindrance potentials evaluated at the M06-2X/6-311++G(d,p) level of theory. However, the reduced moment of inertia is calculated on the basis of the structure of the most stable species, the axis of rotation, and the identity of all of the atoms on each side of the rotated bond. Although an algorithm is

available in MESS that properly treats the internal rotation variation of both the internal and external rotational constants, for simplicity we assumed that the internal and external moments of inertia are constant (i.e., they are not a function of the dihedral angle). Note that this assumption is justified by the fact that the neglect of the coupling of external and internal rotation often counter-balances the neglect of the dihedral angle variance of the internal rotor moment of inertia. For the collisional model used in the master equation simulation, the interaction between the reactant and N_2 bath gas was modeled using the Lennard-Jones (L-J) potential. The L-J parameters were calculated using the method described in reference [9].

The calculated rate coefficients were fitted to a modified Arrhenius expression as a function of temperature:

$$k = \mathrm{A}\left(T/T_{ref}\right)^{\mathrm{n}}\exp(-E/RT)$$

where A is the A-factor, T is the temperature in units of Kelvin, T_{ref} = 1 K, n is the temperature exponent at 1 K, and E is related to the activation energy (by Ea = E + nRT).

The calculated thermochemical values of interest (enthalpy of formation, entropy and heat capacity) were calculated as a function of temperature (298.15 − 3000 K), and these resulting values were fitted to NASA polynomials using the Fitdat utility in ANSYS CHEMKIN-PRO [10].

In addition, another theoretical study carried out in this thesis was the optimization of unsaturated hydrocarbons related group values based on an extensive theoretical study on the thermochemical properties of alkene and

allylic radical species. This study was motivated by performing thermochemistry calculations using the group additivity (GA) method [11] for the 1-methylallyl ($\dot{C}_4H_7$1-3) allylic radical mentioned above. As shown in Figure 9, there are two different approaches to calculate the thermochemistry for this radical, one being the "ALLYLP" group optimized by Burke *et al.* [12] from the 2-butene parent, and the second being the "ALLYLS" group from 1-butene as the parent. On analysis, it was found that the entropy of the "ALLYLS" group was found to be about 4 cal K^{-1} mol^{-1} in error, which is quite high.

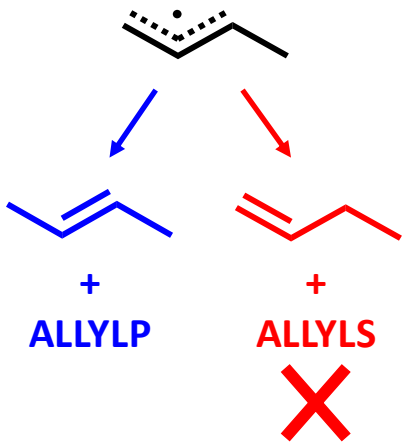

Figure 9. Two different approaches to estimate the thermochemistry of 1-methylallyl ($\dot{C}_4H_7$1-3) allylic radical using the GA method.

In view of the above, this study had two main aims: Firstly, to develop an accurate database of thermodynamic properties for small (C_2 – C_7) alkene and allylic radical species using consistent quantum chemistry (QC) calculations; secondly, to use the developed database to optimize the related groups which will be further used in the group additivity (GA) method. The majority of the values for the groups included in the GA method employed in THERM

originate from Benson [11] who first published group values in 1976. The ideology behind the work presented here is to develop accurate thermochemistry values for allylic radicals; by employing different approaches (parents) for certain radicals with the optimized "ALLYLP, ALLYLS and ALLYLT" group, the GA method should be able to predict similar/identical results from different stable parent alkenes. Moreover, the current GA method will be able to generate reasonable estimates of thermodynamic properties for a large variety of species involved with these groups where accurate high-level calculations are difficult to perform.

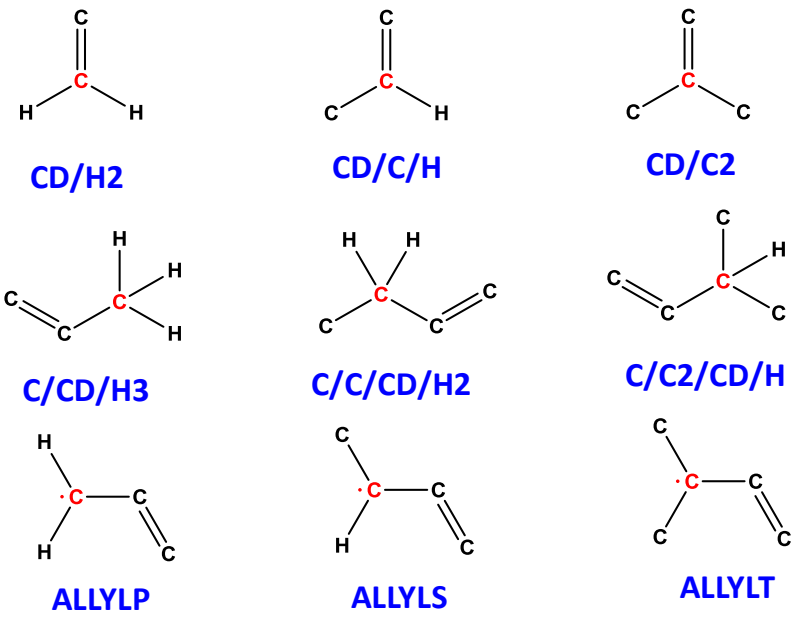

Figure 10. Group targets for optimization.

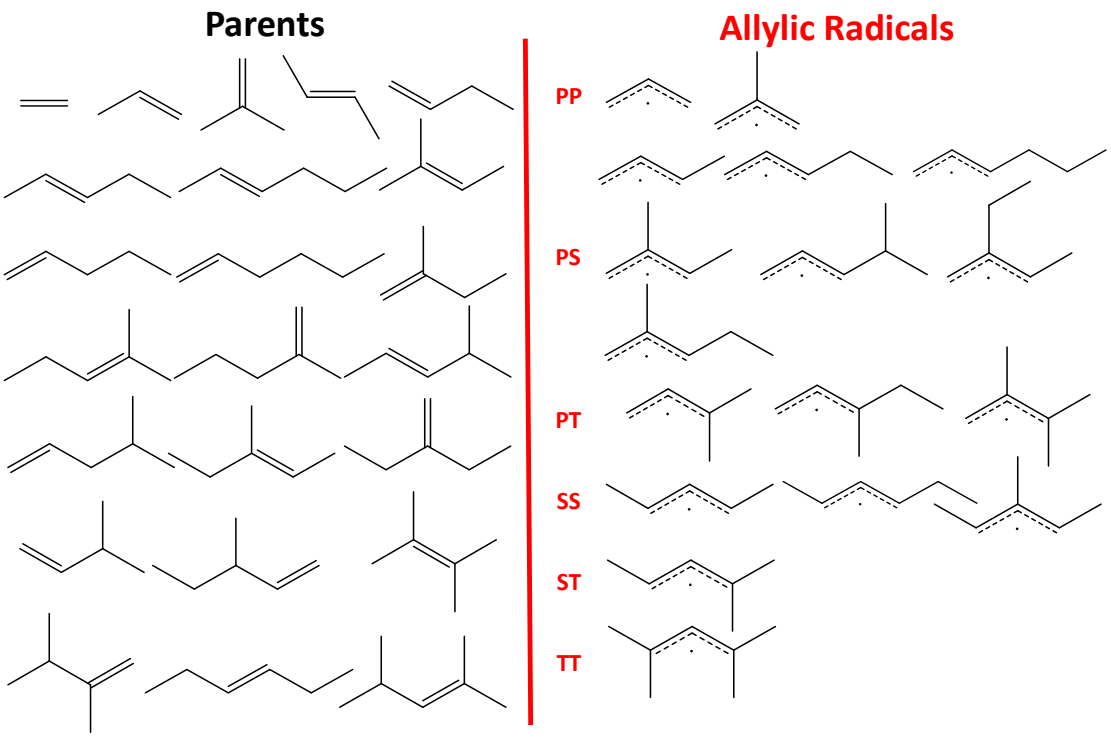

Figure 11. Species resource for quantum chemistry calculation.

To summarize the objective of this study, 9 groups were selected as targets for the optimization, Figure 10, where the thermochemical parameters of 23 alkene molecules and 17 allylic radicals were systematically calculated as the resource for optimization, Figure 11. Moreover, three super allylic BD groups have been newly optimized, Figure 12, where the thermochemical parameters of three diene molecules and two allylic radicals were also simultaneously calculated as a resource for development, Figure 13.

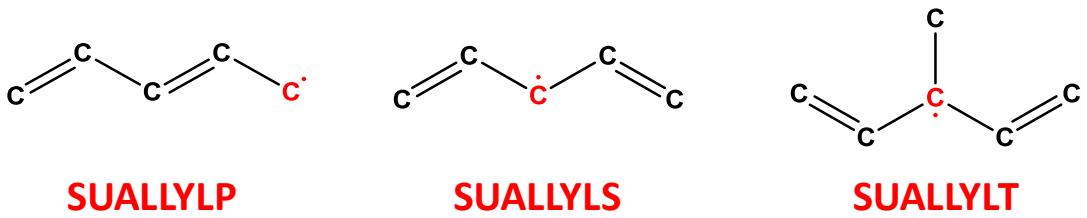

Figure 12. Group targets for development.

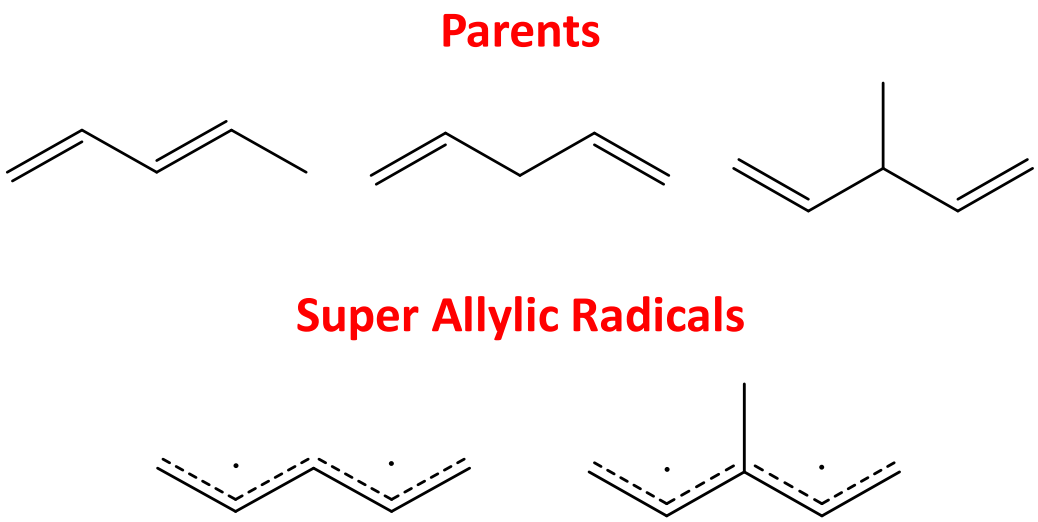

Figure 13. Species resource for quantum chemistry calculation.

Most of the alkene species and allylic radicals studied here are conformationally complex, having more than one conformer that contributes to its final enthalpy of formation. All conformer searches were carried out using the Spartan 10 software package at the B3LYP/6-31G(d,p) level of theory. Gibbs free energies, $\Delta G^{\ominus}$ (298.15 K) were then determined for each conformer and the Boltzmann distribution computed, taking due account of degeneracies, σ. The contribution, x_i, made by each conformer to the overall enthalpy of formation for species X is then calculated from:

$$x_i = \sigma_i exp(-\Delta G_m^{\Theta}(i)/RT) \sum_{i=1}^{n} [\sigma_i exp(-\Delta G_m^{\Theta}(i)/RT)]$$

Each individual enthalpy of formation was then weighted with respect to the population to calculate a final value for a particular molecule using:

$$\Delta_f H_m^{\Theta}(X) = \sum_{i=1}^{n} x_i \Delta_f H_m^{\Theta}(i)$$

Finally, all target groups were optimized by minimizing the total standard deviation:

$$\sum \sqrt{\frac{\sum(x-\bar{x})^2}{n}}.$$

Table 7, Table 8 and Table 9 show the calculated thermochemical values for stable alkenes, allylic radicals, dienes and super allylic radicals at selected temperatures respectively. Table 10 shows the optimized CH, allylic BD and super allylic BD groups.

Ultimately, the optimized group values will be compiled into the "Group Contribution Database", Figure 14, from where accurate thermochemical properties of these C_2 – C_7 and larger alkenes, dienes, allylic radicals and super allylic radicals can be generated for chemical kinetic model development.

Table 7. Thermochemical values* of alkene species calculated by *ab initio* method at selected temperatures.

Name	Structure	$\Delta_f H^\Theta$	S^Θ	C_p						
		298.15 K	298.15 K	300 K	400 K	500 K	600 K	800 K	1000 K	1500 K
Ethylene		12.39	52.33	10.20	12.54	14.77	16.70	19.81	22.20	26.07
Propene	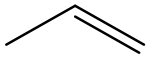	4.61	63.67	15.36	19.08	22.55	25.57	30.45	34.17	40.12
Isobutene	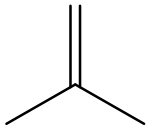	–4.28	70.14	21.12	26.18	30.8	34.82	41.32	46.29	54.22
2-Butene	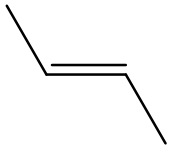	–2.87	70.73	20.96	25.78	30.38	34.45	41.07	46.13	54.17
			73.40							
1-Butene	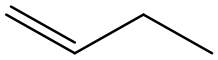	–0.09		20.55	25.98	30.88	35.05	41.62	46.56	54.39

2-Pentene	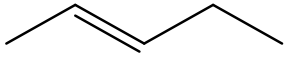	–7.69	81.91	26.13	32.66	38.69	43.91	52.25	58.54	68.45
1-Pentene	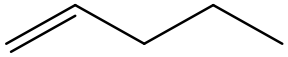	–5.10	83.25	26.18	32.93	39.07	44.30	52.56	58.76	68.55
2-Methyl-2-butene	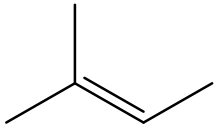	–10.37	80.79	25.04	31.42	37.46	42.76	51.33	57.83	68.06
2-Methyl-1-butene	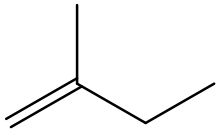	–8.54	81.95	26.03	32.58	38.58	43.76	52.06	58.35	68.31
2-Hexene	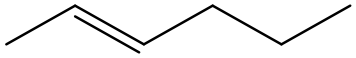	–12.67	91.69	31.90	39.71	46.96	53.22	63.21	70.74	82.61
1-Hexene	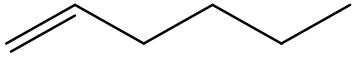	–9.95	93.27	31.85	39.98	47.36	53.65	63.60	71.06	82.79

2-Methyl-2-pentene	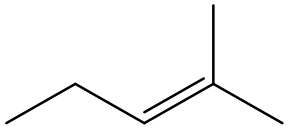	–15.26	91.90	30.13	38.19	45.71	52.23	62.60	70.37	82.47
2-Methyl-1-pentene	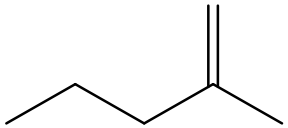	–13.69	91.13	32.63	40.49	47.60	53.73	63.53	70.95	82.70
4-Methyl-2-pentene	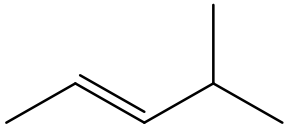	–14.65	89.07	32.16	40.17	47.45	53.68	63.57	71.01	82.75
4-Methyl-1-pentene	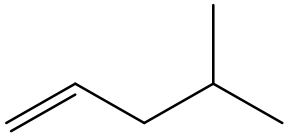	–12.05	89.65	32.18	40.45	47.93	54.26	64.13	71.48	83.01
3-Methyl-2-pentene	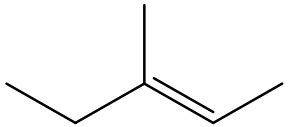	–14.99	90.84	29.95	38.08	45.56	52.01	62.31	70.05	82.22
2-Ethyl-1-butene	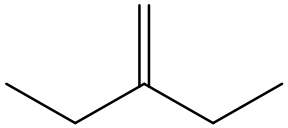	–13.17	90.07	31.23	39.44	46.96	53.38	63.46	70.97	82.75

3-Methyl-1-butene	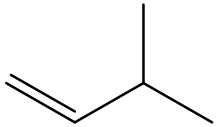	–7.12	80.29	26.44	33.43	39.61	44.80	52.95	59.05	68.69
3-Methyl-1-pentene	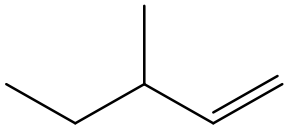	–11.58	89.78	32.70	40.64	47.92	54.15	63.98	71.33	82.92
2,3-Dimethyl-2-butene	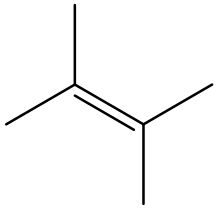	–16.77	86.60	26.69	34.65	42.17	48.77	59.37	67.36	79.86
2,3-Dimethyl-1butene	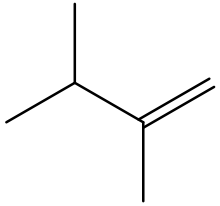	–15.04	88.45	30.68	39.21	46.85	53.32	63.44	70.96	82.73
3-Hexene	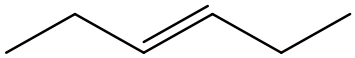	–12.54	91.82	31.36	39.53	46.98	53.35	63.40	70.91	82.71
2,4-Dimethyl-2-pentene	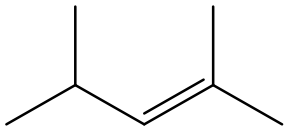	–22.78	85.36	32.14	45.16	55.45	63.31	75.12	83.76	97.21

*Units: enthalpies of formation (kcal mol^{-1}); entropies and heat capacities (cal K^{-1} mol^{-1})

Table 8. Thermochemical values* of allylic radicals calculated by *ab initio* method at selected temperatures.

Name	Structure	$\Delta_f H^\Theta$	S^Θ	C_p						
		298.15 K	298.15 K	300 K	400 K	500 K	600 K	800 K	1000 K	1500 K
Primary Allylic										
Allyl		39.59	61.62	14.94	18.83	22.10	24.76	28.81	31.82	36.63
2-Methylallyl	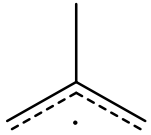	31.84	68.94	19.65	25.05	29.65	33.44	39.31	43.68	50.60
Primary Allylic - Secondary Allylic										
1-Methylallyl		31.85	72.08	19.67	24.75	29.29	33.12	39.11	43.57	50.58
1-Penten-3-yl / 2-Penten-1-yl	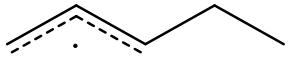	27.01	81.76	25.11	31.77	37.66	42.59	50.24	55.91	64.82
2-Methyl, 1-buten-3-yl / 2-Methyl, 2-buten-1-yl	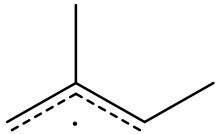	24.55	80.24	24.11	30.72	36.63	41.63	49.47	55.31	64.48

1-Hexen-3-yl / 2-Hexen-1-yl	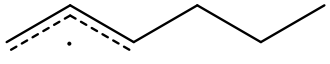	21.85	91.38	30.69	38.80	46.01	52.04	61.38	68.29	79.10
2-Methyl, 1-penten-3-yl/ 2-Methyl, 2-penten-1-yl	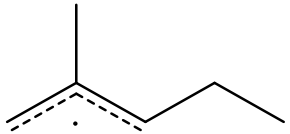	19.70	90.31	29.89	38.12	45.38	51.48	60.96	67.98	78.94
4-Methyl, 1-penten-3-yl / 4-Methyl, 2-penten-1-yl	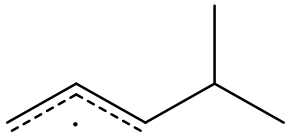	19.98	88.85	31.30	39.38	46.48	52.41	61.58	68.39	79.11
2-Ethyl, 1-buten-3-yl / 2-Ethyl, 2-buten-1-yl	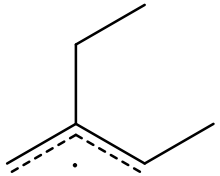	19.70	90.26	30.22	38.18	45.30	51.32	60.78	67.81	78.84
Primary Allylic - Tertiary Allylic										
3-Methyl, 1-buten-3-yl / 2-Methyl, 1-buten-4-yl	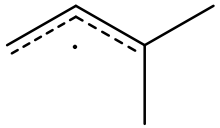	23.04	80.52	24.80	31.13	36.89	41.82	49.62	55.44	64.58
3-Methyl, 1-penten-3-yl / 3-Methyl, 2-penten-1-yl	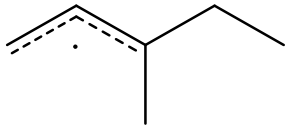	18.35	89.94	30.65	38.45	45.47	51.45	60.85	67.86	78.85
2,3-Dimethyl, 1-buten-3-yl / 2,3-Dimethyl, 2-buten-1-yl	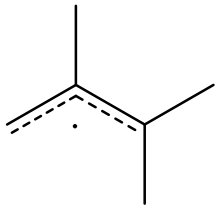	17.16	90.10	30.14	37.80	44.76	50.75	60.25	67.38	78.58

Secondary Allylic										
2-Penten-4-yl		24.29	80.45	24.56	30.76	36.56	41.55	49.45	55.34	64.55
2-Henxen-4-yl / 3-Henxen-2-yl		19.42	90.84	30.02	37.82	44.97	51.07	60.64	67.76	78.85
3-Methyl, 2-penten-4-yl	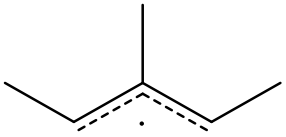	17.70	89.89	29.14	36.86	44.00	50.14	59.88	67.14	78.49
Secondary Allylic - Tertiary Allylic										
2-Methyl, 2-penten-4-yl / 4-Methyl, 2-penten-4-yl		15.59	89.26	29.93	37.31	44.26	50.32	59.99	67.23	78.55
Tertiary Allylic										
2,4-Dimethyl, 2-penten-4-yl		10.74	98.38	35.18	43.77	51.93	59.07	70.53	79.14	92.56

*Units: enthalpies of formation (kcal mol^{-1}); entropies and heat capacities (cal K^{-1} mol^{-1})

Table 9. Thermochemical values* of dienes and super allylic radicals calculated by *ab initio* method at selected temperatures.

Name	Structure	$\Delta_f H^\Theta$	S^Θ	C_p						
		298.15 K	298.15 K	300 K	400 K	500 K	600 K	800 K	1000 K	1500 K
Dienes										
1,3-Pentadiene	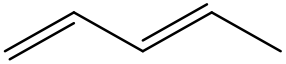	18.73	76.50	24.38	30.85	36.44	40.97	47.77	52.69	60.41
1,4-Pentadiene	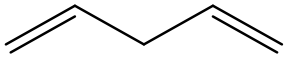	25.44	79.18	23.88	29.71	34.94	39.39	46.37	51.59	59.81
3-Methyl-1,4-pentadiene	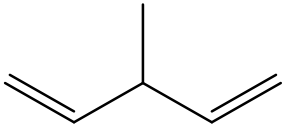	18.97	88.11	29.79	37.15	43.65	49.11	57.64	64.01	74.06
Super allylic radicals										
C_5 super allylic radical	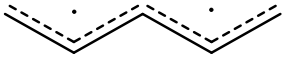	48.05	73.75	22.83	29.00	34.27	38.57	45.08	49.80	57.13
C_6 super allylic radical	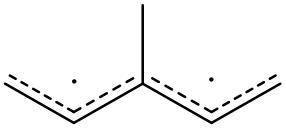	43.00	83.04	28.51	37.17	44.68	50.58	58.67	63.90	71.51

*Units: enthalpies of formation (kcal mol^{-1}); entropies and heat capacities (cal K^{-1} mol^{-1})

Table 10. Thermochemical values* of optimized groups at selected temperatures.

Name	$\Delta_f H^\Theta$	S^Θ	C_p						
	298.15 K	298.15 K	300 K	400 K	500 K	600 K	800 K	1000 K	1500 K
HC Groups									
C/C/H3	–9.59	30.36	6.44	7.94	9.36	10.71	12.58	14.18	16.88
C/CD/H3	–10.10	30.26	6.02	7.64	9.09	10.48	12.54	14.37	16.78
C/C2/H2	–4.90	9.70	5.50	7.03	8.35	9.44	11.12	12.34	14.21
C/C3/H	–2.27	–11.93	4.84	6.40	7.66	8.51	9.92	10.71	–
CD/H2	6.11	27.40	5.23	6.52	7.62	8.54	10.01	11.18	13.06
CD/C/H	8.68	8.05	4.11	4.92	5.82	6.54	7.90	8.63	10.28
CD/C2	11.24	–11.49	2.88	3.59	4.39	4.77	5.86	6.15	7.50
C/C/CD/H2	–5.40	9.79	5.12	6.72	8.11	9.26	11.15	12.61	14.19
C/C2/CD/H	–2.73	–11.88	4.22	6.10	7.45	8.31	9.88	10.90	11.62
Allylic BD Groups									
ALLYLP	87.50	–2.56	–0.50	–0.33	–0.54	–0.92	–1.78	–2.44	–3.55
ALLYLS	84.14	–1.41	–1.23	–1.35	–1.63	–1.92	–2.56	–3.06	–3.85
ALLYLT	83.67	–0.62	–1.35	–2.11	–2.63	–2.93	–3.34	–3.63	–4.15
Super allylic BD Groups									
SUALLYLP	80.68	–3.34	–1.45	–1.66	–1.77	–1.84	–2.07	–2.59	–3.17
SUALLYLS	75.05	–5.56	–0.98	–0.75	–0.94	–1.09	–1.97	–2.29	–3.92
SUALLYLT	74.80	–4.71	–0.39	0.49	0.92	1.40	0.66	–0.22	–3.45

*Units: enthalpies of formation (kcal mol^{-1}); entropies and heat capacities (cal K^{-1} mol^{-1})

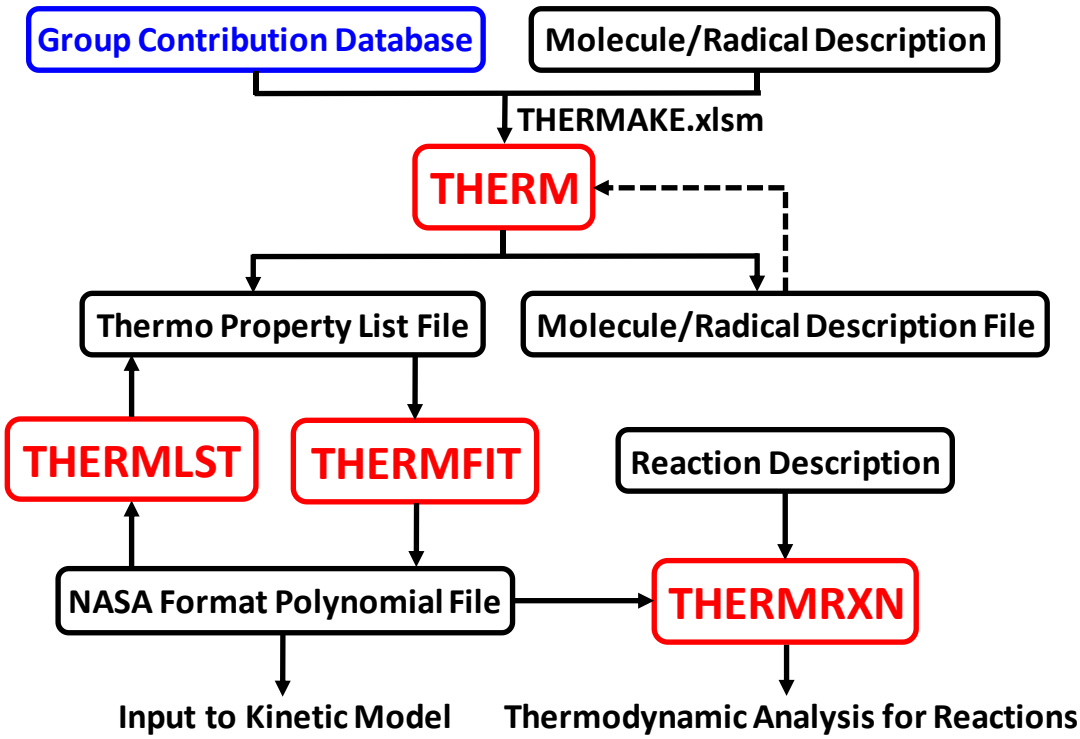

Figure 14. Thermochemistry calculation by GA method using THERM code.

3. Kinetic model development

The detailed 1- and 2-butene kinetic model was developed based on a series of previous work studies, including:

- H_2/O_2 sub-mechanism developed by Kéromnès *et al.* [13].
- C_1–C_2 sub-mechanism (AramcoMech 1.3) developed by Metcalfe *et al.* [14].
- CH_4/DME sub-mechanism developed by Burke *et al.* [15].
- Propene/allene/propyne sub-mechanism developed by Burke *et al.* [16,17].
- Isobutene sub-mechanism developed by Zhou *et al.* [18].

Figure 15 shows the overview of the mechanisms developed in Combustion Chemistry Centre (C^3), the ones highlighted in red were grouped as AramcoMech1.3, and the 1- and 2-butene model was simultaneously released as AramcoMech2.0.

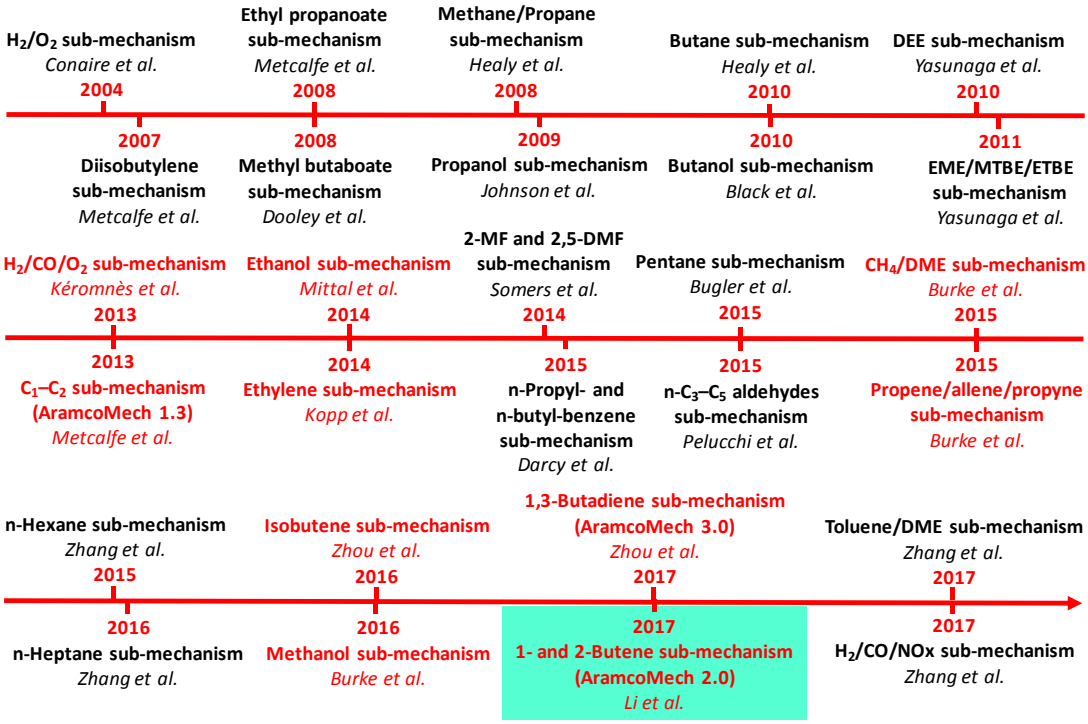

Figure 15. Detailed kinetic model development.

Important reaction classes of unsaturated hydrocarbon oxidation were developed or updated:

- **Fuel Initiation Chemistry**

✓ Ḣ atom addition

✓ ȮH radical abstraction and addition

✓ Molecular O_2 abstraction

- **Allylic Radical Chemistry**

✓ Reactions on $\dot{C}_4H_7$ PES

✓ Molecular O_2 abstraction

✓ $H\dot{O}_2$ radical addition

✓ $\dot{C}H_3$ radical addition

✓ Self-recombination

- **Vinylic Radical Chemistry**

✓ Molecular O_2 abstraction and the subsequent dissociation

- **Alcohol Radical Chemistry**

✓ Waddington mechanism

✓ Typical alkyl radical low temperature chemistry

The model has been validated against large variety of experimental targets:

- IDT in HPST and RCM
- Speciation in JSR
- Speciation in pre-mixed flame
- Speciation in flow reactor
- Flame speed in combustion bomb

These experimental targets cover wide range of conditions:

- Type: oxidation – pyrolysis
- Equivalence ratio: 0.25 – 2.0
- Pressure: 0.004 – 50 atm
- Temperature: 600 – 2000 K

The simulation approaches are explained below in detail.

Ignition delay time simulations

Shock tube ignition delay time simulations were performed assuming a zero-dimensional, constant-volume reactor. The reflected shock pressure (p_5)

and temperature (T_5) were used as the initial simulation pressure and temperature, respectively. For longer IDTs measurements at the lowest temperature conditions, an average dp/dt = 4%, observed in the experiments was included in the simulations. For simulations of ignition delay time results already presented in the literature, the definition of ignition delay time is taken consistent with the particular diagnostic used in the reported experiments. In simulating the rapid compression machine experiments an "adiabatic core expansion" approach was employed, which accounts for the heat loss effect by adopting the volume–time history.

Species simulations

Simulations of species measurements recorded in jet-stirred reactor, flow reactor and pre-mixed flame experiments were performed using the Perfectly Stirred Reactor (PSR), Plug Flow Reactor (PFR) and Premixed Laminar Burner-Stabilized Flame modules in CHEMKIN-PRO. Pressure-distance and temperature-distance profiles from the experiments are used as input files.

Flame speed simulations

Flame speed simulations were performed using the Premixed Laminar Flame-Speed simulator in CHEMKIN-PRO. In order to avoid a high computational cost, a high-temperature version of the model was used to simulate the flame speed, which was created by removing all of the species and reactions involving low temperature oxidation chemistry.

Sensitivity analyses

Sensitivity analyses were carried out in order to identify the key reactions responsible for fuel consumption in the simulation targets.

Flame speed sensitivity analyses were performed using CHEMKIN-PRO's inbuilt utility, which calculates first-order sensitivity coefficients for the predicted mass flow rate, which corresponds to the flame speed.

Ignition delay time "brute force" sensitivity analyses were carried out by increasing and decreasing every reaction rate expression by a factor of two resulting in the effect on the predicted ignition delay time. The sensitivity coefficient is defined as:

$$S = \frac{ln(\tau_+/\tau_-)}{ln(k_+/k_-)} = \frac{ln(\tau_+/\tau_-)}{ln(2.0/0.5)}$$

where τ_+ corresponds to the ignition delay time calculated with the increased rate constant and vice versa. A positive sensitivity coefficient indicates an inhibiting reaction and vice versa.

Flux analyses

Flux analyses were carried out to determine the most important reactions responsible for fuel consumption and the further underlying pathways leading to final products at various temperature regimes. They were performed assuming a constant volume reactor and were taken at the time corresponding to 20% fuel consumption.

Reference

[1] S.S. Goldsborough, S. Hochgreb, G. Vanhove, M.S. Wooldridge, H.J. Curran, C.-J. Sung, Advances in rapid compression machine studies of low- and intermediate-temperature autoignition phenomena, Prog. Energy Combust. Sci. 63 (2017) 1-78.

[2] G. Kalghatgi, H. Babiker, J. Badra, A Simple Method to Predict Knock Using Toluene, N-Heptane and Iso-Octane Blends (TPRF) as Gasoline Surrogates, SAE Int. J. Engines 8 (2015) 505-519.

[3] M. Mehl, W.J. Pitz, C.K. Westbrook, H.J. Curran, Kinetic modeling of gasoline surrogate components and mixtures under engine conditions, Proc. Combust. Inst. 33 (2011) 193-200.

[4] N. Atef, G. Kukkadapu, S.Y. Mohamed, M.A. Rashidi, C. Banyon, M. Mehl, K.A. Heufer, E.F. Nasir, A. Alfazazi, A.K. Das, C.K. Westbrook, W.J. Pitz, T. Lu, A. Farooq, C.-J. Sung, H.J. Curran, S.M. Sarathy, A comprehensive iso-octane combustion model with improved thermochemistry and chemical kinetics, Combust. Flame 178 (2017) 111-134.

[5] J.M. Simmie, K.P. Somers, Benchmarking Compound Methods (CBS-QB3, CBS-APNO, G3, G4, W1BD) against the Active Thermochemical Tables: A Litmus Test for Cost-Effective Molecular Formation Enthalpies. J. Phys. Chem. A 2015, 119, 7235−7246.

[6] K.P. Somers, J.M. Simmie, Benchmarking Compound Methods (CBS-QB3, CBS-APNO, G3, G4, W1BD) against the Active Thermochemical Tables: Formation Enthalpies of Radicals. J. Phys. Chem. A 2015, 119, 8922−8933.

[7] B. Ruscic, Uncertainty Quantification in Thermochemistry, Benchmarking Electronic Structure Computations, and Active Thermochemical Tables. Int. J. Quantum Chem. 2014, 114, 1097−1101.

[8] J.R. Barker, T.L. Nguyen, J.F. Stanton, M.C. Aieta, F. Gabas, T.J.D. Kuma, C.G.L. Li, L.L. Lohr, A. Maranzana, N.F. Ortiz, J.M. Preses, P.J. Stimac, MultiWell-2016 Software Suite; J.R. Barker, University of Michigan: Ann Arbor, Michigan, 2016.

[9] M.J. Pilling, S.H. Robertson, Master Equation Models for Chemical Reactions of Importance in Combustion. Annu. Rev. Phys. Chem. 2003, 54, 245−275.

[10] ANSYS Chemkin-Pro 17.2; ANSYS, Inc.: San Diego, 2016.

[11] S.W. Benson, Thermochemical kinetics: Methods for the Estimation of Thermochemical Data and Rate Parameters, Wiley, (1976).

[12] S.M. Burke, J.M. Simmie, H.J. Curran, Critical Evaluation of Thermochemical Properties of C_1–C_4 Species: Updated Group-Contributions to Estimate Thermochemical Properties, J. Phys. Chem. Ref. Data 44 (2015) 013101.

[13] A. Kéromnès, W.K. Metcalfe, K.A. Heufer, N. Donohoe, A.K. Das, C.-J. Sung, J. Herzler, C. Naumann, P. Griebel, O. Mathieu, M.C. Krejci, E.L. Petersen, W.J. Pitz, H.J. Curran, An experimental and detailed chemical kinetic modeling study of hydrogen and syngas mixture oxidation at elevated pressures, Com- bust. Flame 160 (2013) 995–1011.

[14] W.K. Metcalfe, S.M. Burke, S.S. Ahmed, H.J. Curran, A hierarchical and

comparative kinetic modeling study of C1 −C2 hydrocarbon and oxygenated fuels, Int. J. Chem. Kinet. 45 (2013) 638–675.

[15] U. Burke, K.P. Somers, P. O'Toole, C.M. Zinner, N. Marquet, G. Bourque, E.L. Petersen, W.K. Metcalfe, Z. Serinyel, H.J. Curran, An ignition delay and kinetic modeling study of methane, dimethyl ether, and their mixtures at high pressures, Combust. Flame 162 (2015) 315–330.

[16] S.M. Burke, W. Metcalfe, O. Herbinet, F. Battin-Leclerc, F.M. Haas, J. Santner, F.L. Dryer, H.J. Curran, An experimental and modeling study of propene oxidation. Part 1: Speciation measurements in jet-stirred and flow reactors, Combust. Flame 161 (2014) 2765–2784.

[17] S.M. Burke, U. Burke, R. Mc Donagh, O. Mathieu, I. Osorio, C. Keesee, A. Morones, E.L. Petersen, W. Wang, T.A. DeVerter, M.A. Oehlschlaeger, B. Rhodes, R.K. Hanson, D.F. Davidson, B.W. Weber, C.-J. Sung, J. Santner, Y. Ju, F.M. Haas, F.L. Dryer, E.N. Volkov, E.J.K. Nilsson, A.A. Konnov, M. Alrefae, F. Khaled, A. Farooq, P. Dirrenberger, P.A. Glaude, F. Battin-Leclerc, H.J. Curran, An experimental and modeling study of propene oxidation. Part 2: Ignition delay time and flame speed measurements, Combust. Flame 162 (2015) 296–314.

[18] C.-W. Zhou, Y. Li, E. O'Connor, K.P. Somers, S. Thion, C. Keesee, O. Mathieu, E.L. Petersen, T.A. DeVerter, M.A. Oehlschlaeger, G. Kukkadapu, C.-J. Sung, M. Alrefae, F. Khaled, A. Farooq, P. Dirrenberger, P.A. Glaude, F. Battin-Leclerc, J. Santner, Y. Ju, T. Held, F.M. Haas, F.L. Dryer, H.J. Curran, A comprehensive experimental and modeling study of isobutene oxidation,

Combust. Flame 167 (2016) 353–379.

The oxidation of 2-butene: A high pressure ignition delay, kinetic modeling study and reactivity comparison with isobutene and 1-butene

Author contributions

Yang Li: Obtained all ignition delay time experimental data on high pressure shock tube and rapid compression machine, conducted all modelling work, and wrote the manuscript.

Chong-Wen Zhou: Provided input for the modelling efforts, and reviewed the manuscript.

Kieran P. Somers: Provided input for the modelling efforts, and reviewed the manuscript.

Kuiwen Zhang: Provided input for the modelling efforts, and reviewed the manuscript.

Henry J. Curran: Managed the project throughout, and reviewed manuscript prior to and post the review process.

Brief description of the paper

In this paper, a series of novel ignition delay time (IDT) experiments of trans-2-butene were performed in a high-pressure shock tube (HPST) and in a rapid compression machine (RCM) under conditions of relevance to practical combustors. This is the first IDT data of trans-2-butene taken at engine relevant conditions, and the combination of HPST and RCM results greatly expands the range of data available for the oxidation of trans-2-butene to higher pressures (10–50 atm), lower temperatures (670–1350 K) and a wide range of equivalence ratios (0.5–2.0). A comprehensive chemical kinetic mechanism has simultaneously been developed to describe the combustion of trans-2-butene. It has been validated using the IDT data measured here in addition to a large variety of literature data: jet-stirred reactor (JSR) speciation data, premixed flame speciation data, flow reactor speciation data and laminar flame speed data. Moreover, the reactivity of trans-2-butene is compared to that of the other two isomers, 1-butene and isobutene, and these comparisons are discussed. Important reactions are highlighted via flux and sensitivity analyses and help explain the differences in reactivity among the butene isomers.

The oxidation of 2-butene: A high pressure ignition delay, kinetic modeling study and reactivity comparison with isobutene and 1-butene

Yang Li, Chong-Wen Zhou, Kieran P. Somers, Kuiwen Zhang, Henry J. Curran

Combustion Chemistry Centre, National University of Ireland, Galway, Ireland

Published in: *Proc. Combust. Inst.* 36 (2017) 403–411

Abstract

Butenes are intermediates ubiquitously formed by decomposition and oxidation of larger hydrocarbons (e.g. alkanes) or alcohols present in conventional or reformulated fuels. In this study, a series of novel ignition delay time (IDT) experiments of trans-2-butene were performed in a high-pressure shock tube (HPST) and in a rapid compression machine (RCM) under conditions of relevance to practical combustors. This is the first IDT data of trans-2-butene taken at engine relevant conditions, and the combination of HPST and RCM results greatly expands the range of data available for the oxidation of trans-2-butene to higher pressures (10–50 atm), lower temperatures (670–1350 K) and a wide range of equivalence ratios (0.5–2.0). A comprehensive chemical kinetic mechanism has simultaneously been developed to describe the combustion of trans-2-butene. It has been validated using the IDT data measured here in addition to a large variety of literature data: jet-stirred reactor (JSR) speciation data, premixed flame speciation data, flow reactor speciation data and laminar flame speed data. Moreover, the reactivity of trans-2-butene is compared to that of the other two isomers, 1-butene and

isobutene, and these comparisons are discussed. Important reactions are highlighted via flux and sensitivity analyses and help explain the differences in reactivity among the butene isomers.

1. Introduction

Alkenes are important intermediates formed by the combustion of larger hydrocarbons, e.g., alkanes and alcohols. Moreover, liquefied petroleum gas (LPG) produced during oil refining contains significant amount of olefins, particularly propene and butenes [1], with gasoline fuel containing butenes, pentenes and hexenes in various amounts. Butene is the shortest alkene with structural isomers, namely 2-methylpropene (isobutene), which is a branched isomer, and 1-butene, cis-2-butene (c-2-C_4H_8) and tran-2-butene (t-2-C_4H_8), which are three linear isomers.

Recently, there have been some high-temperature and low-pressure experimental and kinetic modeling studies performed on trans-2-butene combustion, including pyrolysis and oxidation, speciation [2–4], flame speed [2,5], ignition temperature [5], etc., Table S1 of the Supplemental material. However, there is a lack of experimental data available in the literature at engine relevant, high-pressure and low-temperature, conditions. In addition, few studies have been specifically concerned with reactivity effects of the isomeric fuel structures.

In view of the above considerations, we have measured ignition delay times in a high-pressure shock tube (HPST) and in a rapid compression ma-

chine (RCM) under conditions of low temperatures (600–1000 K) and at high pressures (> 10 atm), which are conditions of direct relevance with respect to gasoline, diesel, and low-temperature combustion (LTC) engine technologies. A comprehensive chemical kinetic mechanism to describe trans-2-butene oxidation has been developed including detailed low- and high-temperature reaction pathways specific to unsaturated fuel chemistry, and it is validated against the experimental results. An ignition reactivity comparison of three butene isomers (trans-2-butene, 1-butene and isobutene) has been performed, and a detailed chemical kinetic mechanism (AramcoMech 2.0) has been developed to explain the reactivity differences which account for the isomeric structure effects on ignition/reactivity properties.

2. Experiment

Experiments were performed in the NUI Galway HPST and RCM facilities as described previously [6,7]. All fuels were acquired from Sigma Aldrich at 99.5% purity. Oxygen, nitrogen, argon and carbon dioxide were acquired from BOC Ire- land at high purity (≥ 99.5%).

Table 1 shows that identical experimental conditions at ϕ = 1.0 for cis- and tran-2-butene were selected (p = 10, 30 and 50 atm), and Fig. 1 shows the IDT measurements for these two isomers and they are identical. Therefore, they will be named as 2-butene in the following text. Typical pressure-time traces and original experimental data are shown in the Supplemental material, Fig. S1 and Tables S3–S17.

Table 1 Detailed mixture compositions (%).

	Fuel	O_2	Diluent	φ
	1.72	20.64	77.64	0.5
t-2-C_4H_8	3.38	20.29	76.33	1.0
	6.54	19.63	73.83	2.0
c-2-C_4H_8	3.38	20.29	76.33	1.0

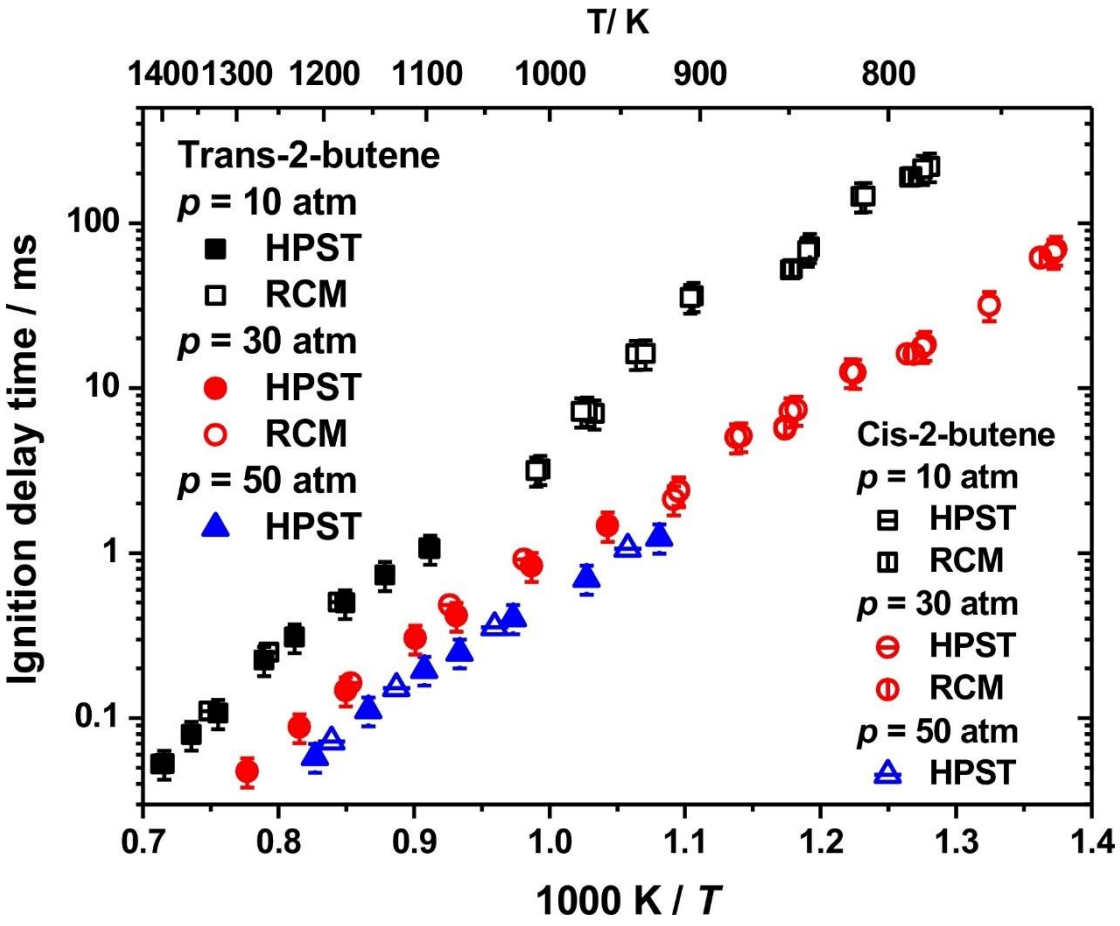

Fig. 1. IDT measurements for trans/cis-2-butene at φ = 1.0 and p = 10, 30, 50 atm.

3. Results and discussions

3.1. Chemical kinetic mechanism development

The current mechanism development is based on the H_2/O_2 sub-mechanism from Kéromnès *et al.* [8], the C_1–C_2 AramcoMech 1.3 sub-mechanism [9] and the propene/allene/propyne sub-mechanism adopted from Burke *et al.* [10,11]. Thermodynamic parameters are estimated using the group additivity method employed by Benson [12] with updated group values by Burke *et al.* [13] as utilized in THERM [14].

During these developments, the mechanism has been validated against numerous experimental conditions and targets. Key reactions for 2-butene oxidation at different temperature and pressure conditions are highlighted using sensitivity and flux analyses for ignition times. The 2-butene combustion chemistry model developed in this work has improved the predictions against a variety of experimental results. The comprehensive kinetic mechanism, thermochemistry, transport files and molecular structure glossary are provided as Supplemental material. In addition, speciation measurements in a JSR [2], laminar flame speeds [2] and ignition temperature measurements [5] shown in the Supplemental material, Figs. S3–S8 also indicates that both isomers (cis- and trans-2-butene) exhibit identical reactivity.

3.2. Important reaction classes highlighted

All simulations, including brute force sensitivity analyses [15] were

performed using CHEMKIN-PRO [16]. Figure 2 highlights the important reactions controlling 2-butene oxidation for a series of representative conditions: ϕ = 1.0, T = 1250 K, 950 K and 700 K, p = 30 atm.

The choice of rate constants for many of the important reactions highlighted above are dis- cussed and explained in Sections 3.4.3 and 3.4.4. The Arrhenius coefficients for all of the important reactions are provided in Table S2 of the Supple- mental material. The performance of the mechanism presented in this study is compared with the performance of selected mechanisms available in the literature [2,3,5], comparisons of which are provided in Figs. S12 and S13 of the Supplemental material. It was found that existing literature mechanisms were unable to simulate our new experimental data at these relatively high-pressure, low-temperature conditions, as they did not include the low-temperature chemistry reactions necessary to describe fuel oxidation in this range.

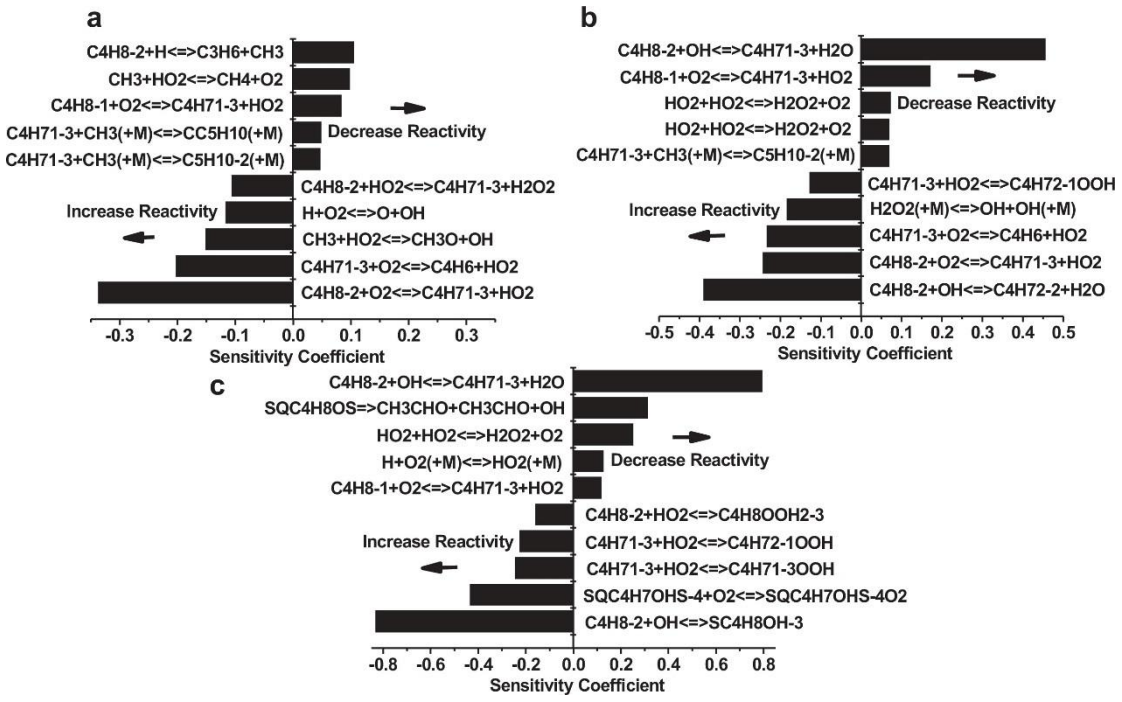

Fig. 2. Sensitivity analyses for 2-butene, ϕ = 1.0, p = 30 atm. (a) T = 1250 K, (b) T = 950 K, (b) T = 700 K.

3.3. Flux analyses

Flux analyses were carried out under the same conditions as the sensitivity analyses: ϕ = 1.0 in 'air' (O_2 : N_2 = 21 : 79), p = 30 atm, T = 700 K, 950 K and 1250 K and at 20% fuel consumed, these being most representative for the experimental conditions studied, Fig. 3. These analyses cover the most common reactions occurring at the various temperature regimes, and for brevity, any reaction paths representing < 5% flux have been excluded.

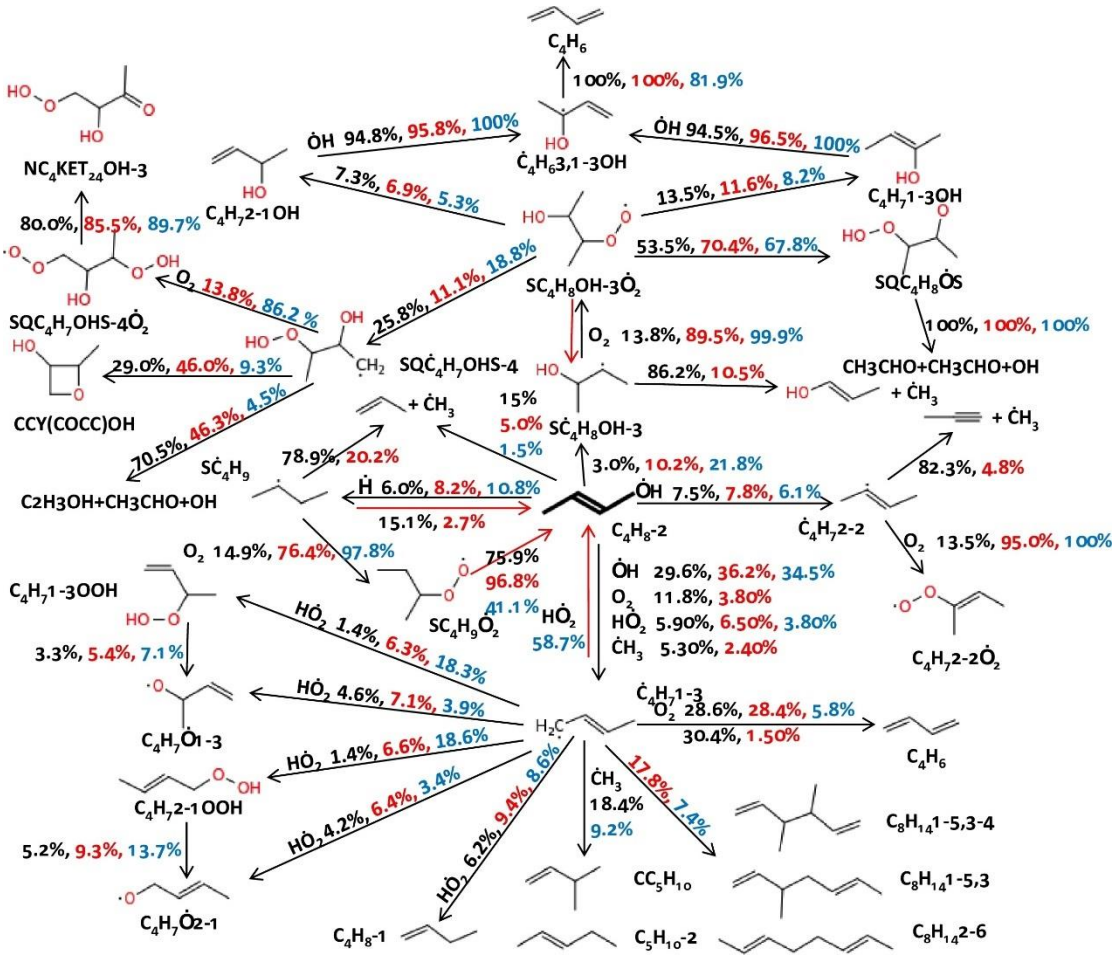

Fig. 3. Flux analysis for 2-butene oxidation at ϕ =1.0, 30 atm and 20% fuel

consumption. Black numbers: 1250 K; red numbers: 950 K; blue numbers: 700 K. (For interpretation of the references to color in this figure legend, the reader is referred to the web version of this article).

3.4. Model validation

Figures 4–6 show both our experimental data and model simulations for all mixtures. Solid symbols represent experimental data obtained in the HPST, open symbols represent experiments taken in the RCM. Solid lines correspond to IDTs calculated via constant-volume, adiabatic simulations. Dashed lines represent IDTs calculated using effective volume histories from the RCM to account for facility effects as discussed previously [15].

3.4.1. Influence of pressure on ignition delay time

Figure 4 shows the effect of pressure on igni- tion times obtained in both the HPST and in the RCM for fuel/air mixtures at ϕ = 0.5, 1.0 and 2.0. The experimental results show that reactivity increases with increasing pressure at all equivalence ratios. As the pressure increases so does the absolute concentration of reactants, resulting in the observed increase in reactivity. The mechanism is able to predict this effect over a wide range of pressures, temperatures and equivalence ratios.

3.4.2. Influence of equivalence ratio on ignition delay time

Ignition delay times were measured at three fuel/air mixture equivalence ratios of 0.5, 1.0 and 2.0 at 10, 30 and 50 atm, Fig. 5. In the range of conditions

studied here, fuel-rich mixtures are fastest to ignite with fuel-lean mixtures being slowest. This is due to an increased concentration of fuel, as the chemistry based on the 2-butanol-3-yl radical, $S\dot{C}_4H_8OH$-3, which is generated from the addition of hydroxyl radical to the C=C double bond, dominates reactivity, as discussed in the section on temperature effects on ignition times. Again, the model shows good agreement across the entire temperature and pressure ranges.

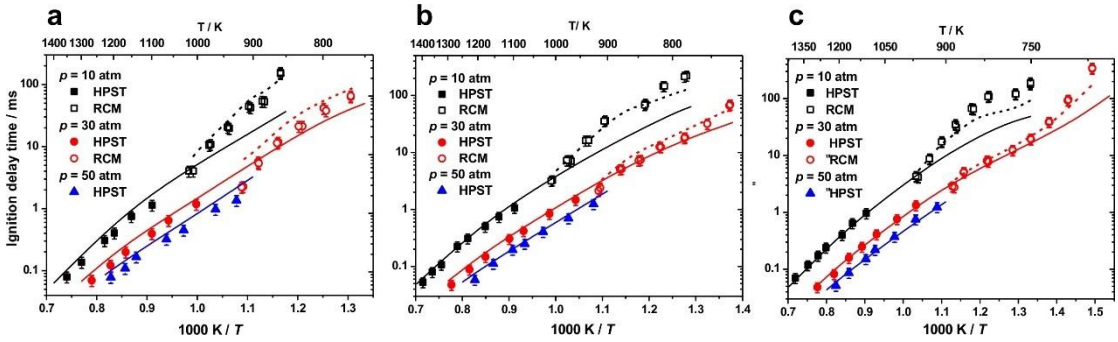

Fig. 4. Influence of pressure on 2-butene IDTs. (a) ϕ =0.5, (b) ϕ =1.0, (c) ϕ =2.0.

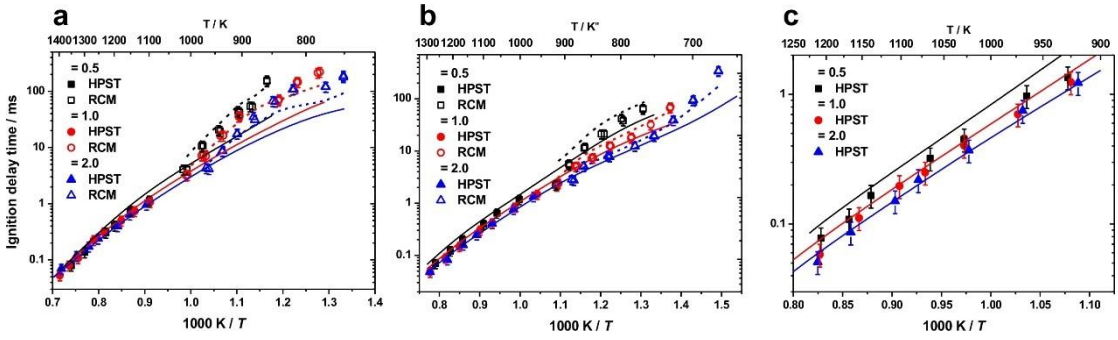

Fig. 5. Influence of equivalence ratio on 2-butene IDTs. (a) p = 10 atm, (b) p = 30 atm, (c) p = 50 atm.

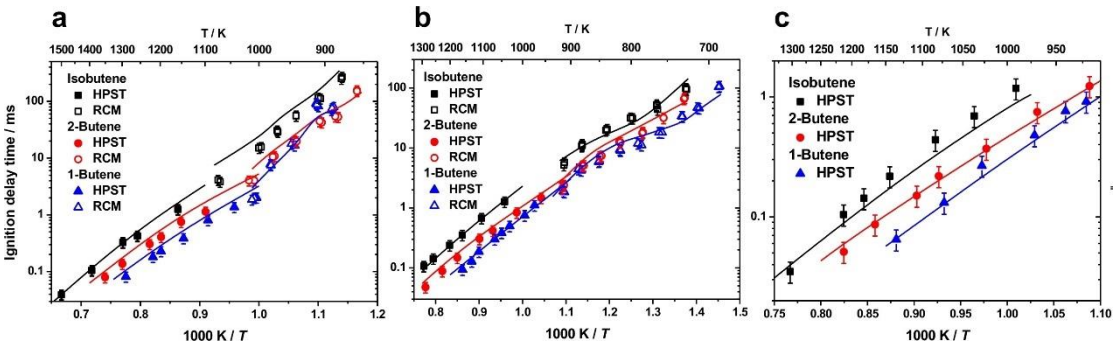

Fig. 6. Influence of isomeric structure on 2-butene IDTs. (a) ϕ = 0.5, p = 10 atm, (b) ϕ = 1.0, p = 30 atm, (c) ϕ = 2.0, p = 50 atm.

At low to intermediate temperatures (~700–1000 K) fuel-rich mixtures ignite faster than fuel-lean ones. This behavior at low temperatures is due to an increase in fuel concentration, as the chemistry of the fuel radicals forms the kinetic bottleneck and has the largest effect on ignition delay times.

The difference in IDTs between the mixtures is much smaller at high temperatures (1000–1300 K) relative to that at low and intermediate temperatures. However, based on the relative slopes of the data, all datasets would appear to converge with increasing temperature, as has been observed and discussed previously [15].

3.4.3. Influence of temperature on ignition delay time

Based on the sensitivity and flux analysis results at high temperature (T = 1250 K) shown in Fig. 2 (a) and Fig. 3 (black numbers), H-atom abstraction by molecular oxygen from allylic carbon atoms which result in the generation of 1-buten-3-yl radicals ($\dot{C}_4H_7$1-3) and their subsequent reaction with molecular oxygen ($\dot{C}_4H_7$1-3 + O_2 ↔ C_4H_6 + $H\dot{O}_2$) are the most promoting reactions. It is

worth nothing that the reaction $\dot{C}_4H_7$1-3 + O_2 ↔ C_4H_6 + $H\dot{O}_2$ is not chemically activated via the sequence: $\dot{R}$ + O_2 ↔ $R\dot{O}_2$ ↔ alkene + $H\dot{O}_2$, instead being a direct abstraction. The well depth of the association reaction $\dot{C}_4H_7$1-3 + O_2 ↔ $C_4H_7$1-3$\dot{O}_2$ has been calculated here to be 19.9 kcal/mol using Gaussian 09 [17] and the composite CBS-QB3 method. The barrier for the subsequent concerted elimination of hydroperoxyl radical is 27.2 kcal/mol, so the reverse reaction to $\dot{C}_4H_7$1-3 + O_2 is kinetically favored over the formation of C_4H_6 + $H\dot{O}_2$. Alternatively, the formation of C_4H_6 + $H\dot{O}_2$ via chemically activated complexes via a direct H-atom abstraction from the primary carbon side is plausible, and the rate constant is adopted from the theoretical work of DeSain *et al.* [18]. The most inhibiting reaction is the chemically activated reaction C_4H_8-2 + $\dot{H}$ ↔ C_3H_6 + $\dot{C}H_3$, the rate constant of which is calculated here on the C_4H_9 potential energy surface at the CCSD(T)/cc-pvXZ//M062X/6-311++G(d,p) level of theory (where X = D, T and Q) and extrapolated to the complete basis set (CBS) limit [19,20]. This reaction results in the consumption of atomic hydrogen, competing with $\dot{H}$ + O_2 ↔ $\ddot{O}$ + $\dot{O}H$, which controls reactivity at high temperatures.

At intermediate temperatures (T = 950 K) the two most sensitive and competitive reactions, Fig. 2 (b), are allylic-hydrogen abstraction reactions, which result in the generation of $\dot{C}_4H_7$1-3 radicals, and hydrogen atom abstractions from secondary vinylic carbon atom which results in the generation of 2-buten-2-yl radicals ($\dot{C}_4H_7$2-2). This promoting/inhibiting effect appears to be linked to the ease-of-oxidation of these respective radicals. As

shown in the flux analysis results in Fig. 3 (red numbers), the $\dot{C}_4H_7$1-3 radical is resistant to oxidation by O_2, and is consumed subsequently by a) chain propagating reactions with hydroperoxyl radical resulting in methyl-allyl-hydroperoxide ($C_4H_7$1-3OOH, $C_4H_7$2-1OOH), methyl-allyl-oxy ($C_4H_7\dot{O}$1-3, $C_4H_7\dot{O}$2-1) and hydroxyl radicals (in a 50:50 ratio); b) chain termination reactions with methyl radicals resulting in the formation of 2-pentene (C_5H_{10}-2) and 3-methyl-1-butene (CC_5H_{10}) (with an assumed 50:50 branching ratio). On the contrary, 2-buten-2-yl radicals ($\dot{C}_4H_7$2-2) react with molecular oxygen producing atomic oxygen, methyl ketene and methyl radicals in a chain-branching sequence.

At lower temperatures (T = 700 K) shown in Fig. 2 (c), again, the most inhibiting reaction is hydrogen abstraction reactions by hydroxyl radicals from allylic carbon atom (C_4H_8 -1 + $\dot{O}H$ ↔ $\dot{C}_4H_7$1-3 + H_2O), because it results in the consumption of a reactive hydroxyl radical and the formation of a resonantly stabilized 1-butenyl-3-yl radical ($\dot{C}_4H_7$1-3) radical. The addition of hydroxyl radical to C=C double bond forming $S\dot{C}_4H_8OH$-3 radical pronouncedly promotes reactivity. Based on flux analysis results in Fig. 3 (blue numbers), the reason being that: chain branching can subsequently occur from the addition of O_2 to the 2-butene + $\dot{O}H$ adduct, isomerization and second O_2 addition, with the decomposition of the nascent ketohydroperoxide ultimately promoting reactivity via generation of $\dot{O}H$ radicals.

It is also worth noting that, at all temperatures presented in Fig. 2, the reaction C_4H_8-1 + O_2 ↔ $\dot{C}_4H_7$1-3 + $H\dot{O}_2$ always ranks among the top five most

sensitive reactions inhibiting reactivity. As we can see from flux analysis results in Fig. 3, this is because the reaction between $\dot{C}_4H_7$1-3 and $H\dot{O}_2$ radicals results in the formation of two stable species. Note also that the $\dot{C}_4H_7$1-3 radical is generated in the oxidation of 1-butene, and thus both the 1- and 2-butene oxidation mechanisms are intrinsically linked and need to be generated simultaneously.

3.4.4. Influence of isomeric structure on ignition delay time

The effect of isomeric structure on ignition de- lay times for three butene isomers (*iso*-, 1-, and 2-butene) are compared, Fig. 6. Representative conditions have been selected: (a) ϕ = 0.5, p = 10 atm, (b) ϕ = 1.0, p = 30 atm, (c) ϕ = 2.0, p = 50 atm. It is shown that 1-butene is the fastest to ignite, followed by 2-butene, with isobutene being the slowest at all equivalence ratios and pressures and throughout the entire temperature range.

In order to explain the differences in reactivity due to isomeric structure, sensitivity analyses for 1-, 2-butene and isobutene oxidation have been carried out at identical conditions: ϕ = 1.0, T = 1250 K, 950 K and 700 K, p = 30 atm, shown in Fig. S2 of the Supplemental material. H-atom abstraction reactions by hydroxyl radicals from an allylic carbon atom inhibit reactivity for all three isomers at all temperatures. The rate constants of C_4H_8-1 + $\dot{O}H$ and C_4H_8-2 + $\dot{O}H$ are adopted from the experimental work and theoretical study of Vasu *et al.* [21] at the CCSD(T)/6- 311 ++ G(d,p)//QCISD/6-31G(d)) level of theory, while the rate constant of iC_4H_8 + OH is calculated at the QCISD(T)/CBS//M062X/6-311++G(d,p) level of theory as part of this study.

Figure 7 (a) shows a comparison of these three rates constants at high temperatures (1000–2000 K). The rate constant of iC_4H_8 + ȮH is faster than that of C_4H_8-2 + ȮH, with C_4H_8-1 + ȮH being the slowest, which means the reactivity of isobutene is inhibited the most by this reaction, followed by 2-butene and 1-butene.

At high temperatures (> 1000 K), the most promoting reactions are H-atom abstraction reactions by molecular oxygen from allylic carbon atom which results in the generation of methyl-allyl radicals (iC_4H_7 and $\dot{C}_4H_7$1-3). The rate constants of iC_4H_8 + O_2 is adopted from Yasunaga *et al.* [22], while the rate constants of C_4H_8-1 + O_2 and C_4H_8-2 + O_2 are determined by the Evans-Polanyi relationship developed by Somers *et al.* [23]. Figure 7 (b) shows a comparison of these three rates constants, with the rates of C_4H_8-1 + O_2 and C_4H_8-2 + O_2 being faster than that of iC_4H_8 + O_2, which means the reactivity of 1-butene and 2-butene are promoted more than isobutene. Moreover, the subsequent reaction $\dot{C}_4H_7$1-3 + O_2 ↔ C_4H_6 + $H\dot{O}_2$ promotes reactivity more for both 1-butene and 2-butene but this reaction doesn't exist for isobutene.

The most inhibiting reactions for 1- and 2-butene oxidation are H atom addition reactions to the fuel on the same potential energy surface. Addition to the terminal carbon atom on 1-butene and non-terminal addition to 2-butene both generate propene and a methyl radical with rate constant comparisons shown in Fig. 7 (c). The rate of addition to 2-butene is faster than for 1-butene at high temperatures, inhibiting the reactivity of 2-butene more than 1-butene. Moreover, addition to the non- terminal carbon in 1-butene results in the

formation of C_2H_4 + $\dot{C}_2H_5$, which ultimately generates two vinyl radicals and a hydrogen atom, promoting reactivity.

At intermediate temperatures (~800–1000 K), unlike isobutene, both 1- and 2-butene can undergo H-atom abstraction by hydroxyl radicals from secondary vinylic carbon atom resulting in the generation of 1-buten-2-yl ($\dot{C}_4H_7$1-2) and 2-buten-2-yl ($\dot{C}_4H_7$2-2) radicals, and their subsequent reactions with molecular oxygen generates alkenylperoxy radicals, $C_4H_7$1-2$\dot{O}_2$ and $C_4H_7$2-2$\dot{O}_2$, followed by O–O bond fission resulting in Ö atoms, a sequence which pronouncedly promotes reactivity. However, the β-scission of 2-butanone-3-yl ($C_4H_7\dot{O}$2-2) radical, generated via O–O bond fission of a $C_4H_7$2-2$\dot{O}_2$ radical, generates methyl radicals which can recombine with $\dot{C}_4H_7$1-3 radicals to produce 2-pentene and 3-methyl-1-butene, which slightly inhibits reactivity.

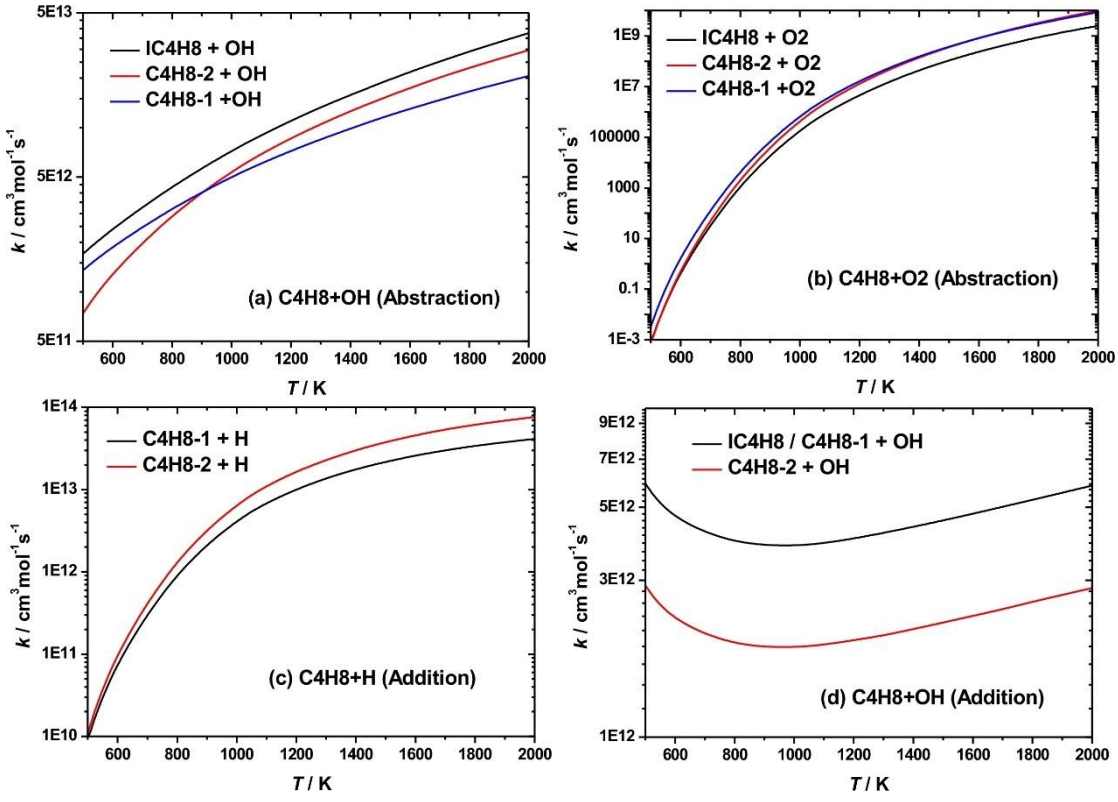

Fig. 7. Rate constants comparison for isobutene, 2-butene and 1-butene mechanism.

At low temperatures (< 800 K), the promoting reactions for the three fuels changes from H-atom abstraction to hydroxyl radical addition to the C=C double bond. Rate constants are compared in Fig. 7 (d), and are estimated by analogy to propene plus OH radical as calculated by Zádor *et al.* [24] (with 75:25 branching ratio for terminal verses central addition for both isobutene and 1-butene [25]), hence the total rate constant of the reaction C_4H_8-2 + ȮH is 2.5 times slower than that of isobutene and 1-butene. Furthermore, the butanol-alkyl (SC_4H_8OH-3, PC_4H_8OH-2, SC_4H_8OH-1, IC_4H_8OH-IT and IC_4H_8OH-TI) radicals generated can react with molecular oxygen followed by an isomerization reaction to form hydroperoxyl-alkyl radicals (QOOH). However, because of the isomeric structural difference between 1-butene and isobutene, 1-butene oxidation facilitates more chain branching reactions than isobutene leading to more rapid chain branching in 1-butene compared to isobutene.

4. Conclusions

This work represents the first ignition delay study of 2-butene oxidation at elevated pressures in a HPST and in a RCM over a wide range of pressures, temperatures and equivalence ratios. The results presented greatly expand the ignition delay time database available for mechanism validation for 2-butene oxidation. Further, the ignition reactivity of the three butene isomers (1-, 2- and

isobutene) has been compared under the same conditions.

It was found that an increase in reflected shock pressure resulted in shorter ignition delay times (higher reactivity) for all equivalence ratios investigated, which is typical of the influence of pressure on fuel reactivity. The effect of equivalence ratio on ignition delay times depended on the temperature of the experiment, where all mixtures had similar reactivity at higher temperatures and fuel-rich mixtures were most reactive at lower temperatures. As to the effect of isomeric structure on ignition delay times for three butene isomers, 1-butene is the fastest to ignite, followed by 2-butene, with isobutene being the slowest.

A detailed chemical kinetic mechanism has been developed to describe the combustion of 2-butene, it includes comprehensive low- and high- temperature reaction pathways specific to unsaturated fuel chemistry. Important reactions were identified through sensitivity and flux analyses. Rate constants have been adopted from experimental and theoretical studies where possible. However, for reactions where the literature is lacking, rate constants were calculated from ab initio methods or estimated. The mechanism is validated against our new experiments and relevant literature data. The current mechanism captures well most of the experimental results of ignition delay times, as well as the flame speeds, speciation results from premixed flame and flow reactor results from the literature.

This is also the first study that explains the reactivity difference between the three butene isomers using detailed chemistry at these relatively

high-pressure, low-temperature conditions. Together with recent studies on ethylene [26,27], propene [10,11], isobutene [28] and 2-methyl-2-butene [29], a consistent and detailed picture of low-temperature vinylic and allylic hydrocarbon combustion kinetics is starting to emerge to supplement our recently re-developed rate rules for n- and *iso*-alkanes [30]. Future research efforts will be focused on: a) reaction class development for unsaturated hydrocarbons, and b) rate rules for important reaction classes.

Acknowledgments

The authors thank the entire group members at Combustion Chemistry Centre for helpful discussions. This work at NUI Galway was supported by Saudi Aramco under the FUELCOM program.

References

[1] K. Morganti PhD thesis, A Study of the Knock Limits of Liquefied Petroleum Gas (LPG) in Spark-Ignition Engines, The University of Melbourne, 2003.

[2] Y. Fenard, P. Dagaut, G. Dayma, F. Halter, F. Foucher, Proc. Combust. Inst. 35 (2015) 317–324.

[3] M. Schenk, L. Leon, K. Moshammer, et al., Com- bust. Flame 160 (2013) 487–503.

[4] Y. Zhang, J. Cai, L. Zhao, et al., Combust. Flame 159 (2012) 905–917.

[5] P. Zhao, W. Yuan, H. Sun, et al., 35, 2015, pp. 309–316.

[6] D. Darcy, C.J. Tobin, K. Yasunaga, et al., Combust. Flame 159 (7) (2012) 2219–2232.

[7] D. Darcy, H. Nakamura, C.J. Tobin, et al., Combust. Flame 161 (1) (2014) 65–74.

[8] A. Kéromnès, W.K. Metcalfe, K.A. Heufer, et al., Combust. Flame 160 (6) (2013) 995–1011.

[9] W.K. Metcalfe, S.M. Burke, S.S. Ahmed, H.J. Curran, Int. J. Chem. Kinet. 45 (10) (2013) 638–675.

[10] S.M. Burke, U. Burke, R. Mc Donagh, et al., Combust. Flame 162 (2) (2015) 296–314.

[11] S.M. Burke, W. Metcalfe, O. Herbinet, et al., Com- bust. Flame 161 (11) (2014) 2765–2784.

[12] S.W. Benson, Thermochemical Kinetics, Wiley, 1976.

[13] S.M. Burke, J.M. Simmie, H.J. Curran, J. Phys. Chem. Ref. Data 44 (1) (2015) 013101.

[14] E.R. Ritter, J.W. Bozzelli, Int. J. Chem. Kinet. 23 (9) (1991) 767–778.

[15] W.K. Metcalfe, S.M. Burke, S.S. Ahmed, H.J. Curran, Int. J. Chem. Kinet. 45 (2013) 638–675.

[16] CHEMKIN-PRO 15131, Reaction Design, San Diego, 2010

[17] M.J. Frisch, G.W. Trucks, H.B. Schlegel, et al., Gaussian 09, revision A.02; Gaussian, Inc.: Wallingford CT, 2009.

[18] J.D. DeSain, S.J. Klippenstein, J.A. Miller, C.A. Taatjes, J. Phys. Chem. A 107 (2003) 4415–4427.

[19] J.M.L. Martin, Chem. Phys. Lett. 259 (5-6) (1996) 669–678.

[20] D. Feller, D.A. Dixon, J. Chem. Phys. 115 (8) (2001) 3484–3496.

[21] S.S. Vasu, L.K. Huynh, D.F. Davidson, R.K. Han- son, D.M. Golden, J. Phys. Chem. A 115 (2011) 2549–2556.

[22] K. Yasunaga, Y. Kuraguchi, R. Ikeuchi, et al., Proc. Combust. Inst. 32 (2009) 453–460.

[23] K.P. Somers, J.M. Simmie, F. Gillespie, et al., Com- bust. Flame 160 (2013) 2291–2318.

[24] J. Zádor, A.W. Jasper, J.A. Miller, Phys. Chem. Chem. Phys. 11 (46) (2009) 11040–11053.

[25] J.C Loison, J. Daranlot, A. Bergeat, F. Caralp, R. Mereau, K.M. Hickson, J. Phys. Chem. A 114 (2010) 13326–13336.

[26] M.M. Kopp, N.S. Donato, E.L. Petersen, W.K. Metcalfe, S.M. Burke, H.J. Curran, J. Prop. Power 30 (3) (2014) 799–811.

[27] M.M. Kopp, N.S. Donato, E.L. Petersen, W.K. Metcalfe, S.M. Burke, H.J. Curran, J. Prop. Power 30 (3) (2014) 790–798.

[28] C. Zhou, Y. Li, E. O'Connor, et al., Combust. Flame 167 (2016) 353–379.

[29] C.K. Westbrook, W.J. Pitz, M. Mehl, et al., J. Phys. Chem. A 119 (28) (2015) 7462–7480.

[30] J. Bugler, K.P. Somers, E.J. Silke, H.J. Curran, J. Phys. Chem. A 119 (2015) 7510–7527.

An extensive experimental and modeling study of 1-butene oxidation

Author contributions

Yang Li: Obtained all ignition delay time experimental data on high pressure shock tube and rapid compression machine, conducted all modelling work, and wrote the manuscript.

Chong-Wen Zhou: Provided input for modelling efforts, and reviewed the manuscript.

Henry J. Curran: Managed the project throughout, and reviewed manuscript prior to and post the review process.

Brief description of the paper

In this paper, a series of ignition delay time (IDT) experiments of 1-butene were performed in a high-pressure shock tube (HPST) and in a rapid compression machine (RCM) under conditions of relevance to practical combustors. This is the first 1-butene IDT data taken at engine relevant conditions, and the combination of HPST and RCM results greatly expands the range of data available for the oxidation of 1-butene to higher pressures (10–50 atm), lower temperatures (670–1350 K) and to a wide range of equivalence ratios (0.5–2.0). A comprehensive chemical kinetic mechanism to describe the combustion of 1-butene has simultaneously been applied. It has been validated using the IDT data measured here in addition to a large variety of literature data: IDTs, speciation data from jet-stirred reactor (JSR), premixed flame, and flow reactor, and laminar flame speed data. Important reactions have been identified via flux and sensitivity analyses including: (a) H-atom abstraction from 1-butene by hydroxyl radicals and molecular oxygen from different carbon sites; (b) addition reactions, including hydrogen atom and hydroxyl radical addition to 1-butene; (c) allylic radical chemistry, including the addition reactions with methyl radical, hydroperoxy radical and self-recombination; (d) vinylic radical chemistry, including the addition reaction with molecular oxygen; (e) alcohol radical chemistry, including the Waddington type propagating reaction pathways and alkyl radical low-temperature branching chemical pathways.

An extensive experimental and modeling study of 1-butene oxidation

Yang Li, Chong-Wen Zhou, Henry J. Curran

Combustion Chemistry Centre, National University of Ireland, Galway, Ireland

Published in: *Combust. Flame* 181 (2017) 198–213

Abstract

In this study, a series of ignition delay time (IDT) experiments of 1-butene were performed in a high-pressure shock tube (HPST) and in a rapid compression machine (RCM) under conditions of relevance to practical combustors. This is the first 1-butene IDT data taken at engine relevant conditions, and the combination of HPST and RCM results greatly expands the range of data available for the oxidation of 1-butene to higher pressures (10–50 atm), lower temperatures (670–1350 K) and to a wide range of equivalence ratios (0.5–2.0).

A comprehensive chemical kinetic mechanism to describe the combustion of 1-butene has simultaneously been applied. It has been validated using the IDT data measured here in addition to a large variety of literature data: IDTs, speciation data from jet-stirred reactor (JSR), premixed flame, and flow reactor, and laminar flame speed data. Important reactions have been identified via flux and sensitivity analyses including: (a) H-atom abstraction from 1-butene by hydroxyl radicals and molecular oxygen from different carbon sites; (b) addition reactions, including hydrogen atom and hydroxyl radical addition to 1-butene; (c) allylic radical chemistry, including the addition reactions with

methyl radical, hydroperoxy radical and self-recombination; (d) vinylic radical chemistry, including the addition reaction with molecular oxygen; (e) alcohol radical chemistry, including the Waddington type propagating reaction pathways and alkyl radical low-temperature branching chemical pathways.

1. Introduction

Alkenes are important intermediates formed during the com- bustion of larger hydrocarbons and alcohols. Moreover, liquefied petroleum gas (LPG) produced during oil refining contains a significant quantity of alkenes, particularly propene and butenes [1], with gasoline fuel containing butenes, pentenes, and hexenes in various amounts. Butene is the shortest alkene with structural isomers including, isobutene, 1-butene, cis-2-butene, and trans-2-butene. 1-butene is the smallest unsaturated hydrocarbon having a secondary allylic carbon group and a primary carbon group which exhibit both alkane- and alkene-type chemistry.

There have been some high-temperature and low-pressure experimental and kinetic modeling studies of 1-butene consumption, including pyrolysis and oxidation. The types of reactors and conditions studied are shown in Table 1.

Most recently, Zhao *et al.* [9] developed a high temperature kinetic model for the four butene isomers (1-, trans-2-, cis-2-, and isobutene) validated using laminar flame speeds and non-premixed counter-flow ignition temperatures at pressures of 2, 5, and 10 atm. Furthermore, the critical reaction paths for butene isomer oxidation during the induction period for ignition, particularly the allylic H-atom abstractions by ȮH radical, were systematically updated with

rate coefficients from ab-initio calculations and kinetic theory.

Table 1 List of experimental literature data for 1-butene pyrolysis and oxidation.

No.	Reactor	φ	Diluent / %	T / K	p / atm	References
1	Shock Tube	0.5, 1.0, 2.0	87.0–96.0 (Ar)	1000–1700	1.2, 4.0, 16.0	Pan *et al.* [2]
2	Shock Tube	0.5, 1.0, 2.0	87.0–96.0 (Ar)	1200–1670	6.6–8.9	Heyberger *et al.* [3]
3	Combustion Vessel	0.7–1.4	75.31–77.11	–	1	Fenard *et al.* [4]
4	Jet-Stirred Reactor	0.25, 0.5, 1.0, 2.0	97.5–99.6	900–1440	1	Fenard *et al.* [4]
5	Jet-Stirred Reactor	0.15, 1.0, 4.0	90.0–93.85	900–1200	1.0–10.0	Chakir *et al.* [5]
6	Flow Reactor	∞	96.0 (Ar)	900–1900	0.004–0.016	Zhang *et al.* [6]
7	Flame Burner	1.7	25.0 (Ar)	2204	0.04	Schenk *et al.* [7]
8	Counterflow	0.7–1.7	74.6–77.1	2329	1.0, 2.0, 5.0, 10	Davis *et al.* [8]
9	Counterflow	–	–	1000–1300	1.0–5.0	Zhao *et al.* [9]

Schenk *et al.* [7] studied premixed, low-pressure (40 mbar), flat, argon-diluted (25%) flames of three of the butene isomers (1-, trans-2-, and isobutene) under fuel-rich (ϕ = 1.7) conditions. This was the first detailed flame study of the butene isomers performed under fuel-rich conditions. The isomer-specific species information and the quantitative mole fraction profiles of more than 30 stable and radical species were measured using a newly developed analytical combination of high-resolution in-situ molecular-beam mass spectrometry (MBMS) and in-situ gas chromatography (GC), and it was

used to validate and improve the subset of C 4 kinetics in a general hydrocarbon oxidation mechanism based on the work of Hoyermann *et al.* [10].

Zhang *et al.* [6] measured product and intermediate concentrations during the pyrolysis of 1-, 2-, and isobutene using synchrotron vacuum ultraviolet photoionization mass spectrometry (SVUV-PIMS) with the molecular-beam sampling technique in the temperature range 900–1900 K at a pressure of 3 Torr. Based on the experimental results, a kinetic model consisting of 76 species and 232 reactions was also developed to simulate the measured species mole fractions.

Fenard *et al.* [4] conducted experiments for the oxidation of 1- and cis-2-butene in a jet-stirred reactor and in a combustion vessel. The concentration profiles of stable species were measured in the temperature range 900−1440 K, at atmospheric pressure, for different equivalence ratios ($0.25 \leq \phi \leq 2$). Laminar burning velocities were determined at $p = 1$ atm, at unburned gas temperatures in the range of 300–450 K, and at equivalence ratios in the range 0.8–1.4. A chemical kinetic mechanism based on a previously pro- posed scheme for the oxidation of hydrocarbons was also used to reproduce their experimental data (201 species involved in 1787 reactions).

Pan *et al.* [2] measured IDTs of 1-butene oxidation at pressures of 1.2, 4.0, and 16.0 atm, in the temperature range 1000–1700 K, and at equivalence ratios of 0.5, 1.0, and 2.0 in 87–96% argon diluent. Three widely used models, NUIG AramcoMech1.3 [11], USC Mech 2.0 [12] and the LLNL C_4 [13] model were used to simulate the measured ignition delay times. It was found that none of

the models could satisfactorily reproduce the experimental data, especially at lower temperatures.

Chakir *et al.* [5] measured the concentrations of molecular species produced from the oxidation of 1-butene in a jet-stirred reactor in the temperature range 900–1200 K, at pressures extending from 1 to 10 atm, for a wide range of fuel-oxygen equivalence ratios (0.15–4.0). A chemical kinetic reaction mechanism developed previously [14, 15] was used to simulate the experimental data.

Heyberger *et al.* [3] automatically generated a kinetic model for 1-butene using EXGAS, and it was used to simulate two sets of experimental results: species measurements in a jet-stirred reactor between 900 and 1200 K [5], and IDT measurements in a ST at temperatures in the range 1200–1670 K, at pressures from 6.6 to 8.9 atm, equivalence ratios from 0.5 to 2.0, using argon as bath gas.

There is still a lack of experimental data for 1-butene oxidation available in the literature at engine relevant, high-pressure, and low-temperature conditions. In addition, based on previous work on propene [16, 17], isobutene [18], and 2-butene [19], a comprehensive kinetic model for 1-butene oxidation will extend our understanding on alkene combustion chemistry.

In view of the above considerations, we have measured ignition delay times in a high-pressure shock tube (HPST) and in a rapid compression machine (RCM) at low temperatures (600–1000 K) and high pressures (> 10 atm), which are of direct relevance to gasoline, diesel, and low-temperature

combustion (LTC) engine technologies. In this work a comprehensive chemical kinetic mechanism to describe 1-butene oxidation has been developed, including detailed low-, intermediate- and high-temperature reaction pathways specific to unsaturated fuel chemistry. The model has been validated against a wide range of ignition de- lay time measurements from this work, the speciation and flame speed results from jet-stirred reactor, flow reactor, flame in the literature.

2. Experimental methods

IDT measurements for 1-butene were performed in a HPST and in an RCM located at NUI Galway (NUIG). Table 2 provides the detailed experimental conditions investigated in the present study. All fuels were acquired from Sigma Aldrich at 99.5% purity. Oxygen, nitrogen, argon and carbon dioxide were acquired from BOC Ireland at high purity (≥ 99.5%).

Table 2 % molar composition of 1-butene mixtures.

	Fuel	O_2	Diluent	φ	p / atm
1-butene	1.72	20.64	77.64	0.5	10, 30, 50
	3.38	20.29	76.33	1.0	10, 30, 50
	6.54	19.63	73.83	2.0	10, 30, 50

2.1. NUIG HPST

The HPST at NUIG was used to measure IDT for 1-butene at intermediate to high temperatures (~900–1300 K) at 10, 30, and 50 atm. The tube has an

inner diameter of 63.5 mm, a 3 m driver section, a 5.7 m driven section, and a 3 cm double diaphragm section that is located between the driver and driven sections. Two pre-scored aluminum diaphragms are placed in the double-diaphragm section, and used to initiate the incident shock wave.

As to the diagnostic system, six PCB 113B24 pressure transducers are mounted in the sidewall of tube at known positions. The shock velocity at the end-wall is calculated by linearly extrapolating the five velocities to the end-wall. A Kistler 603B pressure transducer is mounted in the end-wall to measure the pressure versus time history behind the reflected shock wave. The IDT is de- fined as the interval between the rise in pressure due to the arrival of the shock wave at the end-wall and the rapid rise in pressure due to the ignition event, as shown in Fig. 1.

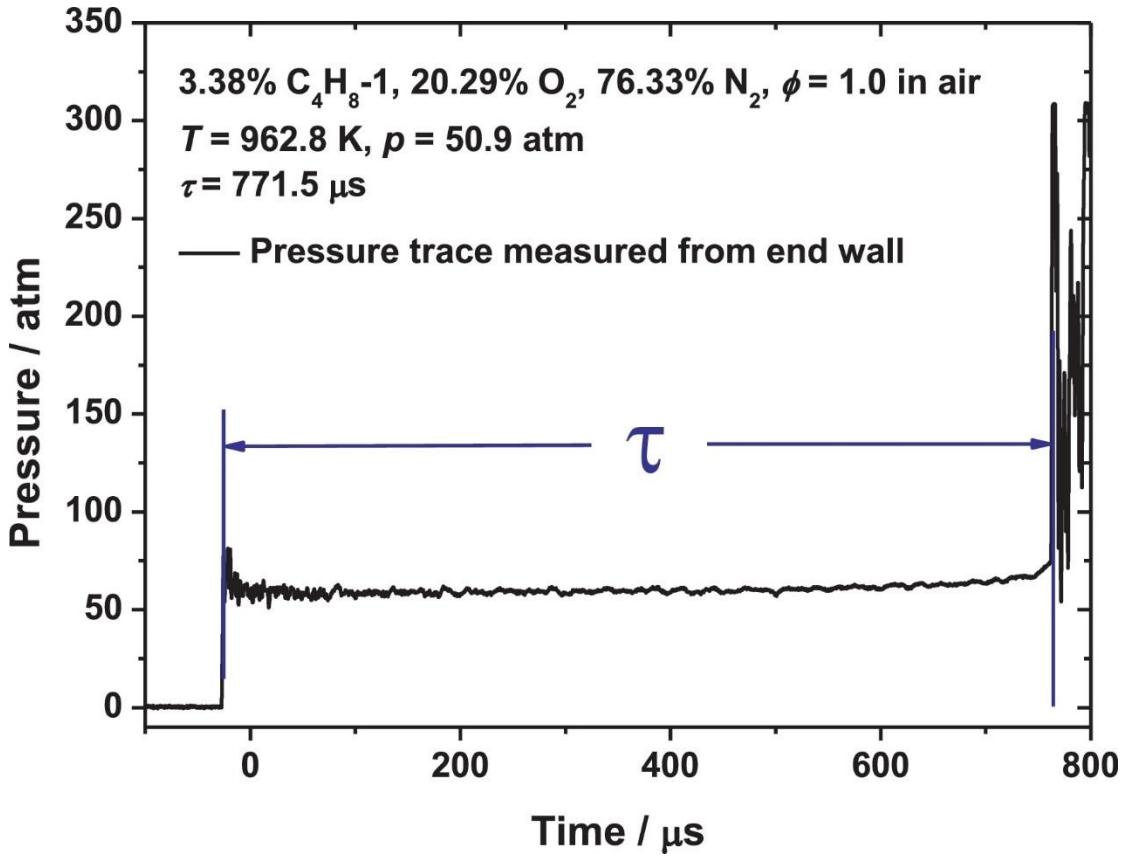

Fig. 1. A typical pressure-time history measured in the HPST.

Post-shock conditions were determined using the normal shock relations as employed by Gaseq [20] utilizing measurements of incident shock velocity, initial temperature and pressure, and the thermodynamic properties of the shock-heated fuel/oxidizer mixtures. More detailed information can be found in a previous paper [21].

As to the uncertainty quantification of IDT measurements in our HPST, it has been reported by Petersen *et al.* [22] that the uncertainty of the reflected shock temperature is mainly attributable to the uncertainty of the incident shock velocity, which is determined by the uncertainties in the precise positions of the pressure trans- duces and the shock pass time recorded by the signal relayed to the oscilloscope from the pressure transducers. We have adopted a standard rt-sum-squares (RSS) method used by Petersen *et al.* [22],

$$T_5 = \frac{T_1[2(\gamma-1)M^2+(3-\gamma)][(3\gamma-1)M^2-2(\gamma-1)]}{(\gamma+1)^2M^2} = AM^2 + B + CM^{-2}$$

$$\mathrm{M} = \frac{V_s}{\sqrt{\gamma R T_1}}$$

$$\delta V_s = \sqrt{\left(\frac{1}{\Delta t}\delta_{\Delta z}\right)^2 + \left(\frac{-\Delta z}{\Delta t^2}\delta_{\Delta t}\right)^2}$$

$$\delta T_5 = \frac{\partial T_5}{\partial M}\delta M = (2AM - 2CM^{-3})\frac{\delta V_s}{\sqrt{\gamma_1 R T_1}}$$

where T_5 is the reflected shock temperature (K); T_1 is the initial temperature (K); γ is the adiabatic exponent; V s is the velocity of the incident shock wave (ms^{-1}); and R is the gas constant. The uncertainty of the time intervals recorded

using the six PCB 113B24 pressure transducers in our HPST and relayed to the TiePie Handyscope HS4 oscilloscope were estimated to be 1 μs, which corresponds to the sampling rate of the pressure transduce and the oscilloscope. The uncertainty in distance between the pressure transducers is estimated to be ± 0.1 mm that stems mainly from the shock front thickness and the diameter of the sensing area of the pressure transducers. Using the above equations, the largest uncertainty in the reflected temperature is estimated to be 20 K. However, this uncertainty of the reflected shock temperature leads to a 20% uncertainty in measured ignition times, τ_{ign}, based on an Arrhenius-type correlation using the RSS method, a detailed description of which can be found in a previous study by Zhang *et al.* [23].

2.2. NUIG RCM

A clone of the original NUIG twin-opposed piston RCM was used in this study, and has been described previously [24]. The twin-opposed piston results in a short compression time of approximately 16 ms while the use of creviced piston heads leads to a homogeneous post-compression temperature distribution in the combustion chamber [25]. These piston heads achieve an approximate compression ratio of 12.5:1.

Different com pressed gas temperatures are achieved by either varying the diluent gas composition or initial temperatures based on the adiabatic compression/expansion equation:

$$ln\left(\frac{p_c}{p_i}\right) = \int_{T_i}^{T_c} \frac{\gamma}{\gamma - 1} \frac{dT}{T}$$

where p_i is the initial gas pressure, p_C is the compressed gas pressure, T_i is the initial gas temperature, T_C is the compressed gas temperature and γ is temperature dependent ratio of specific heat.

Pressure-time profiles are measured using a Kistler 6045A pressure transducer, and the compressed gas pressure in above equation is taken as the pressure at the end of compression. The ignition delay time is measured from the first local maximum in the pressure–time history to the maximum rate of pressure rise due to ignition, as shown in Fig. 2. The reactive pressure traces 1 and 2 show the repeatability of our pressure measurements from two similar experiments.

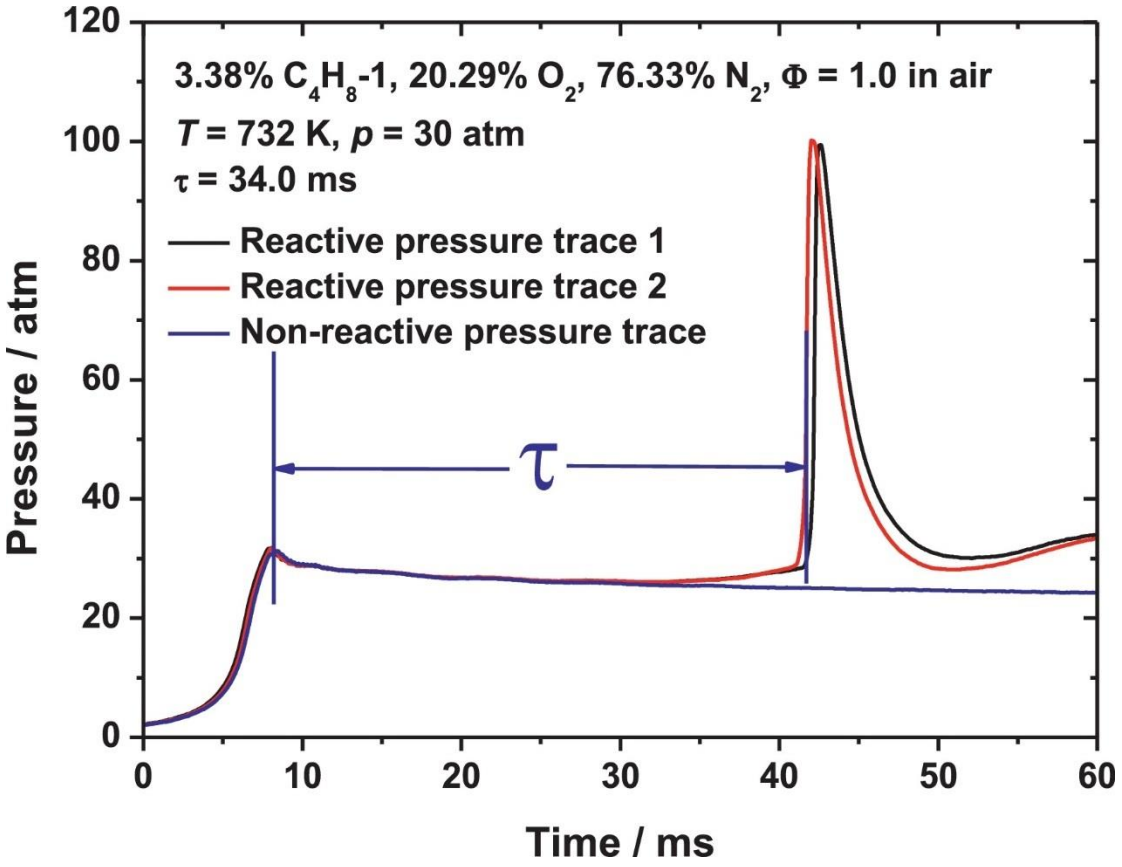

Fig. 2. A typical pressure-time history measured in the RCM.

In order to take heat loss effect into account, a non-reactive experiment, in which O_2 is replaced by an equivalent amount of N_2 in the mixture, was performed for every reactive experiment under the same conditions. For model simulations, non-reactive pressure–time profiles were converted to an "effective volume" history, which is then used as input file in CHEMKIN-PRO [26].

We have explored the uncertainty quantification of IDT measurements in an RCM in a previous study of isobutene oxidation [18]. We also recognize that uncertainty quantification for experimental data is an essential step in assessing the agreement be- tween experimental data and kinetic mechanism simulation results. It is natural to think in terms of two types of uncertainties for RCM

experiments; uncertainties in the measured ignition delay time, and uncertainties in the measured and inferred thermodynamic state of the reacting gas.

Ignition delay times can be measured quite accurately in the RCM. The high natural frequency of the transducer (80 kHz) used to monitor in-cylinder pressure along with the sufficient time- resolution of the data acquisition unit (20 kHz) permits the capture of both the end of compression time and the occurrence of the ignition event to within approximately 50 μs. The a-synchronicity of the pistons' arrival at maximum compression in our dual-piston machine contributes to shot-to-shot scatter in ignition delay measurements due to the stochastic change in piston seating. This a-synchronicity can cause inconsistencies for the defined end of compression time between reactive and non-reactive traces of up to 0.5 ms, which only induces large uncertainties when comparing experimental and simulated ignition delay times for short ignition events (for example, ± 5% for an ignition delay of 5 ms and ± 0.5 at 50 ms).

While the RCM is accurate in recording ignition delay measurements, the characterization of the thermodynamic state of the re- acting gas is more difficult, especially with regard to compressed temperatures that are evaluated from the adiabatic core hypothesis. Initial mixture mole fractions are expected to be accurate to within about ± 2% of their reported nominal value, where the main contribution of uncertainty comes from partial pressure measurements. Time resolved measurements of in-cylinder pressures are readily achievable

with modern static and dynamic pressure transducers, which result in the measurement of the initial reactor pressure and transient pressure history to within approximately ± 0.05% and ± 1 bar, respectively. Assuming perfect applicability of the adiabatic core hypothesis to the experiments conducted in this study and accounting for both uncertainties in the initial temperature and pressure measurements, the uncertainty of the inferred adiabatic core compressed temperature is less than approximately ± 15 K.

3. Simulation methods

3.1. Ignition delay time simulations

Shock tube ignition delay time simulations were performed assuming a zero-dimensional, constant-volume reactor. The reflected shock pressure (p_5) and temperature (T_5) were used as the initial pressure and temperature, respectively. The non-ideal facility effect (dp/dt) for the reflected shock wave was found to be less than 2%/ms. However, due to the longer IDTs measured by Pan *et al.* [2] a dp/dt = 4% was taken into account for the simulations of their data presented as Supplementary material. For simulations of ignition delay time results already presented in the literature, the definition of ignition delay time is taken consistent with the particular diagnostic used in the reported experiments.

In simulating the rapid compression machine experiments an “adiabatic core expansion” approach [27–29] was employed, which accounts for the heat loss effect by adopting the volume–time his- tory as discussed in Section 2.2.

3.2. Species simulations

Simulations of species measurements recorded in jet-stirred reactor, flow reactor and pre-mixed flame experiments were performed using the Perfectly Stirred Reactor (PSR), Plug Flow Reactor (PFR) and Premixed Laminar Burner-Stabilized Flame modules in CHEMKIN-PRO [26]. Pressure-distance and temperature-distance profiles from the experiments [6,7] are used as input files.

3.3. Flame speed simulations

Flame speed simulations were performed using the Premixed Laminar Flame-Speed simulator in CHEMKIN-PRO [26]. In order to avoid a high computational cost, a high-temperature version of the model was used to simulate the flame speed, which was created by removing all of the species and reactions involving low temperature oxidation chemistry, which is discussed in the following section.

3.4. Sensitivity analyses

Sensitivity analyses were carried out in order to identify the key reactions responsible for fuel consumption in the simulation targets.

Flame speed sensitivity analyses were performed using CHEMKIN-PRO's inbuilt utility [26], which calculates first-order sensitivity coefficients for the predicted mass flow rate, which corresponds to the flame speed.

Ignition delay time "brute force" sensitivity analyses were carried out by increasing and decreasing every reaction rate expression by a factor of two

resulting in the effect on the predicted ignition delay time. The sensitivity coefficient is defined as:

$$S = \frac{ln(\tau_+/\tau_-)}{ln(k_+/k_-)} = \frac{ln(\tau_+/\tau_-)}{ln(2.0/0.5)}$$

where τ_+ corresponds to the ignition delay time calculated with the increased rate constant and vice versa. A positive sensitivity coefficient indicates an inhibiting reaction and vice versa.

3.5. Flux analyses

Flux analyses were carried out to determine the most important reactions responsible for fuel consumption and the further underlying pathways leading to final products at various temperature regimes. They were performed assuming a constant volume reactor and were taken at the time corresponding to 20% fuel consumption.

4. Computational method

4.1. Rate constant calculation

Rate constant calculations have been carried out for the im- portant reactions associated with 1-butene oxidation. The M062X method [30] with the 6-311 ++ G(d,p) basis set were used in the geometry optimizations and frequency calculations of all of the species involved in this reaction using Gaussian 09 [31] . The same method was used to determine the potential energy surface scans for the individual hindered rotors associated with reactant

and transition state. The electronic single point energies have been calculated at CCSD(T)/cc-pvXZ level of theory (where X = D, T and Q) which were extrapolated to the complete basis set (CBS) limit [32,33].

Conventional transition-state theory [34] with an asymmetric Eckart tunneling correction [35] has been used to calculate the high-pressure limit rate constants in this work. The low-frequency torsional conserved modes were treated as hindered rotors.

For systems containing arbitrary numbers of wells and product/isomer channels, pressure dependent rate constants were calculated by using the ChemDis code [36,37], based on Quantum- Rice–Ramsperger–Kassel (QRRK) theory using a Modified Strong Collision (MSC) approximation for Collisional Energy Transfer (CET).

4.2. Thermochemistry calculation

The thermodynamic parameters for all of new species pertaining to the 1-butene sub-mechanism were calculated based on the group additivity method developed by Benson [38] with updated group values by Burke *et al.* [39] and utilizing the THERM program developed by Ritter and Bozzelli [40]. The thermodynamic parameters for all of the species involved in the 1-butene sub-mechanism in addition to the entire mechanism are provided as Supplementary material.

5. Chemical kinetic mechanism development

The current mechanism was developed based on a series of previous work

studies, including:

- H_2/O_2 sub-mechanism developed by Kéromnès *et al.* [41].
- C_1–C_2 sub-mechanism (AramcoMech 1.3) developed by Metcalfe *et al.* [11].
- CH_4/DME sub-mechanism developed by Burke *et al.* [42].
- Propene/allene/propyne sub-mechanism developed by Burke *et al.* [16, 17].
- Isobutene sub-mechanism developed by Zhou *et al.* [18].
- 2-Butene sub-mechanism developed by Li *et al.* [19].

The current model has been developed and presented in our 2-butene study [19]. In this paper, the model will be validated, not only against the new experimental data presented in this study, but also against a large variety of experimental data and a number of other literature models, provided as Supplementary material. Key reactions for 1-butene oxidation at different temperatures and pressures have been highlighted using the "brute force" and flame speed sensitivity analyses and flux analyses, discussed in detail in the following sections. The 1-butene combustion chemistry model predicts well a variety of experimental data, including ignition delay times, speciation measurements as a function of time and/or temperature and height above the burner surface in addition to flame speed measurements. The comprehensive kinetic mechanism AramcoMech 2.0, thermochemistry, transport files and glossary are provided as Supplementary material and are available for download at http://c3.nuigalway.ie/mechanisms.html.

Table 3 Arrhenius coefficients for the important reactions (cm^3/mol/s/cal units).

No.	Reactions	*A*	*n*	*Ea*	Reference
1	C_4H_8-1+O_2<=>$\dot{C}_4H_7$1-3+$H\dot{O}_2$	1.00E+14	0.00	37190.	[43]
2	C_4H_8-2+O_2<=>$\dot{C}_4H_7$1-3+$H\dot{O}_2$	2.00E+14	0.00	39390.	[43]
3	C_4H_8-1+$\dot{O}H$<=>$\dot{C}_4H_7$1-3+H_2O	1.01E+06	2.20	–437.2	[44]
4	C_4H_8-1+$\dot{O}H$<=>$\dot{C}_4H_7$1-4+H_2O	8.60E+06	2.03	2623.1	[44]
5	C_4H_8-1+$\dot{O}H$<=>$\dot{C}_4H_7$1-2+H_2O	3.00E+06	1.97	2847.7	[44]
6	C_4H_8-1+$\dot{O}H$<=>p$\dot{C}_4H_8$OH-2	2.10E+06	1.81	–3292.3	[45,46]
7	C_4H_8-1+$\dot{O}H$<=>s$\dot{C}_4H_8$OH-1	7.00E+05	1.80	–3290.2	[45,46]
8	C_4H_8-1+$\dot{H}$<=>C_3H_6+$\dot{C}H_3$ (DUP1)	1.32E+20	–1.46	15383.	[19]
9	C_4H_8-1+$\dot{H}$<=>C_3H_6+$\dot{C}H_3$ (DUP2)	1.00E+33	–5.49	31922.	[19]
10	$\dot{C}_4H_7$1-3<=>$\dot{C}_4H_7$1-4	5.62E–12	7.19	36200.8	[19]
11	$\dot{C}_4H_7$1-4<=>C_2H_4+$\dot{C}_2H_3$	2.84E+10	0.99	38998.8	[19]
12	$\dot{C}_4H_7$1-3+O_2<=>C_4H_6+$H\dot{O}_2$	1.07E+00	3.71	9322.	[47]
13	$\dot{C}_4H_7$1-3+$H\dot{O}_2$<=>$C_4H_7$2-1OOH	2.80E+20	–2.96	–2503.	[48]
14	$\dot{C}_4H_7$1-3+$H\dot{O}_2$<=>$C_4H_7$1-3OOH	3.45E+19	–2.71	–3140.	[48]
15	$\dot{C}_4H_7$1-3+$H\dot{O}_2$<=>$C_4H_7$1$\dot{O}$+$\dot{O}H$	4.44E+42	–8.67	21071.	[48]
16	$\dot{C}_4H_7$1-3+$H\dot{O}_2$<=>$C_4H_7\dot{O}$2-1+$\dot{O}H$	2.18E+42	–8.58	21090.	[48]
17	$\dot{C}_4H_7$1-3+$\dot{C}H_3$(+M)<=>C_5H_{10}-2(+M)	1.00E+14	–0.32	–262.3	[49]
18	$\dot{C}_4H_7$1-3+$\dot{C}H_3$(+M)<=>cC_5H_{10}(+M)	1.00E+14	–0.32	–262.3	[49]
19	sQC_4H_7OHp-4+O_2<=>sQC_4H_7OHp-4O_2	3.43E+16	–1.63	198.7	[50]
20	sQC_4H_8Op=>C_2H_5CHO+CH_2O+$\dot{O}H$	5.36E+12	–0.08	10790.	[51]

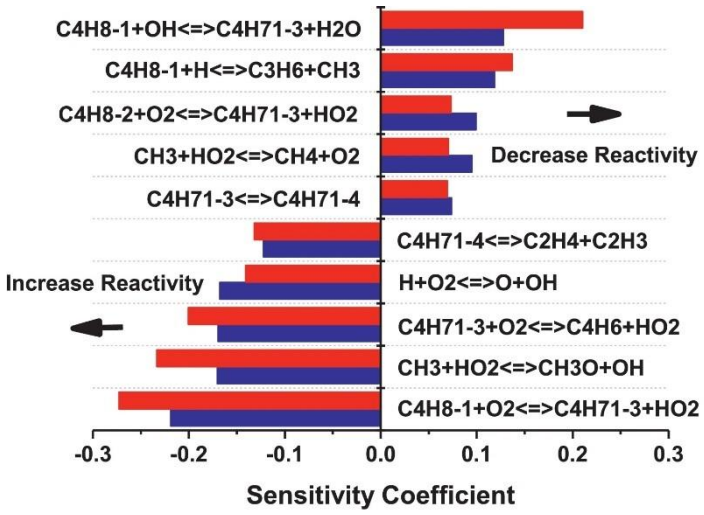

(a) $T = 1250$ K

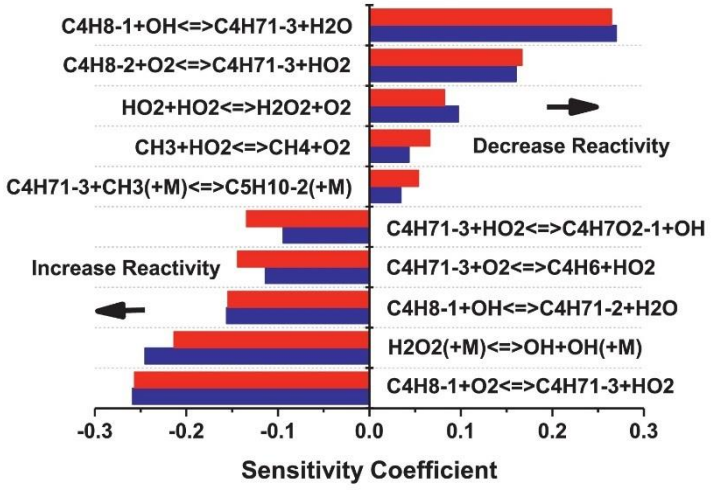

(b) $T = 950$ K

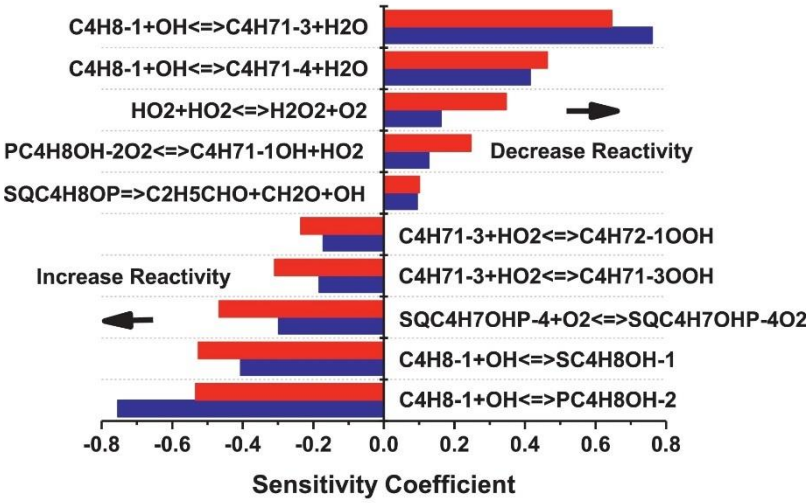

(c) $T = 700$ K

Fig. 3. Sensitivity analyses for 1-butene, $\phi = 1.0$ in 'air', $p =$ ● 10 atm, ● 30 atm.

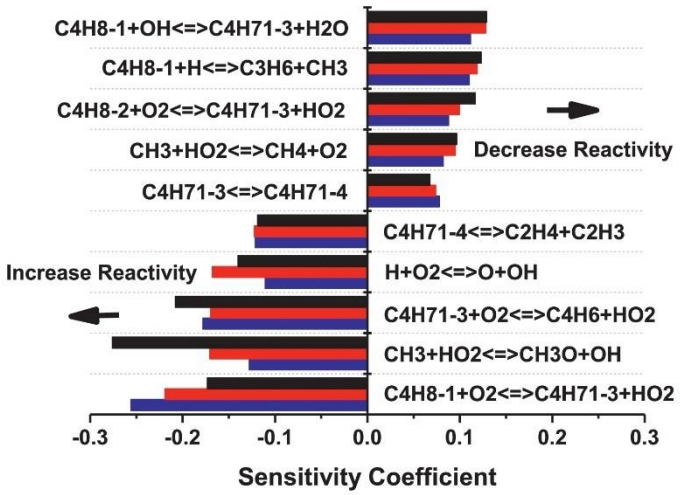

(a) T = 1250 K

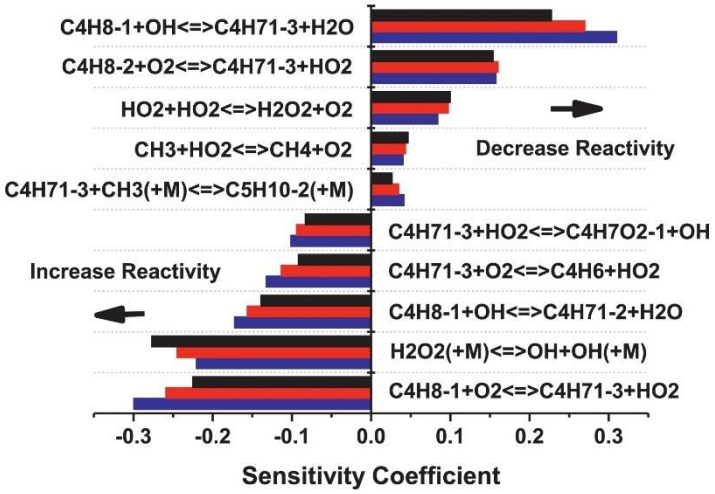

(b) T = 950 K

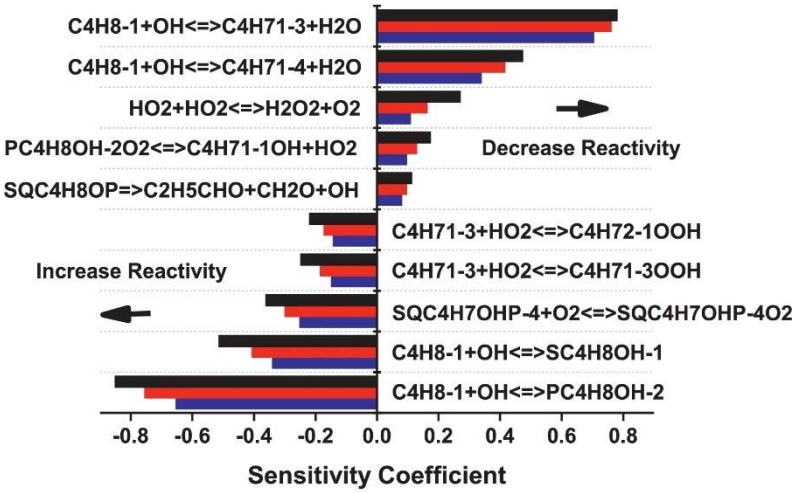

(c) T = 700 K

Fig. 4. Sensitivity analyses for 1-butene oxidation, p = 30 atm, ϕ = ● 0.5, ● 1.0 and ● 2.0 in 'air'.

5.1. Important reaction classes highlighted

The important reactions for 1-butene ignition delay times in an RCM and/or a shock tube are highlighted by our "brute force" sensitivity analyses. Figure 3 shows the sensitivity result comparison for the pressure of 10 and 30 atm, at ϕ= 1.0 in 'air' (21% O_2 : 79% N_2), T = 1250, 950 and 700 K, Fig. 4 shows the sensitivity result comparison for ϕ = 0.5, 1.0 and 2.0, at p = 30 atm, T = 700, 950 and 1250 K. All of the reactions highlighted here will be discussed and explained in detail in the following sections and the major reaction pathways are shown in Fig. 5 and their associated Arrhenius coefficients are provided in Table 3.

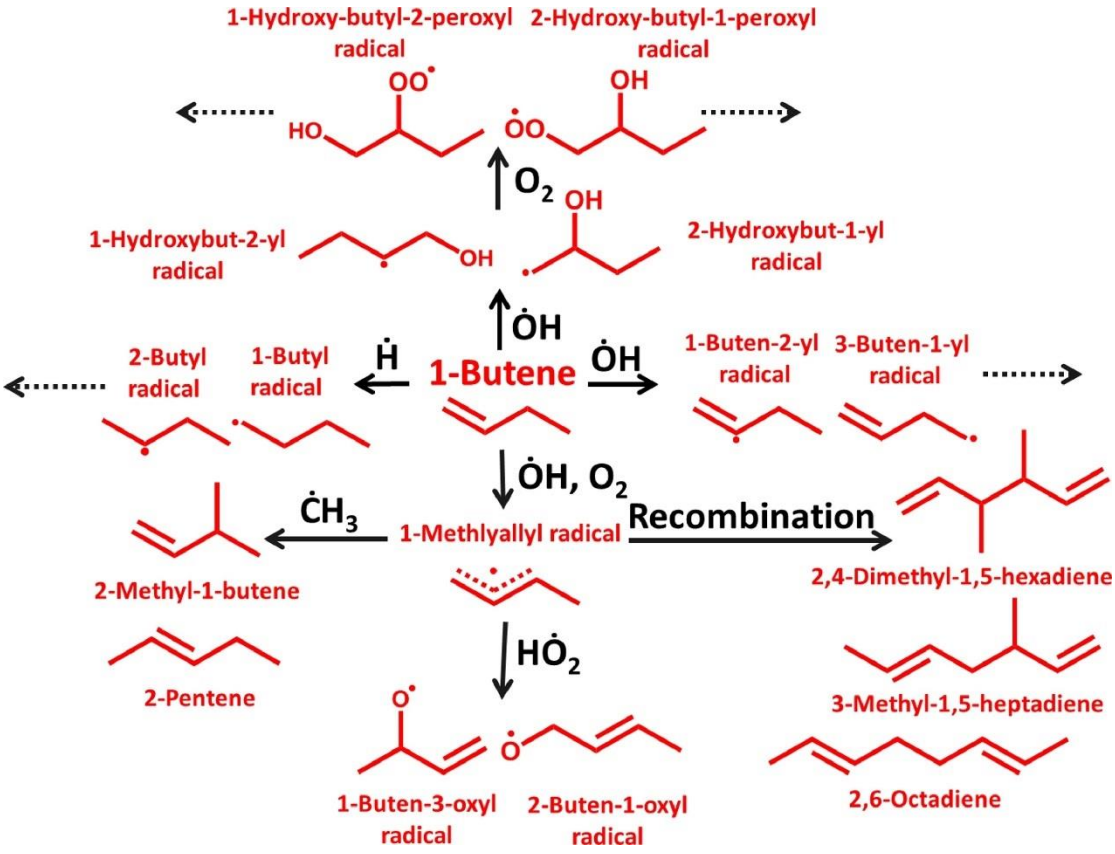

Fig. 5. Generalized reaction pathways included in this work for 1-butene oxidation.

5.2. Unimolecular decomposition

Speciation measurements of 1-butene pyrolysis in flow reactor [6] are sensitive to 1-butene decomposition. Four important reactions involving C–C and C–H bond breaking of 1-butene, which we described in the recombination direction, were included in this work:

- $\dot{C}_3H_5$-a + $\dot{C}H_3$ (+M) ↔ C_4H_8-1 (+M)
- $\dot{C}_2H_5$ + $\dot{C}_2H_3$ (+M) ↔ C_4H_8-1 (+M)
- $\dot{C}_4H_7$1-3 + $\dot{H}$ (+M) ↔ C_4H_8-1 (+M)
- $\dot{C}_4H_7$1-4 + $\dot{H}$ (+M) ↔ C_4H_8-1 (+M)

The pressure-dependent rate constants for the two C–C bond fission reactions were adapted from the study by Tsang *et al.* [49,52]. The allylic site C–H bond fission reaction was found to be the most favored channel, and the rate constant was estimated to best validate the 1-butene pyrolysis experiments presented by Zhang *et al.* [6].

5.3. Fuel–O_2 reactions

For H atom abstraction by molecular oxygen, only the reaction resulting in the formation of 1-methlyallyl ($\dot{C}_4H_7$1-3) and hydroperoxyl radicals was found to be sensitive, while abstractions from the other carbon atom sites were not competitive.

- C_4H_8-1 + O_2 ↔ $\dot{C}_4H_7$1-3 + $H\dot{O}_2$
- C_4H_8-2 + O_2 ↔ $\dot{C}_4H_7$1-3 + $H\dot{O}_2$

As shown in Figs. 3 and 4, at intermediate (T = 950 K) and high temperatures (T = 1250 K), H atom abstraction from the allylic car- bon atom site on 1- and 2-butene results in the formation of the same products, but these two reactions have different effects in either promoting or inhibiting reactivity. This is because the chain branching reaction between 1-butene and molecular oxygen forms two radicals ($\dot{C}_4H_7$1-3 and $H\dot{O}_2$) promoting reactivity. Conversely, in the second reaction the thermodynamics results to the formation of the two stable molecules (C_4H_8-2 + O_2), thus inhibiting re- activity. In this way both the 1- and 2-butene oxidation mechanisms are intrinsically linked and a mechanism for one must contain the other.

The rate constants for these two abstraction reactions were determined based on the Evans–Polanyi relationship developed by Somers *et al.* [43], in which the activation energy was found to relate to the heat of reaction via:

E_a=1.06*$\Delta_r H$ – 9.44

in kJ mol^{-1} units. The frequency factors were estimated based on a best fit to experimental data over a wide range of conditions from the jet-stirred reactor, pre-mixed flame and shock tube. Figure 6 shows the influence of this adjustment on IDT prediction.

5.4. Fuel–radical reactions

H-atom abstraction reactions by various radicals from 1-butene have been included in this work. There are four different types of hydrogen atom (methyl site, secondary allylic C atom site, seondary vinylic C atom site and primary

vinylic C atom site) on 1-butene as shown in Fig. 7.

Figure 7 shows the bond dissociation energies of 1-butene molecule. Due to the much lower bond dissociation energy (BDE) of the secondary allylic hydrogen atoms (85.5 kcal mol^{-1}) which are approximately 20 kcal mol^{-1} weaker than the other three types of C–H bonds in the molecule, abstraction of these H-atom and thus the formation of 1-methylallyl ($\dot{C}_4H_7$1-3) radicals is dominant.

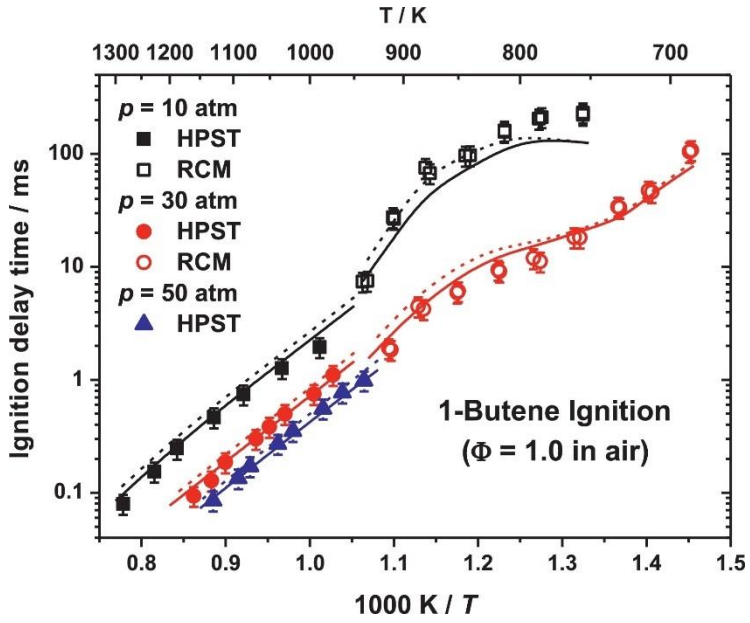

Fig. 6. Effect of changing the C_4H_8-1 + O_2 ↔ $\dot{C}_4H_7$1-3 + $H\dot{O}_2$ rate constant on IDT at ϕ = 1.0 in air, p = 10, 30 and 50 atm. Solid line: this study, dashed line: A-factor × 0.5.

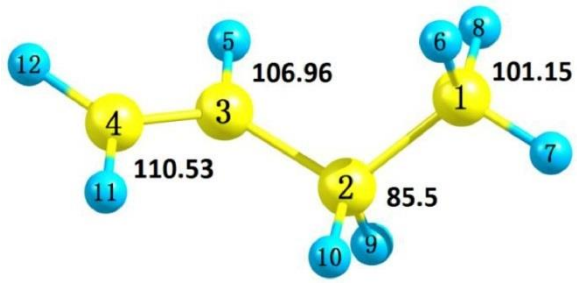

Fig. 7. 1-Butene structure and C–H bond dissociation energies (in kcal mol^{-1}),

● C atom, ● H atom.

5.4.1. C_4H_8-1 + ȮH ↔ products

The hydroxyl radical is extremely important in promoting reactivity in combustion processes. For the reaction of hydroxyl radical with 1-butene, both abstraction and addition pathways are included in the current kinetic mechanism

- C_4H_8-1 + ȮH ↔ $\dot{C}_4H_7$1-4 + H_2O
- C_4H_8-1 + ȮH ↔ $\dot{C}_4H_7$1-3 + H_2O
- C_4H_8-1 + ȮH ↔ $\dot{C}_4H_7$1-2 + H_2O
- C_4H_8-1 + ȮH ↔ $\dot{C}_4H_7$1-1 + H_2O

As shown in Figs. 3 and 4, the reaction leading to the formation of 1-methylallyl radicals is the most inhibiting reactivity through- out the entire temperatures range. The rate constants for the C_4H_8-1 + ȮH abstraction reactions were adopted from the experimental and theoretical study of Vasu *et al.* [44] at the CCSD(T)/6- 311++G(d,p)//QCISD/6-31G(d,p) level of theory, and it has been de- creased by a factor of 2.6 which is the uncertainty provided by Vasu et al. in taking the contribution from the pathway for ȮH radical addition and the uncertainty in their experiments into consideration. Figure 8 shows a rate constant comparison for abstraction by ȮH radicals on different sites on 1-butene on a per H-atom basis. It can be seen that abstraction from the allylic site is the fastest followed by primary carbon site, with vinylic site being

the slowest, corresponding to the C–H bond dissociation energies. Figure 9 shows the rate constants comparison for the allylic radical formation reactions C_3H_6, iC_4H_8, C_4H_8-1 and C_4H_8-2 + ȮH (per H-atom basis).

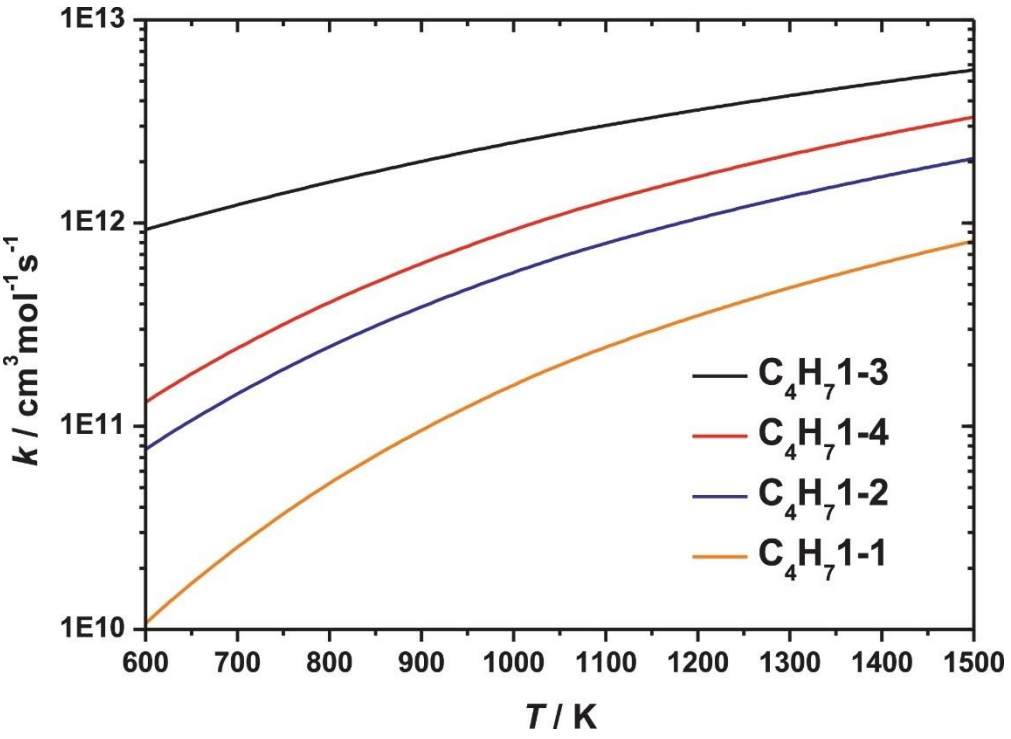

Fig. 8. Comparison of rate constants for C_4H_8-1 + ȮH at different sites on a per H-atom basis.

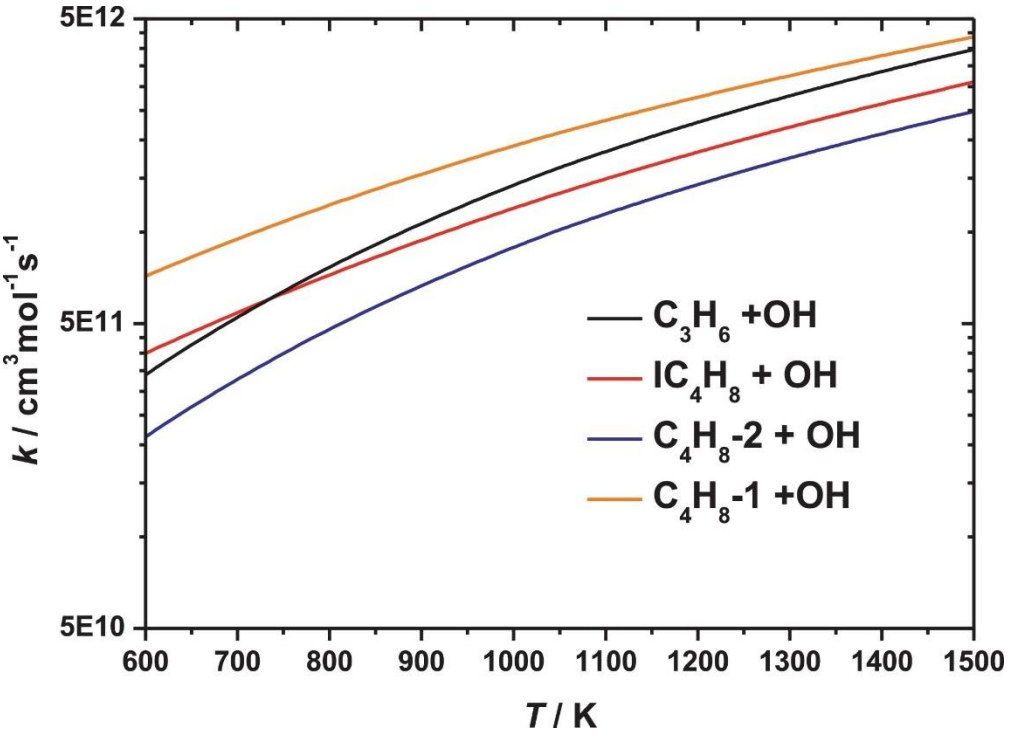

Fig. 9. Comparison of rate constants for abstraction of allylic H-atom by ȮH from C_3H_6, iC_4H_8, C_4H_8-2 and C_4H_8-1 + ȮH on a per H-atom basis.

It can be seen that the rate constants for abstraction from the primary allylic sites on C_3H_6, iC_4H_8, C_4H_8-1 and C_4H_8-2 are within 30% of one another at combustion temperatures (700–1500 K). Further- more, the rate constant for abstraction from the secondary allylic site on 1-butene is faster compared to abstraction of a primary allylic H-atom, which is consistent with the differences in the C–H bond dissociation energies.

- C_4H_8-1 + ȮH ↔ p$\dot{C}_4H_8$OH-2
- C_4H_8-1 + ȮH ↔ s$\dot{C}_4H_8$OH-1

As shown in Figs. 3 and 4, ȮH radical addition to C_4H_8-1 is the most important reaction promoting reactivity at low temperatures (T = 700 K). This is because chain branching can subsequently occur via radical addition of the

1-butene + ȮH adduct to O_2, internal H-atom isomerization, a second addition to O_2, with the decomposition of the nascent ketohydroperoxide species ultimately promoting reactivity via the generation of ȮH radicals, as shown in Fig. 10. The rate constants for these reactions were estimated by analogy with the propene/ȮH radical system as calculated by Zádor *et al.* [45]. Moreover, a branching ratio of 75:25 in favor of addition to the terminal carbon was adopted based on the experimental study by Loison *et al.* [46]. The influence of this branching ratio on the ignition delay times in the low temperature range can be seen in Fig. 11.

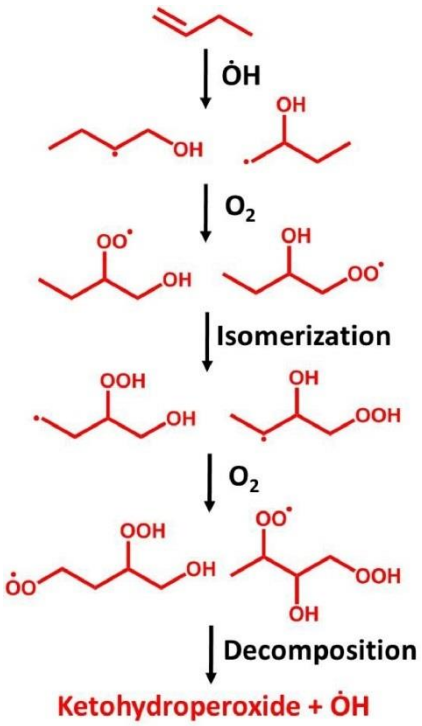

Fig. 10. Low temperature chain branching reaction pathways for 1-butene oxidation.

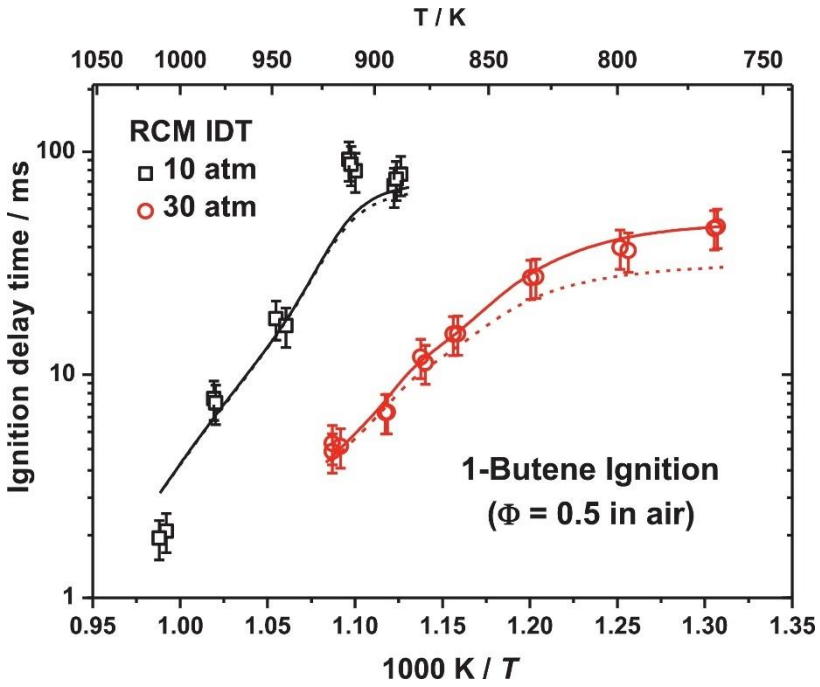

Fig. 11. Branching ratio effects from the ȮH terminal and central addition to C_4H_8-1 to ignition delay times at ϕ = 0.5, fuel in air, p = 10 and 30 atm. Terminal vs. central: solid line (75:25); dash line (50:50).

5.4.2. C_4H_8-1 + Ḣ ↔ products

- C_4H_8-1 + Ḣ ↔ $\dot{C}_4H_7$1-4 + H_2
- C_4H_8-1 + Ḣ ↔ $\dot{C}_4H_7$1-3 + H_2
- C_4H_8-1 + Ḣ ↔ $\dot{C}_4H_7$1-2 + H_2
- C_4H_8-1 + Ḣ ↔ $\dot{C}_4H_7$1-1 + H_2
- C_4H_8-1 + Ḣ ↔ p$\dot{C}_4H_9$
- C_4H_8-1 + Ḣ ↔ s$\dot{C}_4H_9$
- C_4H_8-1 + Ḣ ↔ C_2H_4 + $\dot{C}_2H_5$
- C_4H_8-1 + Ḣ ↔ C_3H_6 + $\dot{C}H_3$
- C_4H_8-1 + Ḣ ↔ C_4H_8-2 + Ḣ

As shown in Figs. 3 and 4, when Ḣ atom adds to the terminal carbon atom, the chemically activated reaction C_4H_8-1 + Ḣ ↔ C_3H_6 + $\dot{C}H_3$ becomes sensitive, inhibiting reactivity. This reaction results in the consumption of atomic hydrogen producing relatively unreactive methyl radicals. In the flame speed sensitivity analysis shown in Fig. 12, this reaction is the only sensitive fuel chemistry reaction, also inhibiting reactivity.

However, Ḣ-atom addition to the non-terminal carbon atom in 1-butene results in the formation of C_2H_4 + $\dot{C}_2H_5$, which ultimately generates two vinyl radicals and a hydrogen atom, promoting reactivity. The rate constants for this reaction class were calculated on the $\dot{C}_4H_9$ potential energy surface (PES) at the CCSD(T)/cc-pVXZ//M062X/6-311++G(d,p) level of theory (where X = D, T and Q) and extrapolated to the complete basis set (CBS) limit [32, 33].

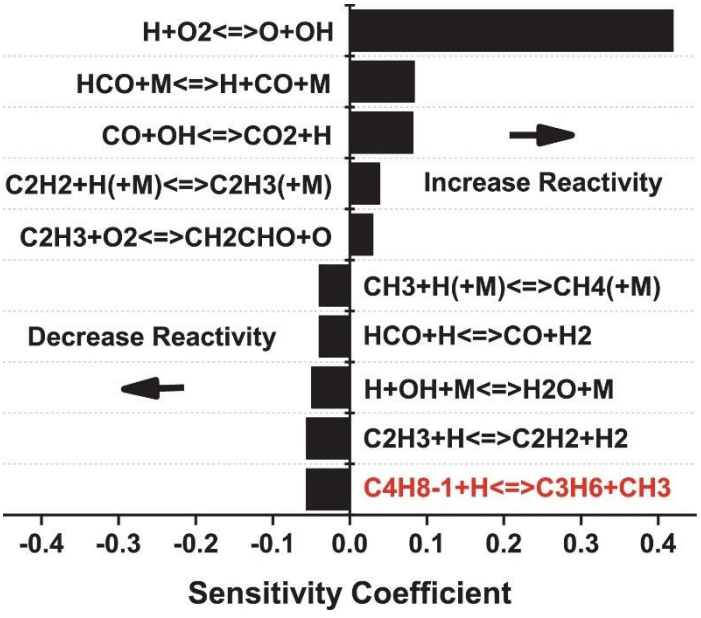

Fig. 12. Flame speed sensitivity analysis of C_4H_8-1/air laminar flame at ϕ = 1.1, Tu = 298 K, p = 1 atm.

5.4.3. C_4H_8-1 + $H\dot{O}_2$ ↔ products

Reactions that involve hydroperoxyl radicals are most influential at elevated pressures and lower temperatures. Under these conditions, the stabilization of $\dot{H} + O_2 (+M) \leftrightarrow H\dot{O}_2 (+M)$ is favored over the chain branching reaction $H + O_2 \leftrightarrow \ddot{O} + \dot{O}H$.

H-abstraction reaction by $H\dot{O}_2$

- $C_4H_8\text{-}1 + H\dot{O}_2 \leftrightarrow \dot{C}_4H_7\text{1-4} + H_2O_2$
- $C_4H_8\text{-}1 + H\dot{O}_2 \leftrightarrow \dot{C}_4H_7\text{1-3} + H_2O_2$
- $C_4H_8\text{-}1 + H\dot{O}_2 \leftrightarrow \dot{C}_4H_7\text{1-2} + H_2O_2$
- $C_4H_8\text{-}1 + H\dot{O}_2 \leftrightarrow \dot{C}_4H_7\text{1-1} + H_2O_2$

The rate constants for abstraction reactions of 1-butene and hydroperoxyl radicals are adopted by analogy with the theoretical study on propene + $H\dot{O}_2$ from Zádor *et al.* [53].

$H\dot{O}_2$ addition to C_4H_8-1

- $C_4H_8\text{-}1 + H\dot{O}_2 \leftrightarrow \dot{C}_4H_8OOH\text{1-2}$
- $C_4H_8\text{-}1 + H\dot{O}_2 \leftrightarrow \dot{C}_4H_8OOH\text{2-1}$
- $C_4H_8\text{-}1 + H\dot{O}_2 \leftrightarrow \dot{C}_4H_8OOH\text{2-3}$
- $C_4H_8\text{-}1 + H\dot{O}_2 \leftrightarrow C_4H_8O\text{1-2} + \dot{O}H$
- $C_4H_8\text{-}1 + H\dot{O}_2 \leftrightarrow C_4H_8O\text{2-3} + \dot{O}H$
- $C_4H_8\text{-}1 + H\dot{O}_2 \leftrightarrow pC_4H_9\dot{O}_2$
- $C_4H_8\text{-}1 + H\dot{O}_2 \leftrightarrow sC_4H_9\dot{O}_2$
- $C_4H_8\text{-}1 + H\dot{O}_2 \leftrightarrow p\dot{C}_4H_9 + O_2$
- $C_4H_8\text{-}1 + H\dot{O}_2 \leftrightarrow s\dot{C}_4H_9 + O_2$

- $pC_4H_9\dot{O}_2 \leftrightarrow \dot{C}_4H_8OOH1\text{-}2$
- $pC_4H_9\dot{O}_2 \leftrightarrow \dot{C}_4H_8OOH1\text{-}3$
- $pC_4H_9\dot{O}_2 \leftrightarrow \dot{C}_4H_8OOH1\text{-}4$
- $sC_4H_9\dot{O}_2 \leftrightarrow \dot{C}_4H_8OOH2\text{-}1$
- $sC_4H_9\dot{O}_2 \leftrightarrow \dot{C}_4H_8OOH2\text{-}3$
- $sC_4H_9\dot{O}_2 \leftrightarrow \dot{C}_4H_8OOH2\text{-}4$
- $\dot{C}_4H_8OOH1\text{-}2 \leftrightarrow C_4H_8O1\text{-}2 + \dot{O}H$
- $\dot{C}_4H_8OOH1\text{-}3 \leftrightarrow C_4H_8O1\text{-}3 + \dot{O}H$
- $\dot{C}_4H_8OOH1\text{-}4 \leftrightarrow C_4H_8O1\text{-}4 + \dot{O}H$
- $\dot{C}_4H_8OOH2\text{-}4 \leftrightarrow C_4H_8O1\text{-}3 + \dot{O}H$
- $\dot{C}_4H_8OOH2\text{-}1 \leftrightarrow C_4H_8O1\text{-}2 + \dot{O}H$
- $\dot{C}_4H_8OOH2\text{-}3 \leftrightarrow C_4H_8O2\text{-}3 + \dot{O}H$
- $\dot{C}_4H_8OOH1\text{-}3 \rightarrow C_3H_6 + CH_2O + \dot{O}H$
- $\dot{C}_4H_8OOH2\text{-}4 \rightarrow C_2H_4 + CH_3CHO + \dot{O}H$

The rate constants for the addition reactions of hydroperoxyl radicals to 1-butene and the related reactions on the $C_4H_9O_2$ PES have been investigated by different groups [50,53–58]. Zádor *et al.* [53] calculated the rate constants for $H\dot{O}_2$ radical addition to the non-terminal unsaturated carbon atom in 1-butene to form a hydroperoxyl-alkyl radical and its following reaction to form a cyclic ether and a hydroxyl radical. The QCISD(T)/cc-pV∞Z//B3LYP/6-311 ++ G(d,p) level of theory was used to obtain the electronic energy barrier heights. A MULTIWELL master equation analysis

[59,60] was carried out based on these calculations resulting in pressure and temperature dependent rate constants. Villano *et al.* [54] presented high-pressure rate rules and branching ratios for the addition of $H\dot{O}_2$ to olefins through the concerted addition channel to form an alkylperoxyl radical ($H\dot{O}_2$ + olefin ↔ $R\dot{O}_2$) and through the radical addition channel to form a hydroperoxyl-alkyl radical ($H\dot{O}_2$ + olefin ↔ QOOH) at the CBS-QB3 level of theory combined with TST calculations. Pressure- and temperature-dependent rate constants were calculated for $H\dot{O}_2$ addition to the terminal site of 1-butene using an energy-grained master equation approach and QRRK calculations with a modified strong collision (MSC) approximation. Sharma *et al.* [55], Villano *et al.* [56,57], and Miyoshi *et al.* [50,58] carried out systematic investigations on the low-temperature chemistry reaction classes on the $C_4H_9O_2$ PES. Results from these studies were found to be in general good agreement.

5.4.4. C_4H_8-1 + $\dot{C}H_3$ ↔ products

Similar to H-atom abstraction by ȮH radicals described above, methyl radical can abstract a hydrogen atom from 1-butene from any of the four sites. However, only the channel producing 1-methylallyl radical and methane was found to be competitive. This reaction is predicted to be an important source of methane detected in the JSR. The recommendation in this study is an estimation taken from the recommendation of Tsang [49].

5.4.5. C_4H_8-1 + Ö ↔ products

Both abstraction and addition reactions of 1-butene with atomic oxygen

did not show any significant sensitivity to any of the data sets presented in this study. Rate constants for abstraction reactions are adopted from the review by Tsang [49] while those for addition and taken by analogy with propene [16].

5.5. H-atom abstraction from the allylic site

In view of the importance of the above H-atom abstraction re- actions from the secondary allylic site on 1-butene by various radicals and by molecular oxygen, and together with the consistent rate constants for primary allylic H-atom abstraction from propene [16,17], isobutene [18] and 2-butene [19] used in developing AramcoMech 2.0, a recommendation of rate rules for these important abstraction reactions are summarized in Table 4.

Table 4 Recommended rate rules for H-atom abstraction from primary and secondary allylic sites on a per H-atom basis (cm^3/mol/s/cal units).

	Primary			Secondary		
	A	*n*	*Ea*	*A*	*n*	*Ea*
Ḣ	1.21E+05	2.46	4360.	1.21E+03	3.05	2000.
ȮH	7.33E+03	2.68	–827.	5.05E+05	2.20	–437.
$H\dot{O}_2$	4.87E–02	4.12	12800.	3.91E–01	3.97	11700.
O_2	5.90E+00	3.64	37300.	2.44E+01	3.48	34800.

5.6. Allylic radical chemistry

The allylic radical is a resonantly-stabilized radical in each of the two

resonance forms of which the unpaired electron is on an allylic carbon. As shown in Fig. 13, a 1-methylallyl radical can be formed by H atom abstraction from the secondary allylic carbon in 1-butene or the primary allylic carbon in 2-butene. This radical appears in all of the most sensitive reactions at all conditions of temperature and pressure presented in Figs. 3 and 4 as part of our sensitivity analyses.

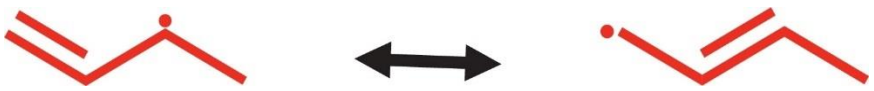

Fig. 13. Stabilization of 1-methylallyl ($\dot{C}_4H_7$1-3) radical.

5.6.1. Allylic radical reactions on C_4H_7 potential

- $\dot{C}_4H_7$1-3 ↔ $\dot{C}_4H_7$1-4
- $\dot{C}_4H_7$1-4 ↔ C_2H_4 + $\dot{C}_2H_3$
- $\dot{C}_4H_7$1-1 ↔ C_4H_6-1 + $\dot{H}$
- $\dot{C}_4H_7$1-1 ↔ C_2H_2 + $\dot{C}_2H_5$
- $\dot{C}_4H_7$1-2 ↔ C_4H_6-1 + $\dot{H}$
- $\dot{C}_4H_7$1-2 ↔ $C_4H_6$12 + $\dot{H}$
- $\dot{C}_4H_7$1-2 ↔ C_3H_4-a + $\dot{C}H_3$
- $\dot{C}_4H_7$1-3 ↔ $C_4H_6$12 + $\dot{H}$
- $\dot{C}_4H_7$1-3 ↔ C_4H_6 + $\dot{H}$
- $\dot{C}_4H_7$1-4 ↔ C_4H_6 + $\dot{H}$
- $\dot{C}_4H_7$2-2 ↔ C_4H_6-2 + $\dot{H}$
- $\dot{C}_4H_7$2-2 ↔ $C_4H_6$12 + $\dot{H}$

- $\dot{C}_4H_7$2-2 ↔ C_3H_4-p + $\dot{C}H_3$
- $\dot{C}_4H_7$1-3 ↔ $\dot{C}_4H_7$2-2

As shown in Figs. 3 and 4 at high temperatures (T = 1250 K), the isomerization of 1-methylallyl ($\dot{C}_4H_7$1-3) radical to 3-buten- 1yl ($\dot{C}_4H_7$1-4) radical and vice versa, and the related β-scission reaction of 3-buten-1yl ($\dot{C}_4H_7$1-4) radical are sensitive reactions. The high-pressure limit rate constants for this reaction class were calculated on the C_4H_7 PES at CCSD(T)/cc-pvXZ//M062X/6- 311 ++ G(d,p) (where X = D, T and Q) level of theory, which have been discussed in Section 4.1.

5.6.2. Allylic radical reaction with O_2

- $\dot{C}_4H_7$1-3 + O_2 ↔ C_4H_6 + $H\dot{O}_2$

The reaction of 1-methylallyl ($\dot{C}_4H_7$1-3) radical with molecular oxygen promotes reactivity, as it consumes a stabilized allylic radical to generate a more reactive hydroperoxy radical. It is worth nothing that the reaction $\dot{C}_4H_7$1-3 + O_2 ↔ C_4H_6 + $H\dot{O}_2$ is not chemically activated via the sequence: $\dot{R}$ + O_2 ↔ $R\dot{O}_2$ ↔ alkene + $H\dot{O}_2$, but is instead a direct abstraction. The well depth of the association reaction $\dot{C}_4H_7$1-3 + O_2 ↔ $\dot{C}_4H_7$1-3$\dot{O}_2$ has been calculated here to be 19.9 kcal mol^{-1} using Gaussian 09 [31] and the composite CBS-QB3 method. The barrier for the subsequent concerted elimination of hydroperoxyl radical is 27.2 kcal mol^{-1} and so the reverse reaction to $\dot{C}_4H_7$1-3 + O_2 is kinetically favored over the formation of C_4H_6 + $H\dot{O}_2$. Alternatively, the formation of C_4H_6 + $H\dot{O}_2$ via a direct H-atom abstraction from the primary

carbon side is possible, and the rate constant is adopted from the theoretical work of DeSain *et al.* [47].

5.6.3. Allylic radical reactions with $\dot{C}H_3$ radical

- $\dot{C}_4H_71\text{-}3 + \dot{C}H_3 (+M) \leftrightarrow C_5H_{10}\text{-}2 (+M)$

$\dot{C}_4H_71\text{-}3 + \dot{C}H_3 (+M) \leftrightarrow cC_5H_{10} (+M)$**Error! Reference source not found.**As shown in Figs. 3 and 4, at intermediate temperatures (T = 950 K), chain terminating reactions with methyl radicals resulting in the formation of 2-pentene (C_5H_{10}-2) and 3-methyl-1-butene (CC_5H_{10}) inhibit the reactivity of the system. Rate constants for these reactions are taken from Tsang [49] by analogy with allyl plus methyl radical recombination and adopting a branching ratio of 50:50 based on the spin densities of carbon atoms calculated with the M062X method [30] and the 6-311++G(d,p) basis set.

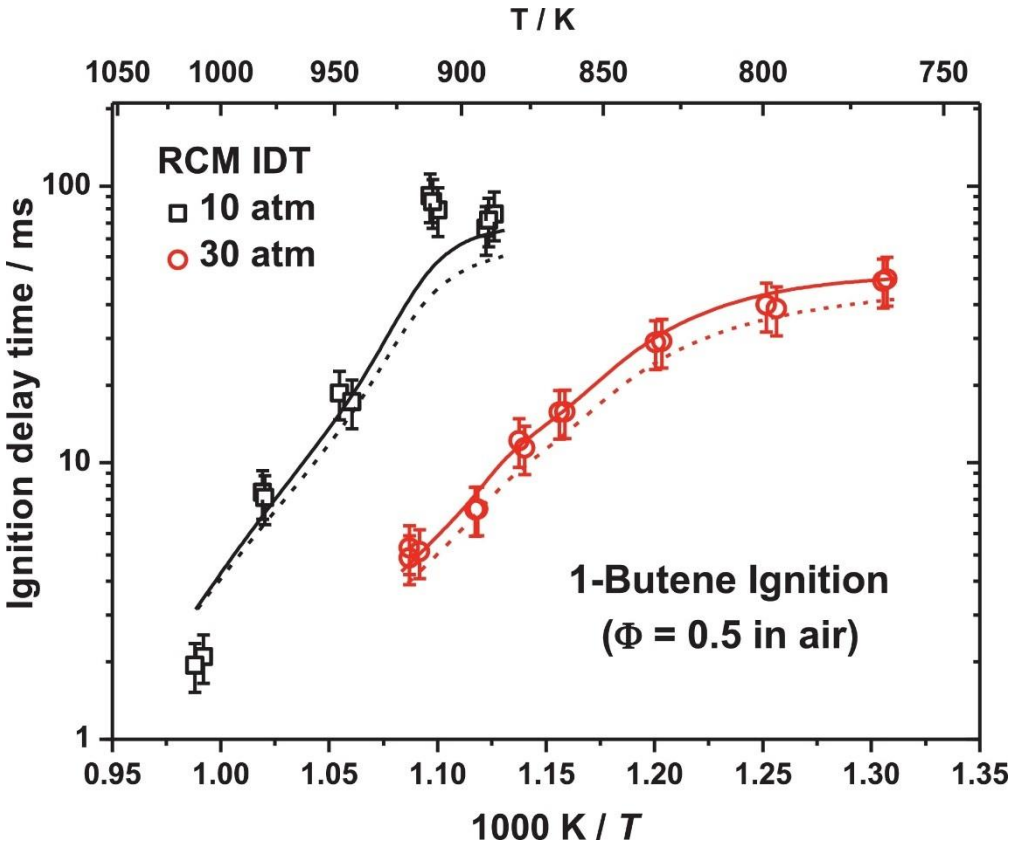

Fig. 14. Influence of rate constants for $\dot{C}_4H_7$1-3 + $\dot{C}_4H_7$1-3 to ignition delay times at ϕ = 0.5 in 'air', p = 10 and 30. Solid line: this study; dash line: excluding recombination channel.

5.6.4. Allylic radical self-recombination

- $\dot{C}_4H_7$1-3 + $\dot{C}_4H_7$1-3 ↔ C_8H_{14}1-5,3-4
- $\dot{C}_4H_7$1-3 + $\dot{C}_4H_7$1-3 ↔ C_8H_{14}1-5,3
- $\dot{C}_4H_7$1-3 + $\dot{C}_4H_7$1-3 ↔ C_8H_{14}2-6

1-methylallyl ($\dot{C}_4H_7$1-3) radical can also undergo self- recombination to form 2,6-octadiene, 3-methyl,1-5-heptadiene and 3,4-dimethyl,1-5-hexadiene, and we adopted a branching ratio of 1:2:1 as explained in Section 5.6.3. These chain terminating reactions inhibit reactivity at low and intermediate

temperatures. 1-methlyallyl radical self-reaction can also result in the formation of two alkene products. However, this reaction channel can be neglected as the rate constant is about two orders of magnitude lower than the self-recombination rate constants and does not contribute to fuel reactivity. The rate constants for this reaction class were taken by analogy with the allyl radical self-recombination study from Tranter and co-workers [61]. The influence of this reaction class to ignition delay time prediction is shown in Fig. 14.

5.6.5. Allylic radical reactions with $H\dot{O}_2$ radical

- $\dot{C}_4H_71\text{-}3 + H\dot{O}_2 \leftrightarrow C_4H_71\text{-}3OOH$
- $\dot{C}_4H_71\text{-}3 + H\dot{O}_2 \leftrightarrow C_4H_71\text{-}\dot{O} + \dot{O}H$
- $\dot{C}_4H_71\text{-}3 + H\dot{O}_2 \leftrightarrow C_2H_3COCH_3 + H_2O$
- $C_4H_71\text{-}3OOH \leftrightarrow C_4H_71\text{-}\dot{O} + \dot{O}H$
- $C_4H_71\text{-}3OOH \leftrightarrow C_2H_3COCH_3 + H_2O$
- $\dot{C}_4H_71\text{-}3 + H\dot{O}_2 \leftrightarrow C_4H_72\text{-}1OOH$
- $\dot{C}_4H_71\text{-}3 + H\dot{O}_2 \leftrightarrow C_4H_7\dot{O}2\text{-}1 + \dot{O}H$
- $\dot{C}_4H_71\text{-}3 + H\dot{O}_2 \leftrightarrow sC_3H_5CHO + H_2O$
- $C_4H_72\text{-}1OOH \leftrightarrow C_4H_7\dot{O}2\text{-}1 + \dot{O}H$
- $C_4H_72\text{-}1OOH \leftrightarrow sC_3H_5CHO + H_2O$

Unlike saturated alkanes in which the fuel molecule radical ($\dot{R}$) adds to molecular oxygen to form an $R\dot{O}_2$ radical with a stabilization energy of ~35 kcal mol^{-1}, the well depth for the reaction of $\dot{C}_4H_71\text{-}3$ radicals with O_2

producing $\dot{C}_4H_7$1-3 radicals has been calculated here (CBS-QB3) to be 19.9 kcal mol^{-1}. Thus, the back dissociation to $\dot{C}_4H_7$1-3 + O_2 is favored over the higher barrier isomerization or concerted elimination reaction processes. Instead, the reactions of 1-methylallyl and hydroperoxyl radicals are observed to be very important across a range of conditions, especially at low-to-intermediate temperatures, Figs. 3 and 4. The high-pressure limit rate constants of this reaction class were taken by analogy with the reaction of allyl radicals with hydroperoxyl radicals studied by Goldsmith *et al.* [48]. A branching ratio of 1:1 based on the spin densities of carbon atoms calculated with the M062X method [30] and the 6-311++G(d,p) basis set was adopted. Pressure dependent rate constants were calculated using QRRK/MSC theory.

5.7. Vinylic radical chemistry

- $\dot{C}_4H_7$1-2 + O_2 ↔ $C_4H_7$1-2$\dot{O}_2$
- $C_4H_7$1-2$\dot{O}_2$ ↔ $C_4H_7\dot{O}$1-2 + Ö
- $C_4H_7\dot{O}$1-2 ↔ CH_2CO + $\dot{C}_2H_5$
- $\dot{C}_4H_7$1-1 + O_2 ↔ $C_4H_7$1-1$\dot{O}_2$
- $C_4H_7$1-1$\dot{O}_2$ ↔ $C_4H_7\dot{O}$1-1 + Ö
- $C_4H_7$1-1$\dot{O}_2$ ↔ C_2H_5CHCO + $\dot{O}H$
- $C_4H_7\dot{O}$1-1 ↔ C_2H_3CHO + $\dot{C}H_3$

Vinylic radicals react with molecular oxygen to generate alkenylperoxy radicals ($C_4H_7$1-2$\dot{O}_2$ and $C_4H_7$1-1$\dot{O}_2$), followed by O–O bond fission resulting in the formation of Ö atoms, which pronouncedly promote reactivity. To the

best of our knowledge there have been no previous studies of the reactions of 1-buten-2-yl ($\dot{C}_4H_7$1-2) radical and 1-buten-1-yl ($\dot{C}_4H_7$1-1) radical with molecular oxygen. During recent studies of ethylene [11,62,63] and propene [16,17] combustion, it was found that the vinyl ($\dot{C}_2H_3$) radical, 2-propenyl ($\dot{C}_3H_5$-t) radical and 1-propenyl ($\dot{C}_3H_5$-s) radical were consumed almost entirely by reactions with molecular oxy- gen. The total rate constants for the reactions of both 1-buten-2-yl ($\dot{C}_4H_7$1-2) radical and 1-buten-1-yl ($\dot{C}_4H_7$1-1) radical with molecular oxygen and the subsequent O–O bond fission reactions recommended in this study are estimated by analogy to the reaction of vinyl radical with molecular oxygen from the high-level ab initio study by Goldsmith *et al.* [64]. The rate constants for the decomposition of the aldehyde and ketone radicals ($C_4H_7\dot{O}$1-1 and $C_4H_7\dot{O}$1-2) formed were calculated here at the CCSD(T)/CBS//M062X/6- 311++G(d,p) level of theory. Note that, based on the geometry optimization and C–C bond scan calculations, the C=C–$\dot{O}$ structure in both $C_4H_7\dot{O}$1-1 and $C_4H_7\dot{O}$1-2 radicals stabilize to the $\dot{C}$–C=O structure, as shown in Fig. 15. Therefore, the β-scission of these two molecules will form $C_2H_3CHO + \dot{C}H_3$ and $CH_2CO + \dot{C}_2H_5$, respectively.

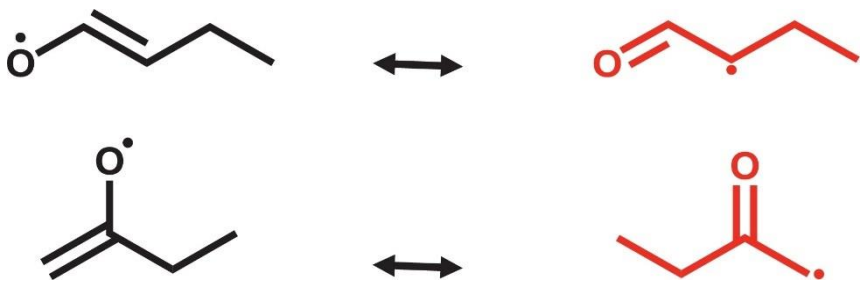

Fig. 15. Stabilization of $C_4H_7\dot{O}$1-1 and $C_4H_7\dot{O}$1-2 radicals.

5.8. Alcohol radical chemistry

- $p\dot{C}_4H_8OH\text{-}2 + O_2 \leftrightarrow pC_4H_8OH\text{-}2\dot{O}_2$
- $s\dot{C}_4H_8OH\text{-}1 + O_2 \leftrightarrow sC_4H_8OH\text{-}1\dot{O}_2$

Alcohol radical chemistry forms a part of alkene oxidation as alcohol radicals ($p\dot{C}_4H_8OH$-2 and $s\dot{C}_4H_8OH$-1), formed by the addition of hydroxyl radicals to alkene fuels reactions are the most promoting reactions at low temperatures, Figs. 3 and 4. In a recent experimental and kinetic modeling study of the oxidation of the butanol isomers Sarathy *et al.* [65] presented detailed elementary reaction classes for the oxidation of these alcohol fuels It was also shown that the reaction of hydroxybutyl radicals with O_2 was and an important reaction class in controlling the reactivity of the system at low temperature, as this reaction is the first step in the low-temperature chain branching and propagation process.

- $pC_4H_8OH\text{-}2\dot{O}_2 \leftrightarrow sQC_4H_8\dot{O}p$
- $sQC_4H_8\dot{O}p \rightarrow C_2H_5CHO + CH_2O + \dot{O}H$
- $sC_4H_8OH\text{-}1\dot{O}_2 \leftrightarrow pQC_4H_8\dot{O}s$
- $pQC_4H_8\dot{O}s \leftrightarrow C_2H_5CHO + CH_2O + \dot{O}H$

The hydroxyalkyl peroxy radical ($R\dot{O}_2$) so generated can undergo Waddington-type reaction pathways [66,67], which have been included in the model. These reaction pathways involve the beta-$R\dot{O}_2$ radical undergoing a six-membered ring isomerization to abstract a hydrogen atom from the hydroxyl moiety (i.e. alkylhydroperoxide alkoxy radical), followed by a rapid decomposition to generate two aldehydes and an $\dot{O}H$ radical. For the

p$\dot{C}_4H_8OH$-2 and s$\dot{C}_4H_8OH$-1 radicals this pathway leads to the formation of propanal, formaldehyde, and an $\dot{O}H$ radical. These reactions are chain propagating and compete directly with the alkyl type low-temperature chain branching pathways, thereby inhibiting reactivity. The rate constants for this reaction class were estimated by analogy with the theoretical work on 2-hydroxy-1,1-dimethylethyl (i$\dot{C}_4H_8OH$-it) and 2-hydroxy-2-methylpropyl (i$\dot{C}_4H_8OH$-ti) radicals addition to O_2 from Sun *et al.* [51].

- $RO\dot{O} \leftrightarrow QOOH$
- $RO\dot{O} \leftrightarrow enol + H\dot{O}_2$
- $QOOH \leftrightarrow$ cyclic ether + $\dot{O}H$
- $QOOH + O_2 \leftrightarrow \dot{O}_2QOOH$
- $\dot{O}_2QOOH \leftrightarrow$ carbonyl-hydroperoxide + $\dot{O}H$

The low-temperature branching pathways promote reactivity with the rate constants for the intra-molecular H-abstraction of hydroxyalkyl peroxy radicals ($R\dot{O}_2$) to form hydroxyalkyl hydroperoxide (QOOH) radicals are adopted from the calculations of Sharma *et al.* [55]. The rate constants for the subsequent formation of a cyclic ether were adopted from the calculations of Villano *et al.* [56], while the rate constants for the second addition to molecular oxygen and the subsequent decomposition were adopted from the theoretical study of Miyoshi *et al.* [50].

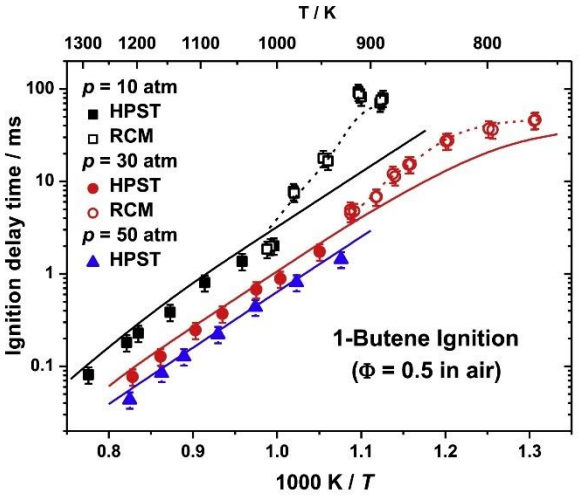

(a)

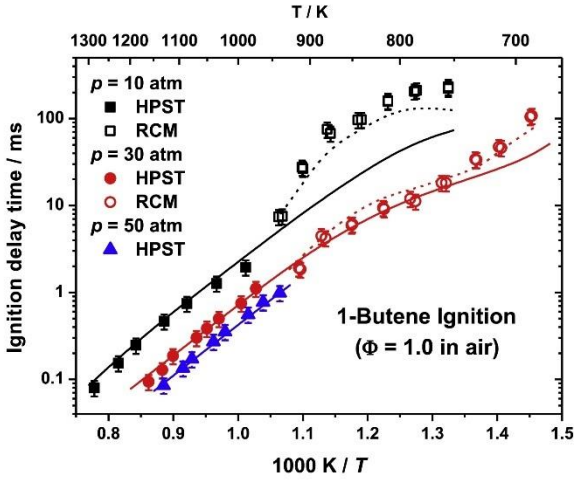

(b)

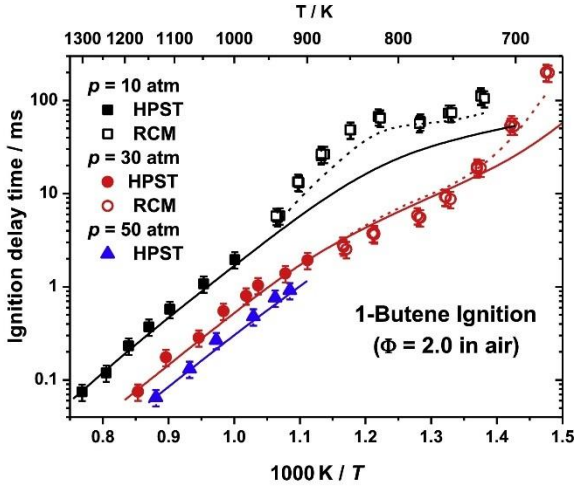

(c)

Fig. 16. Influence of pressure on 1-butene IDTs. (a) ϕ = 0.5, (b) ϕ = 1.0, (c) ϕ = 2.0. Solid lines are constant volume simulations, dashed lines include facility effects in the RCM experiments.

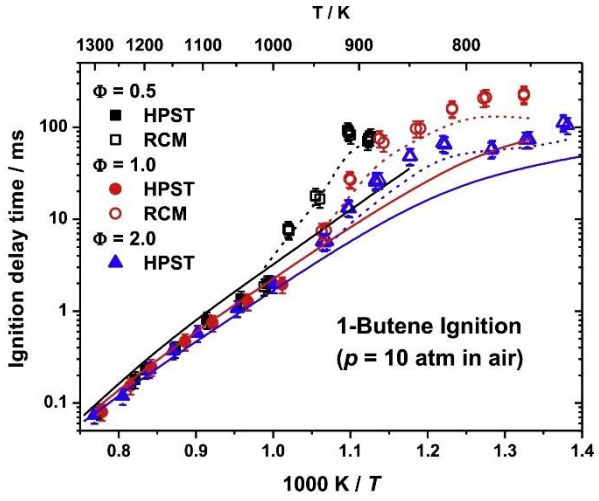

(a)

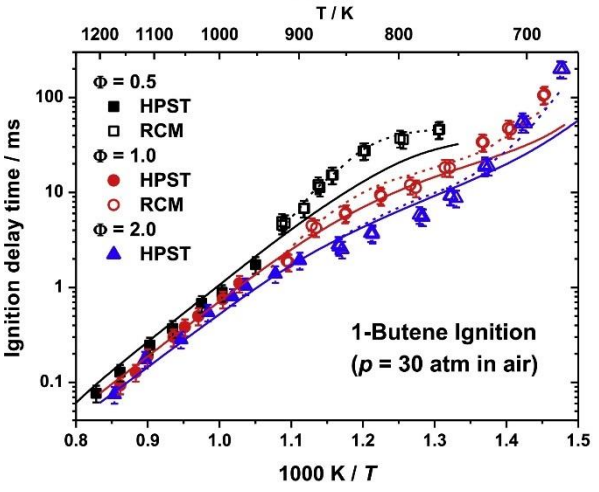

(b)

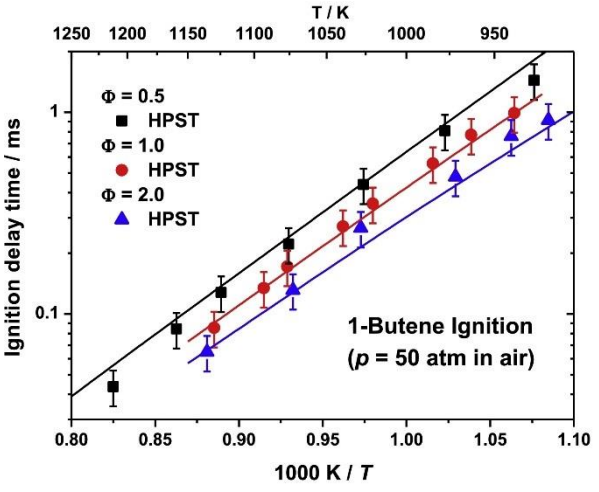

(c)

Fig. 17. Influence of equivalence ratio on 1-butene IDTs. (a) p = 10 atm, (b) p = 30 atm, (c) p = 50 atm. Solid lines are constant volume simulations, dashed lines include facility effects in the RCM experiments.

6. Model validation

Figures 16 and 17 show model simulations compared with the experimental data for all mixtures. The overall uncertainty for each individual ignition delay time was estimated to be 20%, which are represented with y-axis error bars. Uncertainties in pressure, temperature, mixture composition, and those associated with the determination of the ignition delay time from the measured traces all contribute to the overall uncertainty. In these figures, solid symbols represent the experimental data obtained in the HPST and open symbols that recorded in the RCM with solid lines corresponding to IDTs calculated via constant-volume simulations, while dashed lines represent IDTs calculated using effective volume–time histories from the RCM to account for heat loss effects. For the IDTs simulations versus the experimental data recorded by Pan *et al.* [2] the non-ideal facility effect (dp/dt = 4%) is included. In addition, the model has also been validated against the literature data listed in Table 1, and these results are presented as Supplementary material.

6.1. Influence of pressure on ignition delay time

Figure 16 shows the effect of pressure on ignition times obtained in both the HPST and in the RCM for fuel/air mixtures at ϕ = 0.5, 1.0 and 2.0. The experimental results show that reactivity increases with increasing pressure at all equivalence ratios. As the pressure increases so does the absolute concentration of reactants, resulting in the observed increase in reactivity. The mechanism is able to predict this effect over a wide range of pressures,

temperatures and equivalence ratios.

6.2. Influence of equivalence ratio on ignition delay time

Ignition delay times were measured for fuel/air mixtures at equivalence ratios of 0.5, 1.0 and 2.0 at 10, 30 and 50 atm, Fig. 17. Again, the model is in good agreement across the entire temperature and pressure ranges. In the range of low temperature conditions studied here, fuel- rich mixtures are fastest to ignite while fuel-lean mixtures being slowest. This is due to an increased concentration of fuel, as the chemistry based on the 1-butanol-2-yl ($p\dot{C}_4H_8OH$-2) radicals and 2-butanol-1-yl ($s\dot{C}_4H_8OH$-1) radicals, which are generated from the addition of hydroxyl radical to the C=C double bond, dominates reactivity, as discussed in Section 6.1 above. However, at high temperatures, the difference in IDTs between three mixtures is much smaller, and based on the relative slopes of the data all datasets would appear to converge with the increasing temperature. This is due to the increasing importance of the chain branching reaction $\dot{H} + O_2 \leftrightarrow \ddot{O} + \dot{O}H$ at higher temperatures.

6.3. Flux analyses

Flux analyses were carried out at the same conditions as those presented in the sensitivity analyses, namely at ϕ =1.0 in 'air' (21% O_2 : 79% N_2), p = 30 atm, T = 700 K, 950 K and 1250 K and at 20% fuel consumed (Fig. 18). These analyses cover the important reactions occurring at the various temperature regimes, particularly, for H-atom abstraction from the vinylic carbon site, only

secondary vinylic Ḣ atom abstraction is shown here, and for the ȮH radical addition to the C=C double bond, only terminal carbon site addition is selected as a representative.

Initially the fuel is mainly consumed via H-atom abstraction by ȮH radicals across the entire temperature regime. Particularly at high temperature (T = 1250 K), Ḣ atoms can add to the C=C double bond to form propene and a methyl radical which contributes about 5% to overall fuel consumption. At intermediate temperatures (T = 950 K), H-atom abstraction from the vinylic carbon sites followed by the molecular oxygen addition and O–O bond fission consumes about 3.4% of the fuel, and this reaction pathway pro- motes the reactivity as discussed previously. At low temperatures (T = 700 K), the fuel is mainly consumed by the ȮH radical addition to the C=C double bond.

The allylic $\dot{C}_4H_7$1-3 radical is formed in most abundance and at high temperatures (T = 1250 K), it is mainly consumed via two pathways: (1) a unimolecular decomposition to form 1,3-butadiene and a Ḣ atom; (2) a bimolecular reaction with methyl radical to form either 2-pentene or 3-methyl-1-butene. The first reaction pathway promotes the reactivity, as it transfers a stabilized allylic radical into a very reactive ·H atom, which can undergo the typical chain branching reaction $\dot{H} + O_2 \leftrightarrow \ddot{O} + \dot{O}H$. The second reaction pathway is a chain terminating reaction which inhibits reactivity. At intermediate temperature (T = 950 K), $\dot{C}_4H_7$1-3 radicals are mainly consumed by two reaction pathways: (1) H-atom abstraction by molecular oxygen to form 1,3-butadiene and hydroperoxy radical; (2) self-recombination to form C_8

dienes. Again, these two reaction pathways promote and inhibit reactivity respectively as discussed in Sections 5.6.1 and 5.6.2. At low temperatures (T = 700 K), $\dot{C}_4H_7$1-3 radicals are mainly consumed by the addition and chemically activated reactions with $H\dot{O}_2$ radicals.

As to the alcohol radical ($p\dot{C}_4H_8OH$-2) consumption, at high temperature (T = 1250 K), they are mainly consumed by C–H bond β-scission to form an enol ($C_4H_7$1-1OH) and a ˙H atom. At low and intermediate temperatures (T = 700 and 950 K), $p\dot{C}_4H_8OH$-2 radicals are mainly consumed by two reaction pathways: (1) Wadding- ton type reaction pathways; (2) alkyl type low-temperature reaction pathways.

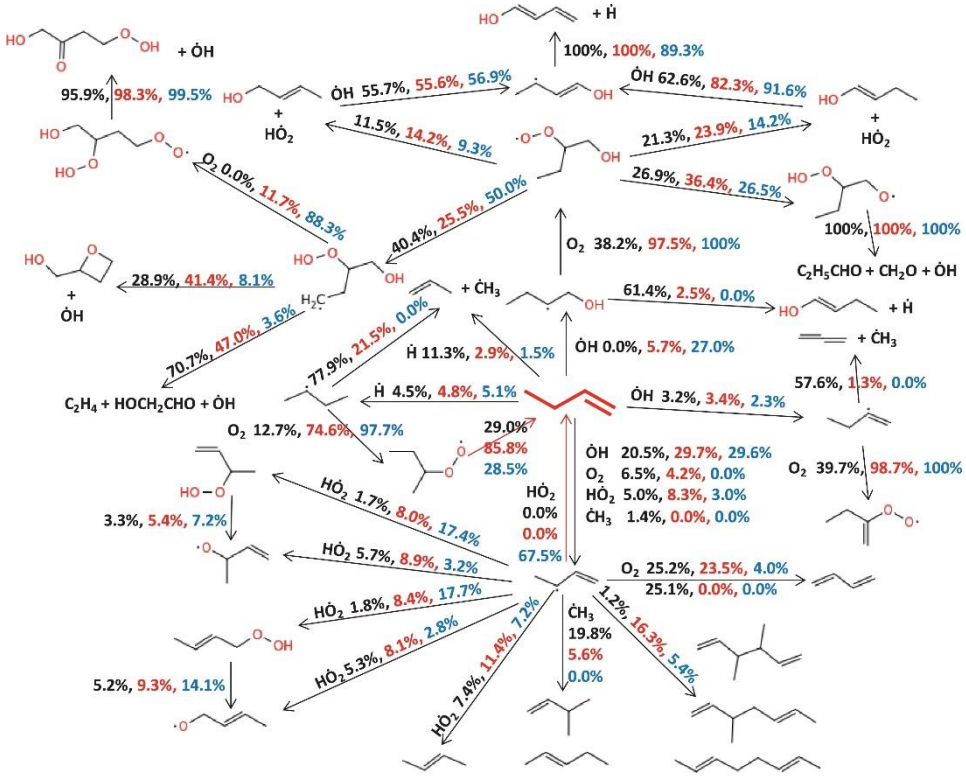

Fig. 18. Flux analysis for 1-butene oxidation at ϕ = 1.0, 30 atm and 20% fuel consumption. Black numbers: 1250 K; red numbers: 950 K; blue numbers: 700 K. (For interpretation of the references to color in this figure legend, the reader

is referred to the web version of this article).

7. Conclusions

This work represents the first ignition delay study of 1-butene oxidation at elevated pressures in a HPST and in a RCM over a wide range of pressures, temperatures and equivalence ratios. The results presented greatly expand the ignition delay time database available for mechanism validation for 1-butene oxidation.

It was found that an increase in reflected shock pressure resulted in shorter ignition delay times (higher reactivity) for all equivalence ratios investigated, which is typical of the influence of pressure on fuel reactivity. The effect of equivalence ratio on ignition delay times depended on the temperature of the experiment, where all mixtures had similar reactivity at higher temperatures and fuel-rich mixtures were most reactive at lower temperatures.

A detailed chemical kinetic mechanism has been developed to describe the combustion of 1-butene. It includes comprehensive low- and high temperature reaction pathways specific to unsaturated fuel molecules. Important reactions were identified through sensitivity and flux analyses. Rate constants have been adopted from experimental and theoretical studies where possible. How- ever, for reactions where the literature is lacking, rate constants were calculated from ab initio methods or estimated. The mechanism is validated against our new experiments and relevant literature data. The current mechanism captures well most of the experimental results of ignition delay times, as well as flame speeds [9], species profiles from a JSR [4], a premixed flame [7] and a flow reactor

[6].

From a kinetic point of view, it is found that H-atom abstraction from 1-butene by hydroxyl radicals significantly inhibits reactivity through the entire temperature range, as this reaction consumes very reactive hydroxyl radical to produce relatively unreactive stabilized 1-methyallyl ($\dot{C}_4H_7$1-3) radical. So the reactivity of 1-butene largely relies on the oxidation chemistry of this allylic radical, at high temperatures, it is mainly involved in the reactions on C_4H_7 potential and direct H-atom abstraction by molecular oxygen, and at intermediate and low temperatures, it is mainly involved in the bimolecular reactions with methyl and hydroperoxyl radicals. In addition, H-atom abstraction reactions from the other three different types of hydrogen atom (methyl site, primary and secondary vinylic C atom site) also show the importance at different temperature range, with methyl site H-atom abstraction inhibiting the reactivity at low temperature and vinylic site H-atom abstraction promoting the reactivity at intermediate temperature.

Together with the 2-butene study by Li *et al.* [19], it is also worth noting that, in 1-butene oxidation system, H-atom abstraction by molecular oxygen from allylic H-atom site in 1-butene and 2-butene promotes and inhibits reactivity respectively, and vice versa in 2-butene oxidation system. This is because the chain branching reaction between 1-butene and molecular oxygen forms two radicals, which ultimately promotes the reactivity, however the thermochemistry drives $\dot{C}_4H_7$1-3 and $H\dot{O}_2$ radicals results in the formation of two stable species: 2-butene and molecular oxygen, this chain terminating

reaction inhibits the reactivity. Thus both the 1- and 2-butene oxidation mechanisms are intrinsically linked and need to be considered simultaneously.

As to the future research efforts, theoreticians and experimentalists are motivated to: a) accurately determine the low- temperature kinetic (rate constants and thermodynamic proper- ties) of 1-methylallyl and n -butanol radicals and b) develop the rate rules of the important reaction classes for larger unsaturated hydrocarbons.

Acknowledgments

The authors thank the entire group members at Combustion Chemistry Centre for helpful discussions. This work at NUI Galway was supported by Saudi Aramco under the FUELCOM program.

Supplementary materials

Supplementary material associated with this article can be found, in the online version, at doi:10.1016/j.combustflame.2017.03. 023.

References

[1] G.E.H. James H. Gary, Mark J. Kaiser, Petroleum Refining: Technology and Economics, CRC Press2007.

[2] L. Pan, E. Hu, J. Zhang, Z. Tian, X. Li, Z. Huang, A high pressure shock tube study of 1-butene oxidation and its comparison with n-butane and alkenes, Fuel 157 (2015) 21-27.

[3] B. Heyberger, N. Belmekki, V. Conraud, P.-A. Glaude, R. Fournet, F. Battin-Leclerc, Oxidation of small alkenes at high temperature, Int. J. Chem. Kinet. 34 (2002) 666-677.

[4] Y. Fenard, G. Dayma, F. Halter, F. Foucher, Z. Serinyel, P. Dagaut, Experimental and Modeling Study of the Oxidation of 1-Butene and cis-2-Butene in a Jet-Stirred Reactor and a Combustion Vessel, Energy & Fuels 29 (2015) 1107-1118.

[5] A. Chakir, M. Cathonnet, J.C. Boettner, F. Gaillard, Kinetic study of 1-butene oxidation in a jet-stirred flow reactor, Symposium (International) on Combustion 22 (1989) 873-881.

[6] Y. Zhang, J. Cai, L. Zhao, J. Yang, H. Jin, Z. Cheng, Y. Li, L. Zhang, F. Qi, An experimental and kinetic modeling study of three butene isomers pyrolysis at low pressure, Combust. Flame 159 (2012) 905-917.

[7] M. Schenk, L. Leon, K. Moshammer, P. Oßwald, T. Zeuch, L. Seidel, F. Mauss, K. Kohse-Höinghaus, Detailed mass spectrometric and modeling study of isomeric butene flames, Combust. Flame 160 (2013) 487-503.

[8] S.G. Davis, C.K. Law, Determination of and Fuel Structure Effects on

Laminar Flame Speeds of C1 to C8 Hydrocarbons, Combust. Sci. Technol. 140 (1998) 427-449.

[9] P. Zhao, W. Yuan, H. Sun, Y. Li, A.P. Kelley, X. Zheng, C.K. Law, Laminar flame speeds, counterflow ignition, and kinetic modeling of the butene isomers, Proc. Combust. Inst. 35 (2015) 309-316.

[10] K. Hoyermann, Mau, T. Zeuch, A detailed chemical reaction mechanism for the oxidation of hydrocarbons and its application to the analysis of benzene formation in fuel-rich premixed laminar acetylene and propene flames, PCCP 6 (2004) 3824-3835.

[11] W.K. Metcalfe, S.M. Burke, S.S. Ahmed, H.J. Curran, A Hierarchical and Comparative Kinetic Modeling Study of C1 − C2 Hydrocarbon and Oxygenated Fuels, Int. J. Chem. Kinet. 45 (2013) 638-675.

[12] Y.X. Wang H, Joshi AV, Davis SG, Laskin A, Egolfopoulos F, USC Mech Version II. High-temperature combustion reaction model of H2/CO/C1–C4 compounds.

[13] N.M. Marinov, W.J. Pitz, C.K. Westbrook, A.M. Vincitore, M.J. Castaldi, S.M. Senkan, C.F. Melius, Aromatic and Polycyclic Aromatic Hydrocarbon Formation in a Laminar Premixed n-Butane Flame, Combust. Flame 114 (1998) 192-213.

[14] W.J. Pitz, C.K. Westbrook, W.M. Proscia, F.L. Dryer, Twentieth Symposium (International) on CombustionA comprehensive chemical kinetic reaction mechanism for the oxidation of N-butane, Symposium (International) on Combustion 20 (1985) 831-843.

[15] W.J. Pitz, C.K. Westbrook, Chemical kinetics of the high pressure oxidation of n-butane and its relation to engine knock, Combust. Flame 63 (1986) 113-133.

[16] S.M. Burke, W. Metcalfe, O. Herbinet, F. Battin-Leclerc, F.M. Haas, J. Santner, F.L. Dryer, H.J. Curran, An experimental and modeling study of propene oxidation. Part 1: Speciation measurements in jet-stirred and flow reactors, Combust. Flame 161 (2014) 2765-2784.

[17] S.M. Burke, U. Burke, R. Mc Donagh, O. Mathieu, I. Osorio, C. Keesee, A. Morones, E.L. Petersen, W. Wang, T.A. DeVerter, M.A. Oehlschlaeger, B. Rhodes, R.K. Hanson, D.F. Davidson, B.W. Weber, C.-J. Sung, J. Santner, Y. Ju, F.M. Haas, F.L. Dryer, E.N. Volkov, E.J.K. Nilsson, A.A. Konnov, M. Alrefae, F. Khaled, A. Farooq, P. Dirrenberger, P.-A. Glaude, F. Battin-Leclerc, H.J. Curran, An experimental and modeling study of propene oxidation. Part 2: Ignition delay time and flame speed measurements, Combust. Flame 162 (2015) 296-314.

[18] C.-W. Zhou, Y. Li, E. O'Connor, K.P. Somers, S. Thion, C. Keesee, O. Mathieu, E.L. Petersen, T.A. DeVerter, M.A. Oehlschlaeger, G. Kukkadapu, C.-J. Sung, M. Alrefae, F. Khaled, A. Farooq, P. Dirrenberger, P.-A. Glaude, F. Battin-Leclerc, J. Santner, Y. Ju, T. Held, F.M. Haas, F.L. Dryer, H.J. Curran, A comprehensive experimental and modeling study of isobutene oxidation, Combust. Flame 167 (2016) 353-379.

[19] Y. Li, C.-W. Zhou, K.P. Somers, K. Zhang, H.J. Curran, The oxidation of 2-butene: A high pressure ignition delay, kinetic modeling study and reactivity

comparison with isobutene and 1-butene, Proc. Combust. Inst. 36 (2017) 403-411.

[20] C. Morley, Gaseq, version 0.76, (2004).

[21] D. Darcy, C.J. Tobin, K. Yasunaga, J.M. Simmie, J. Würmel, W.K. Metcalfe, T. Niass, S.S. Ahmed, C.K. Westbrook, H.J. Curran, A high pressure shock tube study of n-propylbenzene oxidation and its comparison with n-butylbenzene, Combust. Flame 159 (2012) 2219-2232.

[22] E.L. Petersen, M.J.A. Rickard, M.W. Crofton, E.D. Abbey, M.J. Traum, D.M. Kalitan, A facility for gas- and condensed-phase measurements behind shock waves, Meas. Sci. Technol. 16 (2005) 1716-1729.

[23] Z. Zhang, E. Hu, L. Pan, Y. Chen, J. Gong, Z. Huang, Shock-Tube Measurements and Kinetic Modeling Study of Methyl Propanoate Ignition, Energy & Fuels 28 (2014) 7194-7202.

[24] W.S. Affleck, A. Thomas, An Opposed Piston Rapid Compression Machine for Preflame Reaction Studies, Proceedings of the Institution of Mechanical Engineers 183 (1968) 365-387.

[25] L. Brett, J. Macnamara, P. Musch, J.M. Simmie, Simulation of methane autoignition in a rapid compression machine with creviced pistons, Combust. Flame 124 (2001) 326-329.

[26] CHEMKIN-PRO 15101, Reaction Design, San Diego, 2010.

[27] C.K. Westbrook, W.J. Pitz, J.E. Boercker, H.J. Curran, J.F. Griffiths, C. Mohamed, M. Ribaucour, Detailed chemical kinetic reaction mechanisms for autoignition of isomers of heptane under rapid compression, Proc. Combust.

Inst. 29 (2002) 1311-1318.

[28] S. Tanaka, F. Ayala, J.C. Keck, A reduced chemical kinetic model for HCCI combustion of primary reference fuels in a rapid compression machine, Combust. Flame 133 (2003) 467-481.

[29] M. Ribaucour, R. Minetti, L.R. Sochet, H.J. Curran, W.J. Pitz, C.K. Westbrook, Ignition of isomers of pentane: An experimental and kinetic modeling study, Proc. Combust. Inst. 28 (2000) 1671-1678.

[30] Y. Zhao, D.G. Truhlar, The M06 suite of density functionals for main group thermochemistry, thermochemical kinetics, noncovalent interactions, excited states, and transition elements: two new functionals and systematic testing of four M06-class functionals and 12 other functionals, Theor. Chem. Acc. 120 (2008) 215-241.

[31] M. J.E.A Frisch, Gaussian 09, Gaussian, Inc., Wallingford, 2009.

[32] J.M.L. Martin, Ab initio total atomization energies of small molecules — towards the basis set limit, Chem. Phys. Lett. 259 (1996) 669-678.

[33] D. Feller, D.A. Dixon, Extended benchmark studies of coupled cluster theory through triple excitations, The Journal of Chemical Physics 115 (2001) 3484-3496.

[34] S. Glasstone, K.J. Laidler, H. Eyring, Theory of rate processes, McGraw-Hill, New York, 1941.

[35] C. Eckart, The Penetration of a Potential Barrier by Electrons, Physical Review 35 (1930) 1303-1309.

[36] A.Y. Chang, J.W. Bozzelli, A.M. Dean, Kinetic Analysis of Complex

Chemical Activation and Unimolecular Dissociation Reactions using QRRK Theory and the Modified Strong Collision Approximation, Zeitschrift für Physikalische Chemie International journal of research in physical chemistry and chemical physics, 2000, pp. 1533.

[37] P.R. Westmoreland, J.B. Howard, J.P. Longwell, A.M. Dean, Prediction of rate constants for combustion and pyrolysis reactions by bimolecular QRRK, AlChE J. 32 (1986) 1971-1979.

[38] S.W. Benson, Thermochemical kinetics, Wiley, 1976.

[39] S.M. Burke, J.M. Simmie, H.J. Curran, Critical Evaluation of Thermochemical Properties of C1–C4 Species: Updated Group-Contributions to Estimate Thermochemical Properties, J. Phys. Chem. Ref. Data 44 (2015) 013101.

[40] E.R. Ritter, J.W. Bozzelli, THERM: Thermodynamic property estimation for gas phase radicals and molecules, Int. J. Chem. Kinet. 23 (1991) 767-778.

[41] A. Kéromnès, W.K. Metcalfe, K.A. Heufer, N. Donohoe, A.K. Das, C.-J. Sung, J. Herzler, C. Naumann, P. Griebel, O. Mathieu, M.C. Krejci, E.L. Petersen, W.J. Pitz, H.J. Curran, An experimental and detailed chemical kinetic modeling study of hydrogen and syngas mixture oxidation at elevated pressures, Combust. Flame 160 (2013) 995-1011.

[42] U. Burke, K.P. Somers, P. O'Toole, C.M. Zinner, N. Marquet, G. Bourque, E.L. Petersen, W.K. Metcalfe, Z. Serinyel, H.J. Curran, An ignition delay and kinetic modeling study of methane, dimethyl ether, and their mixtures at high pressures, Combust. Flame 162 (2015) 315-330.

[43] K.P. Somers, J.M. Simmie, F. Gillespie, C. Conroy, G. Black, W.K. Metcalfe, F. Battin-Leclerc, P. Dirrenberger, O. Herbinet, P.-A. Glaude, P. Dagaut, C. Togbé, K. Yasunaga, R.X. Fernandes, C. Lee, R. Tripathi, H.J. Curran, A comprehensive experimental and detailed chemical kinetic modelling study of 2,5-dimethylfuran pyrolysis and oxidation, Combust. Flame 160 (2013) 2291-2318.

[44] S.S. Vasu, L.K. Huynh, D.F. Davidson, R.K. Hanson, D.M. Golden, Reactions of OH with Butene Isomers: Measurements of the Overall Rates and a Theoretical Study, J. Phys. Chem. A 115 (2011) 2549-2556.

[45] J. Zador, A.W. Jasper, J.A. Miller, The reaction between propene and hydroxyl, PCCP 11 (2009) 11040-11053.

[46] J.-C. Loison, J. Daranlot, A. Bergeat, F. Caralp, R. Mereau, K.M. Hickson, Gas-Phase Kinetics of Hydroxyl Radical Reactions with C3H6 and C4H8: Product Branching Ratios and OH Addition Site-Specificity, J. Phys. Chem. A 114 (2010) 13326-13336.

[47] J.D. DeSain, S.J. Klippenstein, J.A. Miller, C.A. Taatjes, Measurements, Theory, and Modeling of OH Formation in Ethyl + O2 and Propyl + O2 Reactions, J. Phys. Chem. A 107 (2003) 4415-4427.

[48] C.F. Goldsmith, W.H. Green, S.J. Klippenstein, Role of O2 + QOOH in Low-Temperature Ignition of Propane. 1. Temperature and Pressure Dependent Rate Coefficients, J. Phys. Chem. A 116 (2012) 3325-3346.

[49] W. Tsang, Chemical Kinetic Data Base for Combustion Chemistry Part V. Propene, J. Phys. Chem. Ref. Data 20 (1991) 221-273.

[50] A. Miyoshi, Systematic Computational Study on the Unimolecular Reactions of Alkylperoxy (RO2), Hydroperoxyalkyl (QOOH), and Hydroperoxyalkylperoxy (O2QOOH) Radicals, J. Phys. Chem. A 115 (2011) 3301-3325.

[51] H. Sun, J.W. Bozzelli, C.K. Law, Thermochemical and Kinetic Analysis on the Reactions of O2 with Products from OH Addition to Isobutene, 2-Hydroxy-1,1-dimethylethyl, and 2-Hydroxy-2-methylpropyl Radicals: HO2 Formation from Oxidation of Neopentane, Part II, J. Phys. Chem. A 111 (2007) 4974-4986.

[52] W. Tsang, R.F. Hampson, Chemical Kinetic Data Base for Combustion Chemistry. Part I. Methane and Related Compounds, J. Phys. Chem. Ref. Data 15 (1986) 1087-1279.

[53] J. Zádor, S.J. Klippenstein, J.A. Miller, Pressure-Dependent OH Yields in Alkene + HO2 Reactions: A Theoretical Study, J. Phys. Chem. A 115 (2011) 10218-10225.

[54] S.M. Villano, H.-H. Carstensen, A.M. Dean, Rate Rules, Branching Ratios, and Pressure Dependence of the HO2 + Olefin Addition Channels, J. Phys. Chem. A 117 (2013) 6458-6473.

[55] S. Sharma, S. Raman, W.H. Green, Intramolecular Hydrogen Migration in Alkylperoxy and Hydroperoxyalkylperoxy Radicals: Accurate Treatment of Hindered Rotors, J. Phys. Chem. A 114 (2010) 5689-5701.

[56] S.M. Villano, L.K. Huynh, H.-H. Carstensen, A.M. Dean, High-Pressure Rate Rules for Alkyl + O2 Reactions. 2. The Isomerization, Cyclic Ether

Formation, and β-Scission Reactions of Hydroperoxy Alkyl Radicals, J. Phys. Chem. A 116 (2012) 5068-5089.

[57] S.M. Villano, L.K. Huynh, H.-H. Carstensen, A.M. Dean, High-Pressure Rate Rules for Alkyl + O2 Reactions. 1. The Dissociation, Concerted Elimination, and Isomerization Channels of the Alkyl Peroxy Radical, J. Phys. Chem. A 115 (2011) 13425-13442.

[58] A. Miyoshi, Molecular size dependent falloff rate constants for the recombination reactions of alkyl radicals with O2 and implications for simplified kinetics of alkylperoxy radicals, Int. J. Chem. Kinet. 44 (2012) 59-74.

[59] J.A. Miller, S.J. Klippenstein, From the Multiple-Well Master Equation to Phenomenological Rate Coefficients: Reactions on a C3H4 Potential Energy Surface, J. Phys. Chem. A 107 (2003) 2680-2692.

[60] J.A. Miller, S.J. Klippenstein, Master Equation Methods in Gas Phase Chemical Kinetics, J. Phys. Chem. A 110 (2006) 10528-10544.

[61] A. Fridlyand, P.T. Lynch, R.S. Tranter, K. Brezinsky, Single Pulse Shock Tube Study of Allyl Radical Recombination, J. Phys. Chem. A 117 (2013) 4762-4776.

[62] M.M. Kopp, N.S. Donato, E.L. Petersen, W.K. Metcalfe, S.M. Burke, H.J. Curran, Oxidation of Ethylene–Air Mixtures at Elevated Pressures, Part 1: Experimental Results, J. Propul. Power 30 (2014) 790-798.

[63] M.M. Kopp, E.L. Petersen, W.K. Metcalfe, S.M. Burke, H.J. Curran, Oxidation of Ethylene—Air Mixtures at Elevated Pressures, Part 2: Chemical

Kinetics, J. Propul. Power 30 (2014) 799-811.

[64] C.F. Goldsmith, L.B. Harding, Y. Georgievskii, J.A. Miller, S.J. Klippenstein, Temperature and Pressure-Dependent Rate Coefficients for the Reaction of Vinyl Radical with Molecular Oxygen, J. Phys. Chem. A 119 (2015) 7766-7779.

[65] S.M. Sarathy, S. Vranckx, K. Yasunaga, M. Mehl, P. Oßwald, W.K. Metcalfe, C.K. Westbrook, W.J. Pitz, K. Kohse-Höinghaus, R.X. Fernandes, H.J. Curran, A comprehensive chemical kinetic combustion model for the four butanol isomers, Combust. Flame 159 (2012) 2028-2055.

[66] D.J.M. Ray, D.J. Waddington, Gas phase oxidation of alkenes—Part II. The oxidation of 2-methylbutene-2 and 2,3-dimethylbutene-2, Combust. Flame 20 (1973) 327-334.

[67] M.I. Sway, D.J. Waddington, Reactions of oxygenated radicals in the gas phase. Part 12. The reactions of isopropylperoxyl radicals and alkenes, Journal of the Chemical Society, Perkin Transactions 2, doi:10.1039/P29830000139(1983) 139-143.

Theoretical Kinetics Analysis for Ḣ Atom Addition to 1,3-Butadiene and Related Reactions on the $\dot{C}_4H_7$ Potential Energy Surface

Author contributions

Yang Li: Obtained all ignition delay time experimental data on high pressure shock tube and rapid compression machine, conducted all modelling work, and wrote the manuscript.

Stephen J. Klippenstein: Provided the MESS code, input for calculation efforts, and reviewed the manuscript.

Chong-Wen Zhou: Provided input for calculation efforts, and reviewed the manuscript.

Henry J. Curran: Managed the project throughout, and reviewed manuscript prior to and post the review process.

Brief description of the paper

In this paper, the rate constants and thermodynamic properties for Ḣ-atom addition to 1,3-butadiene and related reactions on the $\dot{C}_4H_7$ potential energy surface have been calculated using two different series of quantum chemical methods and two different kinetic codes. Excellent agreement is obtained between the two different kinetics codes. The calculated results including zero-point energies, single-point energies, rate constants, barrier heights, and thermochemistry are systematically compared among the two quantum chemical methods. 1-Methylallyl ($\dot{C}_4H_7$1-3) and 3-buten-1-yl ($\dot{C}_4H_7$1-4) radicals and C_2H_4 + $\dot{C}_2H_3$ are found to be the most important channels and reactivity-promoting products, respectively. We calculated that terminal addition is dominant (>80%) compared to internal Ḣ-atom addition at all temperatures in the range 298−2000 K. However, this dominance decreases with increasing temperature. The calculated rate constants for the bimolecular reaction C_4H_6 + Ḣ → products and C_2H_4 + $\dot{C}_2H_3$ → products are in excellent agreement with both experimental and theoretical results from the literature. For selected C_4 species, the calculated thermochemical values are also in good agreement with literature data.

Theoretical Kinetics Analysis for Ḣ Atom Addition to 1,3-Butadiene and Related Reactions on the $\dot{C}_4H_7$ Potential Energy Surface

Yang Li, Stephen J. Klippenstein, Chong-Wen Zhou, Henry J. Curran

Combustion Chemistry Centre, National University of Ireland, Galway, Ireland

Chemical Sciences and Engineering Division, Argonne National Laboratory, Argonne, Illinois 60439, United States

School of Energy and Power Engineering, Beihang University, Beijing 100191, P. R. China

Published in: *J. Phys. Chem. A 121 (2017) 7433-7445*

Abstract

The oxidation chemistry of the simplest conjugated hydrocarbon, 1,3-butadiene, can provide a first step in understanding the role of polyunsaturated hydrocarbons in combustion and, in particular, an understanding of their contribution toward soot formation. On the basis of our previous work on propene and the butene isomers (1-, 2-, and isobutene), it was found that the reaction kinetics of Ḣ-atom addition to the C=C double bond plays a significant role in fuel consumption kinetics and influences the predictions of high-temperature ignition delay times, product species concentrations, and flame speed measurements. In this study, the rate constants and thermodynamic properties for Ḣ-atom addition to 1,3-butadiene and related reactions on the $\dot{C}_4H_7$ potential energy surface have been calculated using two different series of quantum chemical methods and two different kinetic codes. Excellent agreement is obtained between the two different kinetics codes. The

calculated results including zero-point energies, single-point energies, rate constants, barrier heights, and thermochemistry are systematically compared among the two quantum chemical methods. 1-Methylallyl ($\dot{C}_4H_7$1-3) and 3-buten-1-yl ($\dot{C}_4H_7$1-4) radicals and C_2H_4 + $\dot{C}_2H_3$ are found to be the most important channels and reactivity-promoting products, respectively. We calculated that terminal addition is dominant (>80%) compared to internal Ḣ-atom addition at all temperatures in the range 298−2000 K. However, this dominance decreases with increasing temperature. The calculated rate constants for the bimolecular reaction C_4H_6 + Ḣ → products and C_2H_4 + $\dot{C}_2H_3$ → products are in excellent agreement with both experimental and theoretical results from the literature. For selected C_4 species, the calculated thermochemical values are also in good agreement with literature data. In addition, the rate constants for H atom abstraction by Ḣ atoms have also been calculated, and it is found that abstraction from the central carbon atoms is the dominant channel (>70%) at temperatures in the range of 298−2000 K. Finally, by incorporating our calculated rate constants for both Ḣ atom addition and abstraction into our recently developed 1,3-butadiene model, we show that laminar flame speed predictions are significantly improved, emphasizing the value of this study.

1. Introduction

In our recent mechanism development studies for propene,[1,2] 1-butene,3 2-butene,[4] isobutene,[5] and 1,3-butadiene[6] oxidation, the reaction kinetics for

Ḣ-atom addition to the C=C double bond was found to be critical in predicting high-temperature ignition delay times, speciation and flame speeds. For the 1-methylallyl ($\dot{C}_4H_7$1-3) radical, which is a key intermediate in 1,3-butadiene oxidation, isomerization, Ḣ-atom elimination, and β-scission reactions are the major consumption pathways at high temperatures (>1100 K). Over the past 30 years, there have been a number of modeling, theoretical, and experimental studies of 1,3-butadiene oxidation. For example, Laskin et al.[7] studied the kinetics of 1,3-butadiene oxidation over the 1035−1185 K temperature regime using a detailed kinetic model. They found that the chemically activated reaction of Ḣ atoms with 1,3-butadiene to produce ethylene and vinyl radicals is the most important channel in all of their experimental conditions. These observations point to the importance of understanding the kinetics of reactions on the Ċ4H7 potential energy surface (PES).

Reactions on the $\dot{C}_4H_7$ PES have been the subject of a number of prior theoretical studies. Miller et al.8 used the G3//B3LYP quantum chemical method to calculate the geometries, vibrational frequencies, and energies of five $\dot{C}_4H_7$ radical isomers and transition states for the corresponding dissociation and isomerization reactions on the Ċ4H7 PES. Miyoshi et al.[9] reported CBS-QB3-based ab initio Rice Ramsperger Kassel Marcus (RRKM) and master equation (ME) calculations of the reaction kinetics for 3-butenyl and 3-butenylperoxy radicals. Xu et al.[10] performed a series of CBS-QB3 based quantum RRK/modified strong collider analyses for the reactions on the $\dot{C}_3H_7$, $\dot{C}_4H_7$, and $\dot{C}_4H_9$ potential energy surfaces in order to characterize the radical

addition reactions that lead to molecular weight growth. Most recently, Huang et al.[11] explored the complete $\dot{C}_4H_7$ PES at the CCSD(T)-F12/cc-pVTZ-F12//QCISD/6-311++G(2df,2p) level, including both straight-chain and branched backbones. They also explored the kinetics with RRKM/ME calculations covering the range from 800 to 2500 K and 0.01 to 100 atm. Their calculations indicate that the transformation from i-$\dot{C}_4H_7$ to the straight-chain $\dot{C}_4H_7$ radical is kinetically unfavorable due to the high strain energy of the three-membered ring structure in the transition state.

Shestov et al.[12] investigated the bimolecular reaction $C_2H_4 + \dot{C}_2H_3$ using the laser photolysis/photoionization mass spectrometry technique in the temperature range of 625−950 K and bath gas (helium) densities of (6−12) × 1016 atom cm^{-3}. C_4H_6 and $\dot{C}_4H_7$ were detected as the primary products, and the thermal stability of the $\dot{C}_4H_7$ radical at 950 K indicated that it is a delocalized radical. The observed total reaction rate constant was represented by the expression $k_1 = 10^{-11.69\pm0.44} \exp(-2830 \pm 790\ K/T)\ cm^3\ molecule^{-1}\ s^{-1}$.

Ismail et al.[13] reported direct measurements of absolute rate coefficients for the $\dot{C}_2H_3 + C_2H_4$ reaction over the temperature range of 300−700 K and at 20 and 133 mbar. The measured results at a pressure of 20 mbar were in good agreement with previous determinations for the $\dot{C}_2H_3 + C_2H_4$ bimolecular reaction at higher temperatures (600−750 K). At a pressure of 133 mbar, the observed rate constants were fit to a modified three-parameter Arrhenius expression: $k = (7 \pm 1) \times 10^{-14}\ (T/298\ K)^2 \exp[-(1430 \pm 70)\ K/T]\ cm^3\ molecule^{-1}\ s^{-1}$.

The objectives of the current study are to calculate the thermodynamic properties and rate coefficients for Ḣ-atom addition to 1,3-butadiene and its related reactions on the $\dot{C}_4H_7$ PES using ab initio TST methods. Moreover, comprehensive comparisons are carried out between (i) two different series of ab initio methods, (ii) two different kinetic program codes, namely, MultiWell[14] and PAPR[15] and (iii) calculated results and experimental data in the literature.

2. Theoretical and Computational Approach

In this study, two different series of ab initio electronic structure methods have been applied using Gaussian 09[16] as summarized in Table 1.

Table 1: Quantum chemical methods used for rate coefficient and thermochemistry calculations.

	Method 1	Method 2
Geometry & Frequency	M06-2X/6-311++G(d,p)	wB97XD/aug-cc-pVTZ
Scan & IRC	M06-2X/6-311++G(d,p)	
Electronic Energy	–	CCSD(T)/aug-cc-pVTZ
	CCSD(T)/cc-pVTZ	MP2/aug-cc-pVTZ
	CCSD(T)/cc-pVQZ	MP2/aug-cc-pVQZ
Zero Kelvin Energy	CBS-APNO/G3/G4	

In the first series of calculations, the M06-2X[17] method with the 6-311++G(d,p)[18,19] basis set was used for the geometry optimizations, vibrational frequency calculations, and also the hindered rotation treatments for lower-frequency modes. All vibrational frequencies and zero-point vibrational

energies (ZPVEs) were scaled by 0.983 and 0.9698, respectively, which was recommended for the M06-2X functional by Zhao and Truhlar.[17] The electronic single-point energies (SPEs) were calculated at the CCSD(T)/cc-pVXZ level of theory (where X = T and Q),[20,21] and the resulting SPEs were extrapolated to the complete basis set (CBS) limit using the following formula:[22,23]

$$E_{CBS} = E_{CCSD(T)/cc-pVQZ} + (E_{CCSD(T)/cc-pVQZ} - E_{CCSD(T)/cc-pVTZ}) * 4^4/(5^4 - 4^4)$$

In the second series, the geometry optimizations and frequency calculations were carried out at the wB97XD/aug-cc-pVTZ[24–26] level of theory. Meanwhile, single-point energies were obtained from a combination of CCSD(T)/aug-cc-pVTZ, MP2/aug-cc-pVTZ and MP2/aug-cc-pVQZ[27] calculations:

$$E_{CBS} = (E_{MP2/aug-cc-pVQZ} - E_{MP2/aug-cc-pVTZ}) + E_{CCSD(T)/aug-cc-pVTZ}$$

In both quantum chemical methods, internal rotations that correspond to low-frequency torsional modes were scanned in 10 degree increments as a function of dihedral angle using the M06-2X/6-311++G(d,p) method. This method was also used to perform intrinsic reaction coordinate (IRC) calculations[28] on each transition state (TS) to ensure it was connected to the desired reactants and products. The T_1 diagnostic[29] for all reactant species is ≤0.025, which indicates the reliability of single-reference methods for describing the wave function. T_1 values for all the TSs are ≤0.044. Klippenstein et al.[30] mentioned that T_1 values of radical species that are greater than 0.03

become a cause for concern. On this $\dot{C}_4H_7$ PES, only 5 of the 23 complexes have T_1 values greater than 0.035. For those few cases, either multireference or higher-order coupled cluster calculations would be recommended for higher accuracies.

For the MultiWell[14] program suite calculation, the Lamm module was used to calculate both external rotational constants and reduced moment of inertia for the hindered internal rotations. The calculated results were then fitted to truncated Fourier series, which were further used as 1-D hindered internal rotation input in the Thermo module. The high-pressure limit (HPL) rate coefficients were finally calculated by the Thermo module as a function of temperature (298.15−2000 K) based on canonical transition-state theory (TST).[31]

In the PAPR[15] program suite calculation, the Master Equation System Solver (MESS) was used to calculate temperature and pressure-dependent rate coefficients for complex-forming reactions via solution of the one-dimensional ME, with the chemical transformations described using RRKM theory.[32−36] Rate coefficients for the thermally and chemically activated reactions are obtained at temperatures ranging from 298.15 to 2000 K, and at pressures ranging from 0.01 to 100 atm. The internal rotors corresponding to methyl and ethyl like torsions were treated as one-dimensional hindered rotors with hindrance potentials evaluated at the M06-2X/6-311++G(d,p) level of theory. However, the reduced moment of inertia is calculated on the basis of the structure of the most stable species, the axis of rotation, and the identity of all

the atoms on each side of the rotated bond. Although an algorithm that properly treats the internal rotation variation of both the internal and external rotational constants is available in MESS, for simplicity we assumed that the internal and external moments of inertia are constant (i.e., not a function of the dihedral angle). Note that this assumption is justified by the fact that the neglect of the coupling of external and internal rotation often counterbalances the neglect of the dihedral angle variance of the internal rotor moment of inertia. For the collisional model used in the master equation simulation, the interaction between the reactant and N_2 bath gas was modeled using the Lennard-Jones (L-J) potential.[37] The L-J parameters were calculated by the method described in ref [38]. For N_2, σ = 3.6 Å and ε = 68 cm^{-1} were used, while for $\dot{C}_4H_7$, σ = 4.5 Å and ε = 1450 cm^{-1} were used. The collisional energy transfer function was represented by a single-parameter exponential down model with $\langle\Delta E\rangle_{down}$ = 200 × $(T/300)^{0.75}$ cm^{-1}, which has served as a fairly good model for C_3, C_4 hydrocarbons.[9,39,40]

In both program suites, quantum mechanical tunneling was taken into account for an unsymmetrical Eckart barrier model.[41] The calculated rate coefficients were fitted to a modified Arrhenius expression as a function of temperature:

$$k = \mathrm{A}\left(T/T_{ref}\right)^{\mathrm{n}}\exp(-E/RT)$$

where A is the A-factor, T is the temperature in units of Kelvin, T_{ref} = 1 K, n is the temperature exponent at 1 K, and E is related to the activation energy (by

Ea = E + nRT).

As to the quantum chemical methods for the thermodynamic properties calculation, the average atomization formation enthalpies for all of the C_4 species on the $\dot{C}_4H_7$ PES were carried out using a combined compound method CBS-APNO/G3/G4,[42–44] which was found to yield results approaching "chemical accuracy" (arbitrarily, ≈4 kJ mol^{-1} or 1 kcal mol^{-1}) when benchmarked against enthalpy of formation values in the Active Thermochemical Tables (ATcT).[45–47] The thermochemical values of interest (enthalpy of formation, entropy and heat capacity) were calculated as a function of temperature (298.15−3000 K), and these resulting values were fitted to NASA polynomials[48] using the Fitdat utility in ANSYS CHEMKIN-PRO.[49]

3. Theoretical and Computational Approach

3.1. $\dot{C}_4H_7$ Potential Energy Surface.

The results of the electronic structure calculations for the association, dissociation, and isomerization pathways are depicted in Figure 1, which contains 19 species and 23 transition states. These relative energies (with ZPE corrections included) were calculated using method 1, as outlined in Table 1, and all isomerization (red lines) and dissociation (blue lines) reaction pathways are highlighted. Note that for all the C_4H_6 and C_4H_7 species in this paper, we focus on the trans-structure, although the cis-structures are generally included implicitly in the kinetic analysis through torsional treatments.

For the reaction of Ḣ atoms with 1,3-butadiene, Ḣ atoms can add to either the terminal carbon atom to form 1-methylallyl ($\dot{C}_4H_7$1-3) radical or to the central carbon to form 3-buten-1-yl ($\dot{C}_4H_7$1-4) radical. The barrier for terminal addition is 3.32 kcal mol^{-1} lower than that for central addition, while the barrier for isomerization between these two radicals lies between the two entrance barriers. Obviously, these two entrance wells are found to be the most important wells on the $\dot{C}_4H_7$ PES. 1-Methylallyl ($\dot{C}_4H_7$1-3) radical has the lowest energy among all of the wells. Meanwhile, 3-buten-1-yl ($\dot{C}_4H_7$1-4) radical is the most "reactivity-promoting" well, leading to the formation of ethylene and vinyl radicals via β-scission.

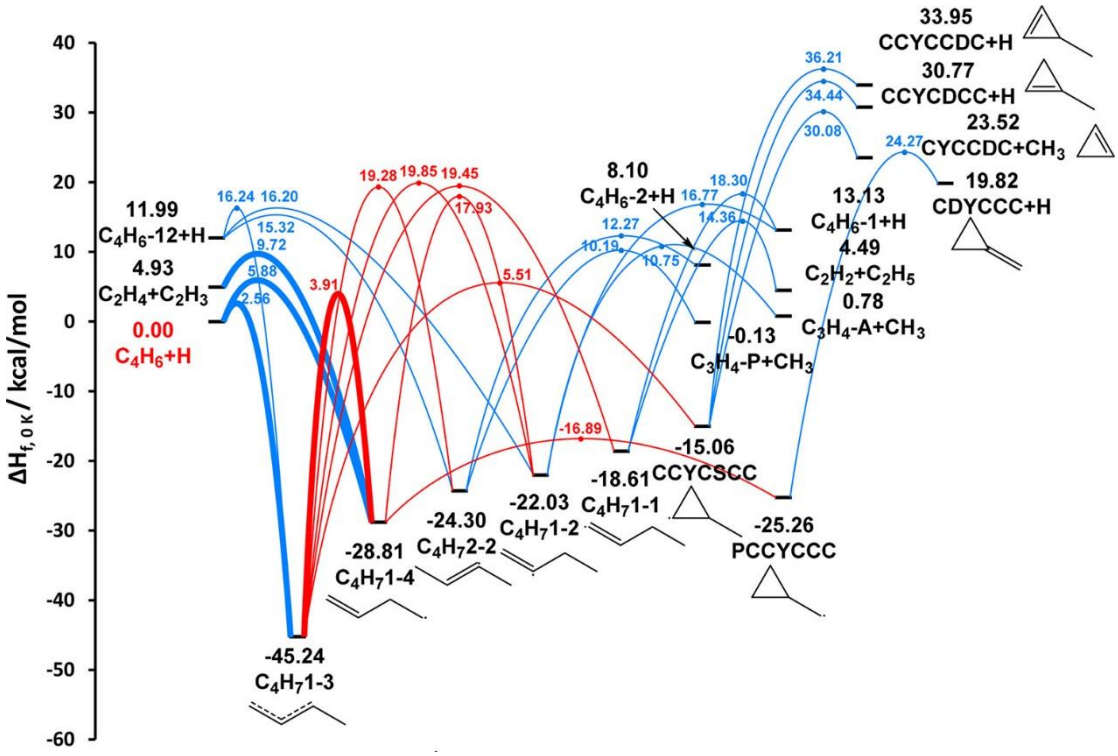

Figure 1. $\dot{C}_4H_7$ potential-energy surface.

As shown in Figure 1, the 1-methylallyl ($\dot{C}_4H_7$1-3) and 3-buten-1-yl ($\dot{C}_4H_7$1-4) radicals can isomerize to form the other three straight-chain and two

cyclic structural $\dot{C}_4H_7$ isomers: 2-buten-2-yl ($\dot{C}_4H_7$2-2), 1-buten-2-yl ($\dot{C}_4H_7$1-2), 1-buten-1-yl ($\dot{C}_4H_7$1-1), 2-methylcyclopropyl (CCYCSCC), and cyclopropyl-methyl (PCCYCCC) radicals. All of these wells can then dissociate via β-scission reactions. For the most part, the isomerization barriers are significantly higher than those of the dissociation reactions. In addition, the TSs for the isomerization reactions are much tighter than those for the dissociations. Therefore, most of the isomerization reactions are not competitive with the dissociation reactions.

Table 2: Comparison of the calculated relative energies (Δ_fH_{0K}) (kcal mol^{-1}) for all species on the $\dot{C}_4H_7$ PES.

	Method 1	Method 2	ATcT[45–47]	Huang *et al.*[11]
		Reactants		
$C_4H_6 + \dot{H}$	0.00	0.00	0.00	0.00
		Wells		
$\dot{C}_4H_7$1-3	–45.24	–44.93	–	–45.1
$\dot{C}_4H_7$1-4	–28.81	–28.79	–	–28.1
$\dot{C}_4H_7$2-2	–24.30	–24.19	–	–
$\dot{C}_4H_7$1-2	–22.03	–21.99	–	–21.7
$\dot{C}_4H_7$1-1	–18.61	–18.65	–	–
CCYCSCC	–15.06	–15.15	–	–14.3
PCCYCCC	–25.26	–25.26	–	–24.8
		Products		
C_4H_6-12 + $\dot{H}$	11.99	11.93	–	13.4
$C_2H_4 + \dot{C}_2H_3$	4.93	4.80	5.02	4.8
C_4H_6-2 + $\dot{H}$	8.10	8.17	8.10	–
C_3H_4-p + $\dot{C}H_3$	–0.13	–0.27	0.36	–

C_4H_6-1 + Ḣ	13.13	13.03	12.98	12.2
C_3H_4-a + $\dot{C}H_3$	0.78	0.66	1.44	1.2
$\dot{C}_2H_5$ + C_2H_2	4.49	4.26	4.46	–
CCYCCDC + Ḣ	33.95	33.78	–	–
CCYCDCC + Ḣ	30.77	30.68	–	–
CYCCDC + $\dot{C}H_3$	23.52	23.30	24.20	–
CDCYCCC + Ḣ	19.82	19.75	–	–

Table 3: Comparison of the calculated relative energies (Δ_fH_{0K}) (kcal mol^{-1}) for all TSs on the $\dot{C}_4H_7$ PES.

	Method 1	Method 2	Huang *et al.*[11]
TSs for Isomerization Reactions			
$\dot{C}_4H_7$1-3 ↔ $\dot{C}_4H_7$1-4	3.91	4.02	3.9
$\dot{C}_4H_7$1-3 ↔ $\dot{C}_4H_7$2-2	19.28	19.30	–
$\dot{C}_4H_7$1-3 ↔ $\dot{C}_4H_7$1-2	19.85	19.85	20.2
$\dot{C}_4H_7$1-3 ↔ $\dot{C}_4H_7$1-1	19.45	19.57	–
$\dot{C}_4H_7$1-4 ↔ $\dot{C}_4H_7$1-2	17.93	17.95	17.8
$\dot{C}_4H_7$1-3 ↔ CCYCSCC	5.51	5.53	5.2
$\dot{C}_4H_7$1-4 ↔ PCCYCCC	–16.89	–16.86	–16.8
TSs for Dissociation Reactions			
$\dot{C}_4H_7$1-3 ↔ C_4H_6-12 + Ḣ	16.24	16.06	–
$\dot{C}_4H_7$1-3 ↔ C_4H_6 + Ḣ	2.56	2.54	1.7
$\dot{C}_4H_7$1-4 ↔ C_2H_4 + $\dot{C}_2H_3$	9.72	9.69	8.8
$\dot{C}_4H_7$1-4 ↔ C_4H_6 + Ḣ	5.88	5.85	5.1
$\dot{C}_4H_7$2-2 ↔ C_4H_6-2 + Ḣ	12.27	12.10	–
$\dot{C}_4H_7$2-2 ↔ C_4H_6-12 + Ḣ	15.32	15.18	–
$\dot{C}_4H_7$2-2 ↔ C_3H_4-p + $\dot{C}H_3$	10.19	9.91	–
$\dot{C}_4H_7$1-2 ↔ C_4H_6-1 + Ḣ	16.77	16.48	16.8
$\dot{C}_4H_7$1-2 ↔ C_4H_6-12 + Ḣ	16.20	16.04	17.8

$\dot{C}_4H_7$1-2 ↔ C_3H_4-a + $\dot{C}H_3$	10.75	10.54	11.9
$\dot{C}_4H_7$1-1 ↔ C_4H_6-1 + $\dot{H}$	18.30	17.96	–
$\dot{C}_4H_7$1-1 ↔ C_2H_2 + $\dot{C}_2H_5$	14.36	14.02	–
CCYCSCC ↔ CCYCCDC + $\dot{H}$	36.21	35.94	–
CCYCSCC ↔ CCYCDCC + $\dot{H}$	34.44	34.23	–
CCYCSCC ↔ CYCCDC + $\dot{C}H_3$	30.08	29.69	–
PCCYCCC ↔ CDCYCCC + $\dot{H}$	24.27	24.04	–

The energies (relative to C_4H_6 + $\dot{H}$) of all of the species and transition states (TSs) on the $\dot{C}_4H_7$ PES have also been calculated using method 2 and are compared to those from method 1, from ATcT,[45–47] and from Huang et al.[11] in Table 2 and Table 3. The calculated energies for the two present quantum chemistry methods are all within 0.4 kcal mol^{-1}, demonstrating the internal consistency of the two methods. The CCSD(T)-F12/cc-pVTZ-F12//QCISD/6-311++G(2df,2p) results of Huang et al. are also quite similar, although differences of as much as 1.7 kcal/mol are observed.

3.2. Barrier Height Comparison.

Ibukl et al.[50] obtained the threshold energy of 33.0 kcal mol^{-1} for the 1,2-H atom shift from 3-buten-1-yl ($\dot{C}_4H_7$1-4) radical to 1-methylallyl ($\dot{C}_4H_7$1-3) radical. Miller et al.[51] investigated the unimolecular reaction dynamics of 1-buten-2-yl ($\dot{C}_4H_7$1-2) radicals using a molecular beam scattering technique. They found that with at least 30.7 ± 2 kcal mol^{-1} of internal energy, this radical underwent C−C fission to form allene and methyl radicals, and with at least 36.7 ± 4 kcal mol^{-1} of internal energy, it underwent C−H fission to form $\dot{H}$

atoms and either 1-butyne or 1,2-butadiene. McCunn et al.[52] studied the unimolecular dissociation of the 2-buten-2-yl ($\dot{C}_4H_7$2-2) radical using a crossed laser-molecular beam technique. They found that the lowest-energy dissociation barrier of C−C bond fission was 31 ± 2 kcal mol^{-1} and that there was a 7.5 ± 2 kcal mol^{-1} energy barrier for the reverse bimolecular reaction of methyl radicals with propyne.

In Table 4, the barrier heights calculated here are compared with the experimental data discussed above. First, the barriers calculated by the two quantum chemical methods are in good agreement, which are consistently within 0.4 kcal mol^{-1} of one another. Second, the calculated results agree well with the experimental data, which indicates the reliability of both methods in terms of energy calculations.

Table 4: Barrier heights for the dissociation reactions from 1-buten-1-yl ($\dot{C}_4H_7$1-1), 1-buten-2-yl ($\dot{C}_4H_7$1-2) and 2-buten-2-yl ($\dot{C}_4H_7$2-2) wells.

Reactions	Experiment	Method 1	Method 2
$\dot{C}_4H_7$1-4 ↔ $\dot{C}_4H_7$1-3	33.0	32.7	32.8
$\dot{C}_4H_7$1-2 ↔ C_3H_4-a + $\dot{C}H_3$	≤ 30.7 ± 2	32.8	32.5
$\dot{C}_4H_7$1-2 ↔ C_4H_6-12 + $\dot{H}$	≤ 36.7 ± 4	38.8	38.5
$\dot{C}_4H_7$1-2 ↔ C_4H_6-1 + $\dot{H}$	≤ 36.7 ± 4	38.2	38.0
$\dot{C}_4H_7$2-2 ↔ C_3H_4-p + $\dot{C}H_3$	≤ 31.0 ± 2	34.5	34.1
C_3H_4-p + $\dot{C}H_3$ ↔ $\dot{C}_4H_7$2-2	≤ 7.5 ± 2	10.3	10.2

3.3. Comparison of HPL Rate Constants between Two Different Quantum Chemical methods and Codes.

The HPL rate constants calculated by the two different quantum chemical methods for the thermal decomposition and isomerization reactions on the $\dot{C}_4H_7$ PES are illustrated in Figure 2a−h. The different colors used there correspond to different reactions from each well, while solid and dashed lines correspond to the results calculated from the first and second methods, respectively. At combustion temperatures (600−2000 K), the rate constants calculated using the first quantum chemical method are consistently smaller than those calculated using the second; however, the differences are within 50% of one another. This finding is consistent with the slightly higher (0.1−0.5 kcal mol^{-1}) barrier heights predicted by the first method. The small magnitude of the difference suggests that the computationally much cheaper second method still yields reasonably accurate kinetic results. All of these HPL rate constants have been fitted in a modified Arrhenius form and are provided as Supporting Information.

In order to compare the performance of the two kinetic codes, the HPL rate constants for terminal and central Ḣ-atom addition to 1,3-butadiene were calculated and their branching ratios compared over the temperature range of 600−2000 K, Table 5. Notably, for both terminal and central atom addition, the rate constants calculated using MultiWell/Thermo and PAPR are in excellent agreement, being within 3% of one another over the entire temperature range. Furthermore, the calculated branching ratio (terminal addition to central

addition) demonstrates that terminal addition dominates, with this dominance decreasing slightly with increasing temperature.

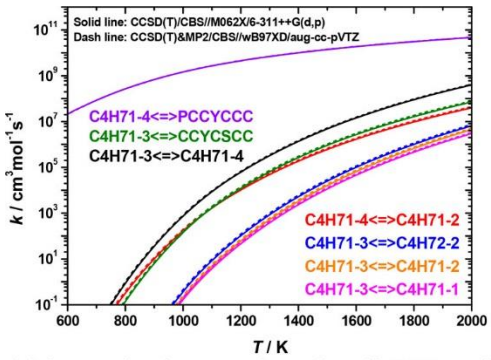

(a) isomerization reactions for all C_4H_7 wells

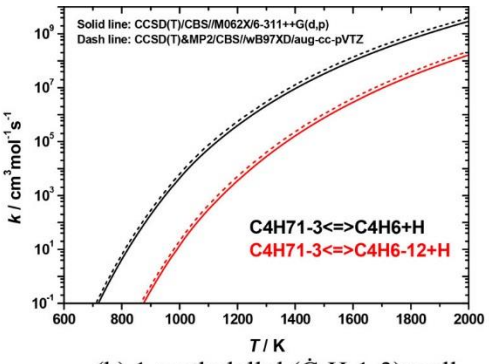

(b) 1-methylallyl ($\dot{C}_4H_7$1-3) well

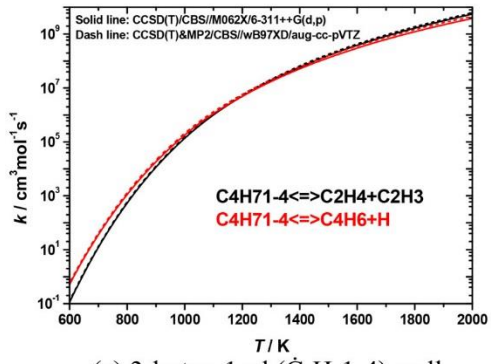

(c) 3-buten-1-yl ($\dot{C}_4H_7$1-4) well

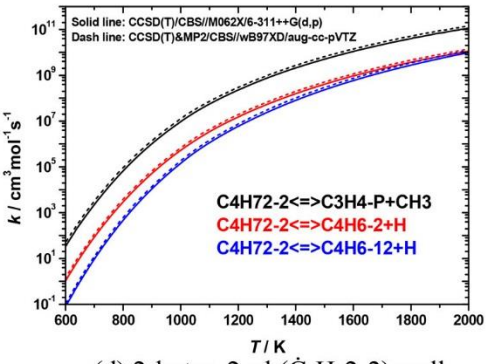

(d) 2-buten-2-yl ($\dot{C}_4H_7$2-2) well

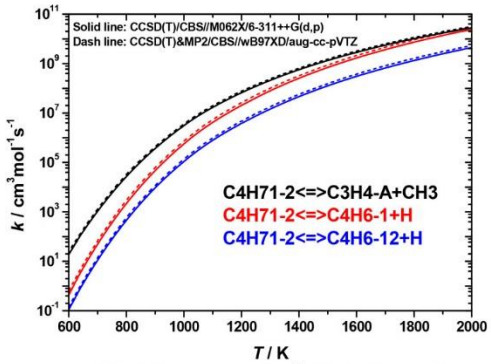

(e) 1-buten-2-yl ($\dot{C}_4H_7$1-2) well

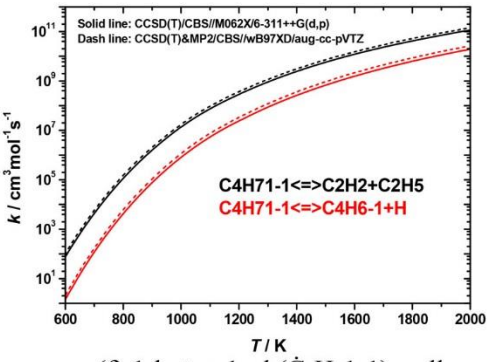

(f) 1-buten-1-yl ($\dot{C}_4H_7$1-1) well

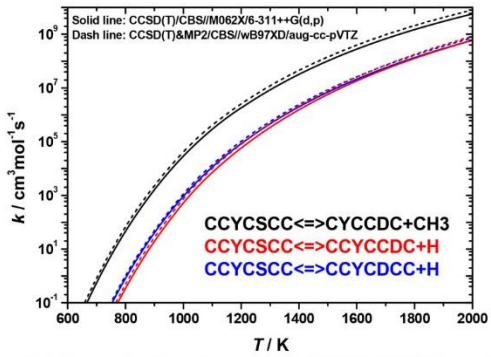

(g) 2-methylcyclopropyl (CCYCSCC) well

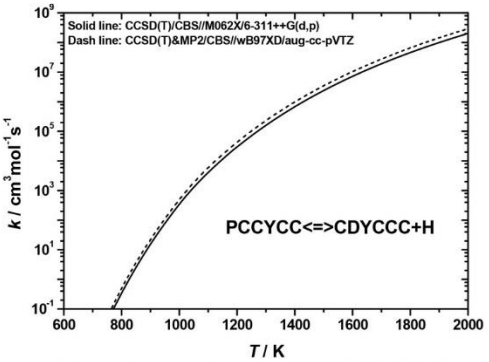

(h) cyclopropylmethyl (PCCYCCC) well

Figure 2. HPL rate constants for the isomerization and thermal decomposition reactions on the $\dot{C}_4H_7$ PES calculated by two quantum chemical methods. Solid lines: method 1; dash lines: method 2.

Table 5: Comparison of the predicted HPL rate constants for terminal and central Ḣ atom addition reactions calculated using two codes.

	MultiWell/Thermo			PAPR		
T / K	Terminal addition	Central addition	Branching ratio	Terminal addition	Central addition	Branching ratio
600	8.96E+12	4.18E+11	96 : 4	8.72E+12	4.09E+11	96 : 4
800	1.99E+13	1.67E+12	92 : 8	1.94E+13	1.64E+12	92 : 8
1000	3.47E+13	4.13E+12	89 : 11	3.37E+13	4.05E+12	89 : 11
1100	4.34E+13	5.86E+12	88 : 12	4.22E+13	5.74E+12	88 : 12
1200	5.29E+13	7.91E+12	87 : 13	5.15E+13	7.76E+12	87 : 13
1300	6.32E+13	1.03E+13	86 : 14	6.15E+13	1.01E+13	86 : 14
1400	7.42E+13	1.30E+13	85 : 15	7.22E+13	1.28E+13	85 : 15
1500	8.59E+13	1.60E+13	84 : 16	8.36E+13	1.57E+13	84 : 16
1600	9.84E+13	1.93E+13	84 : 16	9.57E+13	1.90E+13	83 : 17
1700	1.11E+14	2.29E+13	83 : 17	1.08E+14	2.26E+13	83 : 17
1800	1.25E+14	2.69E+13	82 : 18	1.22E+14	2.64E+13	82 : 18
1900	1.39E+14	3.10E+13	82 : 18	1.36E+14	3.06E+13	82 : 18
2000	1.54E+14	3.55E+13	81 : 19	1.50E+14	3.50E+13	81 : 19

3.4. Rate Constants Comparison Against Experimental and Theoretical Results in Literature.

3.4.1. C_4H_6 + Ḣ Bimolecular Reaction.

There have been a number of experimental investigations on the kinetics

of the C_4H_6 + Ḣ bimolecular reaction, Table 6. Most of these investigations are limited to low temperatures, pressure, and are not product specific. Figure 3 provides a comparison of our calculation results with previously measured[53–61] and computed[11] rate coefficients for C_4H_6 + Ḣ → products. Our calculations are in excellent agreement with the experimental measurements. Moreover, the high pressure limit (HPL), terminal addition, central addition, and chemically activated reaction rate constants are also in good agreement with the theoretical results from Huang et al.,[11] which ultimately suggests the reliability of the quantum chemical and kinetics methods applied in this study and in that by Huang et al.

Table 6: Literature experimental data for the C_4H_6 + Ḣ reaction rate constant.

Temperature / K	Pressure / Torr	Reference
296.5	435	Jennings *et al.* 1961[53]
296.5	501	Yang *et al.* 1962[54]
298	–	Woolley *et al.* 1969[55]
298	–	Cvetanovic *et al.* 1969[56]
298	0.38	Koda *et al.* 1971[57]
298	1.26	Daby *et al.* 1971[58]
305	–	Gordon *et al.* 1978[59]
298	500 – 600	Ishikawa *et al.* 1979[60]
298	50	Oka *et al.* 1979[61]
1070 – 1120	10	Nametkin *et al.* 1975[62]

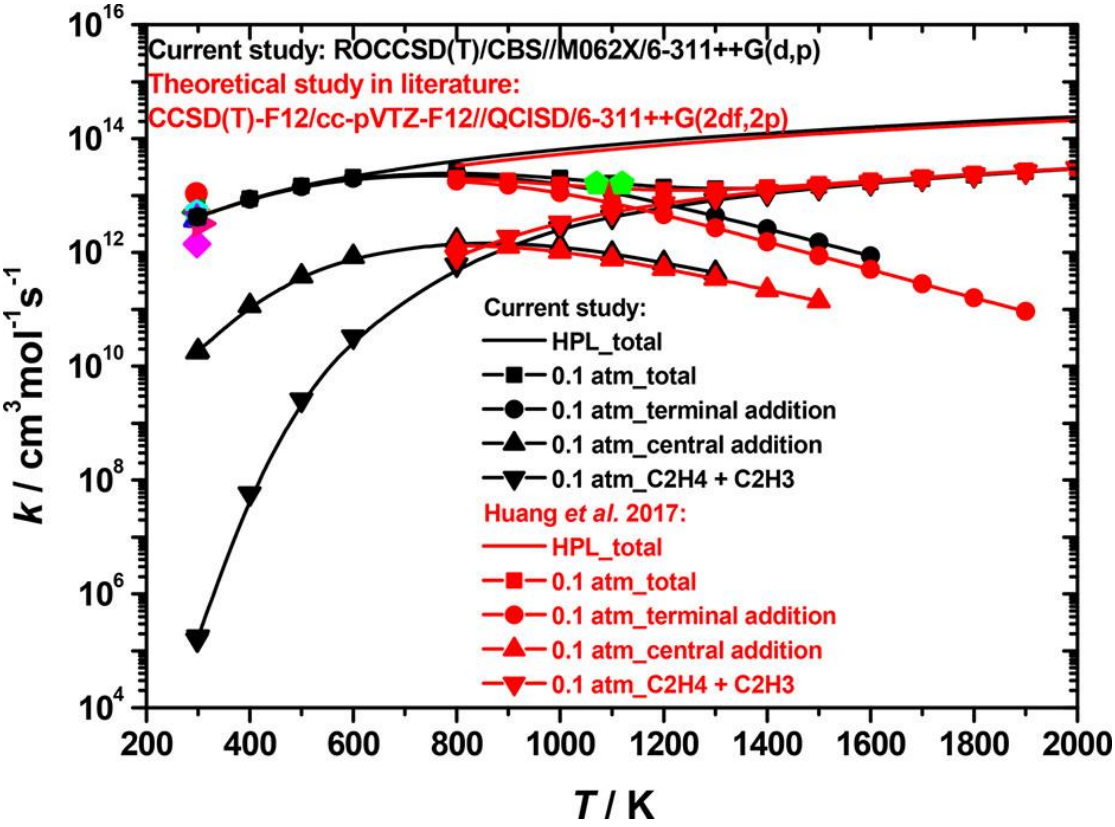

Figure 3. Theoretical and experimental rate coefficients for C_4H_6 + Ḣ → products. (Theoretical study in literature: Huang et al.;[11] Experiments: black ■ Jennings et al.,[53] red ● Yang et al.,[54] blue ▲ Woolley et al.,[55] orange ▼ Cvetanovic et al.,[56] magenta ◆ Koda et al.,[57] olive ◂ Daby et al.,[58] pink ▸ Gordon et al.,[59] cyan ⬢ Ishikawa et al.,[60] violet ★ Oka et al.,[61] green ⬟ Nametkin et al.[62])

Figure 4 illustrates the rate coefficients for the reactions associated with the C_4H_6 + Ḣ → products system plotted as a function of temperature at 0.1, 1.0, and 10 atm. Rate coefficients for the three main reaction pathways are illustrated: terminal Ḣ-atom addition forming 1-methylallyl ($\dot{C}_4H_7$1-3) radicals, central Ḣ-atom addition forming 3-buten-1-yl ($\dot{C}_4H_7$1-4) radicals, and the chemically activated reaction leading to the formation of ethylene + vinyl

radicals. Both the terminal and central addition reactions display a negative temperature dependence at temperatures above about 1100 K, which is enhanced at lower pressure. Both 1-methylallyl ($\dot{C}_4H_7$1-3) and 3-buten-1-yl ($\dot{C}_4H_7$1-4) radicals become thermally unstable with increasing temperature. On the other hand, the chemically activated reaction shows an obvious negative pressure dependence and reaches its low-pressure limit at about 1700 K. This pathway dominates at higher temperatures and at lower pressures since rapid decomposition due to the excess energy in the chemically activated adduct reduces the yield of stabilized $\dot{C}_4H_7$ radicals. In general, the reaction of 1,3-butadiene with Ḣ atoms contributes to molecular growth at high pressures and tends to produce bimolecular products that promote chain branching at low pressures.

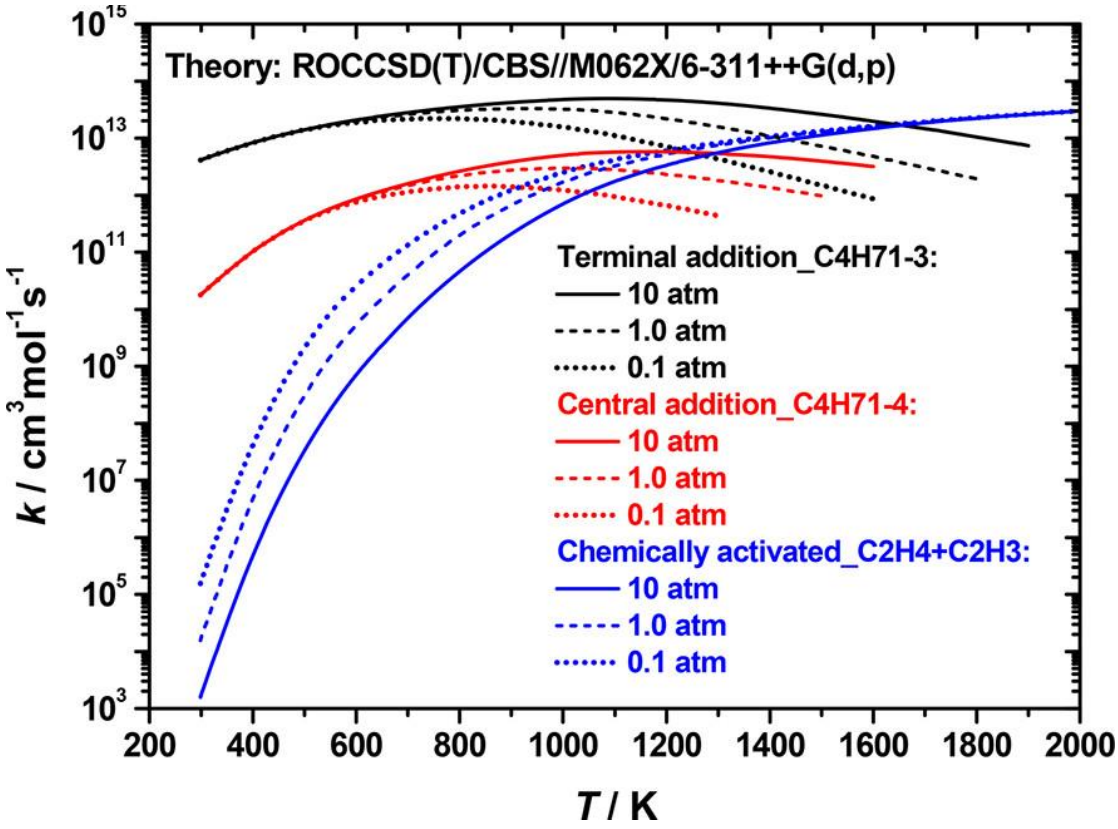

Figure 4. Pressure dependent rate coefficients for C_4H_6 + Ḣ → products reactions at 0.1, 1.0, and 10 atm.

3.4.2. C_2H_4 + $\dot{C}_2H_3$ Bimolecular Reaction.

For the bimolecular reaction C_2H_4 + $\dot{C}_2H_3$ → products, three experimental measurements have been carried out at low pressures from 298−1100 K, as shown in Table 7.

Table 7: Experimental kinetic data for C_2H_4 + $\dot{C}_2H_3$ reaction.

Temperature / K	Pressure / mbar	Reference
1023 – 1273	0.0013 – 0.013	Fahr *et al.* 1988[63]
625 – 950	7 – 15	Shestov *et al.* 2005[12]
298 – 700	20 and 133	Ismail *et al.* 2007[13]

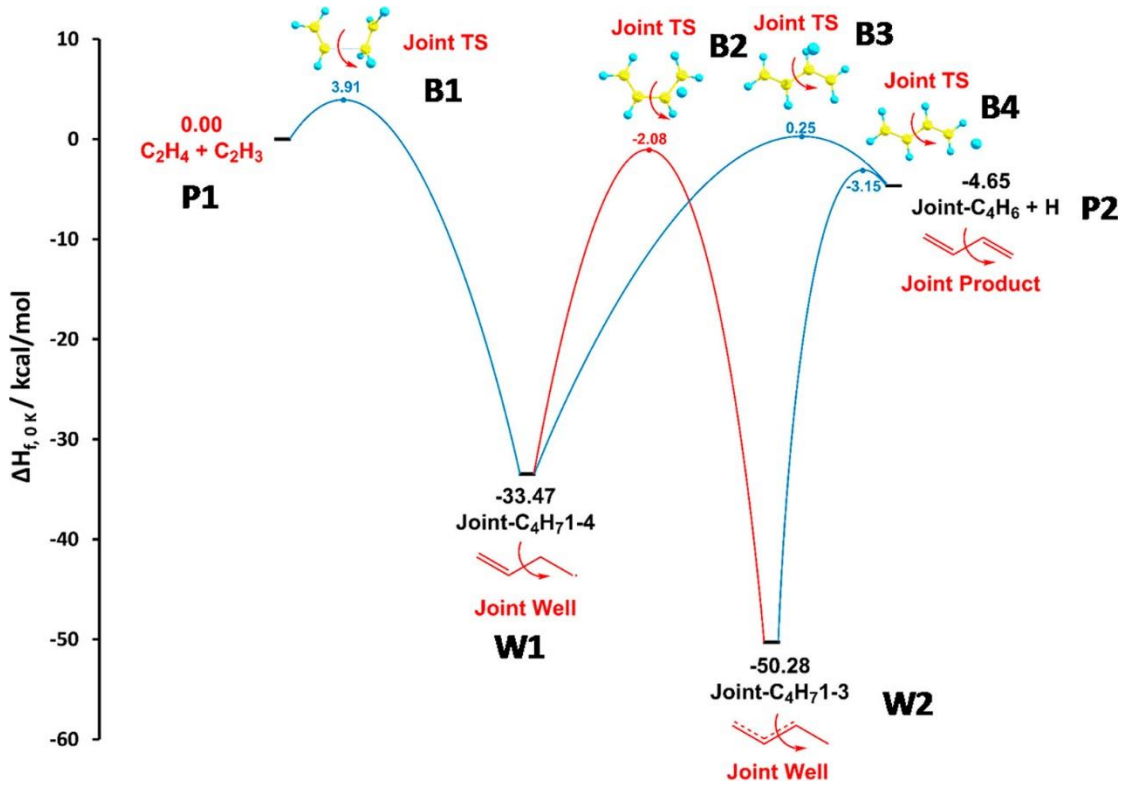

Figure 5. Complete PES for bimolecular reaction $C_2H_4 + \dot{C}_2H_3 \rightarrow$ products.

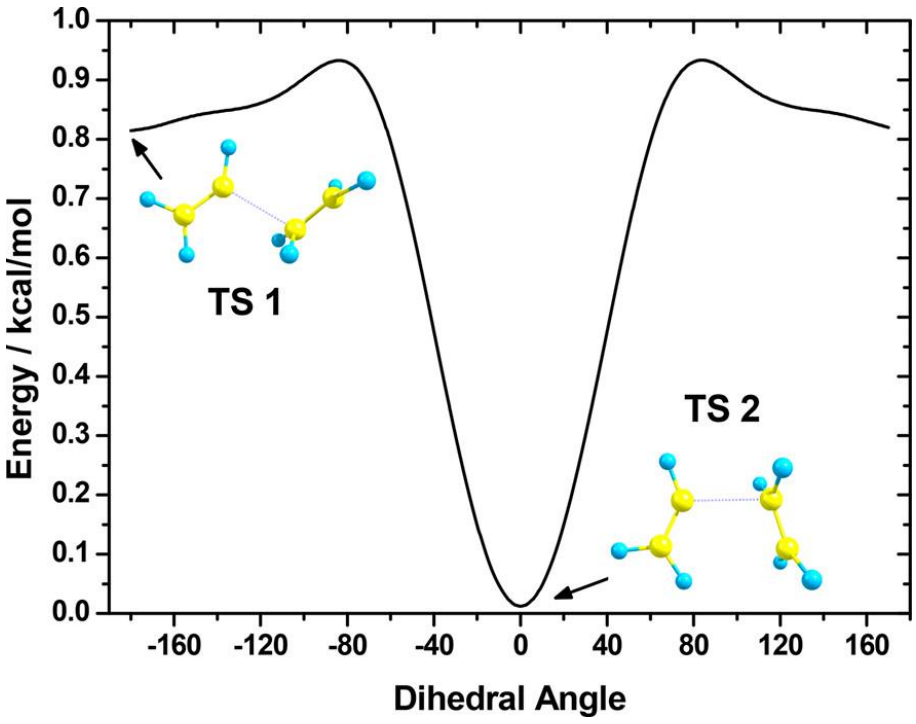

Figure 6. Internal rotor potential of the CC–CC dihedral angle for the joint transition state B1.

As shown in Figure 5, dissimilar to the $\dot{C}_4H_7$ PES discussed above, ethylene can react with vinyl radicals via a joint cis/trans transition state (B1) to form a joint $\dot{C}_4H_7$1−4 well (W1), followed by the isomerization and dissociation pathways with joint-structure species (W2 and P2) and TSs (B2 − B4). Note that the energies on the PES are the sums of ZPEs and SPEs, and torsional scans of all of the joint-structure species and TSs on the PES have been performed. Here, we take joint transition state B1 as an example. Figure 6 shows that trans-structure TS1 and cis-structure TS2 are connected by an internal rotation of the CC−CC dihedral angle, and TS2 is lower in energy than TS1.

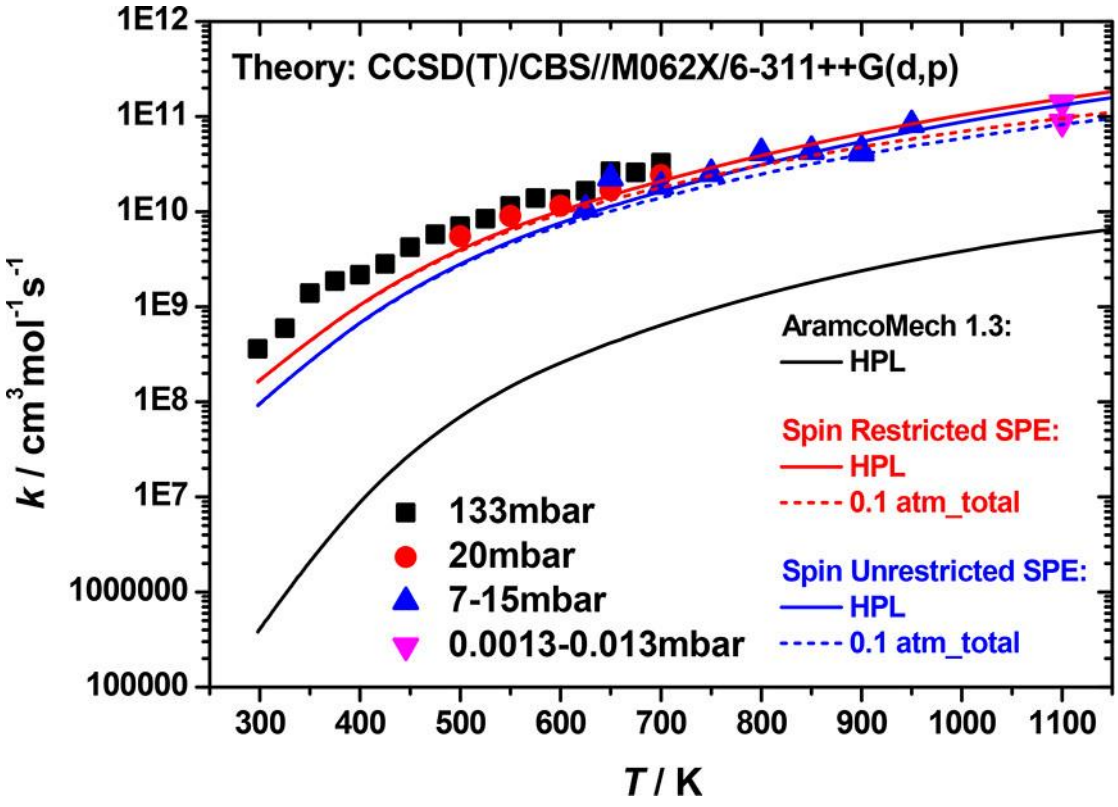

Figure 7. Comparison between theoretical and experimental rate coefficients for $C_2H_4 + \dot{C}_2H_3 \rightarrow$ products. (Theoretical study in literature: Huang et al.;[11] Experiments: ■ & ● Ismail et al.[13] ▲ Shestov et al.,[12] ▼ Fahr et al.,[63])

Figure 7 shows comparisons between theoretical and experimental rate constant calculations/measurements for $C_2H_4 + \dot{C}_2H_3 \rightarrow$ products. The different line colors correspond to the computed rate constants from different sources, with solid and dashed lines representing high-pressure limit rate constants and rate constants at 0.1 atm, respectively. At temperatures in the range of 600−1100 K, our calculations predict well the experimental results. However, at lower temperature (298−600 K), our calculated rate constant is approximately a fact of two smaller than the experimental measurements. Such underprediction reflects the 0.5 kcal/mol overprediction of barrier height of the $C_2H_4 + \dot{C}_2H_3$ entrance channel, and this probably indicates the need for higher level of electronic structure calculations, with treatment of anharmonic ZPE, core−valence corrections, and so on.

3.5. ZPEs and SPEs Evaluation.

Zero-point energies (ZPEs) have been calculated using four different quantum chemical methods for all of the products and transition states associated with the important reaction channels highlighted in Figure 1. These are as follows:

- method 1: M06-2X/6-311++G(d,p)
- method 2: wB97XD/aug-cc-pVTZ
- method 3: B2PLYP-D3/cc-pVTZ
- method 4: CCSD(T)/cc-pVTZ

The calculated ZPEs are compared in Table 8, with all energies relative to the $C_4H_6 + \dot{H}$ reactants. The first two methods are those used for all

calculations throughout our study, and their values are within 0.2 kcal mol^{-1} of one another, which indicates the consistency of these two methods. The latter two methods were recommended by Klippenstein et al.,[64] and the overall comparison of these four methods shows that there is less than 0.7 kcal mol^{-1} difference among them. No value is reported for the 1-methlyallyl ($\dot{C}_4H_7$1-3) radical at the CCSD(T)/cc-pVTZ level due to symmetry breaking problems that arise due to the resonance stabilization in this radical.

Table 8: Relative ZPE comparison between four different quantum chemical methods.[a]

Species & Transition States	Method 1	Method 2	Method 3	Method 4
$C_4H_6 + \dot{H}$	0.00	0.00	0.00	0.00
$C_2H_4 + \dot{C}_2H_3$	1.60	1.48	1.68	1.70
$\dot{C}_4H_7$1-3	5.51	5.69	5.92	–
$\dot{C}_4H_7$1-4	4.86	5.00	5.28	5.55
TS: $C_4H_6 + \dot{H} \rightarrow \dot{C}_4H_7$1-3	0.67	0.60	1.06	0.73
TS: $C_4H_6 + \dot{H} \rightarrow \dot{C}_4H_7$1-4	0.94	0.85	1.26	1.03
TS: $C_2H_4 + \dot{C}_2H_3 \rightarrow \dot{C}_4H_7$1-4	2.72	2.77	3.00	3.06
TS: $\dot{C}_4H_7$1-3 $\rightarrow \dot{C}_4H_7$1-4	2.75	2.78	2.97	2.94

[a] All are relative to that calculated for C_4H_6 + H. Units: kcal mol^{-1}.

Single-point energies (SPEs) were calculated using spin-restricted and spin-unrestricted approaches for the open shell species and transition states of the important reaction channels presented in Figure 1.

- method 1: CCSD(T)/cc-pVTZ, QZ//M06-2X/6-311++G(d,p)
- method 2: CCSD(T) and MP2/aug-cc-pVTZ, QZ//wB97XD/aug-cc-pVTZ

The calculated SPEs are compared in Table 9, with all energies relative to the C_4H_6 + Ḣ reactants. Again, for each approach, there is less than 0.4 kcal mol−1 difference observed for all species and transition states listed when the same spin treatment is used. However, for each method, when comparing the SPEs calculated using the two different spin treatments, 0.3−1.3 kcal mol^{-1} discrepancies are observed. The SPEs calculated using the spin-restricted approach are lower than those using the spin-unrestricted approach.

Table 9: SPEs comparison between two different approaches. (units: kcal mol^{-1}).

Species & Transition States	Method 1		Method 2	
	Spin Restricted	Spin Unrestricted	Spin Restricted	Spin Unrestricted
C_4H_6 + Ḣ	0.00	0.00	0.00	0.00
C_2H_4 + $\dot{C}_2H_3$	3.05	3.34	2.82	3.32
$\dot{C}_4H_7$1-3	–51.14	–50.74	–51.22	–50.62
$\dot{C}_4H_7$1-4	–33.68	–33.67	–33.88	–33.79
TS: C_4H_6 + Ḣ → $\dot{C}_4H_7$1-3	0.83	1.89	0.66	1.94
TS: C_4H_6 + Ḣ → $\dot{C}_4H_7$1-4	3.96	4.94	3.74	5.00
TS: C_2H_4 + $\dot{C}_2H_3$ → $\dot{C}_4H_7$1-4	6.37	7.00	5.95	6.92
TS: $\dot{C}_4H_7$1-3 → $\dot{C}_4H_7$1-4	0.80	1.16	0.69	1.24

Table 10: Barrier height comparisons between two different approaches. (units: kcal mol^{-1}).

	Method 1				Method 2			
	Spin Restricted		Spin Unrestricted		Spin Restricted		Spin Unrestricted	
Reactions	Forward	Reverse	Forward	Reverse	Forward	Reverse	Forward	Reverse
$\dot{C}_4H_7$1-3 ↔ C_4H_6 + $\dot{H}$	47.13	1.49	47.80	2.56	46.79	1.26	47.47	2.54
$\dot{C}_4H_7$1-3 ↔ $\dot{C}_4H_7$1-4	49.19	32.38	49.15	32.72	49.00	32.36	48.95	32.81
$\dot{C}_4H_7$1-4 ↔ C_4H_6 + $\dot{H}$	33.72	4.90	34.69	5.88	33.48	4.59	34.64	5.85
$\dot{C}_4H_7$1-4 ↔ C_2H_4 + $\dot{C}_2H_3$	37.91	4.44	38.53	4.79	37.60	4.41	38.48	4.89

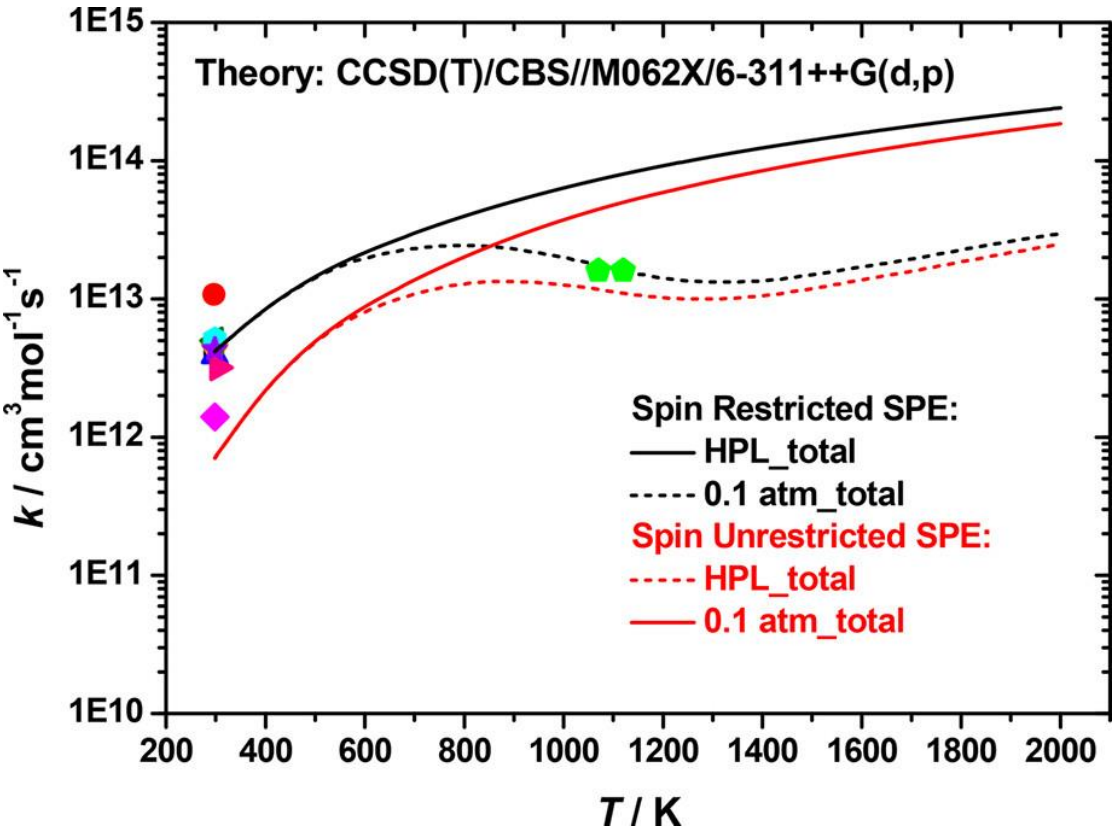

Figure 8. Spin-restricted and unrestricted SPEs effect on the rate constant calculated for C_4H_6 + $\dot{H}$ → products. (Experiments: black ■ Jennings et al.,[53] red ● Yang et al.,[54] blue ▲ Woolley et al.,[55] orange ▼ Cvetanovic et al.,[56]

magenta ◆ Koda et al.,[57] olive ◂ Daby et al.,[58] pink ▸ Gordon et al.,[59] cyan ● Ishikawa et al.,[60] violet ★ Oka et al.,[61] green ⬟ Nametkin et al.[62])

Table 10 shows the forward and reverse barrier heights using the two different approaches and methods (note that the energy values in this table include both ZPEs and SPEs). The biggest discrepancies are generally for reverse barrier heights in the dissociation reactions, where the spin-unrestricted approach gives about 0.4−1.3 kcal mol^{-1} higher barrier than the spin-restricted approach.

The C_4H_6 + Ḣ ↔ products bimolecular reaction has been selected to illustrate the effect of the variation in the SPEs from the two approaches (restricted and unrestricted) on the predicted rate constants. In Figure 8, black and red lines are the rate constants calculated using the spin-restricted and spin-unrestricted SPE approaches, respectively, while solid and dashed lines are the HPL and total rate constants at 0.1 atm, respectively. The spin-unrestricted SPEs approach consistently under predicts rate constants, particularly at lower temperatures. This can be explained by the predicted higher barriers as mentioned above. Our comparison indicates that the results from the spin-restricted approach agree better with experimental data than the spin-unrestricted calculations.

3.6. Thermochemistry Comparison between Two Different Quantum Chemical Methods and Codes.

The thermochemistry of all C_4 species (C_4H_6 and $\dot{C}_4H_7$ isomers) on the PES have been calculated using the two different quantum chemical methods and codes. In order to compare the values calculated, 1,3-butadiene (C_4H_6) and 1-butyne (C_4H_6-1) have been selected as representative species for which data is also available from two other reliable sources, namely, the Active Thermochemical Tables (ATcT)[45–47] and from the bond additivity corrected QCISD(T)/CBS calculations of Goldsmith et al.[65] Table 11 compares the 298 K enthalpies of formation and entropies of 1,3-butadiene (C_4H_6) and 1-butyne (C_4H_6-1) calculated here from our two different quantum chemical methods and the values from the literature.

- method 1: CBS-APNO/G3/G4//M06-2X/6-311++G(d,p)
- method 2: CBS-APNO/G3/G4//wB97XD/aug-ccpVTZ
- ATcT: refs.[45–47]
- Goldsmith: RQCISD(T)/cc-pVT,QZ//B3LYP/6-311++G(d,p), with bond additivity correction

Excellent agreement was obtained for the values from four different sources, with less than 0.5 kcal mol^{-1} and 0.8 cal K^{-1} mol^{-1} differences in the heats of formation and entropy values, respectively. Such agreement once again confirms the consistency and accuracy of the two methods used in this study. Moreover, from the calculation expense viewpoint, significantly “cheaper” methods can still produce accurate results.

Table 11: Comparison of thermochemical values* from two different quantum chemical methods and from literature data.

Species	$\Delta_f H_{298\ K}$				$S_{298\ K}$			
	Method 1	Method 2	ATcT	Goldsmith	Method 1	Method 2	ATcT	Goldsmith
C_4H_6	26.68	26.64	26.43 ± 0.1	26.50	66.60	66.38	–	65.80
C_4H_6-1	39.79	39.77	39.62 ± 0.2	40.10	69.09	68.98	–	69.20

*Units: kcal mol^{-1} for heat of formation, cal K^{-1} mol^{-1} for entropy.

In order to compare thermochemical values calculated by two different codes, the most important C_4 radicals: methylallyl ($\dot{C}_4H_7$1-3) and 3-buten-1-yl ($\dot{C}_4H_7$1-4) radicals have been selected as representatives. Table 12 compares the 298 K enthalpies of formation, entropies, and heat capacity as a function of temperature calculated using the two different codes. Again, excellent agreement is obtained over the entire temperature range, with less than 0.02 kcal mol^{-1}, 0.03 cal K^{-1} mol^{-1}, and 0.09 cal K^{-1} mol^{-1} differences in the heats of formation, entropy, and heat capacity values, respectively.

Table 12: Thermochemical values* comparison between two different codes.

Species	$\dot{C}_4H_7$1-3		$\dot{C}_4H_7$1-4	
	MultiWell/Thermo	PAPR	MultiWell/Thermo	PAPR
$\Delta_f H_{298K}$	31.71	31.71	48.94	48.92
S_{298K}	72.02	72.03	77.23	77.20
Cp_{300K}	19.93	19.90	20.11	20.20
Cp_{400K}	24.92	24.90	24.93	24.98

Cp_{500K}	29.41	29.40	29.23	29.26
Cp_{600K}	33.21	33.20	32.85	32.87
Cp_{800K}	39.17	39.16	38.57	38.58
Cp_{1000K}	43.61	43.60	42.87	42.87
Cp_{1500K}	50.61	50.60	49.72	49.72

*Units: kcal mol^{-1} for heat of formation, cal K^{-1} mol^{-1} for entropy and heat capacity.

3.7. Rate Constants Comparison of H atom Abstraction by H-Atom.

A sensitivity analysis with our recently developed 1,3-butadiene6 oxidation mechanism indicates that the branching ratio between Ḣ-atom addition and abstraction is critical to predicting flame speeds (Figure 9).

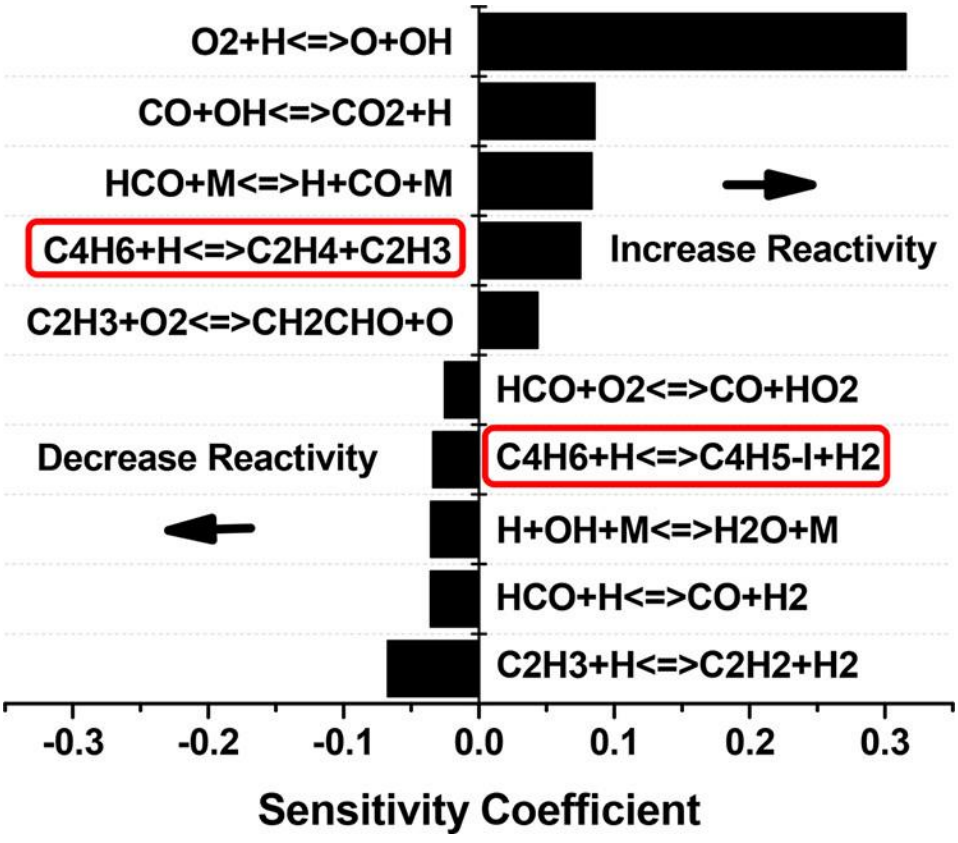

Figure 9. Flame speed sensitivity analysis of C_4H_6/air laminar flame at φ = 1.1,

Tu = 298 K, *p* = 1 atm.

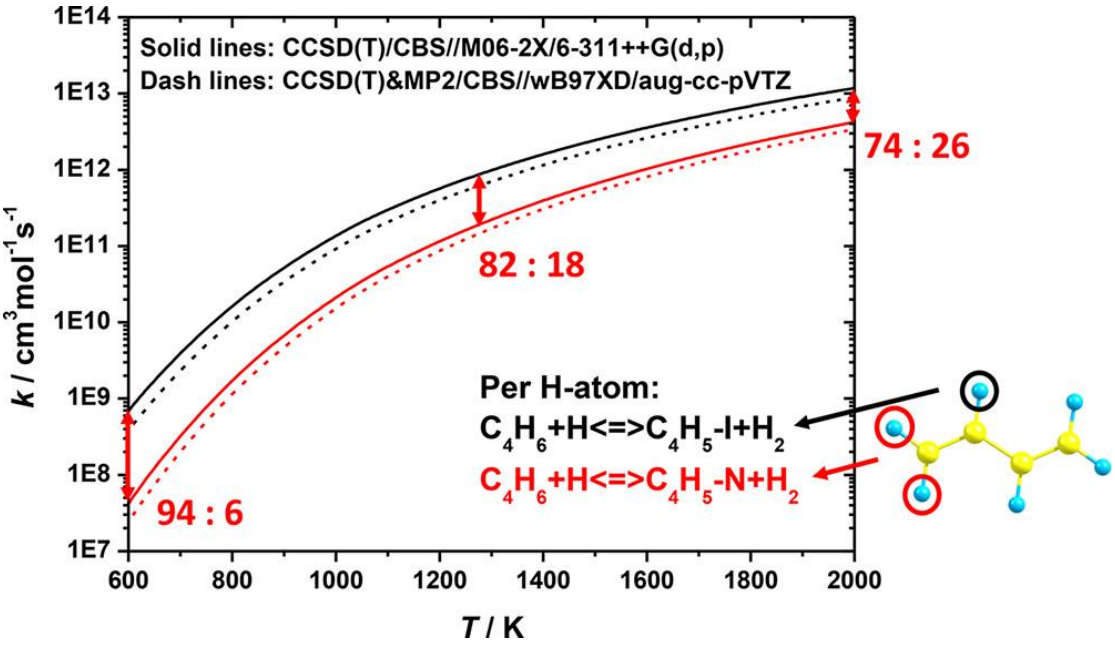

Figure 10. Rate constants for Ḣ-atom abstraction by Ḣ atoms.

Thus, the rate constants for H atom abstraction by Ḣ atoms were calculated with ab initio TST using the two different quantum chemical methods and codes discussed above. The predictions are illustrated in Figure 10, where black and red lines represent rate constants for abstraction of central and terminal H atoms, respectively, and solid and dashed lines correspond to the values calculated using the two different quantum chemical methods. Throughout the temperature range of 600−2000 K, there is less than 40% difference observed between the results. The branching ratio for abstraction from central and terminal carbon atoms are compared at three selected temperatures: 600, 1300, and 2000 K. Central abstraction dominates over terminal abstraction, which is consistent with the calculated bond dissociation energy (BDE) difference between secondary allylic-vinylic (101.5 kcal mol^{-1})

and primary vinylic (110.53 kcal mol^{-1}) C−H bonds in the 1,3-butadiene molecule.

It is worth discussing the $\dot{C}_4H_5$-I free radical formed as a result of abstraction of a H atom from a central carbon atom. This radical is resonantly stabilized due to the presence of vinylic and allenic structures, Figure 11. Table 13 shows the enthalpy of formation at 298 K and distribution xi of these two structures, which is determined from the Boltzmann distribution, taking due account of Gibbs free energies $\Delta G^{\ominus}$ and degeneracies σ:

$$x_i = \sigma_i exp(-\Delta G_m^{\Theta}(i)/RT) \sum_{i=1}^{n} [\sigma_i exp(-\Delta G_m^{\Theta}(i)/RT)]$$

This shows that the allenic structure is about 8.5 kcal mol^{-1} more stable than the vinylic one, and thus, the allenic structure dominates. In addition, a CASPT2(5e,5o)/cc-pVTZ analysis (with all pi and radical orbitals active) shows that the electronic barrier from the vinylic to the allenic structure is only 0.03 kcal mol^{-1}, and ZPE corrections actually make this value negative. Therefore, we believe that the $\dot{C}_4H_5$-I radical will always exist in the allenic form, and the subsequent reaction pathways should be represented accordingly.

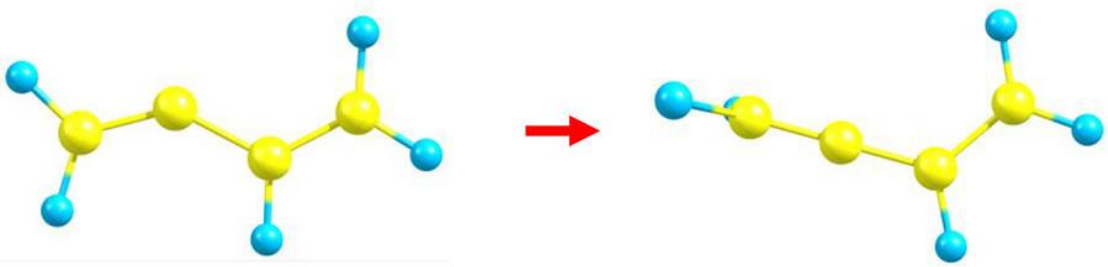

(a) Vinylic Structure (b) Allenic Structure

Figure 11. Vinylic and allenic resonance structures of the $\dot{C}_4H_5$–I radical.

Table 13 Energies and distribution of vinylic and allenic structured $\dot{C}_4H_5$-I radical.

Name	Vinylic Structure	Allenic Structure
$\Delta_f H_{298K}$ (kcal mol^{-1})	83.50	75.08
Distribution (298 – 2000 K)	≤ 25%	≥ 75%

3.8. Application in Kinetic Model Development.

The calculated pressure-dependent rate coefficients of the reactions on the $\dot{C}_4H_7$ PES and H atom abstraction rate coefficients have been incorporated into our recently developed 1,3-butadiene[6] oxidation mechanism. Laminar flame speed measurements have been selected as the representative target as these are particularly sensitive to Ḣ atom chemistry (Figure 12). Herein, the solid lines are the model predictions incorporating the rate coefficients calculated in the current study, and the dashed lines represent those using the rate coefficients from AramcoMech2.0.[4] It is clear that using the rate coefficients from the current study leads to improved flame speed predictions. Such improvement reflects on the accurate prediction of the H atom addition and abstraction branching ratio shown in Figure 9. A further detailed discussion of its effects on model prediction is beyond the scope of this paper and is provided in ref 6.

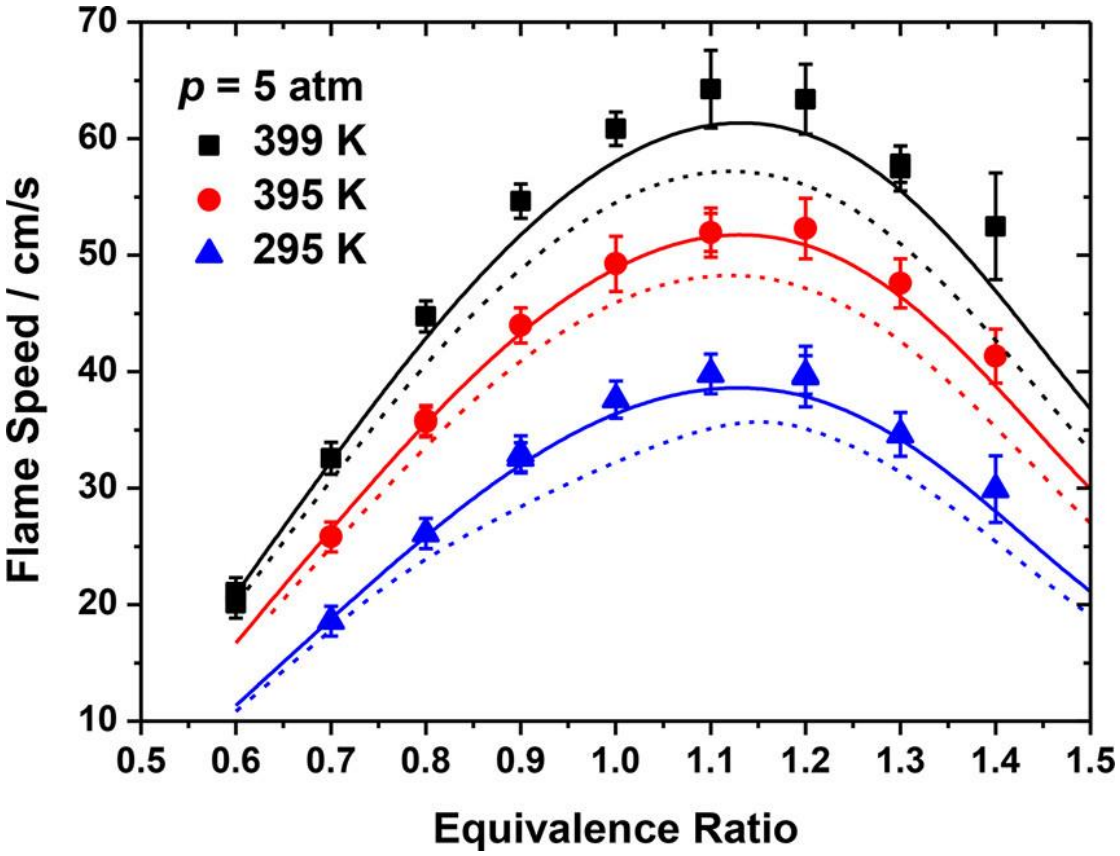

Figure 12. 1,3-Butadiene laminar flame speed. Solid line: Model prediction incorporating the rate coefficients calculated in the current study; Dashed line: Model prediction with original rate coefficients in AramcoMech2.0.

4. Conclusions

This study provides a wide-ranging theoretical treatment of the kinetics associated with the $\dot{C}_4H_7$ PES. The pressure-dependent rate coefficients for isomerization, decomposition, and chemical activation reactions were investigated using RRKM/ME analyses. The thermodynamic properties of all C_4 species were also evaluated. Two entrance channels: 1-methylallyl ($\dot{C}_4H_7$1-3) and 3-buten-1-yl ($\dot{C}_4H_7$1-4) were found to be the most important wells, and production of $C_2H_4 + \dot{C}_2H_3$, which tends to promote reactivity, was found to be

the most important bimolecular reaction. Systematic comparisons were made among different quantum chemical methods, approaches, codes, and literature data for the various results generated in this study including ZPEs, SPEs, rate constants, barrier heights, and thermochemistry.

- ZPEs were compared between four different quantum chemical methods: M06-2X/6-311++G(d,p), wB97XD/aug-cc-pVTZ, B2PLYP-D3/cc-pVTZ and CCSD(T)/ccpVTZ.
- SPEs were compared between spin-restricted and -unrestricted approaches.
- HPL rate constants and thermochemistry were compared between two different codes: MultiWell/Thermo and PAPR.
- HPL rate constants, barrier heights and thermochemistry were compared between two different quantum chemical methods: CCSD(T)/CBS//M06-2X/6-311++G(d,p) and CCSD(T)&MP2/CBS// wB97XD/aug-cc-pVTZ.
- Pressure-dependent rate constants, barrier heights, and thermochemistry were compared against both experimental and theoretical results in literature.

Considering all of the above comparisons, reasonably good agreement was obtained between two different quantum chemical methods and two different codes. Excellent agreement was observed between the theoretical and experimental results available over a wide range of conditions. In addition, the comparison between the two different quantum chemical methods demonstrates

that the second method (CCSD(T) and MP2/CBS//wB97XD/aug-cc-pVTZ) is able to approximate a “higher-level” answer at a lower computational cost, and hence, this method is recommended for the calculation of the pentene + Ḣ and pentadiene + Ḣ reaction systems in the future. Regarding the comparison between spin-restricted and spin-unrestricted approaches for SPEs calculation, it was found that the spin-unrestricted approach tends to overpredict the barrier heights of bimolecular reactions, which results in the underprediction of rate constants especially at lower temperatures (298−1000 K).

Furthermore, the calculated H atom addition and abstraction rate coefficients were incorporated into a recently developed 1,3-butadiene model. The laminar flame speed simulations clearly demonstrate a significant improvement in model predictions, emphasizing the value of this study.

Supporting Information

Rate coefficients (for an N_2 bath) have been fitted to the PLOG[49] format and are provided as a function of temperature by the sum of two modified Arrhenius functions at various pressures. Thermochemical values for all C_4 species are provided at selected temperatures and fitted to ChemKin style NASA polynomials[49] format. In addition, the input files for both MultiWell/Thermo and PAPR codes are also provided (ZIP).

Acknowledgments

This work is supported by the FUELCOM project of Saudi Aramco and by

Science Foundation Ireland via their Principal Investigator Program through project number 15/IA/3177. The work at Argonne was supported by the U.S. Department of Energy, Office of Science, Office of Basic Energy Sciences, Division of Chemical Sciences, Geosciences, and Biosciences under Contract No. DE-AC02-06CH11357. The authors wish to acknowledge the computational resources provided from the Irish Centre for High-End Computing (ICHEC), under project number ngche043c. We also appreciate the provision of automation Perl code from Dr. Kieran Somers, and MESS_TPfit code from Prof. C. Franklin Goldsmith.

References

1. Burke, S. M.; Metcalfe, W.; Herbinet, O.; Battin-Leclerc, F.; Haas, F. M.; Santner, J.; Dryer, F. L.; Curran, H. J., An Experimental and Modeling Study of Propene Oxidation. Part 1: Speciation Measurements in Jet-Stirred and Flow Reactors. Combust. Flame 2014, 161, 2765-2784.

2. Burke, S. M.; Burke, U.; Mc Donagh, R.; Mathieu, O.; Osorio, I.; Keesee, C.; Morones, A.; Petersen, E. L.; Wang, W.; DeVerter, T. A.; Oehlschlaeger, M. A.; Rhodes, B.; Hanson, R. K.; Davidson, D. F.; Weber, B. W.; Sung, C.-J.; Santner, J.; Ju, Y.; Haas, F. M.; Dryer, F. L.; Volkov, E. N.; Nilsson, E. J. K.; Konnov, A. A.; Alrefae, M.; Khaled, F.; Farooq, A.; Dirrenberger, P.; Glaude, P.-A.; Battin-Leclerc, F.; Curran, H. J., An Experimental and Modeling Study of Propene Oxidation. Part 2: Ignition Delay Time and Flame Speed Measurements. Combust. Flame 2015, 162, 296-314.

3. Li, Y.; Zhou, C.-W.; Curran, H. J., An Extensive Experimental and Modeling Study of 1-Butene Oxidation. Combust. Flame 2017, 181, 198-213.

4. Li, Y.; Zhou, C.-W.; Somers, K. P.; Zhang, K.; Curran, H. J., The Oxidation of 2-Butene: A High-Pressure Ignition Delay, Kinetic Modeling Study and Reactivity Comparison with Isobutene and 1-Butene. Proc. Combust. Inst. 2017, 36, 403-411.

5. Zhou, C.-W.; Li, Y.; O'Connor, E.; Somers, K. P.; Thion, S.; Keesee, C.; Mathieu, O.; Petersen, E. L.; DeVerter, T. A.; Oehlschlaeger, M. A.; Kukkadapu, G.; Sung, C.-J.; Alrefae, M.; Khaled, F.; Farooq, A.; Dirrenberger, P.; Glaude, P.-A.; Battin-Leclerc, F.; Santner, J.; Ju, Y.; Held, T.; Haas, F. M.; Dryer, F. L.; Curran, H. J., A Comprehensive Experimental and Modeling Study of Isobutene Oxidation. Combust. Flame 2016, 167, 353-379.

6. Zhou, C.-W.; Li, Y.; Burke, U.; Somers, K. P.; Khan, S.; Hargis, J. W.; Sikes, T.; Petersen, E. L.; AlAbbad, M.; Farooq, A.; Pan, Y.; Zhang, Y.; Huang, Z.; Lopez, J.; Loparo, Z.; Vasu, S. S.; Curran, H. J., An Experimental and Chemical Kinetic Modeling Study of 1,3-Butadiene Combustion: Ignition Delay Time and Laminar Flame Speed Measurements, (under review). Combust. Flame 2017.

7. Laskin, A.; Wang, H.; Law, C. K., Detailed Kinetic Modeling of 1,3-Butadiene Oxidation at High Temperatures. Int. J. Chem. Kinet. 2000, 32, 589-614.

8. Miller, J. L., Theoretical Study of the Straight-Chain C4H7 Radical Isomers and Their Dissociation and Isomerization Transition States. J. Phys. Chem. A

2004, 108, 2268-2277.

9. Miyoshi, A., Computational Studies on the Reactions of 3-Butenyl and 3-Butenylperoxy Radicals. Int. J. Chem. Kinet. 2010, 42, 273-288.

10. Xu, C.; Al Shoaibi, A. S.; Wang, C.; Carstensen, H.-H.; Dean, A. M., Kinetic Modeling of Ethane Pyrolysis at High Conversion. J. Phys. Chem. A 2011, 115, 10470-10490.

11. Huang, C.; Yang, B.; Zhang, F., Pressure-Dependent Kinetics on the C4H7 Potential Energy Surface and Its Effect on Combustion Model Predictions. Combust. Flame 2017, 181, 100-109.

12. Shestov, A. A.; Popov, K. V.; Slagle, I. R.; Knyazev, V. D., Kinetics of the Reaction Between Vinyl Radical and Ethylene. Chem. Phys. Lett. 2005, 408, 339-343.

13. Ismail, H.; Goldsmith, C. F.; Abel, P. R.; Howe, P.-T.; Fahr, A.; Halpern, J. B.; Jusinski, L. E.; Georgievskii, Y.; Taatjes, C. A.; Green, W. H., Pressure and Temperature Dependence of the Reaction of Vinyl Radical with Ethylene. J. Phys. Chem. A 2007, 111, 6843-6851.

14. Barker, J. R.; Nguyen, T. L.; Stanton, J. F.; C. Aieta, M. C.; Gabas, F.; Kuma, T. J. D.; Li, C. G. L.; Lohr, L. L.; Maranzana, A.; Ortiz, N. F.; Preses, J. M.; Stimac, P. J., MultiWell-2016 Software Suite; J. R. Barker, University of Michigan, Ann Arbor, Michigan, USA. 2016.

15. Georgievskii, Y.; Miller, J. A.; Burke, M. P.; Klippenstein, S. J., Reformulation and Solution of the Master Equation for Multiple-Well Chemical Reactions. J. Phys. Chem. A 2013, 117, 12146-12154.

16. Foresman, J.; Ortiz, J.; Cioslowski, J.; Fox, D., Gaussian 09, Revision D. 01; Gaussian, Inc. Wallingford, CT 2009.

17. Zhao, Y.; Truhlar, D. G., The M06 Suite of Density Functionals for Main Group Thermochemistry, Thermochemical Kinetics, Noncovalent Interactions, Excited States, and Transition Elements: Two New Functionals and Systematic Testing of Four M06-Class Functionals and 12 Other Functionals. Theor. Chem. Acc. 2008, 120, 215-241.

18. McLean, A. D.; Chandler, G. S., Contracted Gaussian Basis Sets for Molecular Calculations. I. Second Row Atoms, Z=11–18. J. Chem. Phys. 1980, 72, 5639-5648.

19. Krishnan, R.; Binkley, J. S.; Seeger, R.; Pople, J. A., Self-Consistent Molecular Orbital Methods. XX. A Basis Set for Correlated Wave Functions. J. Chem. Phys. 1980, 72, 650-654.

20. Jr., T. H. D., Gaussian Basis Sets for Use in Correlated Molecular Calculations. I. The Atoms Boron Through Neon and Hydrogen. J. Chem. Phys. 1989, 90, 1007-1023.

21. III, G. D. P.; Bartlett, R. J., A Full Coupled-Cluster Singles and Doubles Model: The Inclusion of Disconnected Triples. J. Chem. Phys. 1982, 76, 1910-1918.

22. Martin, J. M. L., Ab Initio Total Atomization Energies of Small Molecules — Towards the Basis Set Limit. Chem. Phys. Lett. 1996, 259, 669-678.

23. Feller, D.; Dixon, D. A., Extended Benchmark Studies of Coupled Cluster Theory Through Triple Excitations. J. Chem. Phys. 2001, 115, 3484-3496.

24. Chai, J.-D.; Head-Gordon, M., Long-Range Corrected Hybrid Density Functionals with Damped Atom-Atom Dispersion Corrections. Phys. Chem. Chem. Phys. 2008, 10, 6615-6620.

25. Kendall, R. A.; Jr., T. H. D.; Harrison, R. J., Electron Affinities of the First-Row Atoms Revisited. Systematic Basis Sets and Wave Functions. J. Chem. Phys. 1992, 96, 6796-6806.

26. Woon, D. E.; Jr., T. H. D., Gaussian Basis Sets for Use in Correlated Molecular Calculations. III. The Atoms Aluminum Through Argon. J. Chem. Phys. 1993, 98, 1358-1371.

27. Head-Gordon, M.; Head-Gordon, T., Analytic MP2 Frequencies without Fifth-Order Storage. Theory and Application to Bifurcated Hydrogen Bonds in the Water Hexamer. Chem. Phys. Lett. 1994, 220, 122-128.

28. Hratchian, H. P.; Schlegel, H. B., Using Hessian Updating To Increase the Efficiency of a Hessian Based Predictor-Corrector Reaction Path Following Method. J. Chem. Theory Comput. 2005, 1, 61-69.

29. Lee, T. J.; Taylor, P. R., A Diagnostic for Determining the Quality of Single-Reference Electron Correlation Methods. Int. J. Quantum Chem 1989, 36, 199-207.

30. Klippenstein, S. J.; Harding, L. B., Kinetics of the H + NCO Reaction. Proc. Combust. Inst. 2009, 32, 149-155.

31. Eyring, H., The Activated Complex in Chemical Reactions. J. Chem. Phys. 1935, 3, 107-115.

32. Rice, O. K.; Ramsperger, H. C., Theories of Unimolecular Gas Reactions at

Low Pressures. J. Am. Chem. Soc. 1927, 49, 1617-1629.

33. Rice, O. K.; Ramsperger, H. C., Theories of Unimolecular Gas Reactions at Low Pressures. II. J. Am. Chem. Soc. 1928, 50, 617-620.

34. Kassel, L. S., Studies in Homogeneous Gas Reactions. I. J. Phys. Chem. A 1927, 32, 225-242.

35. Marcus, R. A., Unimolecular Dissociations and Free Radical Recombination Reactions. J. Chem. Phys. 1952, 20, 359-364.

36. Marcus, R. A.; Rice, O. K., The Kinetics of the Recombination of Methyl Radicals and Iodine Atoms. J. Phys. Chem. A 1951, 55, 894-908.

37. Pilling, M. J.; Robertson, S. H., Master Equation Models for Chemical Reactions of Importance in Combustion. Annu. Rev. Phys. Chem. 2003, 54, 245-275.

38. Jasper, A. W.; Miller, J. A., Lennard–Jones Parameters for Combustion and Chemical Kinetics Modeling from Full-Dimensional Intermolecular Potentials. Combust. Flame 2014, 161, 101-110.

39. Klippenstein, S. J.; Miller, J. A., The Addition of Hydrogen Atoms to Diacetylene and the Heats of Formation of i-C4H3 and n-C4H3. J. Phys. Chem. A 2005, 109, 4285-4295.

40. Klippenstein, S. J.; Miller, J. A.; Jasper, A. W., Kinetics of Propargyl Radical Dissociation. J. Phys. Chem. A 2015, 119, 7780-7791.

41. Eckart, C., The Penetration of a Potential Barrier by Electrons. Phys. Rev. 1930, 35, 1303-1309.

42. Ochterski, J. W.; Petersson, G. A.; Jr., J. A. M., A Complete Basis Set

Model Chemistry. V. Extensions to Six or More Heavy Atoms. J. Chem. Phys. 1996, 104, 2598-2619.

43. Curtiss, L. A.; Raghavachari, K.; Redfern, P. C.; Rassolov, V.; Pople, J. A., Gaussian-3 (G3) Theory for Molecules Containing First and Second-Row Atoms. J. Chem. Phys. 1998, 109, 7764-7776.

44. Curtiss, L. A.; Redfern, P. C.; Raghavachari, K., Gaussian-4 Theory. J. Chem. Phys. 2007, 126 (8), 084108.

45. Simmie, J. M.; Somers, K. P., Benchmarking Compound Methods (CBS-QB3, CBS-APNO, G3, G4, W1BD) against the Active Thermochemical Tables: A Litmus Test for Cost-Effective Molecular Formation Enthalpies. J. Phys. Chem. A 2015, 119, 7235-7246.

46. Somers, K. P.; Simmie, J. M., Benchmarking Compound Methods (CBS-QB3, CBS-APNO, G3, G4, W1BD) against the Active Thermochemical Tables: Formation Enthalpies of Radicals. J. Phys. Chem. A 2015, 119, 8922-8933.

47. Ruscic, B., Uncertainty Quantification in Thermochemistry, Benchmarking Electronic Structure Computations, and Active Thermochemical Tables. Int. J. Quantum Chem 2014, 114, 1097-1101.

48. Gordon, S.; Mcbride, B. J., Computer Program for Calculation of Complex Chemical Equilibrium Compositions, Rocket Performance, Incident and Reflected Shocks, and Chapman-Jouguet Detonations. NASA STI 1976.

49. ANSYS Chemkin-Pro 17.2, ANSYS, Inc.: San Diego. 2016.

50. Ibuki, T.; Tsuji, A.; Takezaki, Y., Isomerization of Chemically Activated

1-Buten-1-yl and 1-Buten-4-yl Radicals. J. Phys. Chem. A 1976, 80, 8-14.

51. Miller, J. L.; Krisch, M. J.; Butler, L. J.; Shu, J., Dissociation Channels of the 1-Buten-2-yl Radical and Its Photolytic Precursor 2-Bromo-1-butene. J. Phys. Chem. A 2005, 109, 4038-4048.

52. McCunn, L. R.; Krisch, M. J.; Liu, Y.; Butler, L. J.; Shu, J., A Study of the Unimolecular Dissociation of the 2-Buten-2-yl Radical via the 193 nm Photodissociation of 2-Chloro-2-butene. J. Phys. Chem. A 2005, 109, 6430-6439.

53. Jennings, K. R.; Cvetanović, R. J., Relative Rates of Addition of Hydrogen Atoms to Olefines. J. Chem. Phys. 1961, 35, 1233-1240.

54. Yang, K., Free Radical Reactions Initiated by Ionizing Radiation. II. Rate Constants for Hydrogen Atom Addition Reactions with Mono-olefins, Butadiene and Benzene. J. Am. Chem. Soc. 1962, 84, 3795-3799.

55. Woolley, G. R.; Cvetanović, R. J., Production of Hydrogen Atoms by Photolysis of H2S and the Rates of Their Addition to Olefins. J. Chem. Phys. 1969, 50, 4697-4704.

56. Cvetanović, R. J.; Doyle, L. C., Relative Rates of Reaction of Hydrogen Atoms with Olefins. J. Chem. Phys. 1969, 50, 4705-4713.

57. Seiichiro, K.; Tsutomu, H., A Mass Spectrometric Study of the Reaction of Hydrogen Atom with Butadiene. Bull. Chem. Soc. Jpn. 1971, 44, 2888-2888.

58. Niki, H.; Daby, E. E.; Weinstock, B., Mass-Spectrometric Studies of Rate Constants for Addition Reactions of Hydrogen and of Deuterium Atoms with Olefins in a Discharge-Flow System at 300.deg.K. J. Phys. Chem. A 1971, 75,

1601-1610.

59. Gordon, E. B.; Ivanov, B. I.; Perminov, A. P.; Balalaev, V. E., A Measurement of Formation Rates and Lifetimes of Intermediate Complexes in Reversible Chemical Reactions Involving Hydrogen Atoms. J. Chem. Phys. 1978, 35, 79-89.

60. Yo-ichi, I.; Ko-ichi, S.; Shin, S., The Rate Constants for H and D-Atom Additions to O2, NO, Acetylene, and 1,3-Butadiene. Bull. Chem. Soc. Jpn. 1979, 52, 3503-3506.

61. Oka, K.; Cvetanović, R. J., Determination of Rates of Hydrogen Atom Reactions with Alkenes at 298 K by a Double Modulation Technique. Can. J. Chem. 1979, 57, 777-784.

62. Nametkin, N. S.; Shevel'kova, L. V.; Kalinenko, R. A., Rate Constants of the Reactions of Hydrogen Atoms with Ethylene and Butadiene at High Temperatures. Dokl. Chem. 1975, 221, 851.

63. Fahr, A.; Stein, S. E., Reactions of Vinyl and Phenyl Radicals with Ethyne, Ethene and Benzene. Symposium (International) on Combustion 1989, 22, 1023-1029.

64. Klippenstein, S. J., From Theoretical Reaction Dynamics to Chemical Modeling of Combustion. Proc. Combust. Inst. 2017, 36, 77-111.

65. Goldsmith, C. F.; Magoon, G. R.; Green, W. H., Database of Small Molecule Thermochemistry for Combustion. J. Phys. Chem. A 2012, 116, 9033-9057.

A comprehensive experimental and modeling study of isobutene oxidation

Author contributions

Chong-Wen Zhou: Conducted all modelling work, and wrote the manuscript.

Yang Li: Obtained all ignition delay time experimental data on high pressure shock tube, and provided input for modelling efforts, and reviewed the manuscript.

Eoin O'Connor: Obtained all ignition delay time experimental data on rapid compression machine.

Kieran P. Somers: Provided input for modelling efforts, and reviewed the manuscript.

Sébastien Thion *et al.*: Obtained other experimental data.

Henry J. Curran: Managed the project throughout, and reviewed manuscript prior to and post the review process.

Brief description of the paper

IDTs of isobutene oxidation were measured in four different shock tubes and in two rapid compression machines (RCMs) under conditions of relevance to practical combustors. The combination of shock tube and RCM data greatly expands the range of available validation data for isobutene oxidation models to pressures of 50 atm and temperatures in the range 666–1715 K. Isobutene flame speeds were measured experimentally at 1 atm and at unburned gas temperatures of 298–398 K over a wide range of equivalence ratios.

A comprehensive chemical kinetic mechanism has been developed to describe the combustion of isobutene and is validated by comparison to the presently considered experimental measurements. Important reactions, highlighted via flux and sensitivity analyses, include: (a) hydrogen atom abstraction from isobutene by hydroxyl and hydroperoxyl radicals, and molecular oxygen; (b) radical–radical recombination reactions, including 2-methylallyl radical self-recombination, the recombination of 2-methylallyl radicals with hydroperoxyl radicals; and the recombination of 2-methylallyl radicals with methyl radicals; (c) addition reactions, including hydrogen atom and hydroxyl radical addition to isobutene; and (d) 2-methylallyl radical decomposition reactions. The current mechanism accurately predicts the IDT and LFS measurements presented in this study, as well as the JSR and flow reactor speciation data already available in the literature.

A comprehensive experimental and modeling study of isobutene oxidation

Chong-Wen Zhou[a], Yang Li[a], Eoin O'Connor[a], Kieran P. Somers[a], Sébastien Thion[b], Charles Keesee[b], Olivier Mathieu[b], Eric L. Petersen[b], Trent A. DeVerter[c], Matthew A. Oehlschlaeger[c], Goutham Kukkadapu[d], Chih-Jen Sung[d], Majed Alrefae[e], Fathi Khaled[e], Aamir Farooq[e], Patricia Dirrenberger[f], Pierre-Alexandre Glaude[f], Frédérique Battin-Leclerc[f], Jeffrey Santner[g,1], Yiguang Ju[g], Timothy Held[g,2], Francis M. Haas [g], Frederick L. Dryer[g], Henry J. Curran[a,]*

[a]Combustion Chemistry Centre, National University of Ireland, Galway, Ireland
[b]Department of Mechanical Engineering, Texas A&M University, College Station, TX, United States
[c]Department of Mechanical, Aerospace, and Nuclear Engineering, Rensselaer Polytechnic Institute, Troy, NY, United States
[d]Department of Mechanical Engineering, University of Connecticut, CT, United States
[e]Clean Combustion Research Center, King Abdullah University of Science and Technology, Thuwal, Saudi Arabia
[f]Laboratoire Réactions et Génie des Procédés, CNRS-Universitéde Lorraine, Nancy, France
[g]Department of Mechanical and Aerospace Engineering, Princeton University, Princeton, NJ, United States

Published in: *Combust. Flame* 167 (2016) 353–379

Abstract

Isobutene is an important intermediate in the pyrolysis and oxidation of higher-order branched alkanes, and it is also a component of commercial gasolines. To better understand its combustion characteristics, a series of ignition delay time (IDT) and laminar flame speed (LFS) measurements have been performed. In addition, flow reactor speciation data recorded for the pyrolysis and oxidation of isobutene is also reported. Predictions of an updated kinetic model described herein are compared with each of these data sets, as well as with existing jet-stirred reactor (JSR) species measurements.

IDTs of isobutene oxidation were measured in four different shock tubes and in two rapid compression machines (RCMs) under conditions of relevance to practical combustors. The combination of shock tube and RCM data greatly expands the range of available validation data for isobutene oxidation models to pressures of 50 atm and temperatures in the range 666–1715 K. Isobutene flame speeds were measured experimentally at 1 atm and at unburned gas temperatures of 298–398 K over a wide range of equivalence ratios. For the flame speed results, there was good agreement between different facilities and the current model in the fuel-rich region. Ab initio chemical kinetics calculations were carried out to calculate rate constants for important reactions such as H-atom abstraction by hydroxyl and hydroperoxyl radicals and the decomposition of 2-methylallyl radicals.

A comprehensive chemical kinetic mechanism has been developed to describe the combustion of isobutene and is validated by comparison to the presently considered experimental measurements. Important reactions, highlighted via flux and sensitivity analyses, include: (a) hydrogen atom abstraction from isobutene by hydroxyl and hydroperoxyl radicals, and molecular oxygen; (b) radical–radical recombination reactions, including 2-methylallyl radical self-recombination, the recombination of 2-methylallyl radicals with hydroperoxyl radicals; and the recombination of 2-methylallyl radicals with methyl radicals; (c) addition reactions, including hydrogen atom and hydroxyl radical addition to isobutene; and (d) 2-methylallyl radical decomposition reactions. The current mechanism accurately predicts the IDT

and LFS measurements presented in this study, as well as the JSR and flow reactor speciation data already available in the literature.

1. Introduction

Isobutene, one of the butene isomers, is a known component of transportation fuels, as well as being an important intermediate in the pyrolysis and oxidation of higher-order branched hydrocarbons such as isooctane. The pyrolysis and oxidation of methyl and ethyl *tertiary*–butyl ethers, used worldwide as octane enhancers, also produces a significant amount of isobutene. Therefore, kinetic modeling of the combustion of commercial fuels requires a reliable computational tool that can predict the pyrolysis and oxidation behaviors of isobutene and similar compounds (1- and 2-butene). Serving as an archetypal alkene fuel, isobutene is also a precursor for soot formation. Following H-atom abstraction from isobutene, a resonantly stabilized 2-methylallyl radical is formed. Allylic species are implicated in the formation of aromatic and subsequent polyaromatic hydrocarbon species [1]; therefore, understanding the oxidation chemistry of isobutene is important in helping mitigate pollutant formation.

Moreover, understanding the combustion chemistry of the butene isomers is a prerequisite for a comprehensive description of the chemistry of C_1–C_4 hydrocarbon and oxygenated fuels. For the development and validation of combustion models, it is thus crucial to improve our knowledge of detailed C_4 combustion chemistry. Building a comprehensive kinetic model for isobutene is

also an extension of our work on propene [2,3].

Several research groups have investigated isobutene pyrolysis and oxidation in shock tubes [4–10], a turbulent flow reactor [11], a jet-stirred reactor [12] and in premixed laminar flames [13–15]. Yasunaga et al. [9] investigated the pyrolysis and oxidation of isobutene behind reflected shock waves over a temperature range of 1000–1800 K, measuring the product distribution using infrared laser absorption spectroscopy and gas-chromatography. The authors reported species profiles for CH_4 (methane), C_2H_6 (ethane), C_2H_2 (acetylene), C_3H_4-p (propyne), C_3H_4-a (allene), C_3H_6 (propene), 1,3-C_4H_6 (1,3-butadiene) and C_6H_6 (benzene).

Bauge et al. [4] measured ignition delay times of isobutene/oxygen mixture containing 74.45–98.5% argon diluent between 3 ms and 760 ms in the temperature range of 1230–1930 K, over the pressure range of 9.5–10.5 atm and covering the equivalence ratio of 1.0 to 3.0. They also measured speciation data in a continuous-flow stirred-tank reactor at 1 atm in the temperature range 833–913 K. Curran [10] measured ignition delay times for isobutene/oxygen mixtures containing 80.8–98.8% argon diluent in the temperature range 1200–1980 K, at pressures in the range 2.2–4.5 atm, and over the equivalence ratio range of 0.1–4.0.

Dias and Vandooren [13] studied a lean, premixed isobutene/hydrogen/oxygen/argon flame (ϕ = 0.225) using molecular beam mass spectrometry at low pressure (40 mbar). They reported the following detected species: H_2, $\dot{C}H_3$, Ö, $\dot{O}H$, $H\dot{O}_2$, H_2O, C_2H_2 (acetylene), CO, C_2H_4

(ethylene), CH_2O (formaldehyde), O_2, Ar, C_3H_6 (propene), CO_2, CH_3CHO (acetaldehyde), 1,3-C_4H_6 (1,3-butadiene), iC_4H_8 (isobutene), C_3H_6O (acetone), C_4H_6O (1-propen-1-one, 2-methyl) and tautomers of isobutanal (C_4H_8O, prop-1-en-1-ol).

There have been several kinetic mechanisms published in the literature that can be used to simulate isobutene combustion [12,14–16]. Dagaut and co-workers [12] studied the oxidation of isobutene in a jet-stirred reactor at high temperature (~800–1230 K) and at 1, 5 and 10 atm. Measured species profiles were reported as a function of temperature. Molecular species concentration profiles of O_2, H_2, CO, CO_2, CH_2O, CH_4, C_2H_2, C_2H_4, C_2H_6, C_3H_4 (allene and propyne), C_3H_6, acetone, acrolein, methacrolein, 1-C_4H_8, i-C_4H_8, 1,3-C_4H_6, 1-butyne, 2-methyl-1-butene, 2-methyl-2-butene, and benzene were obtained by probe sampling and gas chromatograph (GC) analysis. They also presented a chemical kinetic reaction mechanism capable of reproducing their speciation results. Zhang et al. [16] developed a model to describe the pyrolysis of the butene isomers in the temperature range 900–1900 K at low pressures (~7.5–12.5 Torr), in which kinetic data for the thermal decomposition of butene isomers was measured and recently adopted in the kinetic model of isomeric butanols by Cai et al. [17]. Schenk et al. [14] developed a high-temperature kinetic model for the butene isomers based on a validation against low-pressure laminar premixed flames. However this study did not include some reactions essential to the ignition process in the low- to intermediate-temperature range. Most recently, Law and co-workers [15]

reported laminar flame speeds and ignition temperatures for non-premixed counter-flow flames at normal and elevated pressures. Their mechanism was built on previous studies by Zhang et al. [16] and Cai et al. [17] and included additional rate constants for the reactions of isobutene with Ḣ and Ö atoms and ȮH, HȮ$_2$ and ĊH$_3$ radicals.

In view of the above considerations, we can see that there is a lack of experimental data available in the literature for isobutene at low temperatures (600–1000 K) and at high pressures (> 10 atm), which are conditions of direct relevance with respect to gasoline, diesel, and low-temperature combustion (LTC) engine technologies.

2. Experimental methods

Table 1 compares the experimental conditions investigated as part of this study to those of studies found in the literature. Ignition delay times for isobutene oxidation were measured in four different shock tube facilities and two rapid compression machines (RCMs) shown below. Laminar flame speeds for isobutene were measured at the Universitéde Lorraine (LRPG). Spherical flame speed measurements were also recorded at Princeton University (PU) and Texas A&M University (TAMU). All experimental data are provided in the appended Supplementary material.

Table 1 Ignition delay time, flame speed, and speciation measurements for

isobutene oxidation used in this study for model validation.

Reactor	T (K)	p (atm)	φ	%O2	%Diluent	Ref.
Parameter range for isobutene oxidation available in the literature						
Ignition delay time						
Shock tube	1200–1980	2.2–4.6	0.1–4.0	0.9–18	80.8–98.8 in Ar	[10]
Speciation						
JSR	790–1250	1.0–10.0	0.2–2.0	0.9–4.5	95.35–99.4 in N2	[12]
Flow reactor	1139–1150, 1081	1	0.42–1.29, ∞	1.619–4.757	94.91–99.5 in N2	[11]
Flame speed						
Flat flame burner	298	1.0–10.0	0.7–1.8	19.76–20.5	74.31–77.10 in N2	[15]
Parameter range for isobutene oxidation available in this study						
Ignition delay time						
Shock tube	940–1500	10–50	0.3–2.0	19.63–20.78	73.83–78.18 in N2	
Shock tube	1050–1650	1.7–40	0.5–2.0	0.857–20.65	76.32–99 in Ar	
RCM	666–996	10–50	0.3–2.0	19.63–20.78	73.83–78.18 in N2	
Flame speed						
Flat flame burner	298–398	1	0.6–1.9	19.70–20.60	74.06–77.37 in N2	
Spherical Flame	298	1	0.75–1.5	19.96–20.47	75.05–76.97 in N2	

2.1. Ignition delay time measurements

2.1.1. NUI Galway (NUIG) high-pressure shock tube

Ignition delay times were measured in the high-pressure shock tube at NUIG described in the recent study by Burke et al. [2]. Ignition delay times were recorded for isobutene/‘air’ mixtures at ϕ = 0.3, 0.5, 1.0 and 2.0 at pressures of approximately 10, 30 and 50 atm and in the temperature range of approximately 940–1500 K. The air was considered as a 21/79 vol. oxygen/nitrogen blend. All fuels were acquired from Sigma Aldrich at 99.5% purity. Oxygen, nitrogen, argon and carbon dioxide were acquired from BOC

Ireland at high purity (≥ 99.5%). The overall uncertainty for each individual ignition delay time is estimated to be 20%. Uncertainties in pressure, temperature, mixture composition, and those associated with the determination of the ignition delay time from the measured traces all contribute to the overall uncertainty.

The ignition delay time was defined as the interval between the rise in pressure due to the arrival of the reflected shock wave at the endwall and the maximum rate of rise of the pressure signal, as shown in Fig. 1.

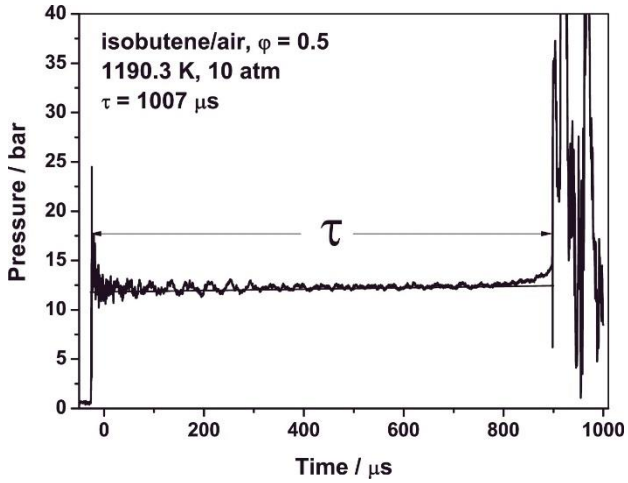

Fig. 1. Sample pressure trace from NUI Galway shock tube.

2.1.2. Texas A&M University (TAMU) shock tube

The single diaphragm, stainless steel, shock tube used at Texas A&M University was 7.18 m long. The driven section had a 15.24 cm i.d., and was 4.72 m long, the driver section had an inner diameter of 7.62 cm. Helium was used as the driver gas during this study. A schematic of the shock-tube setup has been given by Aul et al. [18]. All experimental methods were identical to those used in our recent collaborative study of propene ignition [2]. Ignition

delay times for isobutene/O_2/Ar mixtures were measured at ϕ = 0.5 and 1.0 with isobutene concentration ranges from 0.143% to 2% at pressures of 1.7 and 10 atm and in the temperature range of 1050–1765 K.

In addition to the endwall and sidewall transducers to monitor the test pressure, the chemiluminescence emission from the excited hydroxyl radical (OH^*) located on the sidewall was also used to monitor the kinetics of the reaction. To detect possible pre- ignition events that could occur during the tests, chemiluminescence was also recorded using another photomultiplier but without a filter at the endwall location. Ignition delay time from the three measurements shown in Fig. 2 (a) and (b) lead to very similar results. In Fig. 2 (b), the ignition delay time for the OH^* signal was defined as the time between the arrival of the shock wave at the endwall and the intersection of lines drawn along the steepest rate-of-change of OH^* de-excitation (i.e., chemiluminescence) and a horizontal line which defines the zero-concentration level. Time zero is defined as the time at which the shock wave arrived at the endwall.

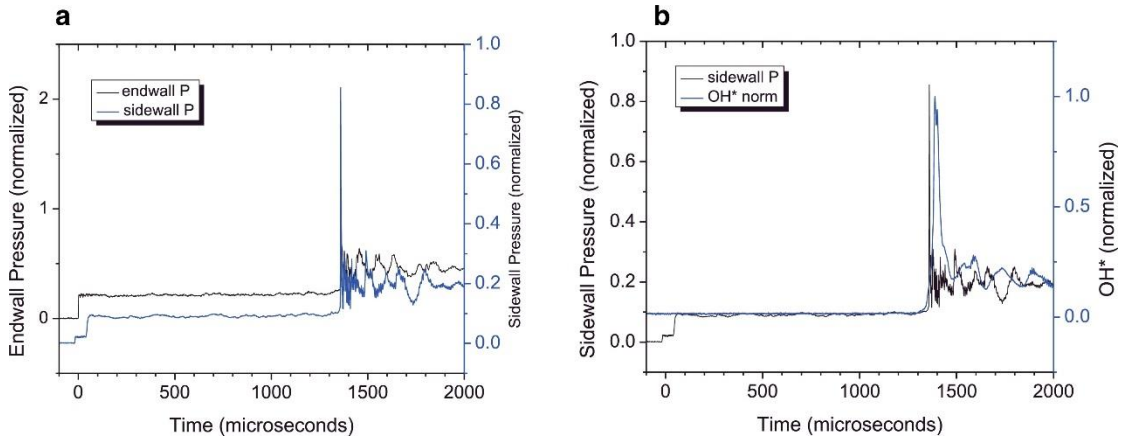

Fig. 2. Ignition delay time measurements in the TAMU shock tube at 1222 K, ϕ = 1.0, 2% isobutene in Ar, 9.34 atm. (a) Pressure sensors located at both the

endwall and sidewall locations. (b) Pressure and OH^* emission measurements.

2.1.3. Rensselaer Polytechnic Institute (RPI) shock tube

Measurements of isobutene ignition delay times were made at RPI in the high-pressure shock tube described by Shen and Oehlschlaeger [19]. All experimental methods were identical to those used in our recent collaborative study of propene ignition [2]. For the present experiments with isobutene, which is gaseous at standard conditions, shock tube heating was not necessary. Ignition delay times were measured for isobutene/air mixtures at ϕ = 0.5, 1.0, and 2.0 at pressures around 10 atm and for isobutene/12% O_2/Ar mixtures at ϕ = 1.0 and 2.0 at pressures around 10 and 40 atm. Reactant mixtures were made outside the shock tube in a mechanically-stirred mixing vessel. Isobutene was from Sigma-Aldrich at 99+% purity and O_2, N_2, and Ar were 99.995% pure from Noble Gas. Following reactant mixture preparation and mechanical mixing (4 h), reactant test gases were loaded into the shock tube driven section and ignition delay experiments performed. Ignition delay time determinations were made behind reflected shock waves by measuring the pressure at a side wall location 2 cm from the driven section end wall and hydroxyl radical emission (OH^*) viewed through the driven section end wall. The onset of ignition was defined by extrapolating the maximum slope in OH^* signal to the baseline and time-zero was defined as the time of shock reflection at the end wall, determined from the measured pressure and incident shock velocity. Figure 3 illustrates an example measurement. The reflected shock conditions were determined using the normal shock relations with input of the measured

incident shock velocity, determined via the incident shock passage over a series of five pressure transducers spaced over the last meter of the driven section. The uncertainty in reflected shock temperature and pressure is estimated at approximately ±1% and ±1.5%, respectively, for the conditions considered in this study. The uncertainty in ignition delay time is estimated at ±20%, based on contributions from uncertainty in reflected shock conditions and in determination of ignition delay from measured signals. The measured reflected shock pressure profiles show non-ideal pressure rise of $(dp/dt)(1/p_0)$ = 2–3%/ms at the conditions studied.

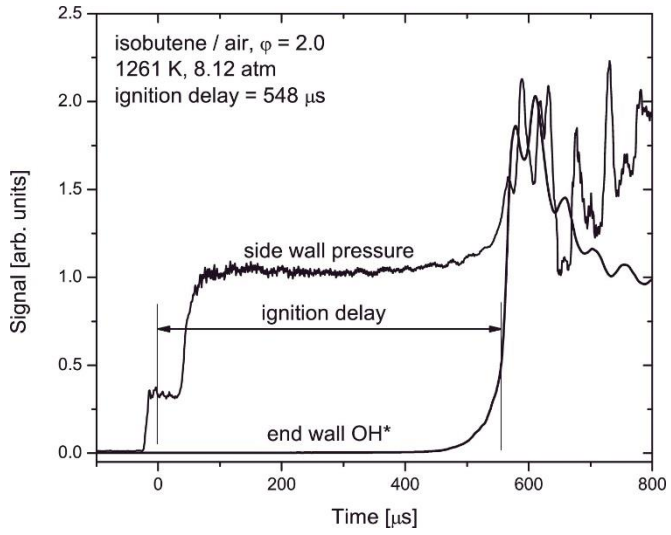

Fig. 3. Example isobutene ignition delay time measurement from the RPI facility.

2.1.4. King Abdullah University of Science and Technology (KAUST) shock tube

The KAUST high-pressure shock tube (HPST) was used to measure the ignition delay times for isobutene/'air' mixtures at ϕ = 0.5, 1.0 and 2.0 at 40

atm. The HPST is described elsewhere [2] and explained briefly here. The HPST is constructed from stainless steel with an inner diameter of 10 cm and a total length of 13.2 m. The driven section is 6.6 m long and the driver section length can be varied to a maximum of 6.6 m; the two sections are separated by pre-scored aluminum diaphragms. The driven section was vacuumed before the experiment to less than 10 –5 mbar using a turbo-molecular pump. A mixing vessel equipped with a magnetic stirrer was used to prepare gaseous mixtures. Helium was used as the driver gas in the experiments reported here. In order to measure the incident shock velocity, six PCB 113B26 piezoelectric pressure transducers (PZTs) were placed axially along the last 3.6 m of the driven section. Shock-jump equations were used to calculate the post-reflected shock conditions (p_5 and T_5). Kistler 603B1 PZT located at 1.0 cm from the end-wall was used to record the pressure behind the reflected shock wave. The measured reflected shock pressure profiles showed non-ideal pressure rise of $(dp/dt)(1/p_0)$ 2–3%/ms at the conditions of current experiments. The OH^* emissions were monitored through Sapphire windows at the endwall and sidewall (1.0 cm from the endwall) locations using PDA36A photo-detectors. The experimental setup is shown in Fig. 7 by Burke et al. [2]. Ignition delay time is defined as the time from the arrival of the reflected shock wave to the onset of ignition at the sidewall. Three diagnostics, pressure trace and the OH^* emission detected at the endwall and the sidewall, were used to determine the onset of ignition. The three methods predict very similar ignition delay times, as illustrated in Fig. 4.

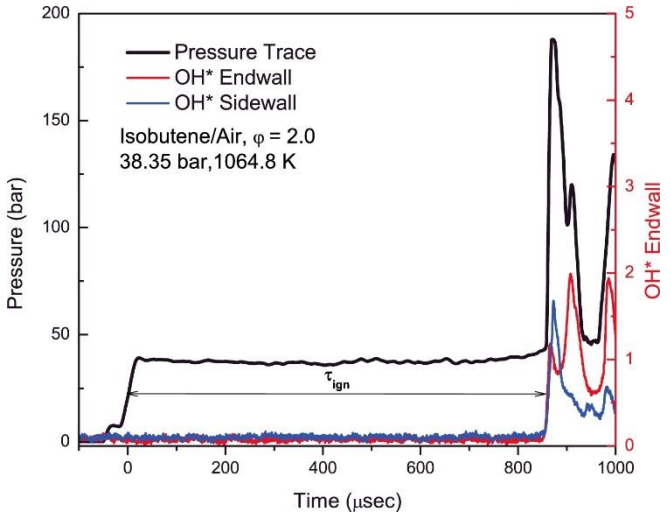

Fig. 4. Example of isobutene ignition delay time measurement from the KAUST shock tube.

2.1.5. NUI Galway rapid compression machine

Ignition delay times for isobutene/'air' mixtures at ϕ = 0.3, 0.5, 1.0 and 2.0 at pressures of approximately 10, 30 and 50 atm were measured at NUIG in the rapid compression machine and are similar to those described in the recent propene study by Burke et al. [2]. The ignition delay time definition in this work is shown in Fig. 5 and is taken from the time of peak pressure at the end of compression to the time of maximum rate of pressure rise due to ignition.

We recognize that uncertainty quantification for experimental data is an essential step in assessing agreement between the experimental data and kinetic mechanism simulation results. It is natural to think in terms of two types of uncertainties for RCM experiments; uncertainties in the measured ignition delay time and also uncertainties in the measured and inferred thermodynamic state of the reacting gas.

We are confident that ignition delay times can be measured quite

accurately within the RCM. This confidence stems from the high natural frequency of the transducer (80 kHz) used to monitor in-cylinder pressure along with the sufficient time-resolution of the data acquisition unit (20 kHz) to adequately capture both the end of compression time and the occurrence of the ignition event to within about 0.05 ms. The a-synchronicity of the pistons' arrival at maximum compression in our dual piston machine contributes to shot-to-shot scatter in ignition delay measurements due to the stochastic change in the piston seating process. This a-synchronicity can cause inconsistencies for the defined end of compression time between reactive and non-reactive traces of up to 0.5 ms, which only induces large uncertainties when comparing experimental and simulated ignition delay times for short ignition events (for example, ±5% for an ignition delay of 5 ms and ±0.5 at 50 ms).

While the RCM exhibits great accuracy for ignition delay measurements the characterization of the thermodynamic state of the reacting gas is more difficult, especially with regard to compressed temperatures that are evaluated from the adiabatic core hypothesis. Initial mixture mole fractions are expected to be accurate to within about ±2% of their reported nominal value, where the main contribution of uncertainty comes from partial pressure measurements. Time resolved measurements of in-cylinder pressures are readily achievable with modern static and dynamic pressure transducers, which result in the measurement of the initial reactor pressure and transient pressure history to within approximately ±0.05% and ±1 bar, respectively. Assuming perfect applicability of the adiabatic core hypothesis to the experiments conducted in

this study and accounting for both uncertainties in the initial temperature and pressure measurements, the uncertainty of the inferred adiabatic core compressed temperature is less than approximately ±15 K.

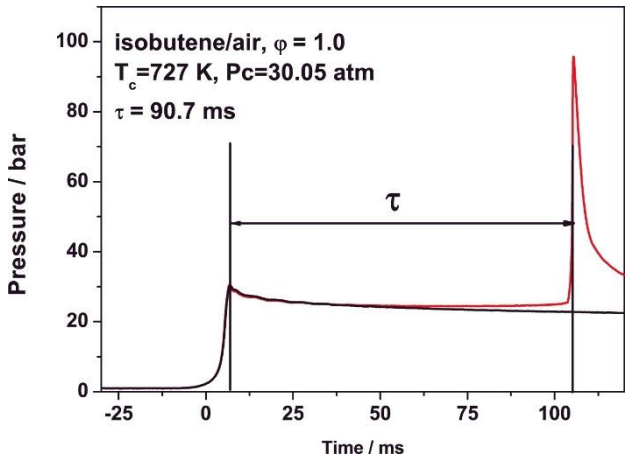

Fig. 5. Sample pressure traces from NUI Galway RCM. – Non-reactive profile, – reactive profile.

2.1.6. University of Connecticut (UConn) rapid compression machine

The rapid compression machine (RCM) at UConn employs a creviced piston to compress test mixtures to elevated pressures and temperatures. The creviced piston is driven pneumatically and brought to rest by hydraulic pin-groove mechanism towards the end of the compression stroke. While the typical compression times are around 30−45 ms, the majority of pressure/temperature rise occurs in the last 6 ms of compression, as shown in Fig. 6. A trigger from LabVIEW ®initiates the compression event and starts data acquisition. Dynamic pressure in the reaction cylinder is measured using a thermal-shock resistant Kistler 6125C transducer in conjunction with 5010 B charge amplifier. Test gas mixtures can be compressed to desired test

conditions, compressed pressure (p_c) and compressed temperature (T_C), by independently varying compression ratio, intake pressure (p_0), and intake temperature (T_0). Compression ratios varying between 7 and 17 can be attained by varying stroke length or/and clearance length. More- over, compressed temperature is deduced using the adiabatic core hypothesis.

The reaction cylinder is filled to the desired intake pressure with a homogenous fuel/oxidizer mixture prepared in a separate stainless-steel mixing chamber of 17.47 L, which is equipped with heaters to preheat the mixture to the desired intake temperature. In the current study, isobutene (> 99%) supplied by Sigma-Aldrich and ultra-high purity (> 99.99%) O_2 and N_2 from Airgas are used to prepare homogenous isobutene/'air' mixtures in mixing chamber. The 'air' used in these experiments is a mixture of O_2 and N_2 in the molar ratio of 1:3.76. Fuel/oxidizer mixtures are prepared manometrically. The mixing chamber, intake manifold, and reaction cylinder are heated to the desired preheat temperature for about 4 hours before starting the experiments. Additionally, the mixing chamber is equipped with a magnetic stirrer which aids in preparation of homogeneous mixtures. Further details about the current RCM design and test procedure can be found in Das et al. [20].

Figure 6 shows the typical experimental repeatability and the definition of ignition delay used for reporting the present data. Ignition delay is defined as the time difference between the end of compression (EOC) and the maximum time derivative of the pressure after EOC. A minimum of four consecutive runs are conducted at each condition and the value close to the mean of the

measured ignition delays is reported as the representative value. The scatter in ignition delays is less than 10% of the representative value for all the cases investigated. Furthermore, to ensure repeatability, ignition delay data obtained from each fresh mixture is checked with that from an earlier mixture.

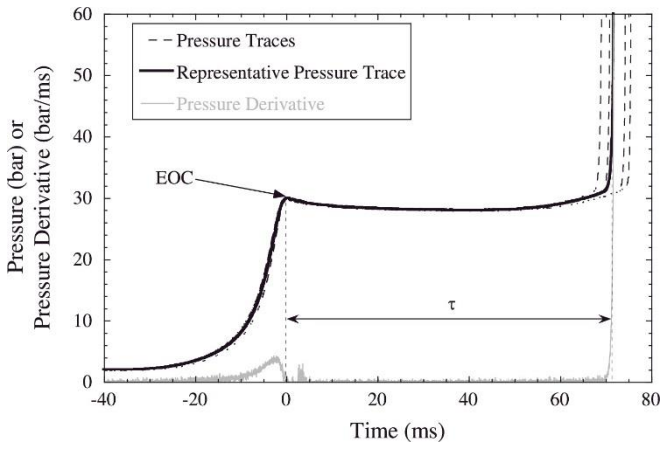

Fig. 6. Plot showing experimental repeatability and definition of ignition delay at $\phi = 2.0$ in air, $p_C = 30$ bar, $T_C = 686$ K, $\tau = 72$ ms.

In order to account for the effect of heat loss to the reactor walls on ignition delay, nonreactive experiments corresponding to each reactive run are taken to infer heat loss characteristics during compression and post compression periods. In these nonreactive experiments, isobutene/N_2 mixtures are prepared by replacing O_2 with N_2 in the corresponding reactive mixtures while maintaining the same fuel concentrations such that a similar specific heat ratio is maintained, and similar heat loss conditions exist between the reactive case and the nonreactive case. Pressure traces from nonre- active runs are further used to generate volume vs. time histories in conjunction with the adiabatic core hypothesis. These volume histories are then imposed on

auto-ignition simulations for characterizing the heat loss effect during the compression stroke and the post compression event.

2.2. Flame speed measurements

Laminar flame speeds for isobutene were measured in three different facilities, which are located at Texas A&M University (TAMU), Princeton University (PU) and Laboratoire Réactions et Génie des Procédés (LRPG).

2.2.1. Texas A&M flames

Laminar flame speed experiments were conducted in the high-temperature, high-pressure, constant-volume bomb at TAMU. This vessel has an internal diameter of 31.8 cm and an internal length of 28 cm. Optical access is gained through fused-quartz windows located on either end of the vessel, each with a diameter of 12.7 cm. The flame is centrally ignited by two electrodes. The relatively large volume of the vessel allows the flame to propagate at near- constant pressure for the course of the experiment, which ends when the flame reaches the diameter of the 12.7-cm window aperture. For the present experiments, the increase in pressure before the optical aperture limit was reached was, worst-case, less than 5%. Full details on this experimental setup are given in Krejci et al. [21].

Mixtures were prepared using the partial pressure method with a 0–1000 Torr pressure transducer. Instrument-grade isobutene and Primary Standard Air were used to conduct all experiments. The initial conditions were 1 atm and 298 ±2 K. Images were taken using a Z-type schlieren setup and a high-speed

camera (Photron Fastcam SA1.1) at a rate of 60 0 0 fps. These images were then processed using an internally developed MATLAB-based edge detection program. The burned, un-stretched laminar flame speed was extracted using the appropriate nonlinear method depending on the Markstein length as outlined by Chen [22]. Images that clearly showed either an ignition effect or a wall effect, based on the dr/dt versus stretch plot, were neglected. The unburned, un-stretched flame speed was then determined using the density ratio calculated from the equilibrium chemistry.

Experimental uncertainty for the TAMU flame speed experiments was calculated using the Kline and McClintock method. The total uncertainty in the experiments is the square root of the square of the bias error plus the square of the random error. The bias error was based on inaccuracies in the temperature and pressure gauges used for the experiments, and the random error was based off of the average difference between the repeated points in the data set. The overall uncertainty was calculated to be just be- low ±1.0 cm/s. Additional consideration was given in this study for differences in the measured values amongst the various apparatuses, as described in the results section.

2.2.2. Princeton University flames

Mass burning rates (the product of flame speed and unburned mixture density) were measured using the spherical flame method in a 10 cm diameter cylindrical chamber with a concentric pressure release chamber and two optical windows with details are shown in [23]. Mixtures were created from bottled air and isobutene (> 99%, Airgas) using the partial pressure method. To reduce

com- positional uncertainty caused by low fuel partial pressure, lean mixtures were prepared by first creating a rich mixture, allowing the mixture to homogenize for 10 min, partially evacuating the chamber, and then diluting with further air to reach the target equivalence ratio and pressure. After allowing the final mixture ten minutes to become quiescent, it is centrally ignited by a spark. High speed (15,000 fps) schlieren imaging is utilized to image the flame propagation up to a radius of 3 cm. The combustion pressure rise is released to the outer chamber after the flame front has passed the edge of the viewing window. A flame edge detection program and circle fitting algorithm are used to determine the flame radius from each image. The stretched propagation speed S b and stretch rate κare extracted from the flame radius time history and corrected for asymmetric compression-induced flow effects as discussed in [24]. The un-stretched flame propagation speed $S_{b,0}$ is then calculated through extrapolation to zero stretch using the linear stretch relation (for mixtures with near unity Lewis number), although the curvature method [22] gives results within 5%. Low extrapolation uncertainty is expected, as $-0.1 < \mathrm{Ma} \times \mathrm{Ka} < 0.2$ for all measurements [25]. Extrapolation endpoints are determined iteratively by locating the range where the residuals from the fit are below a threshold value and using this range to compute a new fit. This process is repeated while decreasing the threshold until stable endpoints (upper limit of flame radius) are found. The value re- ported here is the un-stretched laminar flame speed relative to the unburned gas, $S_{u,0}$, calculated by multiplying $S_{b,0}$ by the density ratio of burned to unburned gas. No data were used for flames that

were observed to be wrinkled due to cellular or spiraling instabilities, affected by buoyancy, or influenced by transient response of the flame speed to stretch rate. The effect of thermal radiation on apparent burning rate is expected to be minor for these relatively fast flames [26].

2.2.3. CNRS-Universitéde Lorraine flames

The laminar burning velocities of isobutene oxidation were measured at Laboratoire Réactions et Génie des Procédés (LRGP) using the same atmospheric pressure heat flux burner as that used to study propene flames [2], as well as of components of natural gas [27] and gasoline [28,29]. The heat flux method proposed first by De Goey and co-workers [4] allowed stabilizing adiabatic flat flames using heat loss compensation in order to derive adiabatic burning velocities directly from inlet gas flow rate measurements. The burner head was a perforated 30 mm diameter brass plate. The head was mounted on a mixing chamber enclosed in a thermo- static oil jacket, the temperature of which was set to the desired initial temperature of the fresh gas mixture. The circumference of the burner plate was heated with thermostatic oil set to about 50 K above the temperature of the unburned gas mixture so that the heat gain of the unburned gas mixture from the burner can compensate for the heat loss from the flame to the burner necessary to stabilize the flame.

The adiabaticity of the flame was checked by eight type K thermocouples inserted into holes of the burner plate and positioned at different distances and angles from the center to the periphery of the burner. When the temperature profile was flat, it meant that no heat was globally lost or gained by the flame

and that the flame became adiabatic with respect to the burner. The adjustment of the flow rate of the gas mixture made it possible to find the appropriate gas velocity, which canceled out the net heat flux so that the radial temperature distribution in the burner plate was uniform. The flow rate at which the net heat flux was zero corresponded to the adiabatic flame burning velocity.

The burning velocity of isobutene/air mixtures has been investigated under atmospheric pressure for fresh gas temperature 298 K, 358 K, and 398 K and equivalence ration ranging from 0.6 to 1.9. The air was considered as a 21/79 vol. oxygen/nitrogen blend. Gas flow rates were measured using Bronkhorst High-Tech Mass Flow Controllers (MFC). Oxygen and nitrogen were delivered by Messer (purity > 99.995 vol%). Isobutene was provided by Air Liquide (purity > 99.5%, without any noticeable content of other hydrocarbons). The uncertainty in the laminar burning velocity can be first attributed to the uncertainty in the mass flow measurements (around 0.5% for each MFC) which can lead to a global uncertainty of 1.5% and around 1% in equivalence ratio. The uncertainty in reading the temperature with thermocouples which could lead to an error of around 0.2 cm/s in the laminar burning velocity, and to errors due directly to flame distortions, such as edge effects (estimated around 0.2 cm/s). In the case of very rich mixtures, the change in the curvature of the temperature profile with the gas flow is more difficult to determine.

2.3. Ignition delay time simulations and sensitivity analyses

2.3.1. Shock tube simulations

Shock tube simulations were performed as zero-dimensional calculations and begin at the onset of the reflected shock period. The reflected shock pressure (p_5) and temperature (T_5) were used as the initial pressure and temperature, respectively. Constant volume, homogeneous and adiabatic conditions are assumed behind the reflected shock wave and no facility effects were necessarily included. For ignition delay calculations, the simulated ignition delay time is defined to be consistent with the particular diagnostic used in the experiment being simulated. The mechanism presented in this study contains a sub-mechanism for both excited CH^* and OH^* which have been adopted from Hall and Petersen [30], and Kathrotia et al. [31], respectively. CHEMKIN-PRO [32] is used to carry out the simulations.

2.3.2. Rapid compression machine simulations

The ignition delay time simulations of the RCM use a volume profile generated from the corresponding nonreactive pressure trace, for which an experiment is performed by replacing oxy- gen with nitrogen in the fuel/air mixtures. The volume history used for the simulation included the heat loss during the com- pression stroke by adding an empirically determined additional volume, and the heat loss after the end of compression was ac- counted for by the "adiabatic core expansion" approach [33-35]. Non-reactive pressure-time traces are taken to correspond to each unique p_c and T_C condition studied. The volume history is then used as an input in the CHEMKIN-PRO [32] input file.

2.3.3. Brute-force sensitivity

"Brute force" sensitivity analyses were carried out in order to identify the key reactions which control fuel reactivity. The analyses were performed by increasing and decreasing each reaction rate expression by a factor of two and calculating the effect on the predicted ignition delay time.

The sensitivity coefficient is defined as: $S = \ln(\tau_+/\tau_-)/\ln(\kappa_+/\kappa_-) = \ln(\tau_+/\tau_-)/\ln(2.0/0.5)$, where, τ_+ is the ignition delay time calculated with the increased rate constant and τ_- is the ignition delay time calculated using the decreased rate constant. A positive sensitivity coefficient indicates an inhibiting reactivity while a negative sensitivity coefficient indicates a reaction promoting reactivity.

2.4. Flame speed simulations and sensitivity analyses

Flame speeds were simulated by the Premix module of CHEMKIN PRO [32]. A high-temperature version of the model which does not include low temperature chemistry was created to simulate the flame speed to avoid the high computational cost of using the full mechanism. The species removed include the 2-methylallyl radical self-recombination product, alkyl-peroxyl radicals, hydroperoxyl-allyl radicals, ketohydroperoxide species, to reduce the size of the mechanism. Metcalfe et al. [36] carried out extensive tests of flame speed calculations for C_0–C_2 molecular species using AramcoMech 1.3 and found that the high-temperature mechanism results in the same predictions as the full mechanism with a considerably reduced computational time.

Simulations were converged to a grid-independent solution by assigning GRAD and CURV values of 0.02. The mixture-averaged diffusion method for calculating the transport coefficients was used. The Transport Data Estimator package of the Reaction Mechanism Generator software of Green and co-workers [37] has been used to provide relevant transport properties. Thermal diffusive effects were also accounted for and generally resulted in a noticeable reduction in flame speed. CHEMKIN-PRO was also used to perform the flame speed sensitivity analyses.

3. Computational method

Rate constant calculations have been carried out for the follow- ing important reactions associated with isobutene oxidation and pyrolysis:

- $iC_4H_8 + OH \leftrightarrow iC_4H_7 + H_2O$
- $iC_4H_8 + OH \leftrightarrow iC_4H_7\text{-}i1 + H_2O$
- $iC_4H_8 + HO_2 \leftrightarrow iC_4H_7\text{-}i1 + H_2O_2$
- $iC_4H_8 \leftrightarrow C_3H_5\text{-}a + CH_3$

The M062X method [38] with the 6-311 ++ G(d,p) basis set were used in the geometry optimizations and frequency calculations of all of the species involved in this reaction using Gaussian 09 [39]. The same method was used to determine the potential energy sur- face scans for the individual hindered rotors associated with reactant and transition state. The electronic single point energies have been calculated at QCISD(T)/cc-pVXZ level of theory (where X = T and Q) which were extrapolated to the complete basis set (CBS) limit [40,41].

Conventional transition-state theory [42] with an asymmetric Eckart tunneling correction [43] has been used to calculate the high-pressure limit rate constants in this work. The low-frequency torsional conserved modes were treated as hindered rotors using a Pitzer–Gwinn-like approximation [44] to calculate the partition function.

4. Chemical kinetic mechanism development

The current mechanism development is based on the H_2/O_2 sub-mechanism adopted from the study of Kéromnès et al. [45], the C_1–C_2 sub-mechanism, AramcoMech 1.3, adopted from the study of Metcalfe and co-workers [36] and the propene/allene/propyne sub-mechanism adopted from the recent publications of Burke et al. [2,3]. The important thermodynamic parameters are estimated using the group additivity method employed by Benson [46] with updated group values by Burke et al. [47] and utilized in the program developed by Ritter and Bozzelli [48]. During these developments, the mechanism has been validated against numerous experimental conditions and targets. Key reactions for isobutene oxidation at different temperature and pressure conditions were highlighted by sensitivity analyses for reflected shock ignition delay times, flux analyses and flame speed sensitivity analyses. The isobutene combustion chemistry model developed in this work has improved the predictions against a variety of experimental results. The comprehensive kinetic mechanism AramcoMech 2.0, thermochemistry and transport files will be provided as Supplementary material and will also be available to download at http://c3.nuigalway.ie/mechanisms.html.

4.1. Important reaction classes highlighted

Figure 7 highlights the important reactions controlling isobutene fuel oxidation at 10 and 30 atm and at fuel-lean (ϕ = 0.3) and fuel-rich (ϕ = 2.0) conditions at intermediate temperatures. The reactions of $iC_4H_8 + OH \leftrightarrow iC_4H_7 + H_2O$, $iC_4H_7 + iC_4H_7 \leftrightarrow$ H15DE25DM and $iC_4H_7 + CH_3 (+M) \leftrightarrow aC_5H_{10} (+M)$ inhibit reactivity for both fuel-lean and fuel-rich conditions at intermediate temperatures. When the pressure increases, the 2-methylallyl (iC_4H_7) radical self-recombination reaction becomes more favored and inhibits the reactivity more pronouncedly than at lower pressures.

The reactions of iC_4H_7 with HO_2 radicals are the most promoting ones at intermediate temperatures in both fuel-lean and fuel-rich mixtures. This is due to the formation of the highly re- active OH radicals and methyl-allyloxyl (iC_4H_7O) radicals; the latter ultimately decompose to produce 2-propenyl (C_3H_5-t) radicals through different reaction pathways. These C_3H_5-t radicals react with O_2 to form CH_3COCH_2 radicals and Öatoms, which ultimately promotes reactivity. It is interesting to note that H-atom abstraction from iC_4H_8 by O_2 to form iC_4H_7 and HO_2 radicals is the most promoting reaction for fuel-rich mixtures (ϕ = 2.0). This is because, at fuel-rich conditions, the concentration of the fuel is high and the two products, iC_4H_7 and HO_2 radicals, will react further to produce methyl-allyloxy radical (iC_4H_7O) and the highly reactive OH radical. The reaction of $iC_4H_8 + OH \leftrightarrow iC_4H_7$–i1 + H_2O promotes reactivity at all conditions studied, as the vinylic isobuten1-yl radical (iC_4H_7–i1) reacts with molecular oxygen to form CH_3COCH_3 +HCO and iC_3H_5CHO + OH,

promoting reactivity. The formation of iC_3H_5CHO mainly through the decomposition of iC_4H_7O radicals via the reaction $iC_4H_7O \leftrightarrow iC_3H_5CHO + H$ is also an important species at intermediate temperatures. With a very weak bond strength ($iC_3H_5CO\ldots H$) of 87.1 kcal mol^{-1}, the aldehydic hydrogen atom is quite easy abstractable to form an iC_3H_5CO radical, which decomposes to form CO and a C_3H_5-t radical which promotes reactivity.

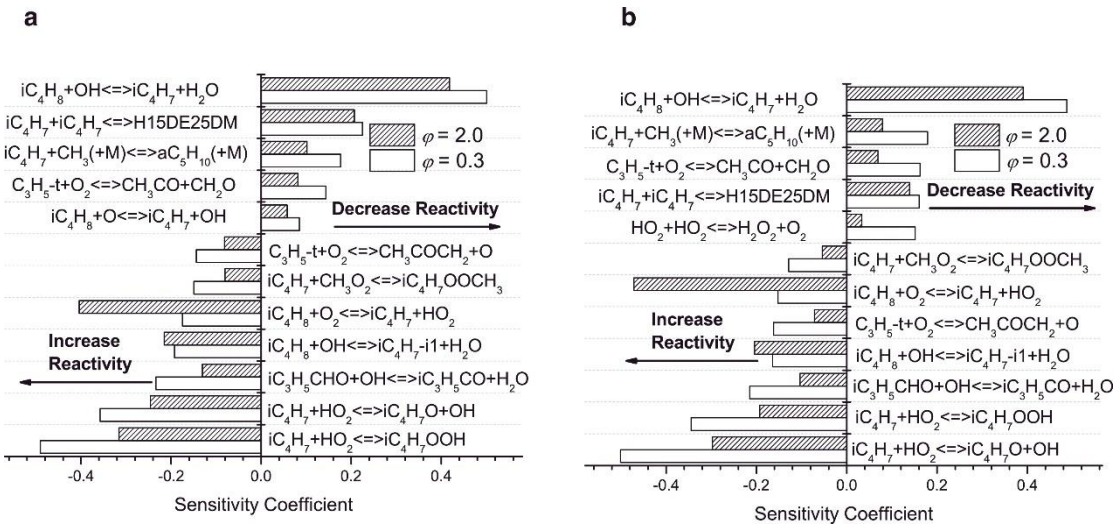

Fig. 7. "Brute force" sensitivity analyses to ignition delay times performed at (a) T = 950 K, p = 30 atm, ϕ = 0.3, and 2.0, (b) T = 900 K, p = 10 atm, ϕ = 0.3, and 2.0.

When the temperature increases to 1250 K, the reaction $iC_4H_8 + O_2 \leftrightarrow iC_4H_7 + HO_2$ is the most dominant one promoting reactivity at both fuel-lean and fuel-rich conditions over the entire pressure range investigated here, Fig. 8. The 2-methylallyl radical self-recombination reaction is not observed to be important at higher temperatures as the adduct readily decomposes.

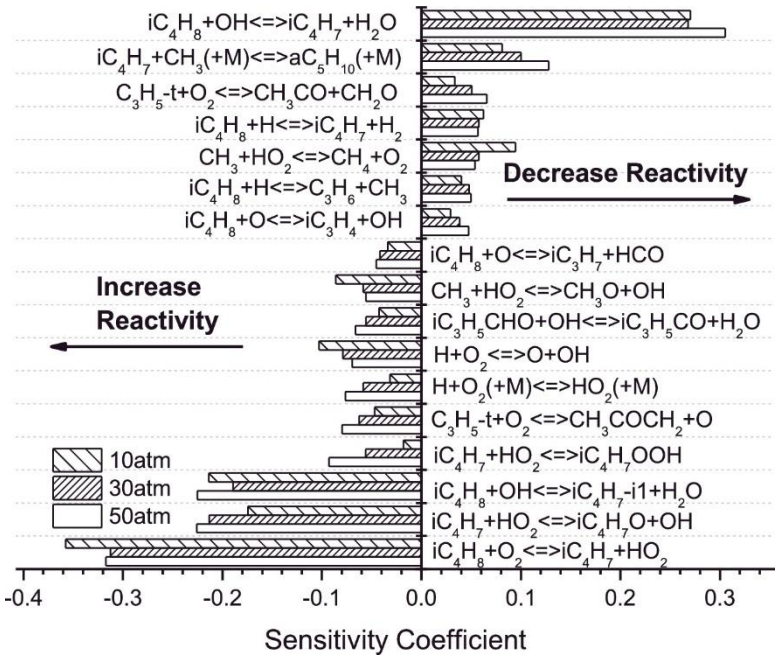

Fig. 8. “Brute force” Sensitivity analyses to ignition delay times performed at ϕ = 1.0, fuel/air, T = 1250 K and different pressures.

All of the reactions highlighted here will be discussed in detail in the following sections and the detailed reaction pathways are shown in Fig. 10. From the bond dissociation energy (BDE) comparison of propene and isobutene shown in Fig. 9, we can see that the BDE of the C–C bond in isobutene is 2.0 kcal mol^{-1} lower than that in propene and the allylic C–H bond in isobutene is 0.8 kcal mol^{-1} higher than in propene. Thus, for some of the important reaction rate constants, we use analogous rate constants from propene for isobutene with some reasonable adjustment; for some of the important reaction rate constants we also carried out ab initio calculations. Moreover, details of the choice of rate constants are discussed and explained in the following sections.

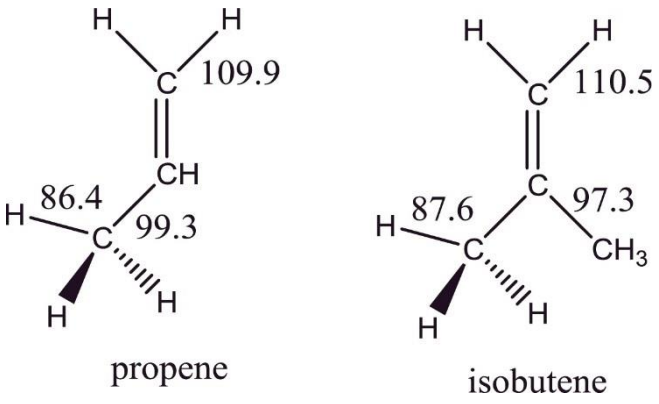

Fig. 9. Bond dissociation energy (in kcal/mol) comparison between propene and isobutene obtained at QCISD(T)/CBS//M062x/6-311 ++ G(d,p) at 0 K.

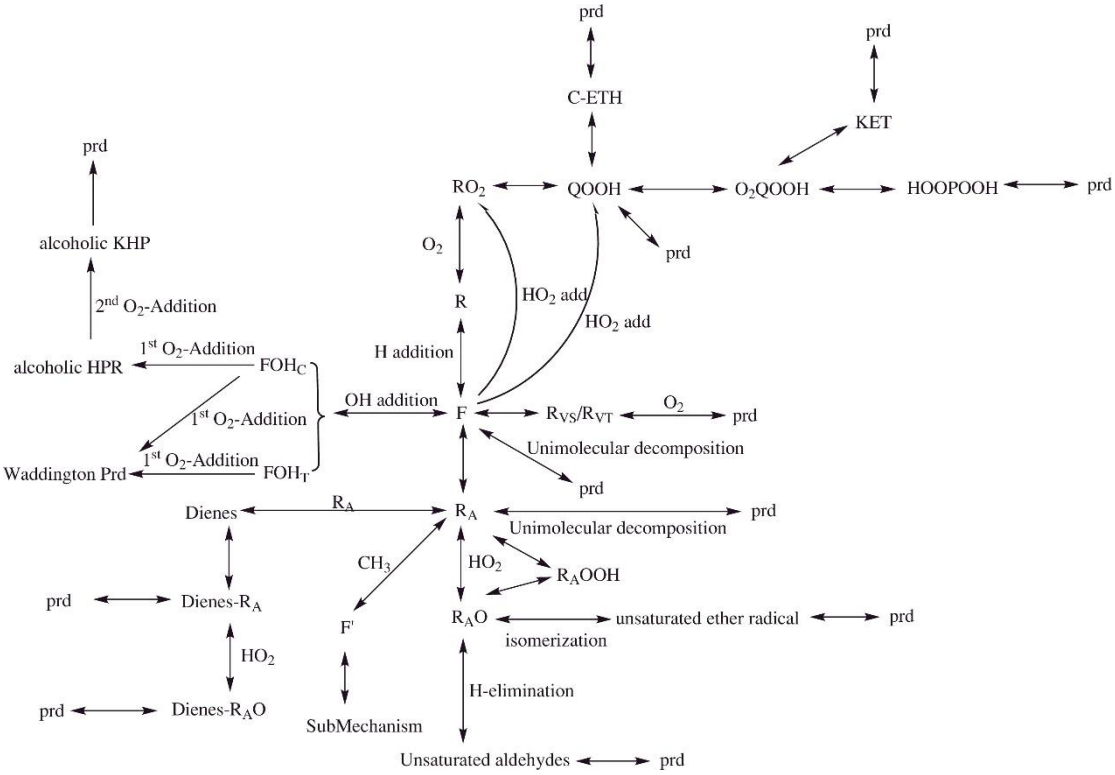

Fig. 10. Generalized reaction pathways included in this work for isobutene oxidation. F: fuel; R_A: allylic radical, R_{VS}: vinylic secondary radical; R_{VT}: vinylic tertiary radical; R_AO: methyl-allyloxyl radical; F′: 2-methyl-1-butene; alcoholic KHP: alcoholic keto-hydroperoxide; dienes: 2,5-dimethyl-1,5-hexadiene.

4.2. Unimolecular decomposition

Two important reaction channels highlighted here are the allylic C–H bond fission reaction channel which has the lowest bond dissociation energy (forming 2-methylallyl (iC_4H_7) radical and a H atom) and the C–C bond fission reaction channel (forming C_3H_5-t and CH_3 radicals):

- $iC_4H_8 \leftrightarrow iC_4H_7 + H$
- $iC_4H_8 \leftrightarrow C_3H_5\text{-t} + CH_3$

Speciation measurements of isobutene pyrolysis in the PU flow reactor [49] are sensitive to isobutene decomposition, Fig. 11. The high-pressure limit rate constant has been adopted by analogy with propene [50] with further QRRK calculations to estimate the pressure fall off. However, in order to improve agreement with flow reactor speciation measurements from [49], the rate constant for the formation of methylallyl radical and atomic hydrogen has been increased by a factor of two. This adjustment is well within the uncertainty of the rate constant estimation. Figure 11 shows the influence of this adjustment.

4.3. Fuel-radical reactions

H-atom abstraction reactions by various radicals from isobutene have been included in this work. There are two different types of hydrogen atom in isobutene that can be abstracted: one from the methyl site forming the resonantly stabilized iC_4H_7 radical and the other from the terminal carbon to form a vinylic radical (iC_4H_7-i1). As shown in Fig. 9, the bond dissociation

energy comparison between those two types of C–H bonds tells us the formation of the 2-methylallyl radical is dominant because it is about 22.9 kcal mol^{-1} weaker than the vinylic one.

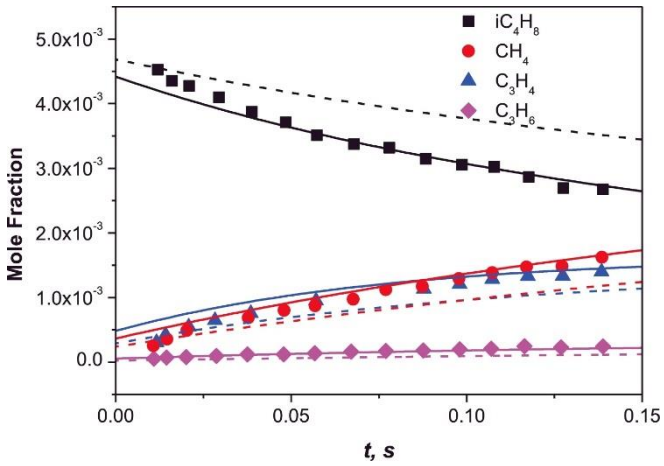

Fig. 11. Influence of rate constants for $iC_4H_8 \leftrightarrow iC_4H_7 + H$ in flow reactor speciation analysis for isobutene pyrolysis (0.503% iC_4H_8, in N_2, p = 1 atm, T = 1150 K. Symbols: APFR experimental measurements [49], lines: mechanism predictions, time shift: –0.26 s.). – This study, — analogy to propene [50].

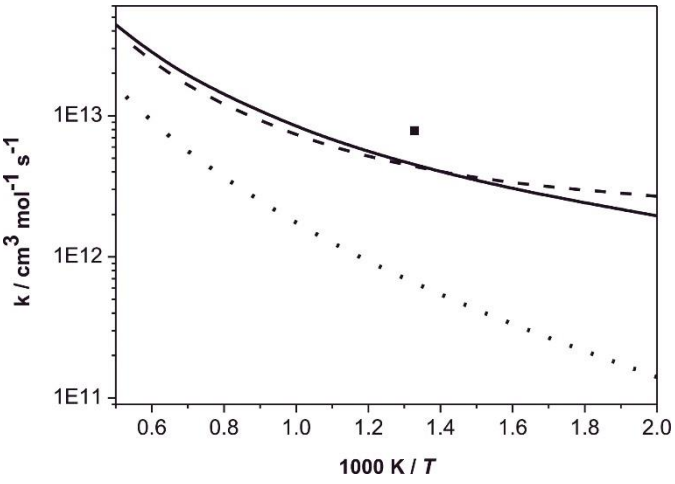

Fig. 12. Rate constants comparison of iC_4H_8 + OH. 2-methylallyl radical formation: – This study (ab-initio), -- Sun et al. [51], ■ Baker [52]; vinylic isobuten1-yl radical formation: – This study (ab-initio).

4.3.1. iC_4H_8 + OH ↔ products

For the reaction of OH radicals with isobutene, both abstraction and addition pathways are included in the current kinetic mechanism.

4.3.1.1. H-Abstraction by OH radicals.

As shown in Figs. 7 and 25, predicted ignition delay times are highly sensitive to the H-atom abstraction reaction by ˙OH radicals from isobutene forming 2-methylallyl (iC_4H_7) radicals in a very large range of temperatures and pressures. This reaction inhibits reactivity throughout the entire temperature range of the ignition delay time measurements, because it consumes a highly reactive OH radical and forms a resonantly stabilized and thus relatively unreactive iC_4H_7 radical. The iC_4H_7 radicals undergo radical–radical self-recombination or can react with methyl radicals via chain terminating reactions which inhibit reactivity, while the reaction of iC_4H_7 with HO_2 promotes reactivity at intermediate temperatures as discussed earlier. Rate constants for the reaction of isobutene with ˙OH radicals has been reported by Sun et al. [51] at the CCSD(T)/6-311++G(d,p)//BH&HLYP/6-311G(d,p) level of theory. As this reaction dominates reactivity over the entire temperature range, we have also calculated the rate constants in this work at a higher level of theory (QCISD(T)/CBS//M062X/6-311 ++ G(d,p)) to obtain more accurate electronic energies and rate constants. Figure 12 shows that the two calculation results are at worst 40% different from one another with different curvature. Comparison with the available experimental measurement taken by Baker et al.

[52] at 753 K is also shown in Fig. 12, and it is a factor of two faster than our calculations.

4.3.1.2. OH addition to iC_4H_8.

OH radical addition to iC_4H_8 is important at temperatures lower than 850 K and the analogous rate constants from propene plus OH radical as calculated by Zádor et al. [53] were used in this work.

- $iC_4H_8 + OH \leftrightarrow iC_4H_8OH\text{-}it$
- $iC_4H_8 + OH \leftrightarrow iC_4H_8OH\text{-}ti$
- $iC_4H_8 + OH \leftrightarrow iC_4H_7OH + H$
- $iC_4H_8 + OH \leftrightarrow sC_3H_5OH + CH_3$
- $iC_4H_8 + OH \leftrightarrow iC_3H_5OH + CH_3$
- $iC_4H_8 + OH \leftrightarrow sC_4H_7OH\text{-}i + H$
- $iC_4H_8 + OH \leftrightarrow CH_3COCH_3 + CH_3$

The competition between the formation of iC_4H_8OH-it and iC_4H_8OH-ti radicals, Fig. 13, plays a significant role in dictating the predicted reactivity in the low temperature range.

Taking the increased steric hindrance by the methyl group in isobutene into consideration, we take the branching ratio of these two channels as being 75:25 rather than 50:50 and keep the total rate constant the same as that for ˙OH addition to propene. The influence to the ignition delay times in the low temperature range can be seen in Fig. 14; this reaction does not influence the high temperature ignition delay time. Baker et al. [52] have also investigated the rate constant of ˙OH addition to isobutene at 753 K, and their rate constants

are about an order of magnitude faster than what we use in this work. A detailed reason for this is unknown. From the flux analysis shown in Fig. 26 we observe that at 730 K and 30 atm, OH radical addition reaction consumes 21.7% of the fuel, with 17.3% of the fuel forming iC_4H_8OH-it radicals through terminal addition and 4.4% forming iC_4H_8OH-ti radicals through addition to the central carbon atom. When the temperature in- creases to 850 K, only 7.9% of iC_4H_8 is consumed through terminal addition and central addition no longer contributes at all. As the temperature increases further to 950 K, OH radical addition reactions do not contribute to fuel consumption.

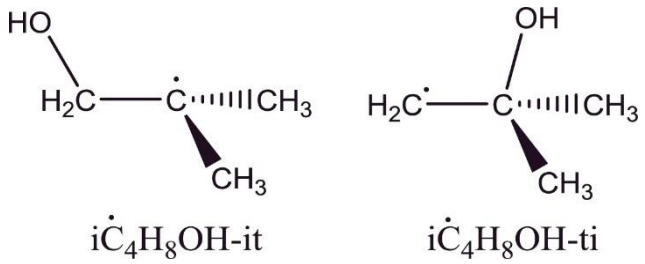

$i\dot{C}_4H_8OH$-it $\quad$ $i\dot{C}_4H_8OH$-ti

Fig. 13. Structures of the two species formed by OH radical addition to iC_4H_8.

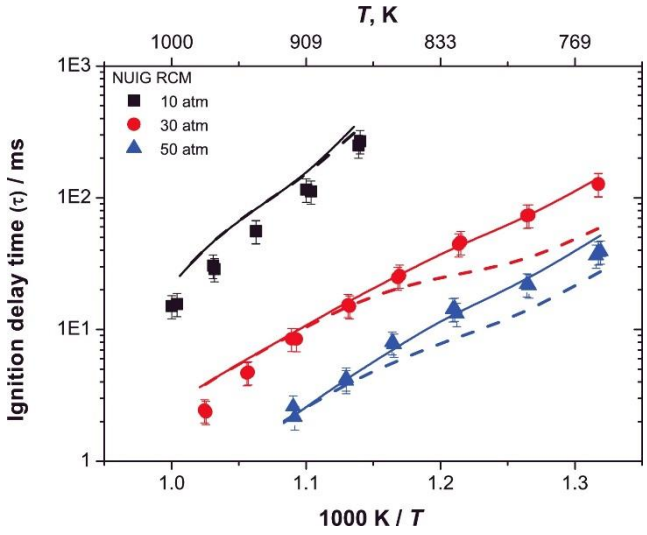

Fig. 14. Branching ratio effects from the OH terminal and central addition to iC_4H_8 to ignition delay times at ϕ = 0.5, fuel in air, p = 10, 30 and 50 atm. Terminal vs. central: solid line (75:25); dashed line (50:50).

4.3.1.3. Addition of iC_4H_8OH-it and iC_4H_8OH-ti radicals to O_2.

Sun et al. [54] calculated the rate constants of iC_4H_8OH-it and iC_4H_8OH-ti radical addition to O_2 and their subsequent decomposition reactions. They used canonical transition state theory to calculate the elementary rate constants and QRRK theory to calculate pressure- and temperature-dependent rate constants. As shown in Fig. 26, the formation of CH_3COCH_3, CH_2O and $^{\cdot}OH$ radical is the dominant product set resulting from iC_4H_8OH-it radical addition to O_2.

The competing two channels for the decomposition of $QCH_2CO(CH_3)_2$ are shown in Fig. 15. The channel forming CH_3COCH_3, CH_2O and OH radical (via the typical Waddington mechanism) inhibits reactivity while the other channel forming CH_3 radical and CH_3COCH_2OOH promotes reactivity. The analogous high-pressure limit rate constants for these two channels calculated by Villano et al. [55] are quite different from the rate constants obtained by Sun et al. [54]. In this work, we use the rate constants for $C_3CCOOH \leftrightarrow C_2C{=}C + CH_2O + OH$ and $C_2CCOOH \leftrightarrow C{=}CCOOH + CH_3$ calculated by Villano et al. [55] as analogies to R1682 and R1683 respectively to give a better ignition delay time prediction, especially at lower temperatures, Fig. 16.

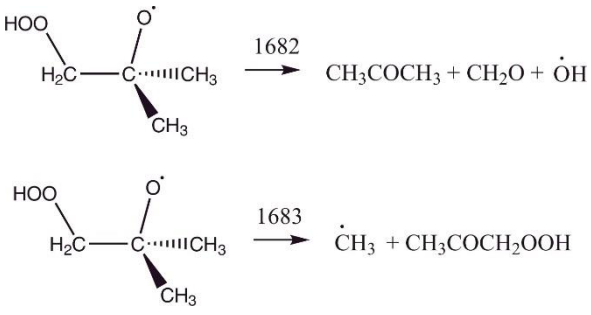

Fig. 15. Competition decomposition channels of the adducts, $QCH_2CO(CH_3)_2$.

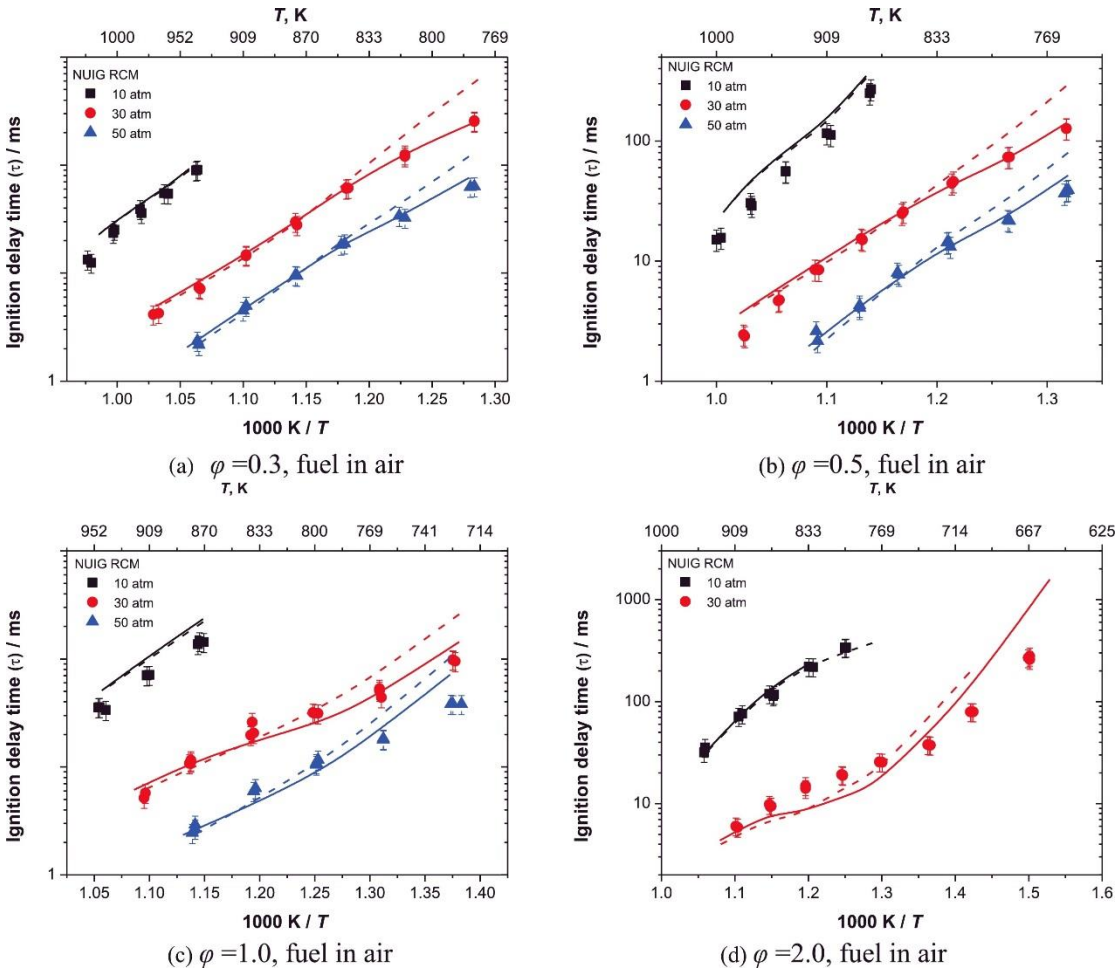

Fig. 16. Influence of replacing rate constants for reactions 1682 and 1683 from Sun et al. [54] (dashed line) to Villano et al. [55] (solid line) to ignition delay time.

The flux analysis presented in Fig. 26 shows only 4.4% of isobutene forms iC_4H_8OH-ti radicals through their reaction with OH radicals at 730 K, but its subsequent chain branching reaction with molecular oxygen pronouncedly promotes low temperature reactivity, Fig. 17. Our current treatment captures the low temperature reactivity of isobutene oxidation quite well; while further fundamental research studies to provide accurate pressure and temperature dependence rate constants for the first and second radical addition to molecular oxygen reactions are needed to give a better understanding of the low

temperature chemistry of alkene fuel oxidation.

The second addition to molecular oxygen has also been included and its influence to the ignition delay times at lower temperatures is shown in Fig. 17. The rate constants for the reaction channels are taken by analogy to rate constants from Miyoshi [56] for the entrance channel of the second (hydroperoxyl-alkyl) radical addition to molecular oxygen and Goldsmith et al. [57] for the following isomerization and decomposition reaction channels.

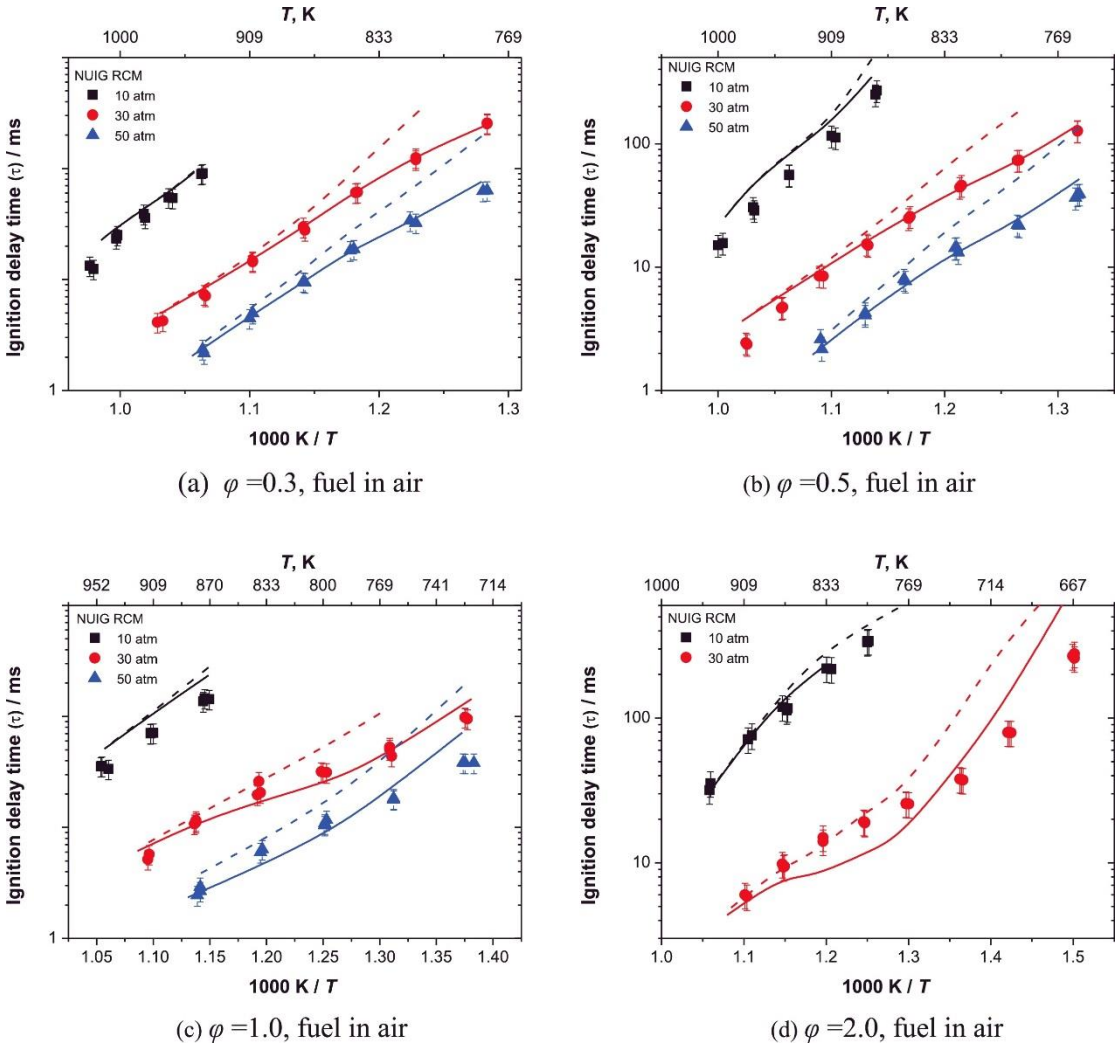

Fig. 17. Model predictions by including (solid line) and excluding (dashed line) the second addition to molecular oxygen reaction class on ignition delay times prediction.

4.3.2. iC_4H_8 + H ↔ products

Flux analyses have identified the reaction between isobutene and hydrogen atom is important (cf., Fig. 26). At low and interme- diate temperatures (< 950 K), hydrogen atom addition to isobutene inhibits reactivity as the tC_4H_9 radicals formed mostly decompose to iC_4H_8 and a H atom. Sensitivity analyses (Fig. 8) shows that the formation of propene and a CH_3 radical inhibits reactivity at higher temperatures as it forms an unreactive CH_3 radical from a very reactive hydrogen atom, and this reaction also competes with the main chain branching reaction promoting reactivity, H + O_2 ↔ Ö + OH. Accurate characterization of this propene formation channel is also important for predicting C_3H_6 profiles in species-resolved experiments.

Previously [2,3], the estimated high-pressure limit rate constants for these reaction channels from Curran [58] were used in the mechanism. In this study, we used analogous rate constants for H atom addition to, and abstraction from, propene calculated by Miller and Klippenstein [59] at a high level of theory to describe the potential energy surface. Conventional transition state theory was used to calculate the abstraction reactions rate constants; RRKM theory was used to calculate micro-canonical, J-resolved rate constants for the dissociation processes, and master-equation methods to determine phenomenological rate constants for all of the non-abstraction reactions. In our mecha- nism, the rate constant for the reaction channel forming C 3 H 6 and ˙CH 3 radicals needs to be divided by a factor of three to predict well propene formation in the flow reactor data taken by Held et al. [49].

4.3.3. $iC_4H_8 + CH_3 \leftrightarrow$ products

Similar to H-atom abstraction by OH radicals described above, methyl radicals can abstract two different types of H-atom from isobutene to form 2-methylallyl radicals plus methane and/or isobuten1-yl radicals plus methane, respectively. However, only the channel producing 2-methylallyl radicals and methane was found to occur. This reaction is predicted to be an important source of methane detected in the JSR. We have adopted the rate constants estimated by Yasunaga et al. [9] in our mechanism.

4.3.4. $iC_4H_8 + HO_2 \leftrightarrow$ products

Both the H-abstraction reaction channels by HO_2 radical and the HO_2 radical addition reaction channels have been taken into consideration.

H-abstraction reaction by HO_2

- $iC_4H_8 + HO_2 \leftrightarrow iC_4H_7 + H_2O_2$
- $iC_4H_8 + HO_2 \leftrightarrow iC_4H_7\text{-}i1 + H_2O_2$

The rate constant for the H-abstraction reactions of isobutene by hydroperoxyl radical forming 2-methylallyl radical (iC_4H_7) is adopted from the theoretical study of Zádor et al. [60]. The rate constant for the other H-abstraction channel forming the vinylic isobuten1-yl (iC_4H_7-i1) radical was calculated in this work.

HO_2 addition to iC_4H_8

- $iC_4H_8 + HO_2 \leftrightarrow iC_4H_9O_2^a$

• $iC_4H_8 + HO_2 \leftrightarrow iC_4H_8O_2H\text{-}t$[b]

• $iC_4H_8 + HO_2 \leftrightarrow tC_4H_9O_2$[c]

• $iC_4H_8 + HO_2 \leftrightarrow tC_4H_8O_2H\text{-}i$[c]

• $iC_4H_8 + HO_2 \leftrightarrow iC_4H_8O + OH$[c]

• $tC_4H_8O_2H\text{-}I \leftrightarrow iC_4H_8O + OH$[c]

[a]rate constants from Villano et al. [61] [b]rate constants from Villano et al. [62] [c]rate constants from Zádor [60].

The rate constants for the addition reactions of hydroperoxyl radicals to isobutene have been investigated by different groups [60–62]. Zádor et al. calculated the rate constants for HO_2 radical addition to the central unsaturated carbon atom in isobutene to form a hydroperoxy-alkyl radical and its following reaction to form a cyclic ether and an hydroxyl radical. The QCISD(T)/cc-pV∞Z//B3LYP/6-311++G(d,p) level of theory was used to obtain the electronic energy barrier heights, based on which the multi-well master equations were solved to calculate the pressure and temperature dependence of the rate constants. Dean and co-workers did a systematic investigation of alkylperoxyl radical decompositions to alkenes and hydroperoxyl radicals [61], and HO_2 + olefin addition channels [62] using electronic structure calculations performed at the CBS-QB3 level of theory. The rate constants for the dissociation reactions were obtained from calculated equilibrium constants and a literature review of experimental rate constants for the reverse association reactions. In this work, we use rate constants from Villano et al. [61,62] for the first two reaction channels and for the last four reaction channels rate constants

from Zádor et al. [60] have been adopted.

4.3.5. $iC_4H_8 + O_2 \leftrightarrow$ products

H-atom abstraction by molecular oxygen from isobutene forming iC_4H_7 + HO_2 radicals was found to be sensitive over the entire temperature range, inhibiting reactivity at temperatures below 900 K and promoting reactivity at temperatures above 900 K.

Several research groups have investigated the reaction between iC_4H_8 and molecular oxygen. Ingham et al. [63] have studied the rate constants in the temperature range 673–793 K. Chen and Bozzelli [64] used canonical transition state theory to calculate the rate constants in the temperature range 300–2000 K. Interestingly, there is a large uncertainty between these two results with a factor of two to five difference in the overlapping temperature range (650–800 K) studied. Goldsmith et al. theoretically investigated the reaction of propene with molecular oxygen as part of their study of the reactions between allyl and hydroperoxyl radicals [65]. In order to directly compare these rate constants, they were written in the opposite direction using the CHEMRev software [66]. Yasunaga et al. [9] estimated this rate constant to give a very good explanation of the product distributions obtained from IR absorption and emission profiles etc. In this work, the rate constant provided by Yasunaga et al. was adopted and was increased by 40% over the temperature range. Comparisons of the rate constants are shown in Fig. 18 and their influence on ignition delay times are shown in Fig. 19.

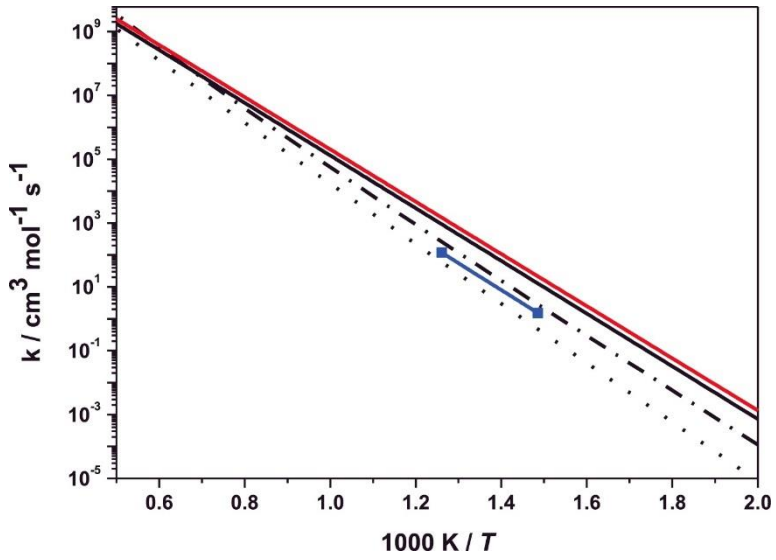

Fig. 18. Rate constants comparison of $iC_4H_8 + O_2$. This study, Yasunaga et al. [9], Ingham et al. [63], Chen and Bozzelli [64], Goldsmith et al. for propene [65].

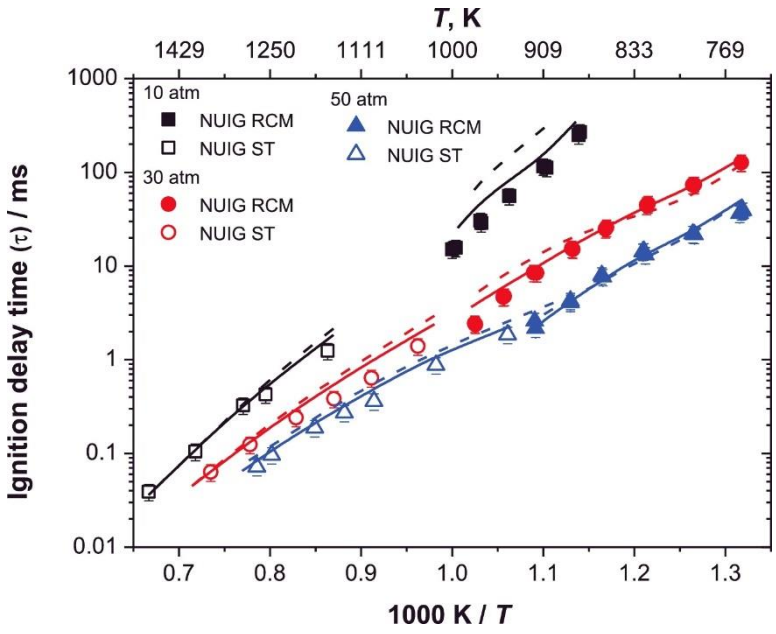

Fig. 19. Influence of rate constants for $iC_4H_8 + O_2 \leftrightarrow iC_4H_7 + HO_2$ to ignition delay times at $\phi = 0.3$, fuel in air, p = 10, 30 and 50 atm. Solid line: this study, dashed line: analogy to propene [3].

4.3.6. $iC_4H_8 + Ö \leftrightarrow$ products

Hydrogen atom abstraction by atomic oxygen did not show significant sensitivity in this work. Rate constants for these reactions are adopted from the ones used by analogy for propene [67]. Oxygen atom can also add to isobutene to produce the following products:

- $iC_4H_8 + Ö \leftrightarrow iC_3H_7 + HCO$
- $iC_4H_8 + Ö \leftrightarrow CH_2CO + CH_3 + CH_3$
- $iC_4H_8 + Ö \leftrightarrow iC_3H_6CO + H + H$

As shown above, oxygen atom addition reactions form two or more radicals through the three reaction pathways; thus these are chain branching reactions. This reaction class has not been studied previously either experimentally or theoretically. Further experimental or theoretical investigation of this reaction class under combustion conditions will be helpful in improving the accuracy of the model.

4.4. $iC_4H_7 \leftrightarrow$ products

- $iC_4H_7 \leftrightarrow C_3H_4\text{-a} + CH_3$

The decomposition of iC_4H_7 radicals will be competitive with its recombination reactions with other radicals such as CH_3, HO_2, iC_4H_7, etc. in the intermediate temperature range. The rate constant for this reaction has been calculated in this work as discussed in Section 3.

4.5. $iC_4H_7 + R \leftrightarrow$ products

4.5.1. $iC_4H_7 + CH_3 \leftrightarrow aC_5H_{10}$

The recombination reaction of 2-methylallyl and methyl radicals to form 2-methyl-1-butene is an important reaction pathway which inhibits reactivity at intermediate and higher temperatures, Figs. 7, 8 and 27. The current mechanism predicts that this reaction produces nearly all of the 2-methyl-1-butene detected in the JSR experiments. Our recommended rate constant is taken from Tsang [67] by analogy with allyl and methyl radical recombination.

4.5.2. $iC_4H_7 + HO_2 \leftrightarrow$ products

The reactions of 2-methylallyl and hydroperoxyl radicals are observed to be very important across a range of conditions, especially at low-to-intermediate temperatures, Figs. 7 and 26. A rate of production analysis shows that at approximately 730 K, 30 atm, and ϕ = 1.0, the reaction of 2-methylallyl radical with hydroperoxyl radical consumes approximately 47.1% of all 2-methylallyl radicals, Fig. 26. Pressure dependent rate constants for the bi-molecular re- actions of allyl radical with hydroperoxyl radical have been extensively studied by Goldsmith et al. [57]; analogous rate constants have been used to describe the reaction between 2-methylallyl radical and hydroperoxyl radical with the following important reaction channels:

- $iC_4H_7 + HO_2 \leftrightarrow iC_4H_7OOH$
- $iC_4H_7 + HO_2 \leftrightarrow iC_4H_7O + OH$
- $iC_4H_7OOH \leftrightarrow iC_4H_7O + OH$

$iC_4H_7O \leftrightarrow$ products

- $iC_4H_7O \leftrightarrow C_3H_5\text{-t} + CH_2O$

• $iC_4H_7O \leftrightarrow iC_3H_5CHO + H$

• $iC_4H_7O \leftrightarrow iC_3H_5OCH_2$

• $iC_4H_7O \leftrightarrow iC_3H_6CHO$

• $iC_4H_7O \leftrightarrow C_3H_6 + HCO$

• $iC_3H_5CHO \leftrightarrow iC_3H_5CO + H$

• $iC_3H_5CO \leftrightarrow C_3H_5\text{-}t + CO$

Methyl-allyloxyl radicals can undergo both decomposition and isomerization reactions to produce different type of products. 2-propenyl radical and formaldehyde, methacrolein and atomic hydrogen, and propene and formyl radicals can be formed through its decomposition reaction. Rate constants for these reactions were taken from the study of Goldsmith et al. [65] for propene by analogy. H-atom abstraction from methacrolein (iC_3H_5CHO) to form iC_3H_5CO radical and H_2O promotes reactivity at intermediate temperatures (Figs. 7, 8, and 25). The rate constant for this reaction channel is taken from the ab initio calculations of Mendes et al. [68]. H-atom abstractions from metharolein by HO_2 and CH_3 radicals and H atoms have also been included from calculations by Mendes et al. [68].

4.5.3. iC_4H_7/iC_4H_7-i1 + $O_2 \leftrightarrow$ products

• $iC_4H_7\text{-}i1 + O_2 \leftrightarrow CH_3COCH_3 + HCO$

• $iC_4H_7\text{-}i1 + O_2 \leftrightarrow tC_3H_6CHO + Ö$

• $iC_4H_7\text{-}i1 + O_2 \leftrightarrow iC_3H_5CHO + OH$

Chen and Bozzelli [64] have theoretically studied the reaction mechanism of 2-methylallyl radical. Unlike saturated alkanes in which the fuel molecule

radical R reacts with O_2 to form an RO_2 radical with a heat release of ~35 kcal mol^{-1}, for the unsaturated alkenes the analogous reaction process only produces ~20 kcal mol^{-1} of heat, or specifically 21.5 kcal mol^{-1} for $iC_4H_7 + O_2 \leftrightarrow iC_4H_7O_2$ in this work. The well of the $iC_4H_7O_2$ radical formed is shallow and thus back dissociation to $iC_4H_7 + O_2$ is favored over the higher barrier isomerization reaction processes. Thus, the reactions of iC_4H_7 radicals with molecular oxygen are not found to be particularly sensitive in this study. Rate constants for reactions and thermodynamics data for species involved in the $iC_4H_7 + O_2$ reactions have been adopted from the study by Chen and Bozzelli [64]. To the best of our knowledge, there are no previous studies of the reaction of isobuten1-yl radical with molecular oxygen; rate constants for this reaction have been adopted by analogy with propene [3].

4.6. 2,5-Dimethyl,1-5-hexadiene

- $iC_4H_7 + iC_4H_7 \leftrightarrow$ H15De25DM
- $iC_4H_7 + iC_4H_7 \leftrightarrow C_3H_4$-a + aC_5H_{10}

2-Methylallyl radicals react via chain terminating self-recombination reaction to form 2,5-dimethyl,1-5-hexadiene, significantly inhibiting reactivity at low- and intermediate- temperatures. The reaction between two 2-methylallyl radicals can also form allene and 2-methyl-1-butene. However, this re- action channel can be neglected as the rate constant is about two orders of magnitude lower than the 2-methylallyl radical self-recombination rate constants and does not contribute to fuel reactivity. Rate constants for this reaction are taken from Tranter and co-workers [69] for the allyl radical self-recombination and have

been divided by a factor of 2.3 to match the low temperature ignition delay time measurements, Fig. 20. If the iC_4H_7 radical self-recombination reaction were removed from the system, the reactivity would increase significantly in the lower temperature range as shown in Fig. 21.

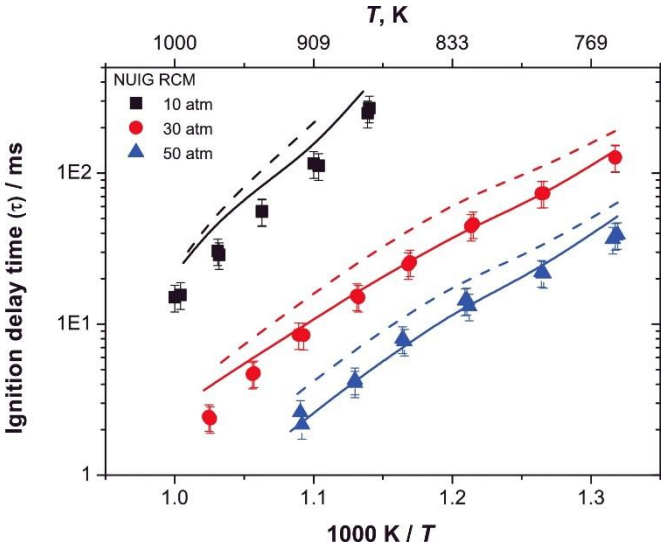

Fig. 20. Influence of rate constants for iC_4H_7 + iC_4H_7 on ignition delay times at ϕ = 0.5 in air, p = 10, 30 and 50 atm. Solid line: this study, dashed line: same as for allyl–allyl from Fridlyand et al. [69].

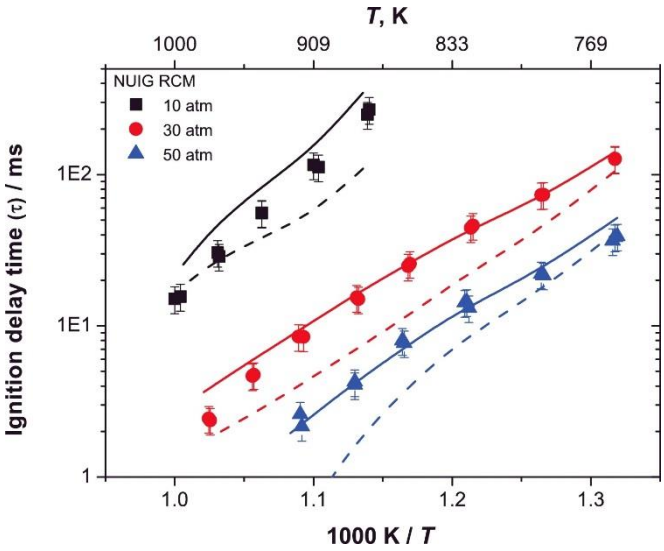

Fig. 21. Influence of rate constants for iC_4H_7 + iC_4H_7 to ignition delay times at

ϕ = 0.5 in ‘air’, p = 10, 30 and 50 atm. Solid line: this study; dashed line: excluding recombination channel.

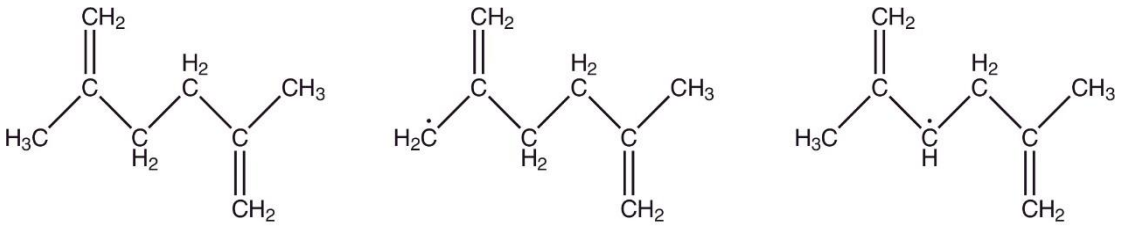

Fig. 22. Molecular structures of 2,5-dimethyl,1-5-hexadiene and the important radicals formed.

4.7. 2,5-Dimethyl,1-5-hexadiene sub-mechanism

As shown in Fig. 22, there are two different types of hydro- gen atom that can be abstracted in the symmetric structure of 2,5-dimethyl,1-5-hexidene to form the allyl-type radical (H15De25DM-a) and secondary allylic-type radical (H15De25DM-s). H-atom abstraction from 2,5-dimethyl,1-5-hexidene by OH, HO_2 and CH_3 radicals, Ö and H atoms, and O_2 have been taken into consideration in the mechanism. The radicals formed can react with HO_2 radicals at this low- and intermediate-temperature range; they can also decompose directly via β-scission. Estimated rate constants are used for their reaction with HO_2 radical based on analogy with normal alkanes. For the latter two β-scission reactions in the following equation array rate constants were estimated by analogy with propene + CH_2O and acetaldehyde + allyl as recommended by Curran [58].

• H15De25DM-a + HO_2 ↔ H15De25DM-aO + OH

- H15De25DM-s + HO_2 ↔ H15De25DM-sO + OH
- H15De2M-t + CH_2O ↔ H15De25DM-aO
- iC_3H_5CHO + iC_4H_7 ↔ H15De25DM-sO

5. Model validation

The current chemical kinetic mechanism is validated against the ignition delay time and flame speed measurements carried out in this work, as well as literature speciation results from a jet-stirred reactor and a flow reactor.

5.1. Ignition delay time validation

Ignition delay times measured in this work (four shock tubes and two rapid compression machines) are presented here, together with the predictions of the current mechanism. The current mechanism captures the experimental results quite well.

A comprehensive comparison between different experimental facilities for both shock tubes and RCMs has been carried out in our previous work in developing the propene mechanism [2] and found that the experimental results of ignition delay time is within 20% between different facilities.

RCMs used in this work are designed differently, and hence each will have different heat loss. In our previous work on propene ignition delay time measurement [2], we found that the NUIG RCM exhibits more heat loss than the UConn facility. This difference in heat loss characteristics could lead to different ignition delay times obtained from the two RCM facilities. When simulating the ignition delay times from RCM measurements, we adopted the

volume his- tory for every experiment as input to account for the specific heat loss for each facility which allows each RCM to be simulated appropriately.

Figure 23 (a)–(d) shows the effect of pressure on ignition de- lay times measured in shock tubes and RCMs for fuel/‘air’ mixtures at ϕ = 0.3, 0.5, 1.0, and 2.0. The experimental results show that high pressure is correlated with shortened ignition delay time at all equivalence ratios. When the pressure increases, the reactant concentrations increases, enhancing overall reactivity. The cur- rent mechanism predicts the influence of pressure on ignition de- lay times over a wide range of temperature and equivalence ratios accurately. Sensitivity analyses (Figs. 7, 8, and 25) together with flux analyses (Figs. 26 and 27) were carried out at different temperatures and pressures to determine the reactivity controlling re- actions at those conditions.

Figure 24 (a)–(f) shows a comparison between the ignition delay time measurements from TAMU and RPI against predictions from the current mechanism. The OH^* concentration/time history from the model was used to compare with the OH^* measurements from TAMU. The model captures most of these fuel-lean conditions except at p = 1.7 atm in Fig. 24 (e) and at conditions in Fig. 24 (f), where the model predicts ignition times that are a little faster than the experimental results which is also true for isobutene/air mixtures at ϕ = 2.0, Fig. 23 (d).

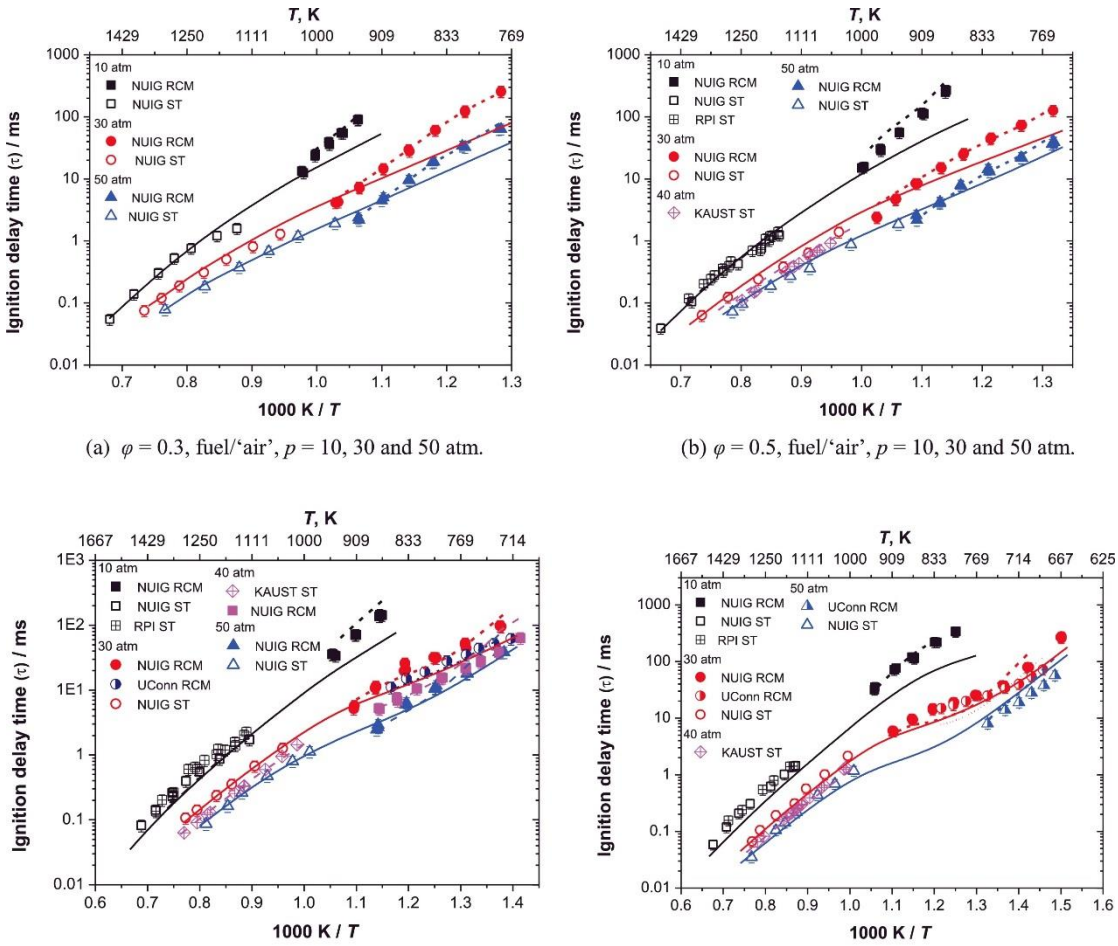

(a) φ = 0.3, fuel/'air', p = 10, 30 and 50 atm.

(b) φ = 0.5, fuel/'air', p = 10, 30 and 50 atm.

(c) φ = 1.0, fuel/'air', p = 10, 30 and 50 atm.

(d) φ = 2.0, fuel/'air', p = 10, 30 and 50 atm.

Fig. 23. Influence of pressure on isobutene IDTs from shock tube and RCMs for fuel/'air' mixtures. Symbols: experimental data; solid lines: constant volume simulation, dashed lines: facilities effect.

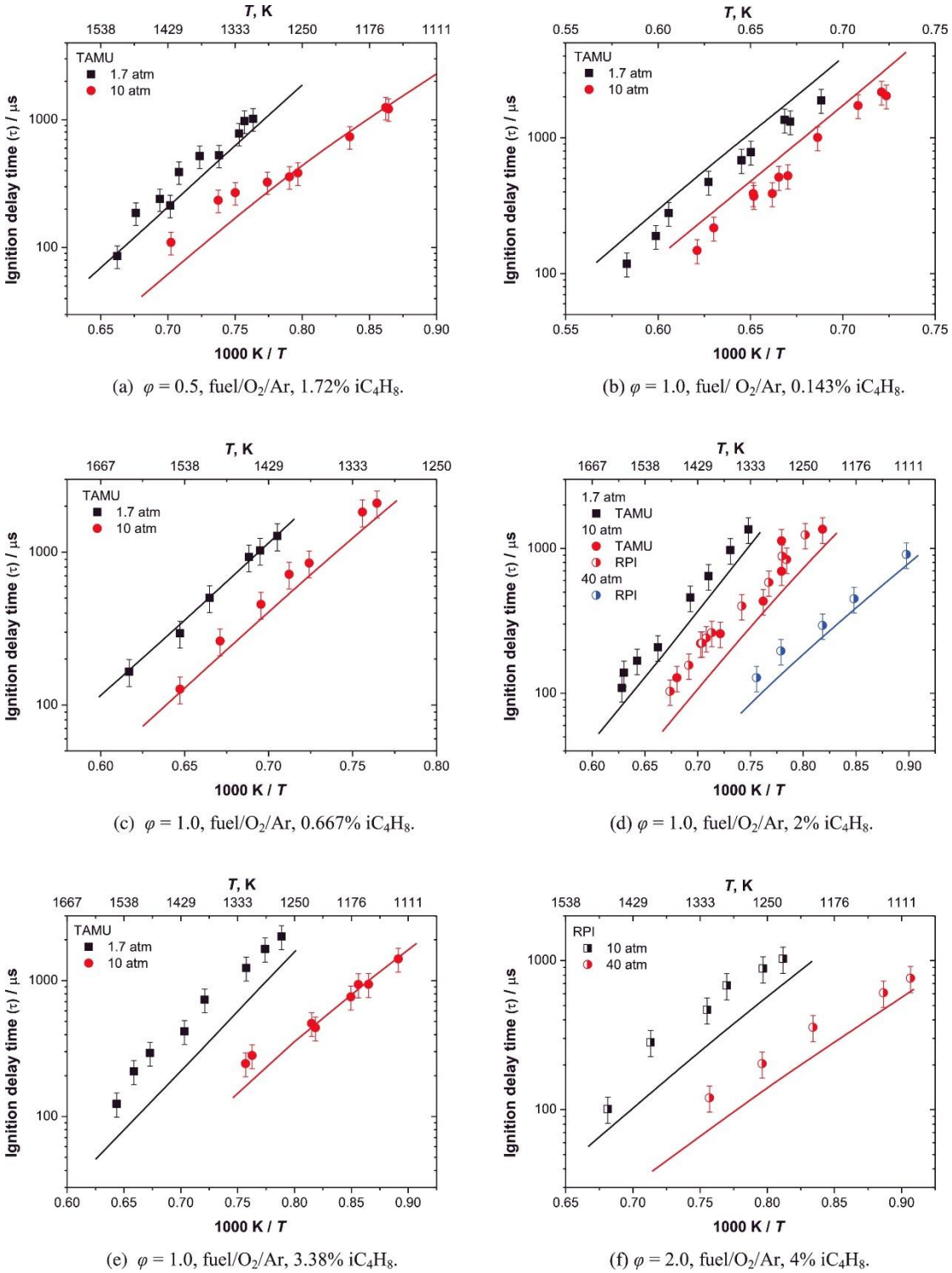

Fig. 24. Influence of pressure on isobutene IDTs from TAMU and RPI shock tube measurements for fuel/O_2/Ar mixtures. Symbols: experimental data; solid lines: constant volume simulation.

5.2. Sensitivity and flux analyses

In order to provide an overview of the isobutene combustion pathways that control reactivity, we performed a series of sensitivity analyses at T = 730 K, 850 K, 950 K and 1250 K at ϕ = 1.0 and p = 30 atm, Fig. 25. Flux analyses at exactly the same conditions have also been carried out, Figs. 26 and 27. It is obvious that the $iC_4H_8 + OH \leftrightarrow iC_4H_7 + H_2O$ reaction inhibits reactivity at all temperatures studied here and its flux increases as the temperature increases.

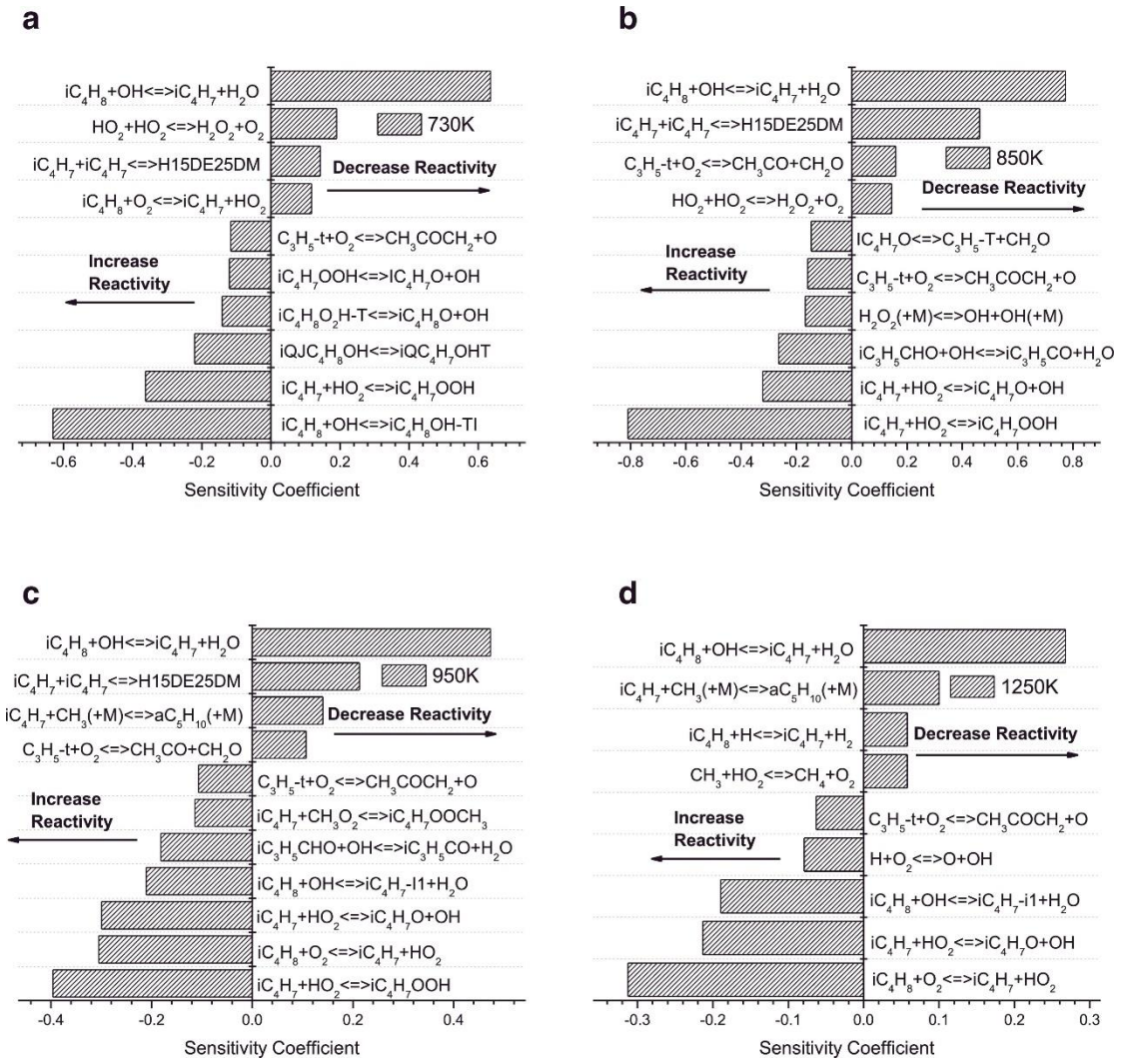

Fig. 25. Sensitivity analyses to ignition delay times performed at ϕ = 1.0, fuel/air, 30 atm, T = 730 K, 850 K, 950 K, and 1250 K.

At 730 K, the addition of OH radicals to the central carbon atom in iC_4H_8 forming iC_4H_8OH-ti radicals pronouncedly promotes reactivity. The flux analysis presented in Fig. 26 shows that, even though this channel accounts for only 4.4% of the total flux, the subsequent radical addition to molecular oxygen reactions generate the radical pool and ultimately promotes reactivity. Even though the $iC_4H_7 + iC_4H_7 \leftrightarrow$ H15DE25DM reaction inhibits reactivity, it only contributes 6.5% of the total flux. The addition of ˙H-atoms to the terminal carbon atom in iC_4H_8 forming tC_4H_9 radicals consumes 18.6% of the fuel. Thereafter, tC_4H_9 radicals add to molecular oxygen and largely reforms iC_4H_8 and an HO_2 radical. It is interesting to find that the reaction of $iC_4H_8 + O_2 \leftrightarrow iC_4H_7 + HO_2$ inhibits reactivity at 730 K, because the reaction proceeds in the reverse direction, consuming iC_4H_7 and HO_2 radicals to form $iC_4H_8 + O_2$, hence preventing chain branching by recombination of methylallyl radicals with HO_2 radicals (cf., Fig. 26). At temperatures above 900 K, this reaction proceeds in the forward direction, promoting reactivity.

At temperatures above 850 K fuel consumption by OH radical addition decreases with the overall flux of ˙OH radical addition to the terminal carbon dropping to 7.9%. The reaction of $iC_4H_7 + iC_4H_7 \leftrightarrow$ H15DE25DM becomes important in inhibiting reactivity as it consumes 20.7% of the iC_4H_7 radicals. This reaction becomes more important at 950 K at which temperature it consumes 39.4% of the iC_4H_7 radicals. In addition, the radical recombination reaction of $iC_4H_7 + CH_3$ (+M) $\leftrightarrow aC_5H_{10}$ (+M) becomes important in inhibiting reactivity, accounting for 7.9% of fuel consumption at 950 K.

At 1250 K, the reaction $iC_4H_8 + O_2 \leftrightarrow iC_4H_7 + HO_2$ is the most one promoting reactivity in the system. The reaction $iC_4H_7 + CH_3$ (+M) $\leftrightarrow aC_5H_{10}$ (+M) which consume 24.6% of the iC_4H_7 radicals, inhibits reactivity. 26.7% of the iC_4H_7 radicals formed de- compose directly to generate allene and a methyl radical. Interestingly, the self-recombination reaction of iC_4H_7 to produce H15DE25DM becomes less important at 1250 K, with only 5.6% of iC_4H_7 radicals consumed by this pathway compared to 39.4% at 950 K. The decreasing dominance of this reaction at high temperatures implies that this reaction pathway will have a minimal effect on ignition delays at high temperatures (Fig. 21) and also on laminar flame speed simulations. Thus, this justifies the decision not to include H15DE25DM chemistry for laminar flame speed simulations.

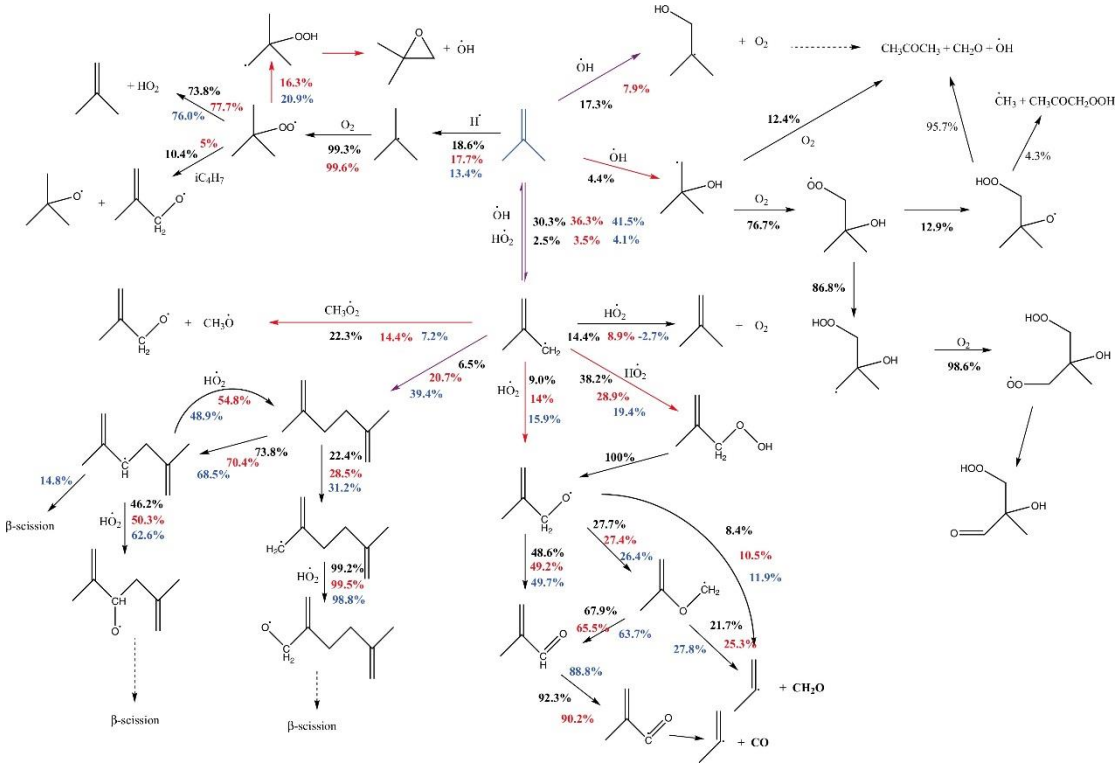

Fig. 26. Flux analysis for the oxidation of ϕ = 1.0, fuel/air mixture at 730 K

(black), 850 K (red) and 950 K (blue) at 20% fuel consumption (red arrows: promote the reactivity; purple ones: inhibit reactivity). (For interpretation of the references to color in this figure legend, the reader is referred to the web version of this article)

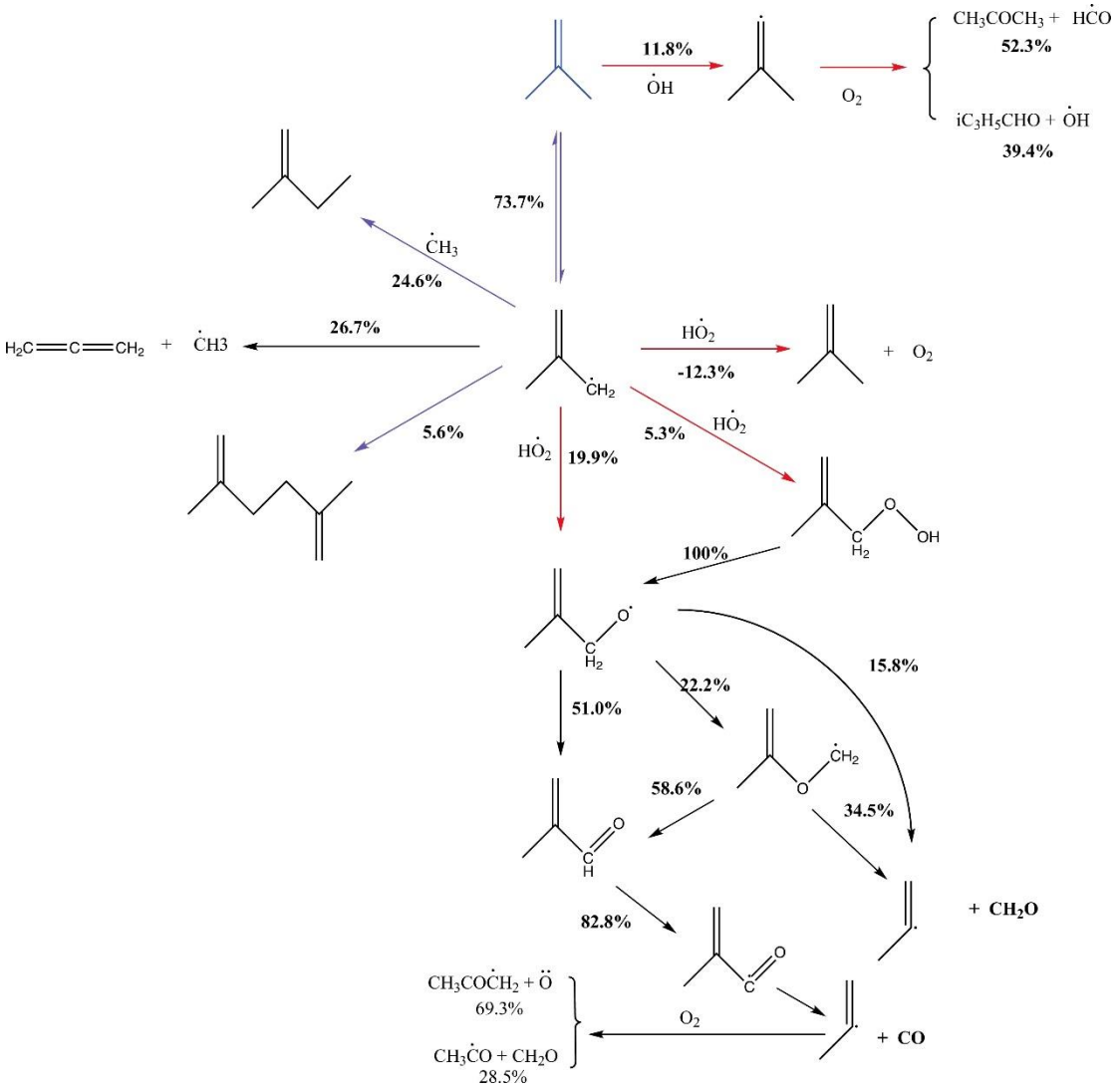

Fig. 27. Flux analysis for the oxidation of ϕ = 1.0, fuel/air mixture at 1250 K at 20% fuel consumption. (red arrows: promote the reactivity; purple ones: inhibit reactivity). (For interpretation of the references to color in this figure legend, the reader is referred to the web version of this article).

5.3. Flame speed validations

Figure 28 compares the predicted laminar burning velocities against those measured experimentally for isobutene in air at 1 atm pressure obtained from three different experimental facilities, LRPG, TAMU, and PU. Both the experiments and the simulation show that the temperature increase does not alter the location of the peak flame speed, which expectedly occurs at $\phi \approx 1.1$. When compared to the experiments performed in the present study, the maximum values are under-predicted by around 5 cm/s, but the locations of these maxima are well predicted. Flame speed sensitivity analyses has been carried out at $\phi = 0.8$, Fig. 28 (b). Many of the important reactions highlighted here are from the H_2/CO sub-mechanism. Competition between the chain branching reaction of $H + O_2 \leftrightarrow$ Ö + OH and chain propagation reaction of $H + O_2$ (+M) $\leftrightarrow$ HO_2 (+M) largely determines the flame speed predictions. Competition between production of HO_2 and H from formyl radical is also sensitive. The reaction of carbon monoxide with hydroxyl radical is also highlighted here. The highlighted isobutene reactions include $iC_4H_8 + OH \leftrightarrow iC_4H_7 + H_2O$, and $iC_4H_8 + OH \leftrightarrow iC_4H_7$–i1 + H_2O, but their sensitivity coefficients are minor in comparison to the others discussed, and hence altering the kinetics of these reactions has limited influence on the predicted flame speed.

Notable in Fig. 28 is the fact that there is about a 5-cm/s difference between the measured flame speeds for the two constant- pressure bomb experiments on the lean side. Some considerable effort was undertaken

between the two groups (TAMU and PU) to resolve this discrepancy, focusing on experimental error, repeatability, and data reduction method. For example, with regard to the latter, the raw images of TAMU were post-processed by PU using their own methods. The results of this exercise led to the conclusion that there was no difference between the results obtained for the TAMU data when using either the TAMU or PU reduction methods. Hence, any potential differences in analysis method cannot make up the difference in the final flame speeds. With regard to repeatability, Fig. 28 contains repeat data points taken at TAMU over a time lag of several months between two different measurement campaigns. As seen in Fig. 28, the TAMU repeatability is within 0.5 cm/s.

One possible source of difference that was considered was the presence of leaks in the experimental setup, which could impact the final mixture composition, particularly for the minor component. A thorough leak rate study was also performed at TAMU, with the result that the worst-case leak rate was less than 0.3 Torr per hour. When filling with the partial pressure method, this worst-case leak rate will have the most impact on the first or mi- nor component, in this case the fuel. Typically the addition of the isobutene to the vessel takes 15–20 min. This time lapse leads to the possibility that up to 0.1 Torr of air could enter the vessel with the fuel, therefore changing the actual partial pressure of the fuel. For a lean mixture nominally at $\phi = 0.8$, this increased amount of air will decrease the equivalence ratio from 0.8 to 0.796, or about a 0.55% decrease. For a rich mixture nominally at $\phi = 1.4$, this level of air leakage will decrease the equivalence ratio to $\phi = 1.395$ or a decrease of

about 0.34%. Hence, for the TAMU rig the worst-case leakage has a minor impact on the final mixture and will not ex- plain the difference between the TAMU and PU data on the lean side.

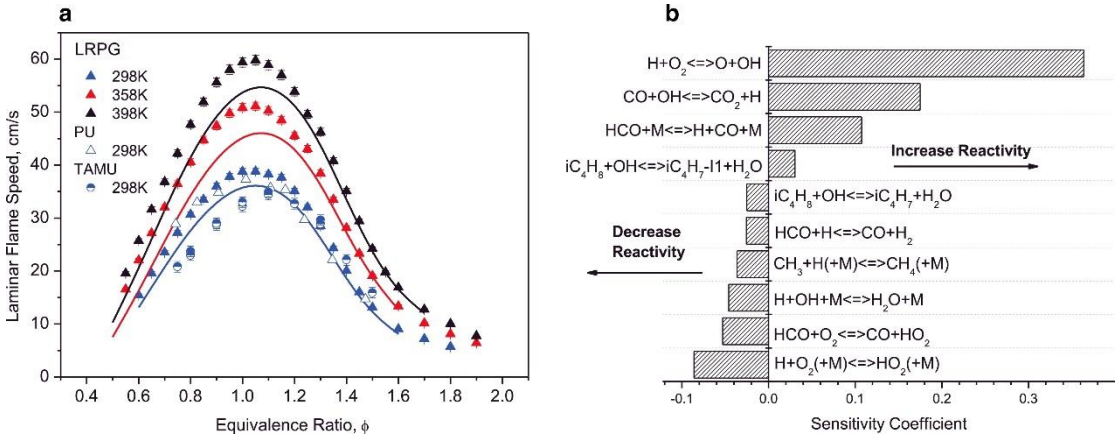

Fig. 28. (a) Laminar flame speed for iC_4H_8 in air at p = 1 atm. Symbols: experimental data, lines: current mechanism. (b) Flame speed sensitivity analysis at $\phi = 0.8$, T = 298 K.

5.4. Speciation validations

5.4.1. Jet-stirred reactor results

Dagaut et al. [12] have measured the concentration profiles of stable species during the oxidation of isobutene in a jet-stirred re- actor at equivalence ratios in the range 0.2–2.0, over a temperature range of 800–1240 K, and in the pressure range 1–10 atm. Overall there is good agreement between the current mechanism and the experimental measurements, Figs. 29–35. As we discussed above, the H15DE25DM formed through the 2-methylallyl radical self-recombination reaction is a very important intermediate species which was not reported in the JSR experimental results here. Methacrolein (iC_3H_5CHO)

which formed through the decom- position of the important methyl-allyoxyl radical is also an important intermediate which is also not reported in the JSR experiments. Future speciation experiments, especially for these species, will be helpful in improving the model predictions. The species 2-methyl-1,3-butadiene is labeled as B13DE2M in Figs. 29 and 35. The species 1,3-butadiene (C_4H_6) is always underestimated in the simulations; the same trends have also been found in our 1-butene [70] and 2-butene [71] combustion models. This may indicate that our current 1,3-butadiene model needs to be updated.

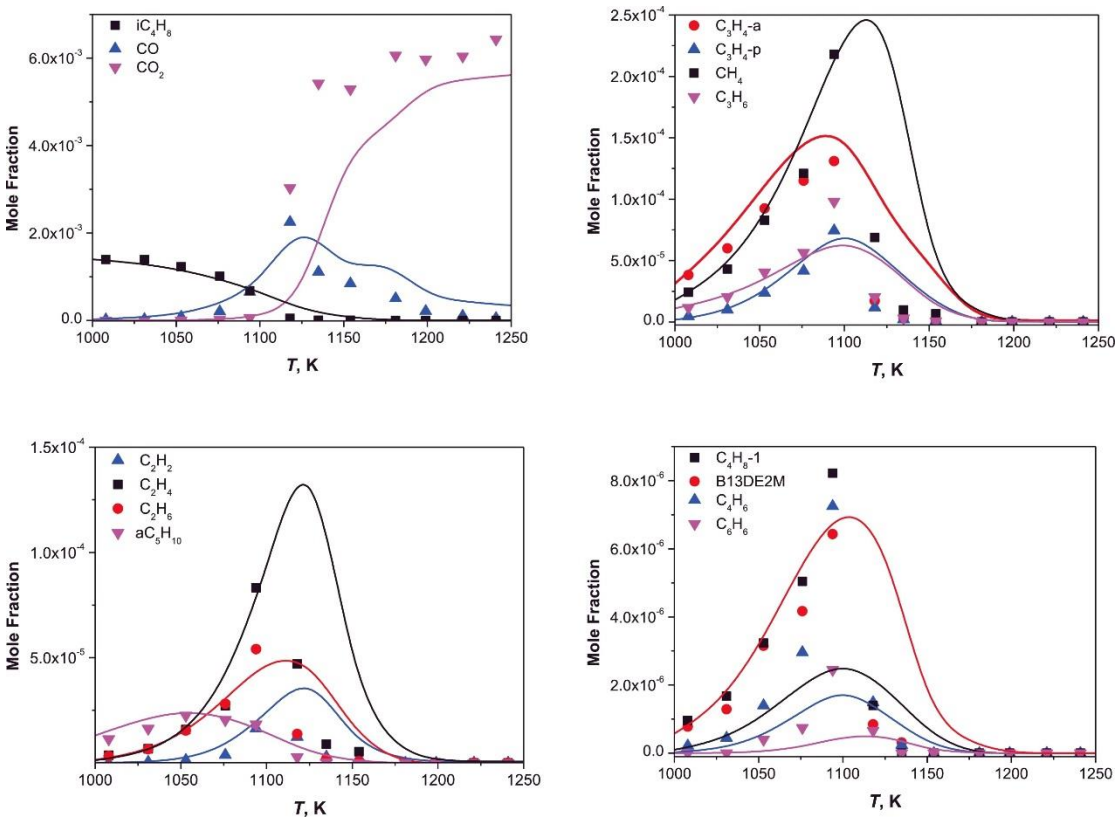

Fig. 29. 0.15% iC_4H_8, 4.5% O_2, 95.35% N_2, ϕ = 0.2, p = 1 atm, τ = 0.15 s. Symbols: JSR experimental measurements [12], lines: current mechanism predictions.

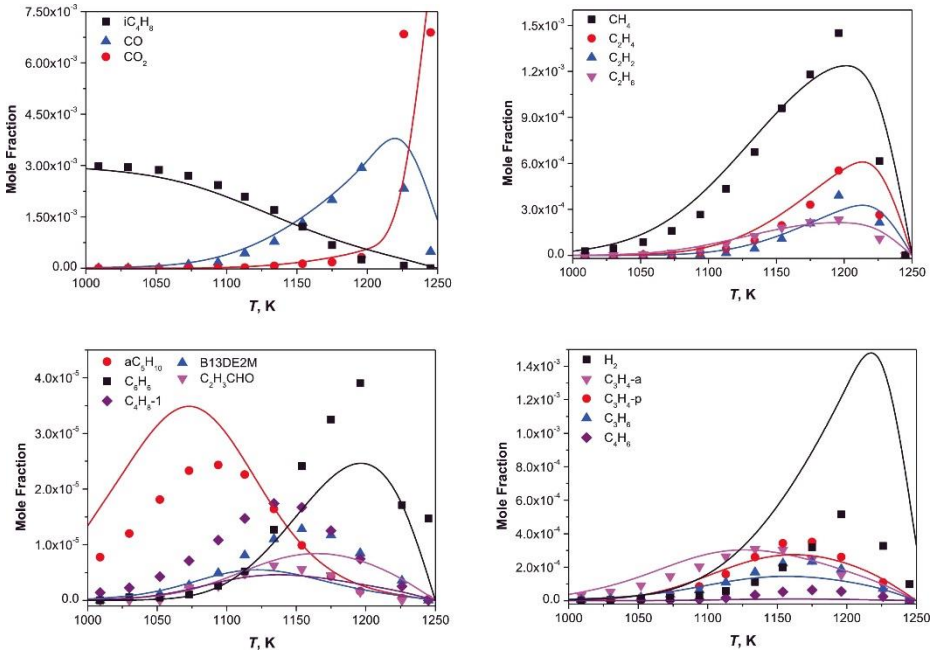

Fig. 30. 0.3% iC_4H_8, 1.8% O_2, 97.9% N_2, ϕ = 1.0, p = 1 atm, τ = 0.15 s. Symbols: JSR experimental measurements [12], lines: current mechanism predictions.

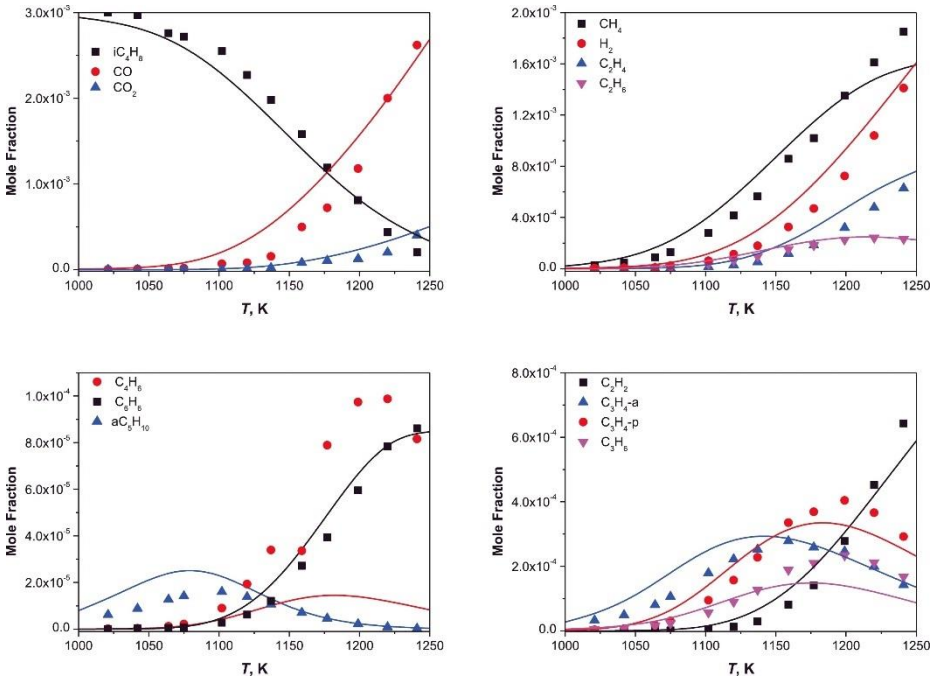

Fig. 31. 0.3% iC_4H_8, 0.9% O_2, 98.8% N_2, ϕ = 2.0, p = 1 atm, τ = 0.15 s. Symbols: JSR experimental measurements [12], lines: current mechanism predictions.

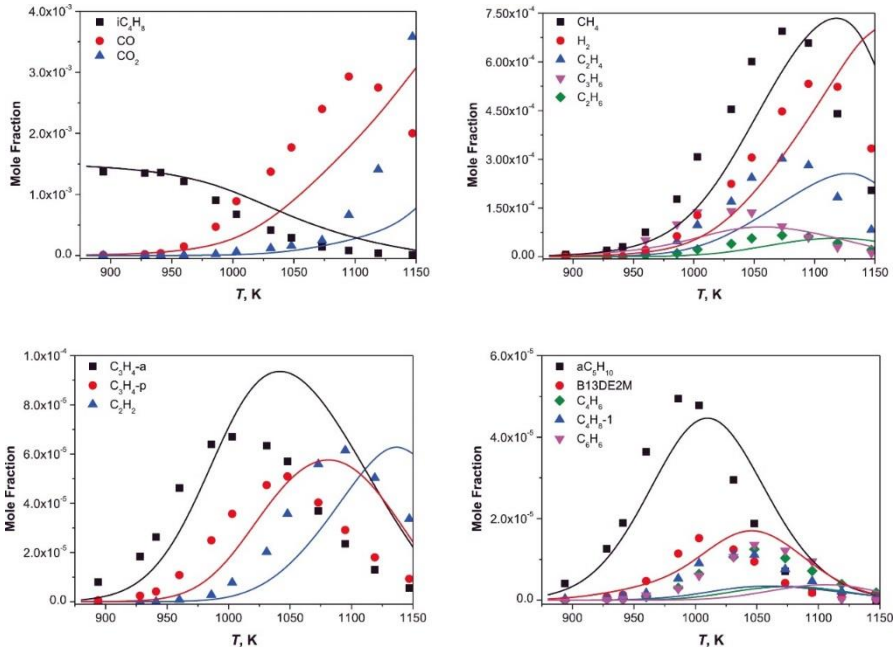

Fig. 32. 0.15% iC_4H_8, 0.9% O_2, 98.95% N_2, ϕ = 1.0, p = 5 atm, τ = 0.75 s. Symbols: JSR experimental measurements [12], lines: current mechanism predictions.

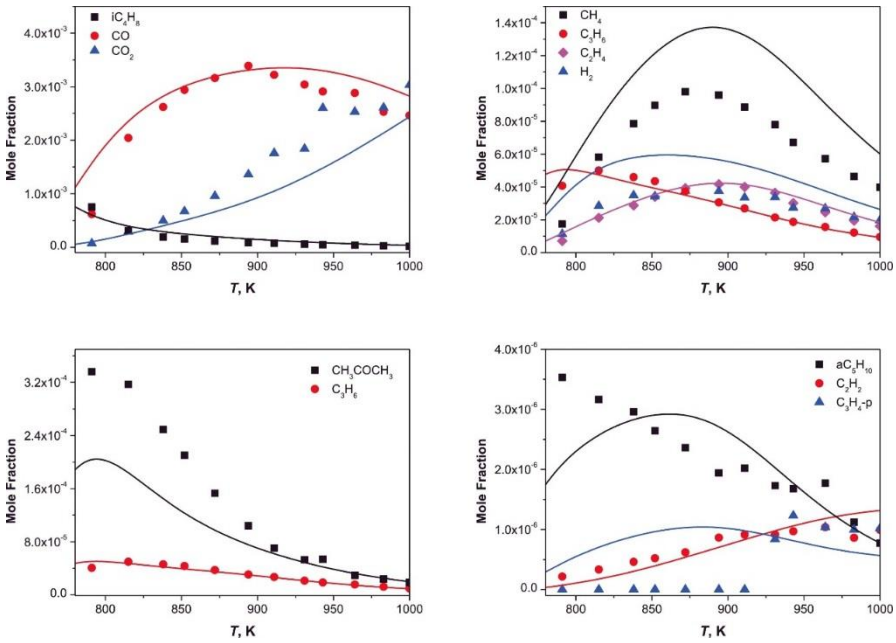

Fig. 33. 0.15% iC_4H_8, 4.5% O_2, 95.35% N_2, ϕ = 0.2, p = 10 atm, τ = 1.5 s. Symbols: JSR experimental measurements [12], lines: current mechanism predictions.

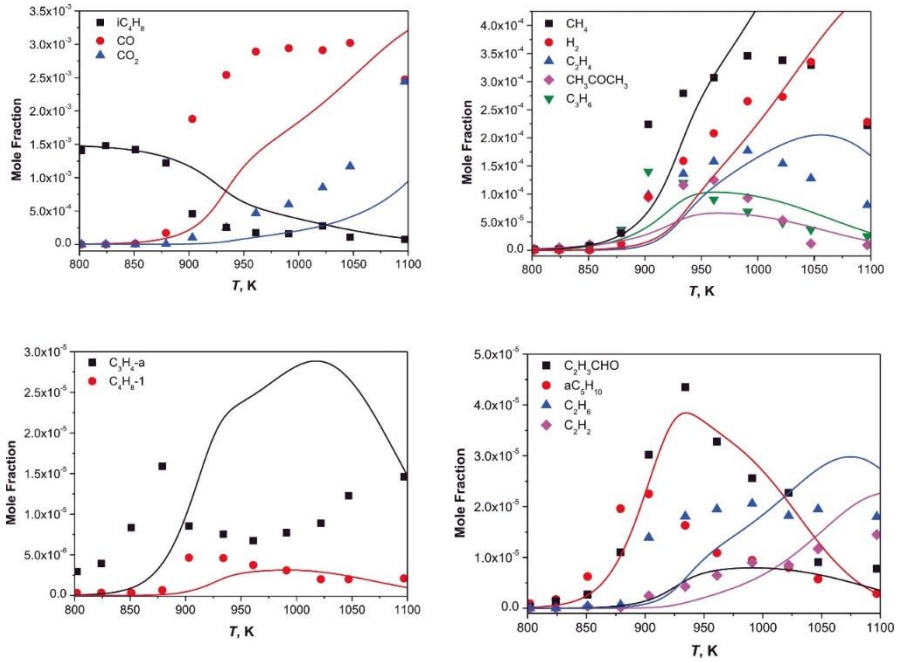

Fig. 34. 0.15% iC_4H_8, 0.9% O_2, 98.95% N_2, ϕ = 1.0, p = 10 atm, τ = 1.5 s. Symbols: JSR experimental measurements [12], lines: current mechanism predictions.

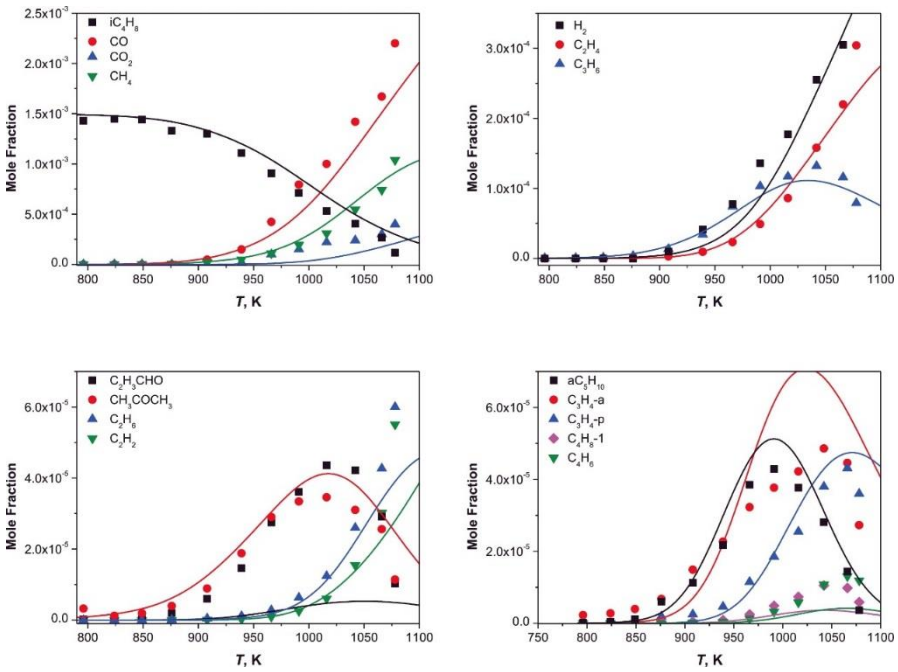

Fig. 35. 0.15% iC_4H_8, 0.45% O_2, 99.4% N_2, ϕ = 2.0, p = 10 atm, τ = 1.5 s. Symbols: JSR experimental measurements [12], lines: current mechanism predictions.

5.4.2. Princeton Atmospheric Pressure Flow reactor (APFR)

Dryer and coworkers [11,49] have experimentally studied the 1 atm pyrolysis and oxidation of isobutene in the Princeton APFR at initial reaction temperatures of 1081 K and 1139–1150 K. Chemical dynamics in the APFR can be simulated using a zero-dimensional, constant pressure adiabatic assumption and a relative time shift between simulation and experimental time. The time-shifting technique has been thoroughly discussed by Dryer et al. [72,73]. Results for C_3H_4 reported for these experiments and their corresponding simulations are for the sum of allene and propyne.

The single APFR isobutene pyrolysis speciation experiment from [49] provides an important test of isobutene destruction pathways that may otherwise be overwhelmed in the oxidizing experimental environments discussed previously. In hierarchical kinetic model construction, accurate description of pyrolytic pathways is prerequisite for developing accurate oxidation chemistry, and such an approach does much to rule out compensatory uncertainties in both the pyrolysis and oxidation sub-mechanisms. As shown in Fig. 36, the present kinetic model generally predicts well the experimentally measured major and minor species profiles. At these conditions, the model indicates that fuel destruction flux is primarily due to the following four reactions:

$iC_4H_8 + CH_3 \leftrightarrow iC_4H_7 + CH_4$

$iC_4H_8 \leftrightarrow iC_4H_7 + H$

$iC_4H_8 + H \leftrightarrow iC_4H_7 + H_2$

$iC_4H_8 + H \leftrightarrow C_3H_6 + CH_3$

Subsequent decomposition of iC_4H_7 generated in these reactions forms CH_3 and C_3H_4-a. Consequently, each of the iC_4H_8, CH_4, C_3H_4-a, and C_3H_6 species evolution profiles provides important constraint for these fuel-related reactions. The relatively abundant pool of CH_3 formed during fuel destruction may undergo self- recombination to form C_2H_6, which subsequently pyrolysis to C_2H_4 and then C_2H_2. Although the chemistry subsequent to CH_3 self-recombination is secondary to the main fuel destruction pathways, its accurate description is critical for prediction of the CH_3 pool, which is a central driver of the overall fuel decomposition process.

Figures 37–39 show the oxidation of isobutene at 1 atm. In each of these cases, the isobutene pyrolysis sub-mechanism remains relatively important, despite the oxidizing environment. At temperature of ~1140 K and for ϕ = 0.42, 0.91, and 1.29, the model generally predicts well the both consumption of iC_4H_8 and the production of the key intermediates identified in the other flow re- actor experiments. Direct comparison of these three experiments on an extent of reaction (iC_4H_8 consumed) basis shows that the principal stable intermediates CH_4 (from CH_3) and C_3H_4–both generated from iC_4H_7 decomposition – have a modest dependence on equivalence ratio. For example, reactions of CH_3 with O_2 and HO_2 compete with formation of CH_4, and so the ϕ = 0.42 case exhibits uniformly lower mole fraction of CH_4 than the other cases. This effect is present (though diminished) with C_3H_4 mole fraction evolutions compared on an extent of reaction basis, and is virtually undetectable (within

experimental uncertainty) for C_3H_6 profiles.

This behavior further suggests the importance of pyrolytic fuel destruction at these flow reactor conditions. The oxidative chemistry primarily couples with smaller species and does not directly compete with reactions specific to iC_4H_8 or its larger decomposition products. Oxidation of CH_3 affects the pools of CH_4 and C_2 species formed subsequent to methyl-methyl recombination, but little affects destruction of the fuel itself.

At 1081 K, very little CO or CO_2 was observed experimentally [11], At this condition, the present model predicts well each of the iC_4H_8, CH_4, C_3H_6, and C_2H_6 species evolution profiles. However, it over-predicts the formation of C_3H_4 species by a factor of ~1.8. Detailed discussion and the figure are provided in the Supplementary information.

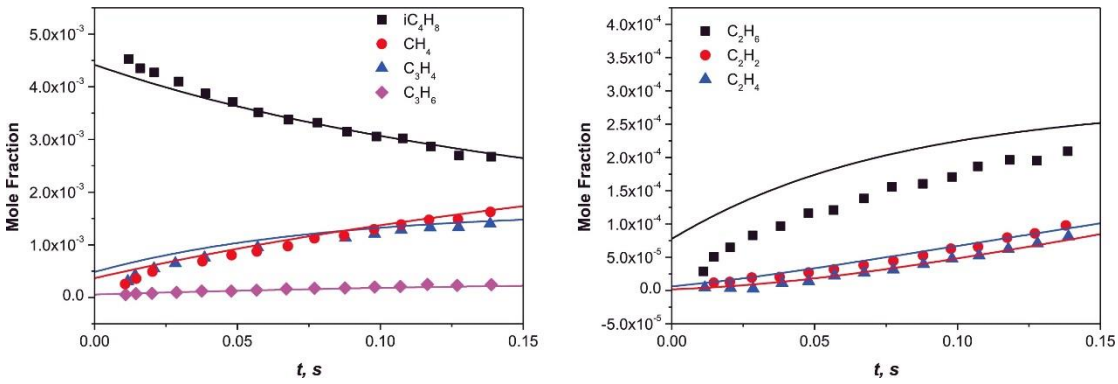

Fig. 36. 0.503% iC_4H_8, in N_2, $\phi = \infty$, p = 1 atm, T = 1150 K. Symbols: APFR experimental measurements [49], lines: current mechanism predictions, time shift: –0.26 s.

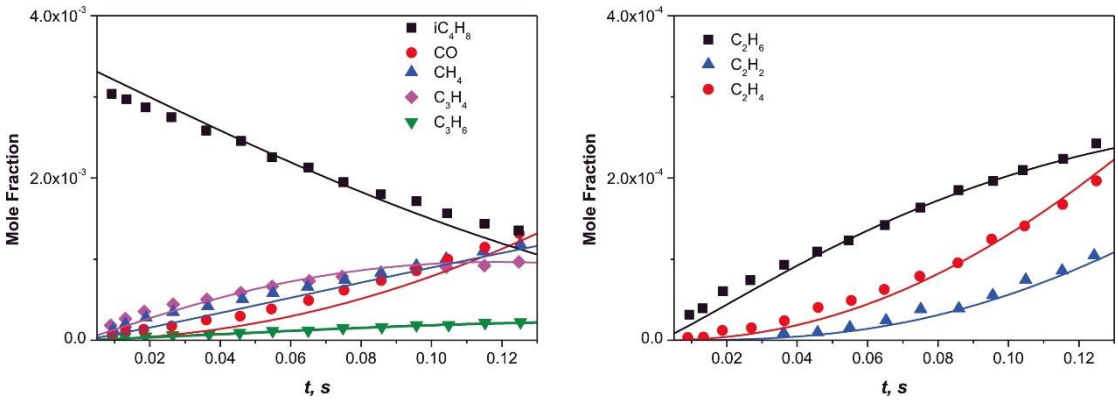

Fig. 37. 0.34% iC_4H_8, 2.242% O_2 in N_2, ϕ = 0.91, p = 1 atm, T = 1140 K. Symbols: APFR experimental measurements [49], lines: current mechanism predictions, time shift: –0.01 s.

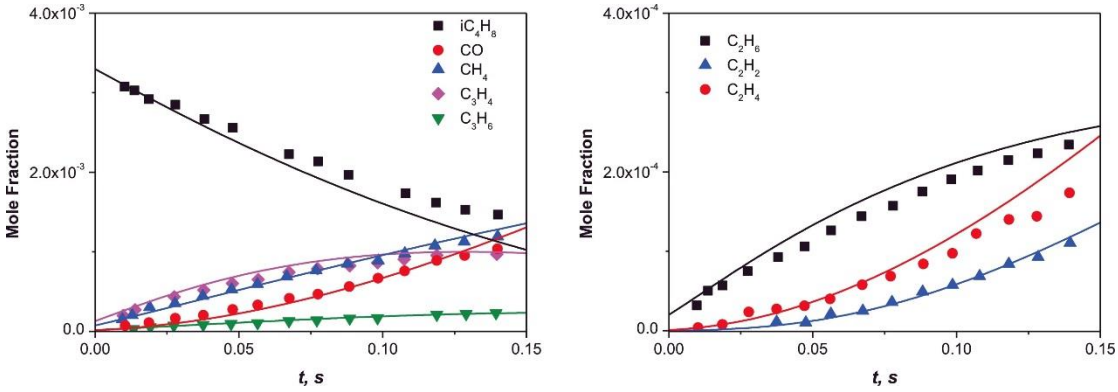

Fig. 38. 0.348% iC_4H_8, 1.619% O_2 in N_2, ϕ = 1.29, p = 1 atm, T = 1142 K. Symbols: APFR experimental measurements [49], lines: current mechanism predictions, time shift: –0.02 s.

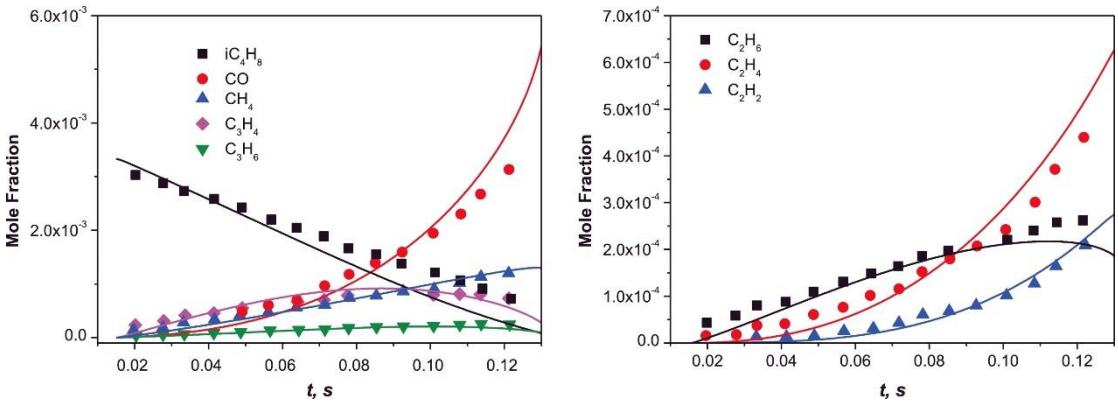

Fig. 39. 0.333% iC_4H_8, 4.757% O_2 in N_2, ϕ = 0.42, p = 1 atm, T = 1139 K.

Symbols: APFR experimental measurements [49], lines: current mechanism predictions, time shift: –0.01 s.

6. Conclusions

This paper presents novel experiments on the ignition delay time and flame speed measurements of isobutene. We also de- scribe the development of a detailed kinetic mechanism which is based on a combination of literature theoretical studies, newly presented ab initio calculations, and estimates by analogy with propene chemistry. The kinetic model includes comprehensive low- and high-temperature reaction pathways specific to unsaturated fuel chemistry. The mechanism is validated against our new experiments and relevant literature data with sensitivity and flux analyses used to identify important reaction pathways and kinetic parameters. The current mechanism captures well most of the experimental results of ignition delay times and flame speeds, as well as the speciation results from jet-stirred reactor and flow reactor results from the literature.

H-atom abstraction from isobutene by hydroxyl radicals significantly inhibits reactivity through the entire temperature and pressure range investigated because the reaction consumes very reactive hydroxyl radical to produce unreactive stabilized 2-methyallyl radical. H-atom abstraction from isobutene by molecular oxygen to form 2-methylallyl and hydroperoxyl radicals ($iC_4H_8 + O_2 \leftrightarrow iC_4H_7 + HO_2$) inhibits reactivity at lower temperatures (< 900 K) because, at these temperatures, the reaction proceeds in the reverse direction. This reaction promotes reactivity as the temperature increases and

contributes significantly to the reactivity at higher temperatures for all mixtures. Its contribution to the reactivity is significant even at intermediate temperatures (~900 K) under fuel-rich conditions. At low temperatures (~750 K), OH radical addition to iC_4H_8 is very important for fuel consumption and contributes significantly to the overall reactivity. At intermediate temperatures (850–1000 K), the reactions of 2-methylallyl (iC_4H_7) with hydroperoxyl radicals and iC_4H_7 self-recombination reaction control the reactivity. At higher temperatures (~1250 K), the reaction of iC_4H_7 radicals with CH_3 radicals becomes important. JSR speciation predictions were shown to be in reasonable agreement with literature experimental data for equivalence ratios from 0.2 to 2, temperatures of 800–1240 K and the pressures from 1 to 10 atm. The product of the 2-methylallyl radical self-recombination reaction, H15DE25DM, is a very important intermediate species which was not reported in the JSR results. Methacrolein, formed through the decomposition of the methyl-allyoxyl radical, is also an important intermediate which is absent from the JSR results. Future speciation experiments, especially for these species, will be helpful to improve the model. Model predictions for flow reactor speciation were shown to be in reasonable agreement with available literature data as well.

7. Research outlook

Isobutene combustion chemistry is very important in describing the combustion behavior of larger alkanes, as well as being a component of commercial fuels. Despite the fact that the current model accurately captures a wide range of reactivity and speciation results, further fundamental research

can aid the important process in improving the accuracy and mechanistic realism of future models. The present study highlights many issues concerning the detailed chemical mechanism development of isobutene combustion, and we summarize these important aspects and present a foundation for future unsaturated alkene combustion mechanism generation.

• The ab initio calculation methods applied in this paper provide very good results for the H-atom abstraction reactions of iC_4H_8 + OH, and iC_4H_8 + HO_2 which are very important in the entire temperature range. The same methods have also been applied to the uni-molecular decomposition reaction of iC_4H_7 radical, which is important at higher temperatures.

• Application of the analogous rate constants for isobutene based on propene for similar reaction classes appears to pro- vide reasonable results for the reaction of iC_4H_7 + HO_2 and iC_4H_7 + iC_4H_7 which are very important at intermediate temperatures. Further ab initio calculations and experiments are needed to test the accuracy of the rate constants estimated by analogy.

• The H-atom abstraction rate constant from iC_4H_8 by molecular oxygen is different from the analogous reaction in propene. As this reaction in the current form results in good predictions of ignition delay times in fuel-rich mixtures, we use the current value. Ab initio calculations for this reaction class in both the propene and isobutene systems are needed in order to improve the fidelity of the model.

• After the fuel radical R reacts with molecular oxygen to form RO_2, this radical then decomposes back to R + O_2 in alkenes, while RO_2 is more stable

for normal alkanes. Based on this work, and related studies of allylic systems, it is becoming apparent that the reactivity for alkene components at very low temperatures (< 800 K) is from the hydroxyl radical addition re- action followed by addition of the resulting radical to molecular oxygen. At intermediate temperatures (800–1300 K), the reactivity is controlled by the competition between hydrogen abstraction by molecular oxygen and ˙OH radicals from alkenes and the reaction between resonantly stabilized iC_4H_7 radical reacting with hydroperoxyl radicals resulting in chain branching reactions. At higher temperatures (> 1300 K), the reactivity is mainly from the hydrogen abstraction reactions from the fuel by molecular oxygen.

• Our current treatment captures the low temperature reactivity of isobutene oxidation well; while further fundamental research studies to provide accurate pressure and temperature dependence of rate constants for the first and second addition to molecular oxygen reactions are needed to give a better under- standing of the low temperature chemistry of alkene fuel oxidation.

• For our future modeling studies of 1-butene, 2-butene and 1,3- butadiene, the following reaction classes need to be accurately described: (1) H-atom abstraction by OH, HO_2, and O_2 from fuel molecules; (2) the reactions of R with HO_2, CH_3, radicals and itself; (3) the decomposition reaction of R radical; and (4) the addition reactions of H, OH, and HO_2 to fuel molecules. Experimental and theoretical investigations on those reaction classes are important to reveal the combustion chemistry of the C_4 alkenes.

The present chemical mechanism study of the isobutene oxidation

provides a comprehensive methodology to develop similar models for alkenes, such as 1-butene, 2-butene and 1,3-butadiene. In addition, this work provides an important sub-mechanism for transportation fuels combustion modeling. The combustion chemistry features that distinguish the alkenes from their branched alkane relatives highlighted in this work are also very interesting. We hope the remaining challenges presented in this final section will motivate theoreticians and experimentalists to discover additional uncertainties of the kinetic properties of important reaction classes for alkene combustion chemistry.

Acknowledgments

Chong-Wen Zhou thanks the entire group members at Combustion Chemistry Centre for helpful discussions. The work at NUI Galway was supported by Saudi Aramco under the FUELCOM program. The TAMU effort was supported by the Texas A&M Engineering Experiment Station and by the TEES Turbomachinery Laboratory. The Rensselaer group was supported by the U.S. Air Force Office of Scientific Research (Grant no. FA9550-11-1-0261). The work at UConn was supported by the National Science Foundation under Grant no. CBET-1402231. The work of KAUST authors was supported by Saudi Aramco under the FUELCOM program and by King Abdullah University of Science and Technology (KAUST). The work at LRGP was supported by the European Commission through the “Clean ICE” Advanced Research Grant of the European Research Council (Grant no. 227669). Collaboration between NUI Galway and LRGP enters in the frame the COST Action CM1404. Y.J.

would like to thank the Grant support from NETL DE-FE0011822 and NSF CBET-1507358. F.L.D. acknowledges support of this at Princeton by the University Turbine Systems Research (UTSR) program, administered by the National Energy Technology Laboratory of the US Department of Energy (DOE), under award DE-FE0012005.

References

[1] C.K. Westbrook, W.J. Pitz, H.J. Curran, "Chemical kinetic modeling study of the effects of oxygenated hydrocarbons on soot emissions from diesel engines", J. Phys. Chem. A 110 (2006) 6912–6922.

[2] S.M. Burke, U. Burke, R. Mc Donagh, O. Mathieu, I. Osorio, C. Keesee, A. Morones, E.L. Petersen, W.J. Wang, T.A. DeVerter, M.A. Oehlschlaeger, B. Rhodes, R.K. Hanson, D.F. Davidson, B.W. Weber, C.J. Sung, J. Santner, Y.G. Ju, F.M. Haas, F.L. Dryer, E.N. Volkov, E.J.K. Nilsson, A.A. Konnov, M. Alrefae, F. Khaled, A. Farooq, P. Dirrenberger, P.A. Glaude, F. Battin-Leclerc, H.J. Curran, "An experimental and modeling study of propene oxidation. Part 2. Ignition delay time and flame speed measurements", Combust. Flame 162 (2015) 296–314.

[3] S.M. Burke, W. Metcalfe, O. Herbinet, F. Battin-Leclerc, F.M. Haas, J. Santner, F.L. Dryer, H.J. Curran, "An experimental and modeling study of propene oxidation. Part 1. Speciation measurements in jet-stirred and flow reactors", Combust. Flame 161 (2014) 2765–2784.

[4] L.H.P. De Goey, A. Van Maaren, R.M. Quax, "Stabilization of adiabatic premixed laminar flames on a flat flame burner", Combust. Sci. Technol. 92

(1993) 201–207.

[5] J.N. Bradley, K.O. West, “Single-pulse shock-tube studies of hydrocarbon pyrolysis. 6. Pyrolysis of isobutene”, J. Chem. Soc. Faraday Trans. I 72 (1976) 558–567.

[6] H.J. Curran, M.P. Dunphy, J.M. Simmie, C.K. Westbrook, W.J. Pitz, “Shock tube ignition of ethanol, isobutene and MTBE: experiments and modeling”, Symp. (Int.) Combust. 24 (1992) 769–776.

[7] S. Santhanam, J.H. Kiefer, R.S. Tranter, N.K. Srinivasan, “A shock tube, Laser-Schlieren study of the pyrolysis of isobutene: relaxation, incubation, and dissociation rates”, Int. J. Chem. Kinet. 35 (2003) 381–390.

[8] W. Tsang, J.A. Walker, “Mechanism and rate constants for the reactions of hydrogen atoms with isobutene at high temperatures”, Symp. (Int.) Combust. 22 (1989) 1015–1022.

[9] K. Yasunaga, Y. Kuraguchi, R. Ikeuchi, H. Masaoka, O. Takahashi, T. Koike, Y. Hidaka, “Shock tube and modeling study of isobutene pyrolysis and oxidation”, Proc. Combust. Inst. 32 (2009) 453–46.

[10] H.J. Curran, “The combustion of isobutene and related compounds” (Ph.D. thesis), Department of Chemistry, University College, Galway, 199.

[11] K. Brezinsky, F.L. Dryer, “A flow reactor study of the oxidation of iso-butylene and an iso-butylene normal-octane mixture”, Combust. Sci. Technol. 45 (1986) 225–232.

[12] P. Dagaut, M. Cathonnet, “Isobutene oxidation and ignition: experimental and detailed kinetic modeling study”, Combust. Sci. Technol. 137 (1998) 237–

275.

[13] V. Dias, J. Vandooren, “Experimental and modeling study of a lean premixed iso-butene/hydrogen/oxygen/argon flame”, Fuel 89 (2010) 2633–2639.

[14] M. Schenk, L. Leon, K. Moshammer, P. Osswald, T. Zeuch, L. Seidel, F. Mauss, K. Kohse-Hoinghaus, “Detailed mass spectrometric and modeling study of iso- meric butene flames”, Combust. Flame 160 (2013) 487–503.

[15] P. Zhao, W.H. Yuan, H.Y. Sun, Y.Y. Li, A.P. Kelley, X.L. Zheng, C.K. Law, “Laminar flame speeds, counterflow ignition, and kinetic modeling of the butene isomers”, Proc. Combust. Inst. 35 (2015) 309–316.

[16] Y.J. Zhang, J.H. Cai, L. Zhao, J.Z. Yang, H.F. Jin, Z.J. Cheng, Y.Y. Li, L.D. Zhang, F. Qi, “An experimental and kinetic modeling study of three butene isomers pyrolysis at low pressure”, Combust. Flame 159 (2012) 905–917.

[17] J.H. Cai, L.D. Zhang, F. Zhang, Z.D. Wang, Z.J. Cheng, W.H. Yuan, F. Qi, “Experimental and kinetic modeling study of n-butanol pyrolysis and combustion”, Energy Fuels 26 (2012) 5550–5568.

[18] C.J. Aul, W.K. Metcalfe, S.M. Burke, H.J. Curran, E.L. Petersen, “Ignition and kinetic modeling of methane and ethane fuel blends with oxygen: a design of experiments approach”, Combust. Flame 160 (2013) 1153–1167.

[19] H.P.S. Shen, J. Vanderover, M.A. Oehlschlaeger, “A shock tube study of isooctane ignition at elevated pressures: the influence of diluent gases”, Combust. Flame 155 (2008) 739–755.

[20] A.K. Das, C.J. Sung, Y. Zhang, G. Mittal, “Ignition delay study of moist

hydrogen/oxidizer mixtures using a rapid compression machine", Int. J. Hydrogen Energy 37 (2012) 6901–6911.

[21] M.C. Krejci, O. Mathieu, A.J. Vissotski, S. Ravi, T.G. Sikes, E.L. Petersen, A. Kérmonès, W. Metcalfe, H.J. Curran, "laminar flame speed and ignition delay time data for the kinetic modeling of hydrogen and syngas fuel blends", J. Eng. Gas Turbines Power Trans. ASME 135 (2013) 9.

[22] Z. Chen, "On the extraction of laminar flame speed and Markstein length from outwardly propagating spherical flames", Combust. Flame 158 (2011) 291–300.

[23] X. Qin, Y. Ju, "Measurements of burning velocities of dimethyl ether and air premixed flames at elevated pressures", Proc. Combust. Inst. 30 (2005) 233–240.

[24] M.P. Burke, Z. Chen, Y. Ju, F.L. Dryer, "Effect of cylindrical confinement on the determination of laminar flame speeds using outwardly propagating flames", Combust. Flame 156 (2009) 771–779.

[25] F. Wu, W. Liang, Z. Chen, Y. Ju, C.K. Law, "Uncertainty in stretch extrapolation of laminar flame speed from expanding spherical flames", Proc. Combust. Inst. 35 (2015) 663–670.

[26] J. Santner, F.M. Haas, Y. Ju, F.L. Dryer, "Uncertainties in interpretation of high pressure spherical flame propagation rates due to thermal radiation", Combust. Flame 161 (2014) 147–153.

[27] P. Dirrenberger, H. Le Gall, R. Bounaceur, O. Herbinet, P.-A. Glaude, A. Konnov, F. Battin-Leclerc, "Measurements of laminar flame velocity for

components of natural gas", Energy Fuels 25 (2011) 3875–3884.

[28] P. Dirrenberger, P.A. Glaude, R. Bounaceur, H. Le Gall, A.P. da Cruz, A.A. Konnov, F. Battin-Leclerc, "Laminar burning velocity of gasolines with addition of ethanol", Fuel 115 (2014) 162-169.

[29] P. Dirrenberger, H. Le Gall, R. Bounaceur, P.A. Glaude, F. Battin-Leclerc, "Measurements of laminar burning velocities above atmospheric pressure using the heat flux method-application to the case of n-pentane", Energy Fuels 29 (2015) 398–404.

[30] J.M. Hall, E.L. Petersen, "An optimized kinetics model for OH chemiluminescence at high temperatures and atmospheric pressures", Int. J. Chem. Kinet. 38 (2006) 714–724.

[31] T. Kathrotia, M. Fikri, M. Bozkurt, M. Hartmann, U. Riedel, C. Schulz, "Study of the H + O + M reaction forming ȮH: kinetics of ȮH chemiluminescence in hydrogen combustion systems", Combust. Flame 157 (2010) 1261–1273.

[32] CHEMKIN-PRO 15101, Reaction Design, San Diego, 2010.

[33] C.K. Westbrook, W.J. Pitz, J.E. Boercker, H.J. Curran, J.F. Griffiths, C. Mohamed, M. Ribaucour, "Detailed chemical kinetic reaction mechanisms for autoignition of isomers of heptane under rapid compression", Proc. Combust. Inst. 29 (2002) 1311–1318.

[34] S. Tanaka, F. Ayala, J.C. Keck, "A reduced chemical kinetic model for HCCI combustion of primary reference fuels in a rapid compression machine", Combust. Flame 133 (2003) 467–481.

[35] M. Ribaucour, R. Minetti, L.R. Sochet, H.J. Curran, W.J. Pitz, C.K. Westbrook, “Ignition of isomers of pentane: an experimental and kinetic modeling study”, Proc. Combust. Inst. 28 (20 0 0) 1671–1678.

[36] W.K. Metcalfe, S.M. Burke, S.S. Ahmed, H.J. Curran, “A hierarchical and comparative kinetic modeling study of C_1 – C_2 hydrocarbon and oxygenated fuels”, Int. J. Chem. Kinet. 45 (2013) 638–675.

[37] W.H. Green, J.W. Allen, R.W. Ashcraft, G.J. Beran, C.A. Class, C. Gao, C.F. Goldsmith, M.R. Harper, A. Jalan, G.R. Magoon, D.M. Matheu, S.S. Merchant, J.D. Mo, S. Petway, S. Raman, S. Sharma, J. Song, K.M. Van Geem, J. Wen, R.H. West, A. Wong, H. Wong, P.E. Yelvington, J. Yu, RMG –Reaction Mechanism Generator v3.3 2011, < http://rmg.sourceforge.net/ >.

[38] Y. Zhao, D.G. Truhlar, “The M06 suite of density functionals for main group thermochemistry, thermochemical kinetics, noncovalent interactions, excited states, and transition elements: two new functionals and systematic testing of four M06-class functionals and 12 other functionals”, Theor. Chem. Acc. 120 (2008) 215–241.

[39] M. J.E.A Frisch, Gaussian 09, Gaussian, Inc., Wallingford, 2009.

[40] J.M.L. Martin, “Ab initio total atomization energies of small molecules – towards the basis set limit”, Chem. Phys. Lett. 259 (1996) 669–678.

[41] D. Feller, D.A. Dixon, Extended benchmark studies of coupled cluster theory through triple excitations, J. Chem. Phys. 115 (2001) 3484–3496.

[42] S. Glasstone, K.J. Laidler, H. Eyring, “Theory of rate processes”, McGraw-Hill, New York, 1941.

[43] C. Eckart, “The penetration of a potential barrier by electrons”, Phys. Rev. 35 (1930) 1303–1309.

[44] K.S. Pitzer, W.D. Gwinn, “Energy levels and thermodynamic functions for molecules with internal rotation I. Rigid frame with attached tops”, J. Chem. Phys. 10 (1942) 428–440.

[45] A. Kéromnès, W.K. Metcalfe, K.A. Heufer, N. Donohoe, A.K. Das, C.J. Sung, J. Herzler, C. Naumann, P. Griebel, O. Mathieu, M.C. Krejci, E.L. Petersen, W.J. Pitz, H.J. Curran, “An experimental and detailed chemical kinetic modeling study of hydrogen and syngas mixture oxidation at elevated pressures”, Combust. Flame 160 (2013) 995–1011.

[46] S.W. Benson, Thermochemical kinetics, Wiley, 1976.

[47] S.M. Burke, J.M. Simmie, H.J. Curran, “Critical evaluation of thermochemical properties of C_1–C_4 species: updated group-contributions to estimate thermochemical properties”, J. Phys. Chem. Ref. Data 44 (2015) 013101.

[48] E.R. Ritter, J.W. Bozzelli, “Therm–thermodynamic property estimation for gas- phase radicals and molecules”, Int. J. Chem. Kinet. 23 (1991) 767–778.

[49] T. Held, F.L. Dryer, “The oxidation of methanol, isobutene and methyl tertiary-butyl ether” (Ph.D. thesis), Department of Mechanical and Aerospace Engineering, Princeton University, 1993.

[50] W. Tsang, “Chemical kinetic data base for combustion chemistry part V. Propene”, J. Phys. Chem. Ref. Data 20 (1991) 221–273.

[51] H.Y. Sun, C.K. Law, “Kinetics of hydrogen abstraction reactions of butene

isomers by OH radical", J. Phys. Chem. A 114 (2010) 12088–12098.

[52] R.R. Baker, R.R. Baldwin, R.W. Walker, "Addition of i-butane to slowly reacting mixtures of hydrogen and oxygen at 480-degrees-C", J. Chem. Soc. Faraday Trans. I 74 (1978) 2229–2251.

[53] J. Zádor, A.W. Jasper, J.A. Miller, "The reaction between propene and hydroxyl", Phys. Chem. Chem. Phys. 11 (2009) 11040–11053.

[54] H.Y. Sun, J.W. Bozzelli, C.K. Law, "Thermochemical and kinetic analysis on the reactions of O_2 with products from OH addition to isobutene, 2-hydroxy-1,1-dimethylethyl, and 2-hydroxy-2-methylpropyl radicals: HO_2 formation from oxidation of neopentane, part II", J. Phys. Chem. A 111 (2007) 4974–4986.

[55] S.M. Villano, L.K. Huynh, H.H. Carstensen, A.M. Dean, "High-pressure rate rules for alkyl + O_2 reactions. 2. The isomerization, cyclic ether formation, and beta- scission reactions of hydroperoxy alkyl radicals", J. Phys. Chem. A 116 (2012) 5068–5089.

[56] A. Miyoshi, "Molecular size dependent falloff rate constants for the recombination reactions of alkyl radicals with O_2 and implications for simplified kinetics of alkylperoxy radicals", Int. J. Chem. Kinet. 44 (2012) 59–74.

[57] C.F. Goldsmith, W.H. Green, S.J. Klippenstein, "Role of O_2 + QOOH in low- temperature ignition of propane. 1. Temperature and pressure dependent rate coefficients", J. Phys. Chem. A 116 (2012) 3325–3346.

[58] H.J. Curran, "Rate constant estimation for C-1 to C-4 alkyl and alkoxyl

radical decomposition", Int. J. Chem. Kinet. 38 (2006) 250–275.

[59] J.A. Miller, S.J. Klippenstein, "Dissociation of propyl radicals and other reactions on a C3H7 potential", J. Phys. Chem. A 117 (2013) 2718–2727.

[60] J. Zádor, S.J. Klippenstein, J.A. Miller, "Pressure-dependent OH yields in alkene plus HO_2 reactions: a theoretical study", J. Phys. Chem. A 115 (2011) 10218–10225.

[61] S.M. Villano, L.K. Huynh, H.H. Carstensen, A.M. Dean, "High-pressure rate rules for alkyl + O_2 reactions. 1. The dissociation, concerted elimination, and isomerization channels of the alkyl peroxy radical", J. Phys. Chem. A 115 (2011) 13425–13442.

[62] S.M. Villano, H.H. Carstensen, A.M. Dean, "Rate Rules, Branching ratios, and pressure dependence of the HO_2 +olefin addition channels", J. Phys. Chem. A 117 (2013) 6458–6473.

[63] T. Ingham, R.W. Walker, R.E. Woolford, "Kinetic parameters for the initiation reaction RH + O2 → R + HO_2", Symp. (Int.) Combust. 25 (1994) 767–774.

[64] C.J. Chen, J.W. Bozzelli, "Thermochemical property, pathway and kinetic analysis on the reactions of allylic isobutenyl radical with O_2: an elementary reaction mechanism for isobutene oxidation", J. Phys. Chem. A 104 (20 0 0) 9715–9732.

[65] C.F. Goldsmith, S.J. Klippenstein, W.H. Green, "Theoretical rate coefficients for allyl + HO_2 and allyloxy decomposition", Proc. Combust. Inst. 33 (2011) 273–282.

[66] S. Rolland, J.M. Simmie, “The comparison of detailed chemical kinetic mechanisms; forward versus reverse rates with CHEMRev”, Int. J. Chem. Kinet. 37 (2005) 119–125.

[67] W. Tsang, “Chemical kinetic data base for combustion chemistry. Part V. Propene”, J. Phys. Chem. Ref. Data 20 (1991) 221–273.

[68] J. Mendes, C.W. Zhou, H.J. Curran, “Theoretical chemical kinetic study of the H- atom abstraction reactions from aldehydes and acids by H atoms and OH, HO_2, and CH_3 radicals”, J. Phys. Chem. A 118 (2014) 12089–12104.

[69] A. Fridlyand, P.T. Lynch, R.S. Tranter, K. Brezinsky, “Single pulse shock tube study of allyl radical recombination”, J. Phys. Chem. A 117 (2013) 4762–4776.

[70] Y. Li, C.-W. Zhou, K. Somers, K. Zhang, H. Curran, “A comprehensive experimental and modelling study of 1-butene oxidation” (in preparation).

[71] Y. Li, C.-W. Zhou, K. Somers, K. Zhang, H. Curran, “The oxidation of 2-butene: a high-pressure ignition delay, kinetic modeling study and reactivity comparison with isobutene and 1-butene”, Proc. Combust. Inst. (2015).

[72] Z. Zhao, M. Chaos, A. Kazakov, F.L. Dryer, “Thermal decomposition reaction and a comprehensive kinetic model of dimethyl ether”, Int. J. Chem. Kinet. 40 (2008) 1–18.

[73] F.L. Dryer, F.M. Haas, J. Santner, T.I. Farouk, M. Chaos, “Interpreting chemical kinetics from complex reaction–advection–diffusion systems: modeling of flow reactors and related experiments”, Prog. Energy Combust. Sci. 44 (2014) 19–39.

An experimental and modeling study of nitromethane + O_2 + N_2 ignition in a shock tube

Author contributions

Jenny D. Nauclér: Obtained most ignition delay time experimental data on high pressure shock tube, conducted all modelling work, and wrote the manuscript.

Yang Li: Obtained some ignition delay time experimental data on high pressure shock tube and low-pressure shock tube, and reviewed the manuscript.

Elna J.K. Nilsson: Provided input for modelling efforts, and reviewed the manuscript.

Alex A. Konnov: Managed the project throughout, and reviewed manuscript prior to and post the review process.

Henry J. Curran: Managed the project throughout, and reviewed manuscript prior to and post the review process.

Brief description of the paper

In this paper, the ignition of nitromethane/O_2/N_2 mixtures was investigated via shock tube experiments in the temperature range 947–1333 K at reflected shock pressures near 8, 16 and 32 atm. The ignition was recorded as the intensity maxima of unfiltered luminosity in the range 240–530 nm. Under the experimental conditions of the present study, ignition was found to proceed via a two-stage process. Dependencies on concentration, pressure and temperature were examined and discussed. The two ignition stages were separated in time, with individual concentration and temperature dependence. The two experimentally determined ignition stages were found to be pressure independent over the pressure range investigated. The activation energy was derived to be 16.15 ± 1.57 kcal mol^{-1} for the first stage ignition and 20.89 ± 0.82 kcal mol^{-1} for the second stage. Modeling using the mechanism by Brequigny et al., published in Proceedings of the Combustion Institute (2014) 703–710, could predict the magnitude of the ignition delay times at 8 atm, but it could not reproduce the temperature dependence of the first stage ignition or the pressure independence of both ignition stages. The measurements are discussed in relation to data from the literature.

An experimental and modeling study of nitromethane + O_2 + N_2 ignition in a shock tube

J.D. Nauclér [a], Y. Li [b], E.J.K. Nilsson [a], H.J. Curran [b], A.A. Konnov [a]*

[a] Division of Combustion Physics, Department of Physics, Lund University, Lund, Sweden
[b] Combustion Chemistry Centre, National University of Ireland, Galway, Ireland

Published in: *Fuel* 186 (2016) 629–638

Abstract

The ignition of nitromethane/O_2/N_2 mixtures was investigated via shock tube experiments in the temperature range 947–1333 K at reflected shock pressures near 8, 16 and 32 atm. The ignition was recorded as the intensity maxima of unfiltered luminosity in the range 240–530 nm. Under the experimental conditions of the present study, ignition was found to proceed via a two-stage process. Dependencies on concentration, pressure and temperature were examined and discussed. The two ignition stages were separated in time, with individual concentration and temperature dependence. The two experimentally determined ignition stages were found to be pressure independent over the pressure range investigated. The activation energy was derived to be 16.15 ± 1.57 kcal mol^{-1} for the first stage ignition and 20.89 ± 0.82 kcal mol^{-1} for the second stage. Modeling using the mechanism by Brequigny et al., published in Proceedings of the Combustion Institute (2014) 703–710, could predict the magnitude of the ignition delay times at 8 atm, but it could not reproduce the temperature dependence of the first stage ignition or

the pressure independence of both ignition stages. The measurements are discussed in relation to data from the literature.

1. Introduction

Nitromethane, CH_3NO_2, is a simple nitrogen containing fuel, which is used in mixtures with methanol or as a pure fuel in racing cars and in model engines [1]. It is also considered as a fuel additive [2–4] in engines, promoting their efficiency and reducing soot from their exhaust. Because of the oxygen content in the molecule, nitromethane can act as both a fuel and as an oxidizer in combustion processes, as noted in the study by Fells and Rutherford [5], where the effect of nitromethane addition on the burning rate of methane flames was investigated. These dual fuel-oxidizer properties motivate studies of combustion characteristics of nitromethane as a single component as well as in mixtures with other oxidizers. Due to its potential as a monopropellant [6], nitromethane has been extensively studied, focusing on thermal decomposition [7–17], and detonation [18–22]. The combustion chemistry of nitromethane is also of interest from a fundamental research viewpoint since it is the simplest representative for fuel-nitrogen species, and as such can facilitate understanding of the reactions relevant to the mutually sensitized oxidation of hydrocarbons and nitrogen oxides [11].

The decomposition of nitromethane has been investigated mainly by kinetic studies of its thermal decomposition in shock tubes [11–17,23]. A common experimental approach is to track the formation of NO_2, and it is well

established that NO_2 + $\dot{C}H_3$ are the significant decomposition products that then undergo further reactions [12,13,16]. It was experimentally shown by Zaslonko et al. [12] that in the temperature and pressure ranges 1030 – 1580 K and 1.0 – 2.8 atm, the thermal decomposition produced $CH_3\dot{O}$ and CH_3ONO. The latter was explained as the result of recombination of $\dot{C}H_3$ and NO_2. In the thermal decomposition study of Hsu and Lin [15] $N\dot{O}$ and CO profiles were measured in the temperature range 940 – 1520 K at pressures 0.4 – 1.0 atm. From the $N\dot{O}$ and CO profiles the authors showed that NO is formed early during ignition, while CO is formed at a later stage. Kuznetsov et al. [16] monitored the formation of NO_2 in nitromethane decomposition through shock tube experiments in the temperature range 1190 – 1490 K at 1.5 atm. The authors confirmed that the NO_2 profile had a convex shape consistent with a typical decomposition product, and that the disappearance of nitromethane and the formation of NO_2 coincided. Through theoretical analysis it was also concluded that isomerization of nitromethane to CH_3ONO was not competitive compared to thermal decomposition. The thermal decomposition of nitromethane has been shown to be pressure dependent in the pressure range of 0.1 – 40 atm [12,13,17,23].

An interesting aspect of nitromethane combustion is that experiments and modeling indicate that it proceeds via two or three steps; detonation has been shown to be a two-step process [19–22,24], a similar pattern is seen in low-pressure flames [25] and in the case of flames of liquid nitromethane three reaction zones have been identified [6].

From detonation studies it is known that fuels and mixtures containing NO2 propagate in a double cellular structure [20–22,24]. Presles et al. [20,21] showed a sub-structure within the first part of the main cell during detonation of pure nitromethane and rich nitromethane/O_2 mixtures ($1.3 < \varphi < 1.75$) at 390 K and 0.05–1.7 bar. This sub-structure behaved independently of the main cell in terms of velocity and structure. Sturtzer et al. [19] compared their numerical results of pure nitromethane and nitromethane + O_2 detonation with the experimental results from Presles et al. [20,21]. It was suggested that the origin of the double cellular structure is an endothermic step of fuel decomposition into $\dot{C}H_3$ and NO_2, followed by two independent exothermic steps and attributed the reaction $NO_2 + \dot{H} = N\dot{O} + H_2$ as the main exothermic source in the first step of detonation.

Experimental and theoretical studies on nitromethane flames have shown a wide total reaction zone, with the chemistry divided into multiple separated zones [6,25]. By performing modeling studies Boyer and Kuo [6] identified three reaction zones in a pure liquid nitromethane flame at pressures of 3–6 MPa. Indications of a two-stage ignition process for pure nitromethane were presented [14,26,27]. Guirguis et al. [27] noted that in their study of 100% nitromethane pyrolysis behind reflected shock waves, for some of the measurements there were two separated pressure spikes where the second was higher in intensity. The presence of a second pressure spike was however not given any further attention. In light of modeling results for flames from previous studies [6,28] and detonation studies [20–22,24], the second pressure

spike could indicate that a second stage ignition occurred in the experiments of Gurguis et al. [27].

In the study by Hall and Wolfhard [25] multiple reaction zones in methyl- and ethyl nitrate, methyl nitrite and nitromethane flames were examined at low pressures. It was concluded that these flames had up to three separate reaction zones. The emission from the reaction zones was analyzed and characterized in terms of emitting species. A nitromethane/O_2 flame was analyzed at 323 K and ~0.1 atm, and two reaction zones were detected. A yellow undefined emission was observed in the first reaction zone, and it was argued by the authors that this was likely due to NO_2^*. In the second reaction zone, emissions from C_2^*, CH^*, CN^*, OH^*, NH^* and NO^* were identified. No emission from formaldehyde was observed for nitromethane/O_2 flames.

Laminar burning velocities of nitromethane/air flames have been determined using the Bunsen flame method [29], spherically expanding flames [30], and the heat flux method [28]. In the work of Nauclér et al. [28] laminar burning velocities of nitromethane/air flames were measured using the heat flux method in the temperature range 338 – 358 K at pressure of 1 atm. The width of the reaction zone of these nitromethane flames was examined using modeling and implications for experimental determinations of laminar burning velocity were discussed. The modeling by Nauclér et al. [28] implied that a two-stage process occurred.

Oxidation studies of nitromethane are not as numerous as compared to detonation and decomposition studies. Oxidation in a static vessel was

investigated by Tricot et al. [31] by studying nitromethane explosion limits in the temperature range 700 – 740 K. Flame structure has been investigated in low-pressure nitromethane/O_2/Ar flames [32,33].

The ignition of nitromethane in the presence of O_2 has been considered as a one-stage process in studies by Borisov et al. [14] and Kang et al. [26]. A two-stage process in the ignition of nitromethane/O_2 was indicated in the literature [34,35], and later shown by the authors of the present work [36] in a conference publication for the 7th European Combustion Meeting 2015. The two-stage ignition process was independently confirmed by Mathieu et al. [37].

A shock tube study on nitromethane + O_2 + Ar at conditions of $0.5 < \varphi < 2$, 875 – 1595 K and 1.71 – 35.8 atm, by Mathieu et al. [38], was published after the original submission of the present work. The study showed two ignition stages, detected by emission from OH^*. Ignition delay times were determined for the second ignition stage by both the maximum OH^* signal and the maximum gradient in the OH^* signal. A kinetic mechanism was presented, which performed satisfactorily for the conditions of the study. In addition, a correlation based on equivalence ratio and pressure at 90% and 98% Ar dilution was presented.

Borisov et al. [14] measured the autoignition of nitromethane/O_2 mixtures in a by-pass apparatus with the diluents Ar, N_2 and He at 700 – 1300 K in order to determine the rate constant for the thermal decomposition of nitromethane. Kang et al. [26] examined the ignition delay times of nitromethane/O_2/Ar mixtures in a shock tube by tracking the von Neuman pressure spike in the

temperature-range 1250–1900 K at a pressure of about 0.2 atm for several different nitromethane/O_2/Ar compositions. A correlation between mixture composition and ignition delay times was presented by Kang et al. [26]. The overall activation energy was calculated to be 21.36 ± 0.51 kcal mol^{-1} through multiple regression analysis. The authors concluded that the presence of oxygen in the NO_2-group in the fuel molecule reduced the role of O_2 as an ignition promoter compared to other hydrocarbon fuels. The decomposition of pure nitromethane, and its ignition in the presence of O_2 was investigated in a shock tube [34] and presented by Djebaili-Chaumeix et al. [35]. Absorption at 235 nm and emission at 235 nm and 306 nm were observed and treated as ignition delay times.

In summary based on the literature discussed above, nitromethane + O_2 ignition occurs in at least two stages. The work of Djebaili-Chaumeix et al. [35] showed that ignition begins with a rapid decomposition of nitromethane and, after a buildup of the radical pool, a second stage of oxidation of the decomposition products follows.

However, the two stages in ignition have not yet been examined and compared. As mentioned above the two-stage behavior was indicated by the present authors in a conference publication [36] where ignition delay times from a shock tube study in the temperature range of 947 – 1333 K and at pressures in the range 8 – 32 atm were presented. In the present paper, that study is discussed in detail. A characterization of the ignition of nitromethane/O_2 over time is conducted by studying pressure and luminosity

profiles to understand the ignition process. Aspects of nitromethane ignition, such as pressure dependence and effects of fuel and oxidizer composition at the same equivalence ratio, are examined. A recent kinetic model developed for nitromethane flames [30] was used in an attempt to interpret the ignition characteristics.

2. Experimental details

Experiments were performed in a high-pressure shock tube at NUI Galway. The experimental setup is described in detail in the work of Nakamura et al. [39].

The experimental pressure profiles were recorded using two pressure transducers, one at the endwall and the other at the side wall, 10 mm from the endwall. The measurable time range in this experimental setup is 4000 μs. The ignition was tracked using unfiltered light emission from an optical window at the side wall, 10 mm from the endwall. The window is transparent within a wavelength range of 150 – 2000 nm and the emission was recorded with a Photodiode array detector (PDA) within the range 240 – 530 nm. Ignition delay times were measured from the time that the reflected shock wave triggered the pressure transducer at the endwall to the maximum intensities in the luminosity trace. This choice of ignition delay definition is further discussed in Section 4.1.

Four different gas compositions with varying fuel and O_2 content were studied, see Table 1. The gas mixtures were prepared and continuously stirred in a mixing tank at low pressure, at a temperature of 323 K. The shock tube

driven section was maintained at the same temperature. Partial pressure was used to control the mixture compositions. An issue when working with nitromethane is the risk of condensation. To avoid this, the liquid nitromethane (Sigma-Aldrich Ireland Limited, 95% purity) was gradually injected into the mixing tank with close monitoring of the pressure. Between each injection the fuel was left to vaporize and equilibrate. The partial pressure of the nitromethane was kept about three times lower than the saturation pressure of nitromethane. The O_2 (99.5%) and N_2 (99.99%) were supplied by BOC Ireland Limited.

Table 1 Experimental conditions visited with respect to mixture composition and pressure. Mixture components are given as mole%.

Mixture	CH_3NO_2	O_2	N_2	φ	Pressure [atm]
1	4	5	91	1	7.4–8.2, 15.9–16.8, 32.5–44.9
2	2	5	93	0.5	7.3–8.2
3	4	10	86	0.5	7.7–9.7, 14.4–15.6
4	4	2.5	93.5	2	14.8–16.6

The experiments were performed in the temperature range 947 – 1333 K at approximately 8, 16 and 32 atm. As explained in detail later, the ignition of nitromethane was found to have two separate stages of ignition with the two stages observed to be pressure independent. Therefore, experimental results with pressures deviating from the target pressure were included in the presentation of the experimental results. The pressures were within 90 – 105%

of the target pressures, with larger deviations for Mixture 1 at 32 atm, with three deviating pressures at 38.8, 39.5 and 44.9 atm, and Mixture 3 at 8 atm, with two deviating pressure of 9.2 and 9.7 atm. All experimental measurements are available in tabulated form as Supplementary material.

Traditionally N_2 has been regarded as the final product for nitromethane combustion [1,7]. For nitromethane flames, NO has been shown to be formed but not consumed [32,33]. For this reason, NO was chosen as the final product for nitromethane containing nitrogen in the definition of u, as further discussed in the work of Nauclér et al. [28].

$$2CH_3NO_2 + 2.5O_2 \rightarrow 2CO_2 + 3H_2O + 2NO \quad (1)$$

The experimental uncertainties, as estimated by Nakamura et al. [39], are ±15 K in reflected shock temperature, T_5, ±15% in ignition delay time, τ, and ±2% in mixture concentration.

3. Modeling details

The shock tube experiments were modeled using the batch reactor module of CHEMKIN IV [40] at constant volume and at a variety of pressure conditions. Two recent kinetic mechanisms were used in modeling nitromethane combustion, one from Brequigny et al. [30] and the second from Mathieu et al. [38].

The Brequigny et al. mechanism [30] contains 88 species and 701 reactions, of which the nitromethane subset involves 13 reactions. The mechanism is an adaptation of a mechanism by Glarborg et al. [11,33], developed to describe oxidation in low-pressure flames, validated for pressures

in the range 0.5–3.0 bar.

The Mathieu et al. mechanism [38] contains 166 species and 1204 reactions. This mechanism is an adaptation of the nitromethane subset from Brequigny et al. [30], updated with new rate constants from the literature. The mechanism was developed for the self-ignition of nitromethane + O_2 mixtures, and validated in the pressure range of 1.71 – 35.8 atm.

4. Results and discussion

The ignition was investigated for various conditions with respect to gas mixture composition, equivalence ratio and pressure. The experimental conditions presented in Table 1 are chosen to provide a matrix of parameters covering a relevant range of pressures and mixture compositions. In the following discussion the experimentally measured properties pressure and luminosity, over time, are first evaluated. It is shown that luminosity has two time-separated maxima, which is treated as two separate ignition stages. These stages are discussed separately from both an experimental and a modeling perspective. Correlation equations are calculated for both of the ignition stages and compared to correlations from the literature [26,35,38]. The effects of mixture composition and pressure on ignition delay times are discussed.

4.1. Experimental traces of pressure and luminosity

To accurately define the ignition, profiles of pressure and luminosity over time are explored. Mixtures 1–4 are discussed separately with respect to the characteristics of each mixture. Figs. 1–4 are typical examples of the measured

pressure and luminosity profiles, clearly illustrating the similarities and differences characterizing the different mixtures. Fig. 1 presents the experimental pressure and luminosity profiles of Mixture 1 at $\varphi = 1$, at a pressure of 8.2 atm and a temperature of 1115 K. From the pressure trace in Fig. 1, it can be seen that after the distinct pressure rise resulting from the arrival of the shock wave, there is a smooth pressure rise with a maximum. The pressure rise indicates that there is a prolonged activity in the gas mixture after the reflected shock wave reaches the end-plate but the pressure trace cannot be used independently to determine if ignition has occurred. In the luminosity trace in Fig. 1 two luminosity maxima separated in time, are evident. First there is a luminosity maximum shortly after the arrival of the shock wave, with a maximum intensity occurring in a time scale smaller than 40 μs. This is followed by a second luminosity peak with a higher maximum intensity and with a broader distribution over time. The second maximum intensity in light emission roughly coincides in time with the pressure maximum. The difference in intensity between the first and second luminosity maxima can be explained either by a higher concentration of light emitting species during the second luminosity maximum, or by different light emitting species present in the two luminosity maxima.

Mixture 2 has $\varphi = 0.5$, with the same oxygen content but with a 50% reduction in nitromethane as compared to Mixture 1. Example pressure and luminosity profiles, representing a measurement for Mixture 2 at 1220 K and 8.5 atm, are shown in Fig. 2. Unlike the pressure in Mixture 1 there is no

clearly defined pressure rise after the arrival of the shock wave, indicating that there is no major change in volume during the ignition, or that no ignition occurs. The chemical activity in this mixture is apparently too low to be detected from the pressure traces. However, from the luminosity traces it is evident that ignition does occur. A similar pattern as in the luminosity profiles from Mixture 1 is seen, with two separated maxima. The first maximum occurs shortly after the arrival of the reflected shock wave, while the second maximum is delayed. The second stage has a stronger emission intensity and wider distribution over time. Considering both the pressure and luminosity traces gives an indication that the lower fuel amount in Mixture 2 decreases the intensity of the luminosity, while preserving similar characteristics over time compared to Mixture 1.

Mixture 3 has $\varphi = 0.5$, which is the same as for Mixture 2, with the same nitromethane content as in Mixture 1 but with the O_2 content doubled. There is no pressure rise after the arrival of the shock wave for Mixture 3 in the measurements at temperatures >1032 K. Measurements at 984 K and 1031 K show a rise in pressure, coinciding in time with the luminosity peaks. Fig. 3 shows the pressure and luminosity traces for Mixture 3 at 1031 K and 8.5 atm. In the luminosity traces for Mixture 3, it can be seen that both luminosity maxima are close together in time, and are almost indistinguishable. The ignition does not start at the arrival of the shock wave in the measurements at 61186 K, but there is a time delay, as can be seen in Fig. 3.

Mixture 4 has $\varphi = 2.0$, with the same nitromethane content as Mixture 1

but it contains 50% of the O_2 content. This mixture was investigated in the temperature range 1109–1780 K at, 16 atm. As can be seen in Fig. 4 the experimental pressure traces shows no significant pressure rise after the arrival of the shock wave. In contrast to the other conditions investigated, luminosity profiles for Mixture 4 show only one peak. This can be either the first stage ignition with the second ignition stage outside the time restrictions in the present study, or the two maxima collapsed to one luminosity peak. From the pressure and luminosity traces it cannot be conclusively determined if the ignition of Mixture 4 corresponds to the first or second stages identified in the luminosity profiles of the other mixtures. In the coming sections the information gained from the analysis of the other conditions are used to elucidate the ignition behavior of Mixture 4.

In the experimental pressure profiles of Mixtures 1–3, the pressure rise after the arrival of the shock wave occurs gradually or not at all, in contrast to the sharp pressure rise commonly used to identify ignition in shock tube experiments. Thus, if ignition were to be defined based on the pressure profiles measured in the present study, there would be a high degree of uncertainty. The luminosity profiles have well defined maxima; therefore, the experimental ignition is defined as the maxima of the luminosity profiles, with each maximum marking separate ignition events.

In the above it was shown that the ignition of nitromethane in the presence of oxygen exhibits an unusual ignition behavior with two separate ignition stages at the majority of the experimental conditions in the present study, as

exemplified by the luminosity profiles in Figs. 1–3. Under these conditions the first stage ignition is fast, with a luminosity maximum at <40 ls, with the exception of Mixture 3 at 984 and 1031 K, while the second stage had a delayed ignition in all mixtures and experimental conditions. This multi stage ignition is considered analogous to the multi stage chemistry found in flames [6,25,28] and in detonations [19]. Both the first and second stages are investigated further.

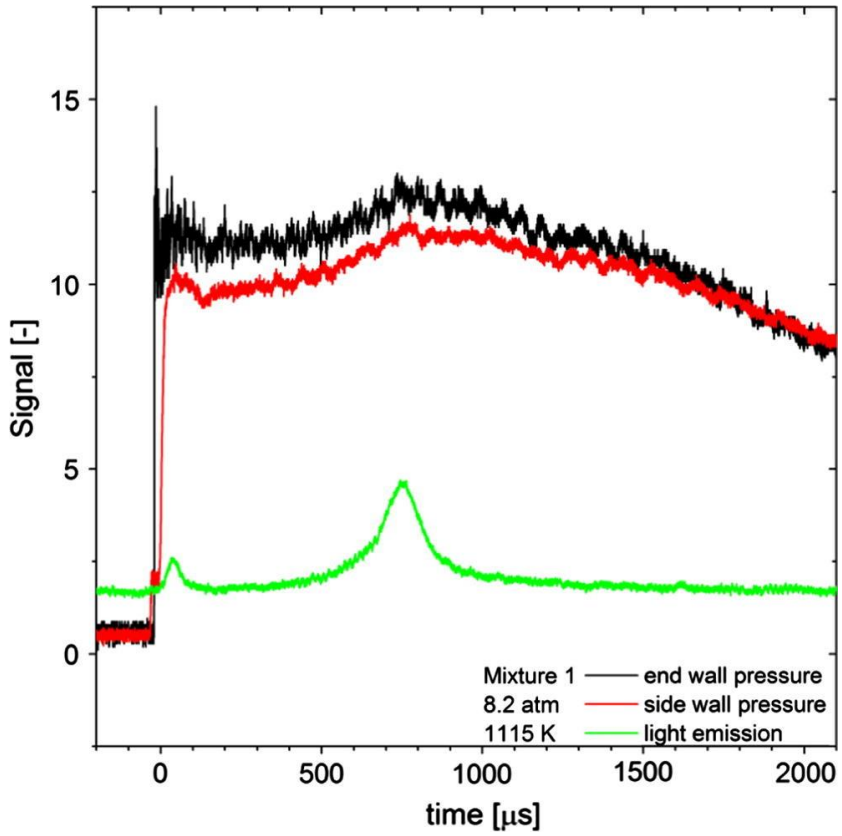

Fig. 1. Traces from pressure and light emission from the ignition of Mixture 1 at 1115 K and 8.2 atm.

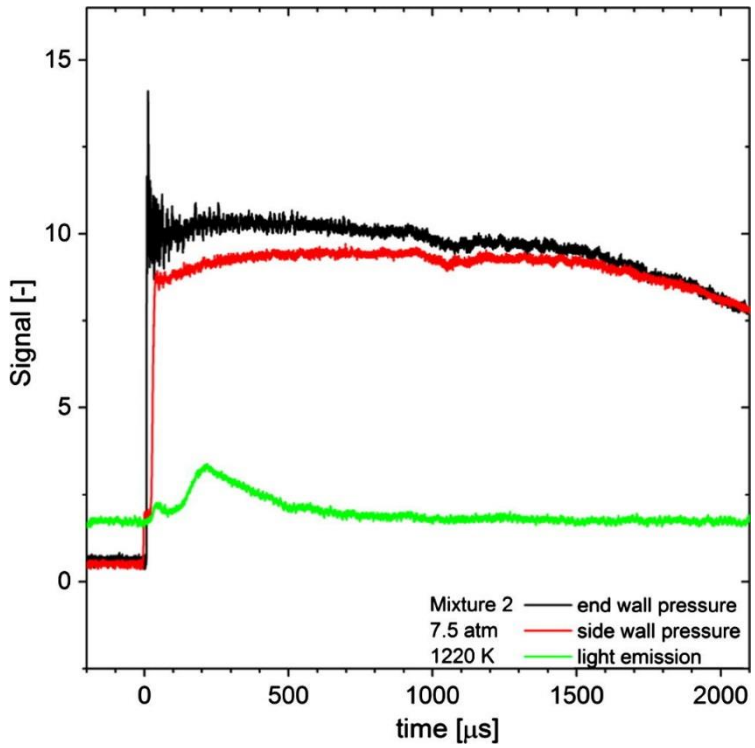

Fig. 2. Traces from pressure and light emission from the ignition of Mixture 2 at 1220 K and 7.5 atm.

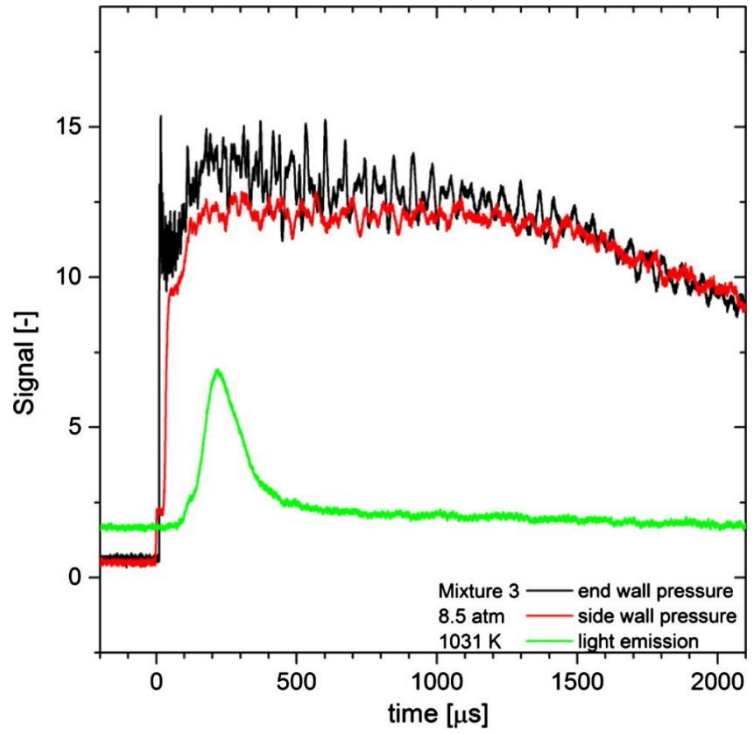

Fig. 3. Traces from pressure and light emission from the ignition of Mixture 3 at 1031 K and 8.5 atm.

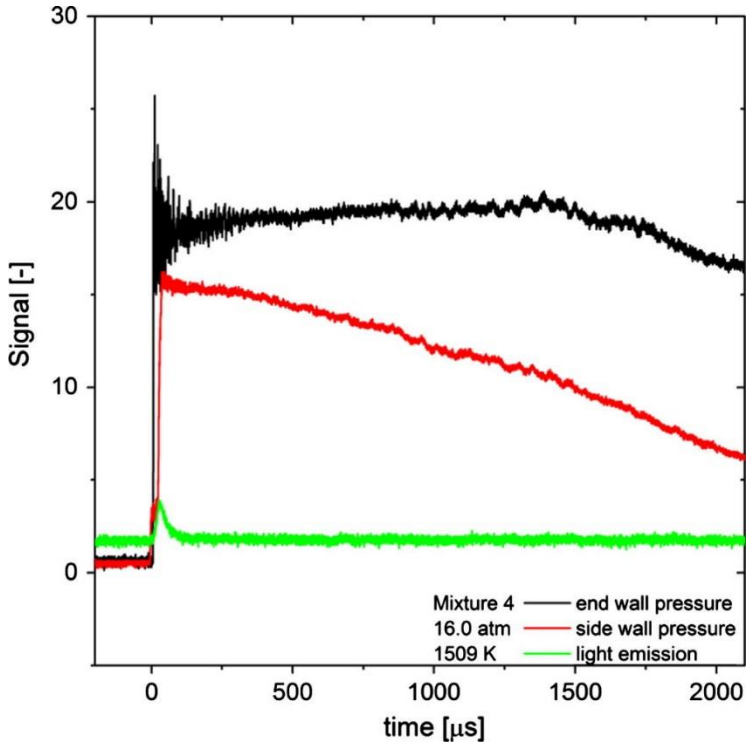

Fig. 4. Traces from pressure and light emission from the ignition of Mixture 4 at 1509 K and 16 atm.

4.1.1. Ignition delay determination

The ignition delay times for first- and second-stage ignition were determined for Mixtures 1–3 in the temperature range 947 – 1333 K. Fig. 5 shows that the ignition delay times for the first stage ignition are the same magnitude for Mixtures 1–3 over the temperature range studied, indicating that the initial gas mixture composition does not affect the ignition delay times. The activation energy for the first stage ignition is similar for the three mixtures. As a result of experimental uncertainties and the short ignition times of this ignition stage scatter in the results are likely not to be attributed to pressure effects. Mixture 4 show a fast ignition and the results are plotted in Fig. 5 together with the first stage ignition from Mixtures 1–3. The ignition delay

times measured for Mixture 4 are of the same order of magnitude as those for Mixtures 1–3, therefore the single stage ignition in Mixture 4 is likely the first stage ignition.

In Fig. 6 the experimental data for the second stage ignition is presented for Mixtures 1–3. The experimental second stage ignition delay decreases with temperature, as the reactivity increases. Reducing the nitromethane content by half has a small activating effect on the second stage ignition by decreasing ignition delay times. By doubling the O_2 content the effect on the ignition delay was considerably stronger with a reduction of the ignition delay times by ~four times compared to Mixture 1. The effective activation energy of the second stage ignition of Mixture 3 is weaker than that for Mixtures 1 and 2.

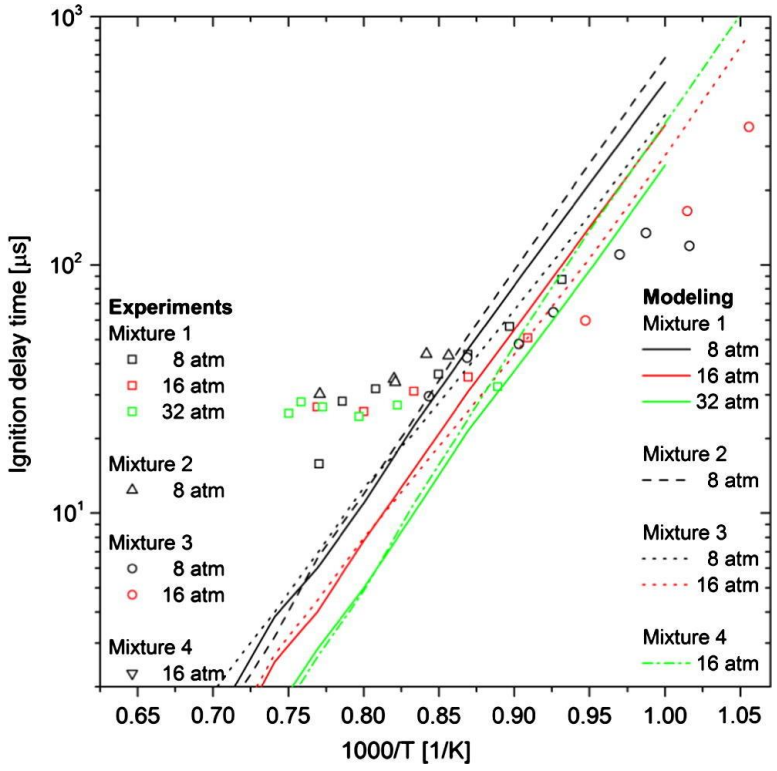

Fig. 5. The experimental results for the ignition delay times for the first stage ignition with predictions from the mechanism of Brequigny et al.

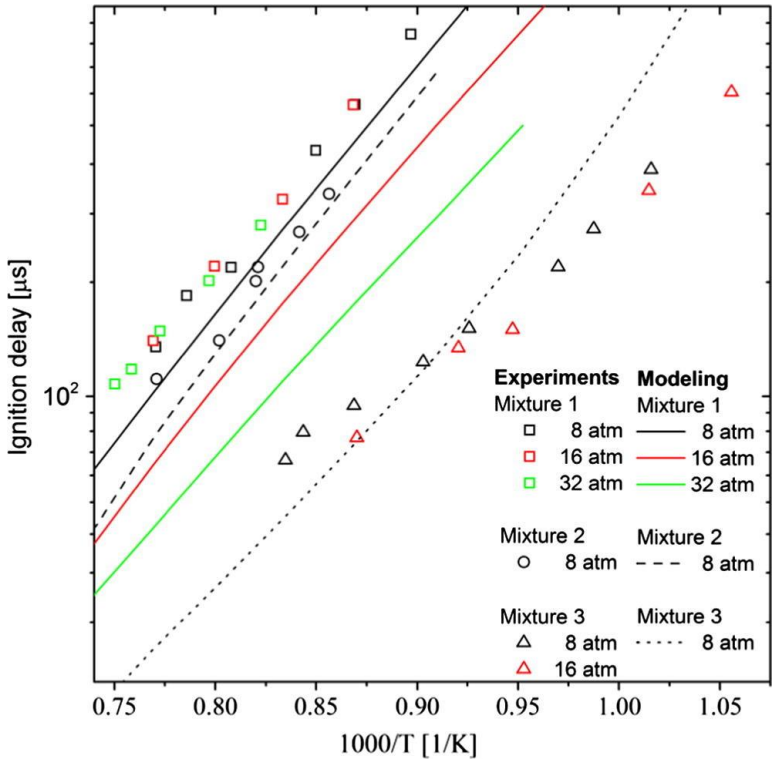

Fig. 6. Experimental results and predictions from the mechanism of Brequigny et al. for the second stage ignition in Mixtures 1–3 at 8, 16 and 32 atm.

Mixture 1 and Mixture 3 were examined in the pressure range of 7.4 – 44.9 atm and 7.7 – 15.6 atm, respectively. For many fuels, the ignition is sensitive to pressure [41]. As a result of the higher concentrations of fuel and O_2 in the gas mixture, ignition is typically faster at higher pressures. However, no change in ignition delay times with pressure is observed for either of the two ignition stages over the pressure range investigated.

4.1.2. Correlation equations based on mixture composition

The use of correlation equations allows comparison of datasets obtained at different conditions as the correlations quantify the dependence of the ignition delay on the concentration of fuel, oxidizer and inert gas over a range of

conditions. The quality of a correlation depends on the range and quality of data used in deriving it. All correlations discussed below are summarized in Table 2. In the present work correlation equations were obtained by fitting an expression to the experimental results from Mixtures 1–3 of the present study for both the first (Eq. (2)) and second (Eq. (3)) stage ignition. Mixture 4 was not included since the single ignition stage cannot be conclusively attributed to one or the other ignition stages identified in the other mixtures. The effect of temperature and mixture composition was evaluated by multiple regression analysis. The concentrations are in mol m^{-3}, temperature in K and R in kcal mol^{-1} K^{-1}.

$$\tau = 10^{-1.71}\, e^{-16.15/RT}\, [CH_3NO_2]^{-0.31}\, [O_2]^{-0.02}\, [N_2]^{-0.48} \qquad (2)$$

$$\tau = 10^{-3.38}\, e^{-20.98/RT}\, [CH_3NO_2]^{-0.59}\, [O_2]^{-2.35}\, [N_2]^{-1.64} \qquad (3)$$

The overall activation energy, Ea, was determined to be 16.15 ± 1.57 kcal mol^{-1} for the first-stage ignition and 20.89 ± 0.82 kcal mol^{-1} for the second stage ignition. The pressure dependence derived from Eqs. (2) and (3) is weak, $P^{0.15}$ and $P^{-0.12}$ respectively. It can be seen in Fig. 7 that the correlations from the present study, Eqs. (2) and (3), represent the experimental results satisfactorily, with an exponential agreement. The ignition delay times determined for Mixture 4 were evaluated by comparison to Eqs. (2) and (3). The agreement with the correlation of the first stage ignition, Eq. (2), was good for the measurements at 1109 K and 1258 K, but the measurements at 1509 K and 1779 K did not fit the correlation. However, because there are no other mixtures examined in the temperature range 1500 – 1700 K, it not possible to

determine whether these measurements are faulty or are an accurate description of the first stage ignition at these temperatures. The fit of Mixture 4 was considerably lower than of the second stage ignition, Eq. (3).

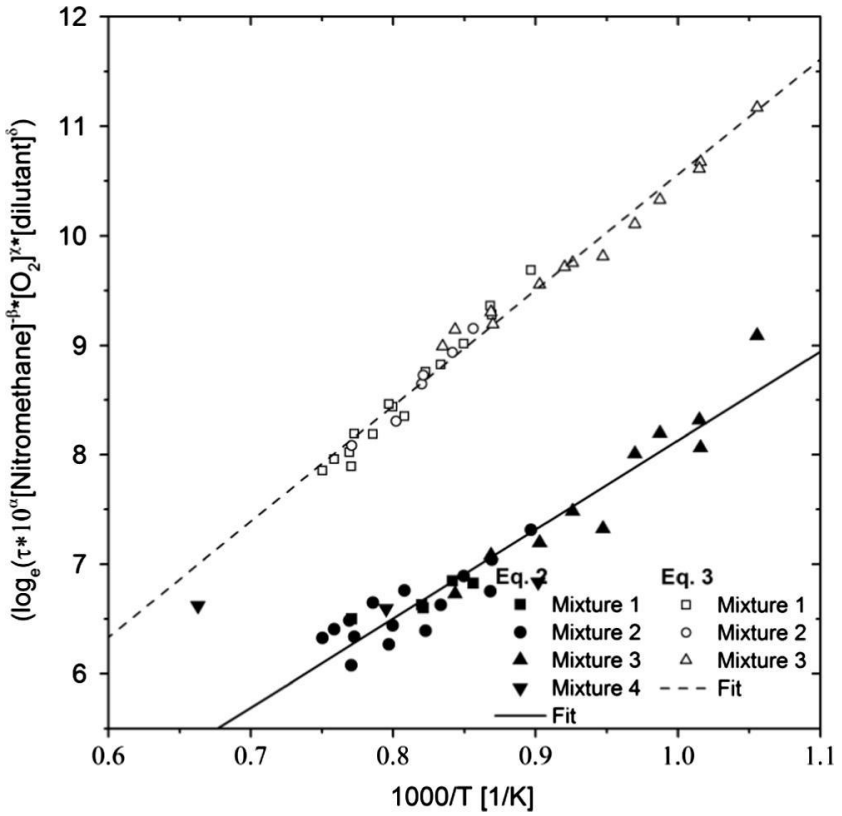

Fig. 7. The experimental data from the present study presented in the form of Eq. (2) for the first stage ignition and Eq. (3) for the second stage ignition.

The present analysis predicts a promoting effect of O_2 on both ignition stages, as evident from the negative sign on the exponents. O_2 has a minor influence on the first stage ignition, $[O_2]^{-0.02}$. However, the second stage ignition exhibits an unusually large influence of O_2, $[O_2]^{-2.35}$. Commonly the influence of O_2 on ignition is in the order of $[O_2]^{-0.5}$ to $[O_2]^{-1.5}$ [26]. Nitromethane concentration has a positive influence on the ignition in the first stage, $[CH_3NO_2]^{-0.31}$, while it has a dampening effect on the second stage

ignition, $[CH_3NO_2]^{0.59}$, according to the correlation analysis in Eqs. (2) and (3). Nitrogen is predicted to have a more pronounced dampening effect on the second stage ignition with a positive exponential dependence of 1.64, compared to the first stage ignition with a dependence of 0.48.

The correlations for the first and second ignition stage were compared to correlations from the literature [26,35,38]. Kang et al. [26] determined the ignition delay at ~0.2 atm by tracking the spike in pressure. The pressure profile presented by Kang et al. has the von Neuman spike, not the gradual increase seen in the present study. As mentioned in the discussion of pressure profiles, the second stage ignition detected by peaks in luminosity, in many cases were accompanied with a pressure increase. In light of this, the ignition delays from Kang et al., derived from pressure profiles, could be interpreted as the second stage ignition. Any indication of a fast ignition stage, near the arrival of the shock wave in time, is absent in the work by Kang et al. However, this can be a question of detection limits and equipment sensitivity. Their results were presented in the form of a correlation equation Eq. (4), derived from the ignition delay data obtained from mixtures with $\varphi \approx 0.8–3.12$. The experimental data was collected for mixture compositions with 8.0 – 37.8% nitromethane, 8.6–39.5% O_2, 33.3–80% Ar in the temperature range 1250 – 1900 K at ~0.2 atm.

$$\tau = 10^{-1.11}\, e^{-21.36/RT}\, [CH_3NO_2]^{0.59}\, [O_2]^{-0.72}\, [Ar]^{0} \qquad (4)$$

In the study by Djebaili-Chaumeix et al. [35], the ignition delay times were determined from a delayed emission signal at 235 nm. The correlation, Eq.

(5), was derived from ignition delay times for mixture compositions 3.56 – 6.4% nitromethane, 3.2 – 12.4% O_2, 84 – 91.97% Ar, and measured at 1040 – 1380 K at 0.8 – 2.8 atm.

$$\tau = 10^{-8.43}\, e^{-15.44/RT}\, [CH_3NO_2]^{-1.02}\, [O_2]^{-1.08}\, [Ar]^{1.42} \qquad (5)$$

The similar activation energies determined in the present study and that of Kang et al., with the uncertainty of both Ea, supports the hypothesis of the present study that the ignition detected in the pressure profiles by Kang et al. is corresponding to the second stage ignition identified in the present study. The trends in nitromethane and O_2, are the same for Eqs. (3) and (4), although with different magnitudes.

The correlation Eq. (5) behaves considerably differently compared to the correlations for the second stage ignition, Eqs. (3) and (4). According to Eq. (5), the ignition is promoted by both oxygen and nitromethane. This behavior is similar to that of the first stage ignition of the present study, Eq. (2). The activation energy in Eq. (5), is significantly lower than in Eqs. (3) and (4), and is in good agreement with the first stage ignition of the present study, Eq. (2), within its uncertainty.

By comparing the correlations for the second stage ignition, Eqs. (3) and (4), it can be seen that O_2 is predicted to have a larger influence on the ignition in the present study, as compared to the analysis by Kang et al. When inserting the experimental results for the second stage ignition into Eq. (4), Mixtures 1 and 2 are well represented, but Mixture 3 is not. This could be attributed to the fact that the equations are generated at different conditions, where Eq. (4) was

calculated from predominantly richer mixtures and higher temperatures than in the present study with one stoichiometric mixture and two mixtures with φ = 0.5, at 947 – 1333 K. As the activation energies in Eqs. (3) and (4) are in close agreement, the difference in temperature dependency between the studies could be due to differences in mixture composition.

Mathieu et al. [38] presented ignition delay times for mixtures in the range $0.5 < \varphi < 2$ at temperatures in the range 875 – 1595 K and at pressures in the range 1.71 – 35.8 atm. The experimental results with 90% and 98% Ar dilution were used to calculate two correlations, Eqs. (6) and (7). In the work of Mathieu et al. the correlations are based on φ and pressure. Here, the coefficients are directly translated to dependences on reactants and diluent, respectively, to facilitate comparison.

$$\tau = 10^{-1.80}\, e^{-19.8/RT}\, [CH_3NO_2]^{0.72}\, [O_2]^{-0.72}\, [Ar]^{0.06} \quad (6)$$

$$\tau = 10^{-2.91}\, e^{-37.5/RT}\, [CH_3NO_2]^{1.55}\, [O_2]^{-1.55}\, [Ar]^{-0.26} \quad (7)$$

The activation energies at 90% and 98% Ar dilution have different magnitudes. With higher dilution, the activation energy increased by 89%. The influence of the reactant also increased with higher dilution.

Correlations based on the predictions of the Brequigny et al. [30] mechanism were calculated in the present study. The predictions were performed in the same temperature and pressure ranges as the corresponding experimental mixtures, with ~50 K steps. The coefficients can be seen in Table 2. Even though the mechanism could capture the ignition delay times at 8 atm for the examined mixtures, the correlation, containing other pressures, cannot

capture the influence of the reactants nor the experimental activation energy.

The data from Borisov et al. [14] cannot be directly compared with the correlations obtained in shock tubes. In fact, earlier measurements performed in a by-pass apparatus were affected by significant heat losses during ignition delay as was revealed and discussed by the same authors [42,43]. Due to heat losses the temperature of the mixture was not equal to the temperature of the walls that affects interpretation of both ignition delays and the apparent activation energy [42,43].

By interpreting the data in light of the present study, where two ignition stages were observed in the same measurements, it is plausible that discrepancies that exist in the literature [26,35] could be due to observations of different stages in the ignition.

Table 2 The correlation coefficients from Eqs. (2) – (7).

Coefficients	Djebaili-Chaumeix et al. (Eq. (5))	Kang et al. (Eq. (4))	Mathieu et al.		Brequigny et al. mechanism 1st stage	Brequigny et al. mechanism 2nd stage	Present study 1st stage (Eq. (2))	Present study 2nd stage (Eq. (3))
			90% Ar (Eq. (6))	98% Ar (Eq. (7))				
$10^{-\alpha}$	8.43	1.11	1.80	2.91	4.94	4.54	1.71	3.38
Ea (kcal)	15.44	21.36	19.8	37.5	40.3	32.29	16.15	−20.98
$[NM]^{\beta}$	−1.02	0.59	0.72	1.55	−0.01	0.71	−0.31	0.59
$[O_2]^{\gamma}$	−1.08	−0.72	−0.72	−1.55	−0.09	−3.01	−0.02	−2.35
$[\text{dilutant}]^{\delta}$	1.42	0	0.06	−0.26	−0.54	1.41	0.48	1.64

4.2. Ignition modeling

4.2.1. Possible origin of luminosity

The presence of two luminosity maxima indicate that the ignition of nitromethane in the presence of O_2 occurs in several zones or steps, as previously seen in detonation [19] and flame [6,25] studies. The possible origins of the luminosity maxima were explored using kinetic modeling and information about the chemiluminescence from exited species in the light emitting wavelength range [44]. When identifying species, considerable experimental work [12,13,25,26,44–46] and the book of Gaydon [44] was considered. Candidate species were those which emit light within the experimentally detectable range of the present study, 240–530 nm.

In the work of Hall and Wolfhard [25] two zones were detected in a nitromethane/air flame. In the first zone the species C_2^*, CH^*, CN^*, $\dot{O}H^*$, NH^* and NO^* were observed, but not CH_2O^*. In the shock tube study of Kang et al. [26] the authors mention that the species CH_2O^*, $\dot{O}H^*$, and NO^* were detected through emission after the reflected shock had passed, which was referenced in [26] as a publication in preparation but is, to the best of our knowledge, not yet published. In the shock tube study of nitromethane decomposition by Zaslonko et al. [12] CH_2O^* was detected, and used as proof of the presence of $CH_3\dot{O}$ radical early in the ignition. In the combustion of liquid nitromethane strong signals of $\dot{O}H^*$ were detected with somewhat smaller signals of CN^* [46]. Dong et al. [45] investigated emission from nitromethane/O2 mixtures in a shock tube and observed emission of $CH3\dot{O}^*$ and $\dot{O}H^*$ appearing simultaneously. In

the shock tube study of Mathieu et al. a weak OH^* signal was detected [38].

NO_2^* is a likely candidate for the first stage emission that is detected as it is established in the literature that ground state NO_2 is produced from the thermal decomposition of nitromethane [12,13], and emits light in the detectable region.

Formaldehyde CH_2O^* emits light in the range 370–480 nm. It was generally considered that the reaction $CH_3\dot{O} + CH_3\dot{O} = CH_2O^* + CH_3OH$ is a source of excited formaldehyde [13].

In the present study, the possibility that luminosity originated from OH^* was examined by OH^*–filtering. No luminosity signal was detected in the filtered experiments. Based on this lack of signal it is, however, not possible with certainty to rule out the presence of OH^*, since the signal might be weaker than the detection limit. As $\dot{O}H^*$ radicals have been detected in previous studies, it is considered among the possible luminosity sources. Precursors to $\dot{O}H^*$ are primarily $\ddot{O} + \dot{H} = \dot{O}H^*$ and $\dot{C}H + O_2 = CO + \dot{O}H^*$, and to a minor extent $N_2O + \dot{H} = N_2 + \dot{O}H^*$.

NO does not decompose at the present temperatures and would therefore not result in one or several concentration maxima with a constrained time interval, but rather be distributed over a wide range in time. The same behavior was also predicted by the model. Considering this NO was excluded as a possible source of the luminosity peaks. The species left for consideration are, CN^*, NH^* and C_2^*. These species all emit light in the experimentally detectable range of the present study; CN^* at 388.3 and 359 nm, NH^* at 337 nm, C_2^* with

two swanbands within the detectable region of the present study at 473.7 and 516.2 nm.

The excited species C_2^* is produced from $\dot{C}H + \dot{C} = C_2^* + \dot{H}$ and $\dot{C}H_2 + \dot{C} = \dot{C}_2^* + H_2$ [47]. Through the reaction $\dot{C}H + NO = NH^* + CO$ the exited species NH^* can be formed [48]. The formation of CN^* is, to the best of the authors' knowledge, not well established in the literature. Therefore, its ground state equivalents are examined further.

Excited species are not present in the chemical kinetic mechanism used to simulate the present results, but the ignition is evaluated using the precursors for the exited species discussed above. Modeling shows two regions of species maxima that could possibly be related to the first- and second-stage ignition, as shown in Fig. 8. The first and second ignition stages are defined as the maximum pressure rises according to the model, and marked in Fig. 8. $CH_3\dot{O}$ and NO_2 peak almost simultaneously at the first ignition stage, with the presence of $CH_3\dot{O}$ indicating that CH_2O^* can be formed. CN has a maximum at the second stage ignition, while NH has two maxima corresponding in time with both the first and second stage ignition events. At both ignition stages, maxima from $\dot{O}H$ radical can be found. The radical $\dot{C}H$ is of interest as a precursor for $\dot{O}H^*$ and C_2^* and NH^*. $\dot{C}H_2$ acts as a precursor to C_2^*. The $\dot{O}H$, $\dot{C}H$ and $\dot{C}H_2$ radicals have three maxima. First there is a maximum at times <5 ms, followed by two delayed maxima corresponding in time with the two ignition stages respectively. The first two maxima are predicted to have a lower molar fraction than the third maximum. Atomic oxygen, Ö, is studied as a

precursor to $\dot{O}H^*$, it has a maximum at both ignition stages. The luminosity of both ignition stages is probably emission from a mixture of several of the exited species discussed above.

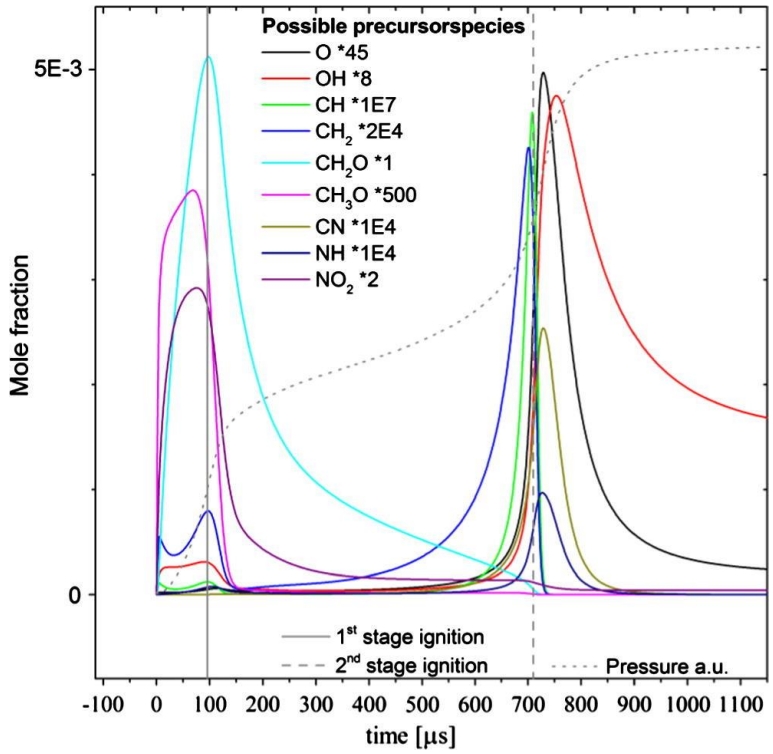

Fig. 8. Predicted concentrations over time for selected precursors to plausible light emitting species in Mixture 1 at 1100 K and 8 atm. The predictions are from the mechanism of Brequigny et al.

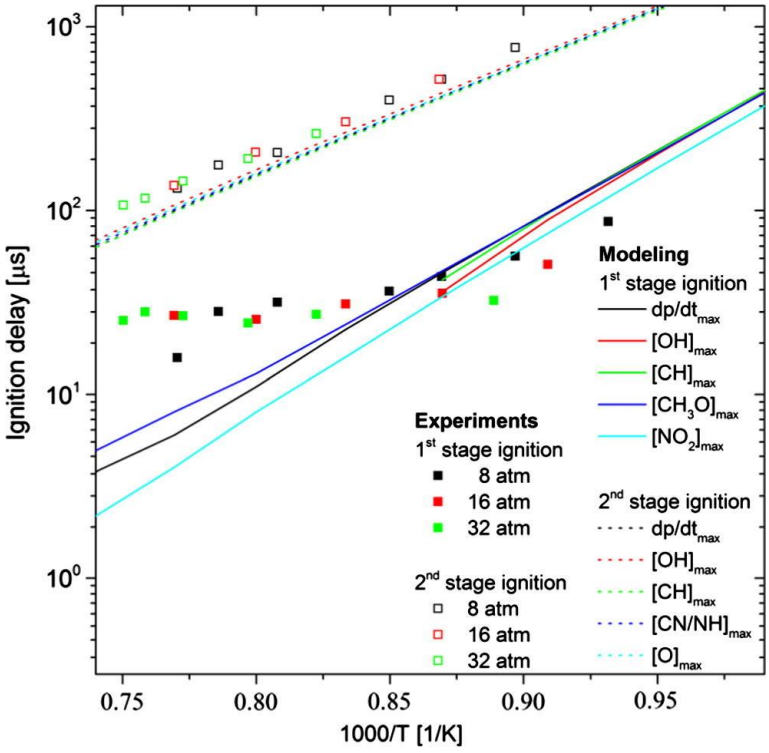

Fig. 9. Comparison of different definitions of the predicted ignition delay time for the first and second stage ignition in Mixture 1. The predictions are from the mechanism of Brequigny et al.

4.2.2. Definition of ignition delay in the modeling

The choice of marker to define the ignition delay time is important when evaluating the performance of the mechanism. In light of the previous discussion, several definitions of ignition were tested in our modeling. Precursors to the radicals considered as likely sources of emission have been tested. These include: dp/dt_{max}, $[\dot{O}H]_{max}$ and $[\dot{C}H + \dot{C}H_2]_{max}$, for both ignition stages, $[CH_3\dot{O}]_{max}$ and $[NO_2]_{max}$ for the first stage ignition, and $[CN]_{max}$, $[NH]_{max}$ and $[N_2O]_{max}$ for the second stage ignition. The definitions dp/dt_{max}, $[\dot{O}H]_{max}$ and $[\dot{C}H + \dot{C}H_2]_{max}$ were chosen as they have all been established in the literature as markers for ignition, and are formed within the explosion and

consumed relatively fast. The results are plotted in Fig. 9 and one can see that there are no major differences in ignition delay time using the different definitions, for either the first or second stage ignition events. The pressure profiles versus time resulted in two pressure rises separated in time; a maximum gradient in pressure dp/dt_{max} was calculated for both pressure rises. The first maximum for ȮH and ĊH + ĊH$_2$ appears at times considerably shorter than the first experimental maximum. This can contribute to the width of the luminosity maximum, but is unlikely to be an appropriate marker for the maximum. Therefore, the second maximum was tested as a marker for the first stage ignition. At temperatures >1150 K, these two first maxima were difficult to distinguish. Therefore, the ignition delay times for the first stage ignition were only calculated up to 1150 K for ȮH and ĊH + ĊH$_2$. For the second stage ignition the ignition delay time from $[\dot{O}]_{max}$ and $[\dot{O}H]_{max}$ were slightly longer compared to predictions using dp/dt_{max}, $[CN/NH]_{max}$ and $[\dot{C}H + \dot{C}H_2]_{max}$, but negligible on the logarithmic scale, as seen in Fig. 8. As there is negligible difference between the definitions for both ignition stages, the choice of ignition marker in modeling the data is of little consequence and does not influence the interpretation of the mechanism's performance. The maximum pressure gradient dp/dt_{max} was used for the modeling predictions as the origin of the experimental luminosity was not experimentally proven.

4.3. Comparison between experimental results and modeling

First, two contemporary kinetic mechanisms by Brequigny et al. [30] and Mathieu et al. [38] are compared for their ability to reproduce the experimental

ignition delay times. The mechanism of Brequigny et al. accurately reproduced the trends in ignition delay times from all mixture compositions at 8 atm. An important point is that the small reduction in ignition delay time when decreasing the nitromethane content was successfully reproduced. The Mathieu et al. mechanism did not reproduce the ignition delay times as well as that of Brequigny et al. in the present work. Therefore, the Brequigny et al. mechanism has been chosen in our further discussion. In Supplementary material, the performance of the mechanism of Mathieu et al., at the condition of the present study, is presented for both ignition stages.

When comparing the experimental results with the modeling predictions for the first stage ignition, the activation energy in the predictions is higher for all mixtures examined, as seen in Fig. 5. The predicted first stage ignition ranges between 1 and 544 μs in the temperature range 1000–1500 K for Mixture 1 at 8 atm, and coincides with the experimental results ~1100 K. There are minor differences between the predicted activation energy of the first stage ignition for the different mixtures, which is slightly lower in Mixture 3 and negligibly higher in Mixture 2 and Mixture 4, as compared to Mixture 1. These differences in activation energy between the different mixtures are small compared to the experimental activation energy.

For Mixtures 1 and 2 the experiments and modeling are in reasonable agreement with the second stage ignition at 8 atm. Moreover, in the simulated second stage ignition the temperature dependence is stronger than observed in the experimental temperature dependence for Mixture 3, as seen in Fig. 6.

The pressure dependence was examined at 8, 16 and 32 atm for Mixture 1. Unlike the pressure independence in the experimental results, the model predicts decreasing ignition delay times (faster reactivity) for both ignition stages with increasing pressure for Mixture 1.

5. Conclusions

The ignition of nitromethane/O_2/N_2 mixtures was characterized as a two-stage process under our experimental conditions. The ignition profiles were examined with respect to pressure and luminosity versus time. Some pressure traces showed a continuous rise stretched over time with one maximum, rather than a sharp von Neuman spike, while some traces had no significant pressure rise at all. From the luminosity traces two maxima were identified; the second coinciding in time with the pressure maximum. The luminosity was used to define the experimental ignition, with the ignition delay times taken at the maximum intensity of the luminosity peaks. Firstly, a fast ignition stage occurs, followed by a second stage ignition with higher luminosity intensity and a larger spread over time. The two-stage ignition process, seen also in detonations [19], and possibly corresponding to the occurrence of several reaction zones in modeled flames [6,28], is thereby proven experimentally in self ignition. Both the first- and second-stage ignition was examined for pressure and mixture composition dependence. An unusual aspect of nitromethane ignition is that over the conditions examined in the current study, there was no pressure dependence in the ignition delay times for

either the first or second stage ignition. Mixture composition had no measurable effect on the first stage ignition delay times. However, for the second stage ignition, the ignition delay time was decreased by a factor of approximately four by doubling the O_2 content of the mixture, but reducing the nitromethane content by half only marginally reduced the ignition delay times.

Possible exited species generating the emission were identified as possible ignition markers for simulations from a theoretical discussion based on species observed in the literature. It was shown that the definition of ignition did not affect the evaluation of the performance for the mechanism of Brequigny et al. [30].

Modeling could reproduce the magnitude of the first stage ignition in reasonable agreement, but the temperature dependence was steeper than for the experimental results. For the second stage ignition the model predictions reproduce the temperature dependence well, and also reproduces well the ignition delay times at 8 atm but under-predicts them at 16 and 32 atm. The mechanism could not reproduce the pressure independence seen in the experimental results for either the first or second stage ignition. The kinetics of nitromethane/O_2/N_2 ignitions cannot be fully explained, and warrants further investigation.

The experimental temperature and mixture dependence was analyzed in terms of a correlation fit for each ignition stage, Eqs. (2) and (3). From this analysis the first stage ignition was concluded to be mainly promoted by the concentration of nitromethane, suggesting that this ignition stage is controlled

by the thermal decomposition of nitromethane and its neighboring chemistry. In the second stage ignition O_2 has a strong promoting effect on the reactivity, while nitromethane has a mild dampening effect on the ignition. From the correlations the overall activation energy was calculated to be 16.15 ± 1.57 kcal mol^{-1} for the first stage ignition, and 21.45 ± 0.82 kcal mol^{-1} for the second stage. Compared to the correlation from Kang et al. [26], the second-stage ignition is in the present study predicted to be more influenced by O_2 and diluent concentrations. The activation energy for the second stage ignition is in good agreement with the activation energy calculated in the work of Kang et al. In the correlation from Djebaili-Chaumeix et al. [35] the activation energy is in good agreement with the first stage ignition of the present study.

The ignition in Mixture 4 was attributed to a first stage ignition, but the measurement points at 1509 K and 1779 K where differentiated as the ignition delay times do not follow the general trend of first stage ignition found in the temperature range 947 – 1333 K.

The chemistry behind ignition of nitromethane/O_2 warrants further studies, in order to elucidate the pressure independence of the ignition and improve capabilities to reproduce this through simulations.

Acknowledgments

The author would like to thank The Centre for Combustion Science and Technology (CECOST) and the Swedish Energy Agency (STEM) for financial support. Special thanks to the Hierta-Retzius foundation for financial support

for an extended research-trip of JDN to National University of Ireland, Galway. Discussions and feedback from Prof. John Simmie are gratefully acknowledged.

References

[1] Starkman ES. Nitroparaffins as potential engine fuels. Ind Eng Chem 1959;51:1477–80.

[2] Litzinger T, Colket M, Kahandawala M, Lee SY, Liscinsky D, McNesby K, et al. Fuel additive effects on soot across a suite of laboratory devices, Part 2: Nitroalkanes. Combust Sci Technol 2011;183:739–54.

[3] Cracknell RF, Andrae JCG, McAllister LJ, Norton M, Walmsley HL. The chemical origin of octane sensitivity in gasoline fuels containing nitroalkanes. Combust Flame 2009;156:1046–52.

[4] Jia Z, Wang Z, Cheng Z, Zhou W. Experimental and modeling study on pyrolysis of n-decane initiated by nitromethane. Combust Flame 2016;165:246–58.

[5] Fells I, Rutherford AG. Burning velocity of methane-air flames. Combust Flame 1969;13:130–8.

[6] Boyer E, Kuo KK. Modeling of nitromethane flame structure and burning behavior. Proc Combust Inst 2007;31:2045–53.

[7] Taylor HA, Vesselovsky VV. The thermal decomposition of nitromethane. J Phys Chem 1934;39:1095–101.

[8] Hillenbrand LJ, Kilpatrick ML. The thermal decomposition of nitromethane.

J Chem Phys 1953;21:525–35.

[9] Bradley JN. Shock-wave decomposition of nitroparaffins. Part 1. -Massspectrometric study of nitromethane decomposition. Trans Faraday Soc 1961;57:1750–6.

[10] Perche A, Tricot JC, Lucquin M. Pyrolysis of nitromethane.1. Experimental study - nitromethane alone and in the presence of additives. J Chem Res-S 1979:116–7.

[11] Glarborg P, Bendtsen AB, Miller JA. Nitromethane dissociation: Implications for the CH3 + NO2 reaction. Int J Chem Kinet 1999;31:591–602.

[12] Zaslonko IS, Kogarko SM, Mozzhukin EB, Petrov Y. Thermal decomposition of nitromethane in Shock waves. Kinet Catal (Engl Transl) 1972;13:1001–5.

[13] Glänzer K, Troe J. Thermische zerfallsreaktionen von nitroverbindungen. I: Dissoziation von nitromethan. Helv Chim Acta 1972;55:2884–93.

[14] Borisov AA, Kogarko SM, Skachkov GI. Thermal decomposition of nitromethane. Kinet Catal (Engl Transl) 1966;7:521–6.

[15] Hsu DSY, Lin MC. Laser probing and kinetic modeling of NO and CO production in shock-wave decomposition of nitromethane under highly diluted conditions. J Energ Mater 1985;3:95–127.

[16] Kuznetsov NM, Petrov YP, Turetskii SV. Kinetics of N_ O2 formation upon the decomposition of nitromethane behind shock waves and the possibility of nitromethane isomerization in the course of the reaction. Kinet Catal 2012;53:1–12.

[17] Zaslonko IS, Petrov YP, Smirnov VN. Thermal decomposition of nitromethane in shock waves: the effect of pressure and collision partners. Kinet Catal 1997;38:321–4.

[18] Menikoff R, Shaw MS. Modeling detonation waves in nitromethane. Combust Flame 2011;158:2549–58.

[19] Sturtzer MO, Lamoureux N, Matignon C, Desbordes D, Presles HN. On the origin of the double cellular structure of the detonation in gaseous nitromethane and its mixtures with oxygen. Shock Waves 2005;14:45–51.

[20] Presles HN, Desbordes D, Guirard M. Detonation in nitromethane and nitromethane-oxygen gaseous mixtures. In: Proceedings of the Zeldovich memorial-international conference on combustion. 1994. p. 382–5.

[21] Presles HN, Desbordes D, Guirard M, Guerraud C. Gaseous nitromethane and nitromethane-oxygen mixtures: a new detonation structure. Shock Waves 1996;6:111–4.

[22] Khasainov B, Virot F, Presles HN, Desbordes D. Parametric study of double cellular detonation structure. Shock Waves 2013;23:213–20.

[23] Petrov YP, Karasevich YK, Turetskii SV. Decomposition of nitromethane in shock waves: the primary stage and the kinetics of decomposition at pressures of about 40 atm. Russ J Phys Chem B 2010;4:566–73.

[24] Joubert F, Desbordes D, Presles H-N. Detonation cellular structure in NO_2/N_2O_4–fuel gaseous mixtures. Combust Flame 2008;152:482–95.

[25] Hall AR, Wolfhard HG. Multiple reaction zones in low pressure flames with ethyl and methyl nitrate, methyl nitrite and nitromethane. Symp (Int)

Combust 1957;6:190–9.

[26] Kang JG, Lee SW, Yun SS, Choi SN, Kim CS. Ignition delay times of nitromethane/oxygen/argon mixtures behind reflected shock. Combust Flame 1991;85:275–8.

[27] Guirguis R, Hsu D, Bogan D, Oran E. A mechanism for ignition of hightemperature gaseous nitromethane—the key role of the nitro group in chemical explosives. Combust Flame 1985;61:51–62.

[28] Nauclér JD, Nilsson EJK, Konnov AA. Laminar burning velocity of nitromethane + air flames: a comparison of flat and spherical flames. Combust. Flame 2015;162:3803–9.

[29] De Jaegere S, Van Tiggelen A. Comparative study of flame propagation in compounds containing nitrogen oxides. Combust Flame 1959;3:187–200.

[30] Brequigny P, Dayma G, Halter F, Mounaïm-Rousselle C, Dubois T, Dagaut P. Laminar burning velocities of premixed nitromethane/air flames: an experimental and kinetic modeling study. Proc Combust Inst 2014;35:703–10.

[31] Tricot JC, Perche A, Lucquin M. Gas-phase oxidation of nitromethane. Combust Flame 1981;40:269–91.

[32] Tian ZY, Zhang LD, Li YY, Yuan T, Qi F. An experimental and kinetic modeling study of a premixed nitromethane flame at low pressure. Proc Combust Inst 2009;32:311–8.

[33] Zhang KW, Li YY, Yuan T, Cai JH, Glarborg P, Qi F. An experimental and kinetic modeling study of premixed nitromethane flames at low pressure. Proc Combust Inst 2011;33:407–14.

[34] Seljeskog M. Shock tube experiments on nitromethane and promotion of chemical reactions by nonthermal plasma. In: Faculty of Engineering Science and Technology Department of Thermal Energy and Hydropower, The Norwegian University of Science and Technology, Trondheim. 2002. p. 328.

[35] Djebaili-Chaumeix N, Abid S, Paillard CE. Shock tube study of the nitromethane decomposition and oxidation. In: Howing AFP, editor. Proceedings of the 21st international symposium on shock tubes and shock waves. Australia: The University of Queensland; 1997.

[36] Nauclér JD, Li Y, Nilsson EJK, Konnov AA, Curran HJ. Ignition of nitromethane + O_2 + N_2 in a shock tube. In: European combustion meeting, Budapest, Hungary. 2015. p. P4–P05.

[37] Mathieu O, Giri B, Mertens JD, Petersen EL. Nitromethane ignition behind reflected shock waves. In: 25th ICDERS, Leeds, UK. 2015.

[38] Mathieu O, Giri B, Agard AR, Adams TN, Mertens JD, Petersen EL. Nitromethane ignition behind reflected shock waves: experimental and numerical study. Fuel 2016;182:597–612.

[39] Nakamura H, Darcy D, Mehl M, Tobin CJ, Metcalfe WK, Pitz WJ, Westbrook CK, Curran HJ. An experimental and modeling study of shock tube and rapid compression machine ignition of n-butylbenzene/air mixtures. Combust Flame 2014;161:49–64.

[40] CHEMKIN IV 15101. Reaction Design: San Diego; 2010.

[41] Westbrook CK, Curran HJ, Pitz WJ, Griffiths JF, Mohamed C, Wo SK. The effects of pressure, temperature, and concentration on the reactivity of

alkanes: experiments and modeling in a rapid compression machine. In: Burgess AR, Dryer FL, editors. Symposium (international) on combustion. Pittsburgh: Combustion Institute; 1998. p. 371–8.

[42] Borisov AA, Knorre VG, Kudryashova EL, Skachkov GI, Troshin KY. On temperature measurements in the induction of homogenous gas mixtures in a static admittance apparatus. Chem Phys Rep c/c Khimicheskaia Fizika 1998;17:1323–32.

[43] Borisov AA, Skachlov GI, Troshin KY. Ignition and combustion kinetics of simple C1–C3 hydrocarbons in their mixtures with air. Chem Phys Rep 1999;18:1665–82.

[44] Gaydon AG. The spectroscopy of flames. 2nd ed. London (UK): Chapman and Hall Ltd; 1974.

[45] Dong H, Yong-Guo W, Hong-Bin L, Zhu-Mei S. Studies on high speed reaction spectrum of nitromethane under high temperature and high pressure. Chin J High Press Phys 1994;8:296–301.

[46] Kelzenberg S, Eisenreich N, Eckl W, Weiser V. Modelling nitromethane combustion. Propel Explos Pyrotech 1999;24:189–94.

[47] Grebe J, Homann KH. Blue-green Chemiluminescence in the system C_2H_2/O/H. Formation of the emitters CH($A^2\Delta$), $C_2(d^3\Pi_g)$ and C_2H^*. Ber Bunsenges Phys Chem 1982;86:587–97.

[48] Lichtin DA, Berman MR, Lin MC. NH($A^3\Pi \rightarrow X^3\Sigma^-$) Chemiluminescence from the CH($X^2\ \Pi$) + NO reaction. Chem Phys Lett 1984;108:18–24.

Overall Conclusions

An extensive set of ignition delay time (IDT) measurements of four C_4 unsaturated hydrocarbons including isobutene, 1-butene, 2-butene and 1,3-butadiene were recorded using both a high-pressure shock tube and a rapid compression machine at engine relevant conditions. The results presented greatly expand the ignition delay time database available for mechanism validation of C_4 unsaturated hydrocarbon fuel oxidation.

A detailed chemical kinetic model to describe the oxidation of 1- and 2-butene was developed, and has been validated against a large variety of experimental data including IDTs, species profiles data from jet-stirred reactors, premixed flames, and flow reactors, and laminar flame speed data. The reactivity difference between the three butene isomers was explained by the detailed low- and high-temperature reaction pathways specific to unsaturated fuel chemistry.

A comprehensive theoretical kinetics analysis for Ḣ atom addition to 1,3-butadiene and related reactions on the $\dot{C}_4H_7$ potential energy surface were performed using two different series of quantum chemical methods and two different kinetic codes. The pressure-dependent rate coefficients for isomerization, decomposition, and chemical activation reactions were investigated using RRKM/ME analyses. The thermodynamic properties of all C_4 species were also evaluated.

In addition to the publications listed in this thesis, the autoignition

characteristics of two gasoline and diesel fuel blends (volume ratio: 75:25 and 50:50) were experimentally investigated over a wide range of temperatures (600 – 1400 K), equivalence ratios (0.5, 1.0 and 2.0), and pressures (10 and 20 atm) using both a high-pressure shock tube and a rapid compression machine. The reactivity of these two gasoline and diesel fuel blends were systematically compared with the other two gasoline fuel samples. Additionally, three surrogates (PRF, TPRF and a multi-component surrogate) were carefully formulated for each fuel blend by matching various fuel characteristics (RON, MON, Octane Sensitivity and AKI). Two gasoline surrogate models from LLNL and KAUST were employed to simulate the experimental data.

Finally, quantum chemical calculations were performed. Firstly, a systematic investigation of abstraction by molecular oxygen of primary, secondary and tertiary hydrogen atoms from a series of allylic radicals was carried out using four different quantum chemical methods and two different kinetic codes. The calculated rate constants were compared, illustrating the general trend in increasing rate of reaction proceeding from the abstraction of primary, secondary and tertiary hydrogen atoms, and rate rules were developed for this reaction class.

Secondly, highly-accurate ab initio gas phase thermochemistry was calculated for 26 alkene molecules and 19 allylic radicals (101 conformers in total) relevant in combustion chemistry in order to develop an accurate database of thermodynamic properties for small (C_2 – C_7) unsaturated species. Based on the quantum calculation results, the relevant groups including six

unsaturated hydrocarbon (HC) groups and three allylic bond dissociation (BD) groups were systematically updated, and three super allylic groups were newly developed which will be used in the future calculations using the Group Additivity (GA) method for thermochemistry calculations.